

STUDIES IN UPPER ATMOSPHERE

A THESIS  
SUBMITTED FOR THE DEGREE OF  
DOCTOR OF PHILOSOPHY  
OF THE

GUJARAT UNIVERSITY

BY  
M. SOUMYA NARAYANAN

DECEMBER 1973

043

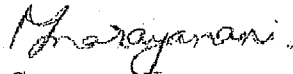


B5447

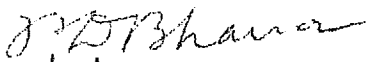
PHYSICAL RESEARCH LABORATORY  
NAVRANGPURA  
AHMEDABAD-9  
INDIA.

CERTIFICATE

I hereby declare that the work presented in this thesis is original and has not formed the basis for award of any degree by any University or Institution.

  
(M. Soumya Narayanan)  
Author

Certified

  
(Praful D. Bhavsar)  
Professor-in-Charge.

## STATEMENT

THE work presented in the thesis was carried out by the author, at the Physical Research Laboratory, Ahmedabad, under the guidance of Professor P. D. Bhavsar and Dr. J. N. Desai.

The first measurements of winds in the equatorial upper atmosphere, at twilight, were made by Bhavsar and Ramanuja Rao from the Thumba Equatorial Rocket Launching Station (TERLS). The present work by the author is an extension of the above, by making measurements of night-time winds and other atmospheric parameters, with the help of chemical releases in the upper atmosphere. In this study, observational results of night-time winds, obtained from experiments conducted for the first time at Thumba, have been presented. The author was associated with the preparation of TMA vapour release payloads for these experiments. General global circulation patterns of winds have also been studied utilising, for the first time, wind results obtained by vapour releases at different latitudes and longitudes.

Diffusion coefficients have been determined for neutral clouds from Ba-Sr point releases. For applying appropriate correction for the effects of strong twilight sky background, a new method has been evolved and used in this study. Also a

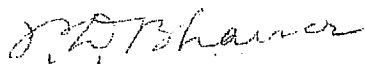
new method is presented to obtain temperature-height profiles from the measured diffusion profiles. This method promises to be of considerable importance for an understanding of the lower thermospheric structure, particularly so, if experiments are made where diffusion coefficient profile is measured simultaneously with temperatures at a few altitudes.

Theoretical investigation of the interaction of neutral and ionised atmospheres has been carried out, and neutral winds and ionisation drifts in the F-region have been derived, utilising measured electron density profiles and model atmospheric parameters. The importance of various processes in maintaining the night-time ionisation has been assessed. The results of this investigation are also presented.

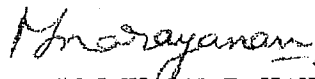
In Chapter I, the author has reviewed the existing knowledge in his field of study. In Chapter II, the observational results of night-time upper atmospheric winds, measured for the first time over Thumba, and results of twilight winds are presented. A general pattern of atmospheric circulation derived from vapour cloud releases in the 100 to 200 km altitude region is also presented in this Chapter. In Chapter III the atmospheric structure measurements, made from



diffusion of vapour releases, are presented and discussed. In Chapter IV, the author has discussed in detail the interaction of neutral and ionised atmospheres. The problem of night-time F-region has been treated, with particular reference to its maintenance by neutral winds. The summary and conclusions of the above study are presented in Chapter V, identifying also areas for future work in this subject. Finally, a list of original papers published in different parts of the world, to which references have been made by the author in the presentation, has been included at the end.



(PRAFUL D. BHAVSAR)



(M. SOUMYA NARAYANAN)

### ACKNOWLEDGEMENTS

The author wishes to express his deep gratitude and indebtedness to Professor P. D. Bhavsar and Dr. J. N. Desai for their invaluable guidance, advice and encouragement in the execution of this study and in the preparation of the thesis.

The author wishes to record his gratitude to Mr. A. N. Ramanathan for his valuable suggestions at all stages during the preparation of this dissertation. The author is also thankful to Professor R. Raghava Rao for many helpful discussions and encouragement during the course of this work. The fruitful discussions with Dr. C. A. Reddy are gratefully acknowledged. Thanks are also expressed to Professor P. R. Pisharoty, Professor R. P. Kane and Professor Satya Prakash for their encouragement and advice.

The helpful suggestions provided by Dr. K. Ramanuja Rao in the initial stages of this work, as well as the many helpful discussions with Dr. M. R. Deshpande, Dr. V. Ramachandra Rao, Dr. B. H. Subbaraya, Dr. Harish Chandra and Mr. M. R. Sivaraman are gratefully acknowledged. Sincere thanks are also expressed to all of the members of the erstwhile Vapour Cloud Project of the Physical Research Laboratory, especially Messrs H. Chakraborti, V. J. Parikh, P. S. Panchal,

T. N. Rajaraman, B. H. Dave and H. I. Pandya, for their enthusiastic and unstinted cooperation.

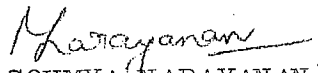
Valuable help in the numerical analysis was provided by Dr. (Mrs.) S. Raghava Rao, Dr. K. S. Rao and Dr. D. R. Kulkarni. Assistance in computer programming was rendered by Dr. D. R. Kulkarni, Mr. P. S. Shah and Mr. H.B. Shah. Computational and other general assistance was rendered by Mr. H. I. Pandya. To all of them, the author is deeply indebted. The computing centre, and the drawing and photographic sections, of PRL are also thanked for their cooperation and help.

Mr. V. C. Mathew was responsible for the neat typing of this dissertation. Mr. P. Gopinathan did the painstaking job of typing the initial draft. Mr. V. H. Kulkarni took the trouble of going through the entire typed thesis and removing typographical and other blemishes. To all of them too, the author expresses his sincere thanks.

The author expresses his gratitude to the Director, TERLS and his staff who carried out the rocket launchings for the experiment and rendered other help, including the making of TMA payloads. The author also expresses his gratitude to the authorities of the Max Planck Institute,

West Germany, for their permission to use the photographs of the neutral clouds for the present study. Thanks are also expressed to the Principal, St. Xaviers College, Palayamcottai and the Governments of Kerala and Tamil Nadu for according their permission and providing facilities for the establishment of necessary Camera Stations for the work.

Finally, the author acknowledges the financial support given to this study by the Department of Atomic Energy and Department of Space, Government of India.

  
(M. SOUMYA NARAYANAN)

## CONTENTS

	Certificate	i
	Statement	ii
	Acknowledgements	v
	Contents	viii
Chapter I	Introduction	1
Chapter II	Winds in the Neutral Upper Atmosphere	75
Chapter III	Atmospheric Structure from Diffusion of Rocket Released Vapour Clouds	148
Chapter IV	Neutral Upper Atmospheric Winds and Mid-latitude Night-time Ionosphere	200
Chapter V	Summary and Conclusions	271
	Appendix	A-1
	References	R-1

CHAPTER I	<u>Introduction</u>	1
1.1	The Upper Atmosphere	2
1.2	Structure of the Upper Atmosphere	7
1.2.1	Temperature	10
1.2.2	Density	16
1.2.3	Composition	19
1.3	Time Variation of Upper Atmospheric Parameters	23
1.3.1	Diurnal Variation	23
1.3.2	27-day Variation	26
1.3.3	Semi-annual Variation	27
1.3.4	Variation Associated with Geomagnetic Activity	28
1.3.5	Seasonal-latitudinal Variation	29
1.3.6	Summary of the Atmospheric Variations	29
1.4	Model Atmospheres	30
1.5	Energy Inputs in the Upper Atmosphere	35
1.5.1	Insolation of Solar Radiation	37
1.5.2	Dynamical Energy Sources	39
1.5.3	Joule Heating	43
1.5.4	Auroral Electrojet, Particle Precipitation etc.	43
1.6	Motions in the Upper Atmosphere	45
1.6.1	Measurement of Upper Atmospheric Movements	46
1.6.2	Ground-based Methods	47
	a) Visual Meteor Method	47
	b) Radio Meteor Method	48

c) Noctilucent Cloud Method	49
d) Airglow Method	49
e) Satellite Drag Method	50
1.6.3 Vehicle-borne Methods	50
a) Pilot Tube Method	50
b) Rocket Grenade Method	51
1.6.4 Chemical Release Method	51
1.6.5 Methods for Determining Plasma Motions in the Ionosphere	55
a) Spaced Receiver Method	56
b) High-frequency Doppler and Phasepath Methods	56
c) Incoherent Scatter Method	57
1.7 Observational Results of Winds in the Upper Atmosphere	57
1.7.1 Periodic Components and Waves	59
1.7.2 Irregular Winds	62
1.7.3 Vertical Winds	64
1.7.4 Observations During Storms and Disturbances	64
1.8 Interaction of Neutral and Ionised Atmospheres	66
1.8.1 Sporadic E	67
1.8.2 Ionospheric Dynamo Currents	69
1.8.3 F-region Plasma Motions	71
1.9 Scope of the Present Thesis	71
CHAPTER II <u>Winds in the Neutral Upper Atmosphere</u>	75
2.1 Experimental Details	76
2.1.1 Ground Equipment and Observation Sites	76
2.1.2 Data Reduction	79

2.2	Error in Cloud Positions	84
2.2.1	Systematic Errors	84
	a) Earth's Curvature	84
	b) Refraction through the Glass Plate	84
	c) Film-shrinkage, Photographic-paper Expansion, Contraction etc.	85
	d) Camera Tilt	85
	e) Atmospheric Refraction	85
	f) Distortion of the Camera Lens	86
2.2.2	Accidental Errors	86
	a) Camera Station Coordinates	86
	b) Trail and Camera Station Orientation	88
	c) Centering and Reading Errors	89
2.2.3	Errors in Wind Velocities	90
2.3	Results and Discussions	91
2.3.1	Chronology of the Experiments	91
2.3.2	Earlier results near the Equator from Studies conducted at Thumba	94
2.3.3	Night-time Neutral Atmospheric Winds over Thumba	95
	a) Meridional Winds	96
	b) Zonal Winds	98
	c) Speed Profiles	100
	d) Rotation of Wind Vectors	102
2.3.4	Results obtained from Ba-Sr Releases at Twilight from Thumba	104
	a) Meridional Component of Winds	104
	b) Zonal Component of Winds	107
	c) Wind speed at Different Altitudes	108
2.3.5	Propagating Waves	108
2.3.6	Turbulence	112



2.3.7	Interaction of Neutral and Ionised Atmospheres	116
2.4	General Circulation in the Upper Atmosphere	120
2.4.1	The Data and Grouping of Stations	123
2.4.2	The Average Flow Above 100 km	125
2.4.3	Super Rotation of the Upper Atmosphere	130
2.4.4	Comparison with Global Pressure Models	134
2.5	Asymmetry in Equatorial Anomaly	143
CHAPTER III	<u>Atmospheric Structure from Diffusion of Rocket-released Vapour Clouds</u>	148
3.1	Diffusion Equation ✓	149
3.2	Radiance of the Cloud ✓	153
3.3	Film Calibration	155
3.4	Measurement of Cloud Densities	157
3.5	Determination of Diffusion Coefficients ✓	163
3.5.1	Effective Radius Method	163
3.5.2	Correction for the Sky Background Brightness	165
	a) When $\xi_b$ Corresponds to the Linear Region	165
	b) When $\xi_b$ Corresponds to the Toe Region	166
3.5.3	Other Methods	168
	a) Maximum Radius Method	168
	b) Gradient ( $\ln B$ ) Method	169
	c) Central Intensity Method	170
	d) Measurements of Faint and Irregular Features	171
3.6	Sources of Error in the Measurement of $r_e$ and D	172

3.6.1	Film Effects	172
3.6.2	Instrumental Errors	173
3.6.3	Non-central Scanning	173
3.6.4	Uncertainty in the Range of the Cloud	174
3.6.5	Atmospheric Effects	175
	a) Turbulence ✓	175
	b) Wind Shear	176
	c) Finite Exposure and Wind Velocity	177
3.6.6	Probable Errors	180
3.7	Diffusion Coefficient Results ✓	181
3.8	Atmospheric Structure from Measured Diffusion Coefficients	183
3.9	Derived Temperature Results	189
3.9.1	Accuracy in Temperatures	193
3.10	Anomalous Temperature Profile Below 150 km	194
3.10.1	Additional Diffusion	194
3.10.2	O/O <sub>2</sub> Ratio	195
3.10.3	Wave Propagation	196
3.10.4	Departures from Barometric Law	198
3.10.5	Desirability of Further Experiments	198
CHAPTER IV	<u>Neutral Upper Atmospheric Winds and Mid-latitude Night-time Ionosphere</u>	200
4.1	Theoretical study of the Ionosphere	200
4.2	Physical Theory of the F-region	203
4.2.1	Production (q)	203
4.2.2	Loss (l)	204
4.2.3	Transport Term (div [Nv] )	205
4.2.4	F-region Parameters and their Relationships	205

4.3	The Night-time Ionosphere	207
4.3.1	Change in Recombination Coefficient	208
4.3.2	Sources of Ionisation	210
	a) Ionisation from Conjugate Point	210
	b) Corpuscular Ionisation	210
	c) Plasma Flux from Protonosphere	212
4.4	Mathematical Formulation of the Problem	215
4.4.1	Definitions and Assumptions	216
	a) Coordinate System	216
	b) Horizontal Derivatives	217
	c) Model Atmosphere	218
	d) Transport Velocities	218
4.4.2	The Equations to be Solved	219
	a) Continuity Equation	219
	b) Equations of Motion for the Ions and Electrons	219
	c) Equation of Motion for Neutral Particles	222
4.4.3	The Data and Calculation of Parameters	224
	a) Pressure Gradients	225
	b) Viscosity and Collision Frequency	225
	c) Rate Constants	226
	d) Mean Ionic Mass	227
4.5	Numerical Procedure for the Solution of the coupled Differential Equations	227
4.5.1	The Finite Difference Method	229
4.5.2	Boundary Conditions	231
	a) Boundary Conditions for Neutral Winds	232
	b) Boundary Conditions for Electron Density	233
	c) Initial Values for Neutral Winds and Electron Density	233

4.5.3	Tri-diagonal System	234
4.5.4	Stability and Accuracy of the Numerical Method	236
4.6	Limitations of the Present Calculations	237
4.6.1	Model Atmosphere	237
4.6.2	Non-linear Term	238
4.6.3	Electron Density	240
4.6.4	Temperatures	240
4.6.5	Magnetic Declination	240
4.6.6	Electric Field	240
4.6.7	Coefficients	241
4.6.8	Numerical Method	241
4.7	Plasma Flux from the Protonosphere	242
4.7.1	Vertical Velocities	244
4.7.2	Accuracies	248
4.7.3	Discussion	249
4.8	Neutral Winds and Electric Field Drifts	251
4.8.1	Results of Neutral Wind Velocities	254
4.9	Explanation of Observed $h_m$ and $N_m$ in Terms of Neutral Winds and Protonospheric Flux	261
4.10	Effects of Different Parameters in Night-time F-region	265
CHAPTER V	Summary and Conclusions	271
5.1	Important Conclusions	272
5.1.1	Results of Night-time Wind Measurements over Thumba	273
5.1.2	Results of Twilight Winds determined from the motion of Ba-Sr Neutral clouds over Thumba	274
5.1.3	General Circulation in the Upper Atmosphere	276

5.1.4	Atmospheric Structure from the Study of Growth Rate of Artificial Vapour Releases	278
5.1.5	Winds at F-region Heights and interaction of Neutral and Ionised Atmospheres	278
5.1.6	Effect of Various Atmospheric Parameters on night-time Ionisation	280
5.2	General Conclusions and Areas for Future Work	281
Appendix-I	Sources of Wind Data from Vapour Releases	A-1
Appendix-II	Mean Winds above 150 km and Winds at the Highest Altitude of observation above 150 km	A-2
	References	R-1

## CHAPTER I

### INTRODUCTION

UPPER atmospheric dynamics has been a subject of great interest in recent times. Though many indirect ground-based methods of measurements are still used, rocket and satellites are now the main sources of providing precise data by means of direct in-situ measurements and indirect inferences from injection of tracers in the high reaches of the atmosphere.

The equatorial upper atmosphere, including the ionosphere and the equatorial electrojet, is as yet insufficiently understood. An extensive programme of study, by a group of scientists at the Physical Research Laboratory (PRL), Ahmedabad, is in progress for this purpose. The programme at PRL includes the study of atmospheric parameters, like neutral temperature, winds, turbulence, electron density, electron temperature, ion and neutral compositions, electric field and drifts of the inhomogeneities in the E- and F-regions of the ionosphere. Release of chemical vapour clouds in the upper atmosphere is a part of this programme, with a view to understand the neutral atmospheric structure and dynamics and its interaction with the ionosphere.

In the first chapter, the author has reviewed the present-day knowledge about the upper atmosphere above 90 km.

Section 1.1 briefly describes the upper atmosphere. In Section 1.2 the available information regarding the temperature, composition and ~~gas~~ density of the upper atmosphere is reviewed. Sections 1.3, 1.4 and 1.5 deal with the time variations of the upper atmospheric parameters, the model atmosphere and the sources of energy inputs in the upper atmosphere respectively. Section 1.6 describes in detail different types of motions in the upper atmosphere and the techniques used for their study. In Section 1.7, the existing observational results of motions in the upper atmosphere are summarised. After describing in Section 1.8 the interaction between the neutral and ionised components of the upper atmosphere, the author deals in Section 1.9 with the purpose of the present study.

## 1.1 THE UPPER ATMOSPHERE

Based on the physical and dynamical properties at various altitudes, the earth's atmosphere has been classified into distinct regions. The nomenclature normally used by the scientific community to designate these regions, which are layers with definite properties, is the direct outcome of the study of the temperature profile of the atmosphere. The atmosphere below about 90 km is in a thoroughly mixed state and the global weather is almost entirely dependent on the physical processes taking place in this region. Thus, the atmosphere below

90 km is the main source of information for the meteorologists for their global weather studies. Detailed discussions and reviews of methods, results and the progress of knowledge of this region of the atmosphere in recent years have been reported by CRAIG (1965), FEDELE (1968), FEDELE AND ZANCLA (1968) and GROVES (1971).

In FIG 1.1 a comprehensive picture of the upper atmosphere is shown. The important atmospheric phenomena, which are responsible for the distinct properties of the upper atmosphere above 90 km, are also indicated in detail in this diagram. This region above 90 km known as the 'Thermosphere', is the subject of interest in the present study.

In the thermosphere the temperature increases rapidly with altitude and attains an asymptotic value of the order of  $1000^{\circ}$  K. This asymptotic value is highly variable with time. It depends on the level of solar activity since sun is the main source of energy input in this region of the atmosphere. The extreme ultra-violet radiation, with wavelengths shorter than  $1000 \text{ \AA}$  is absorbed by the atomic oxygen at heights of about 200 km. The thermal conductivity being high in this region, the heat generated is removed in a short time by downward conduction to about 100 km altitude, where collisions are sufficiently frequent to allow infra-red emissions to remove the heat. This





is the reason for the substantial increase in temperature between 100 and 200 km. The high conductivity is also responsible for the maintenance of the upper atmosphere in an isothermal condition. At greater heights the thermosphere merges with the region called the 'Exosphere' where, because of the small number density of the gas atoms and molecules, the collisions are infrequent. The neutral air particles in this region move in ballistic orbits in the gravitational field; while the ionised particles in this region are mainly constrained by the geomagnetic and the electric fields.

The atmospheric constituents get ionised by the interaction with solar ultra-violet radiation by amounts, varying with altitude. The region of these ionised gases, which extends from an altitude of about 60 km to the outer regions of earth's atmosphere, is termed the 'Ionosphere'. The ionosphere was first alluded as a possibility by Gauss in 1841, and was later postulated by Balfour Stewart in 1883, in order to explain some of the observed variations in the geomagnetic field. The presence of these electrically conducting layers was first experimentally established, by Kennelly and Heaviside independently, in 1902 by the long-range propagation of radio waves expounded by Marconi an year earlier. The radio soundings to estimate the ionisation density with altitude have revealed that there are three main regions of ionisation - the D-region

(60 to 90 km), the E-region (100 to 150 km) and the F-region (beyond 150 km). The F-region is composed of two layers F1 and F2, which merge into one during the night time.

The various regions of the atmosphere can also be designated according to the distribution of the constituent gas species. For example, the region rich in ozone (extending from ground to about 80 km) is known as 'Ozonosphere'. The 'Homosphere' is the region where atmospheric constituents are well mixed because of large-scale convective and turbulent motions and, thus, in this region the composition remains constant with altitude. The 'Heterosphere' (beyond about 100 km altitude) is the region just above the homosphere where photo-chemical reactions and diffusive separation combine to change the relative composition with altitude. The 'Turbopause' (located approximately at 100 km altitude) is the sharp layer dividing the homosphere and the heterosphere. The outer-most portion of the atmosphere, which is almost fully ionised and where hydrogen ions predominate, is called the 'Protonosphere'. The region just below this, where laws derived from equations of state and hydrostatics appear to have limited application and the dominant species is neutral hydrogen, is sometimes called the 'Metasphere'. The metasphere and protonosphere together are also known as 'Geocorona'. The 'Magnetosphere' is the region

in which the earth's magnetic field controls the dynamics of the atmosphere. This includes the whole atmosphere above about 1500 km, where ionised constituents become predominant over neutral constituents.

From the foregoing, it can be seen that the region of the atmosphere above 90 km may be referred to as Thermosphere, when discussing the temperature structure, Chemosphere when discussing the composition and Ionosphere when discussing the ionisation. It is this region, above 90 km, which will be referred to as the Upper Atmosphere in the discussions to follow.

## 1.2 STRUCTURE OF THE UPPER ATMOSPHERE

Before the advent of rockets and satellites, the atmospheric structure at altitudes below 30 km used to be studied by instrumented payloads on balloons, and beyond these heights by the anomalous propagation of sound, which provided the first evidence of ~~pos~~itive temperature gradients in the middle atmosphere. With the availability of rockets, the grenade-explosion and falling-sphere techniques have been used for studying the atmosphere upto 100 km (CRAIG, 1965).

Q-switched giant pulsed lasers have now provided a new powerful technique for probing the earth's atmosphere upto 100 km. Range of application of this 'Lidar' technique has

been discussed in detail by COLLIS (1969). Ruby and Neodymium Glass lasers, with pulse-widths of the order of 10 n sec, and pulse power of the order of 10 joules pulse<sup>-1</sup> have been used to measure atmospheric densities upto 100 km by receiving the Rayleigh-scattered photons due to air molecules. Such measurements have been useful for the study of atmospheric tides as well (KENT ET AL., 1972). Presence of dust layers can be detected and studied even for higher altitudes (upto 140 km) by receiving the Mie-scattered photons from the particulate matter.

Minor constituents can be detected and studied making use of fluorescence and resonance scattering of laser beams tuned to appropriate wavelengths. Such tunable-dye lasers, with Rhodamine G dye excited by flash lamp, have been successfully used to study night-time structure of natural sodium layer at 90 km (HAKE ET AL., 1972).

FIG 1.2 illustrates the various methods applicable in different altitude regions for exploring the atmospheric structure and the dynamics (Section 1.6). These methods, as used for temperature, density and composition measurements, and the results obtained hitherto are reviewed in the following sub-sections.

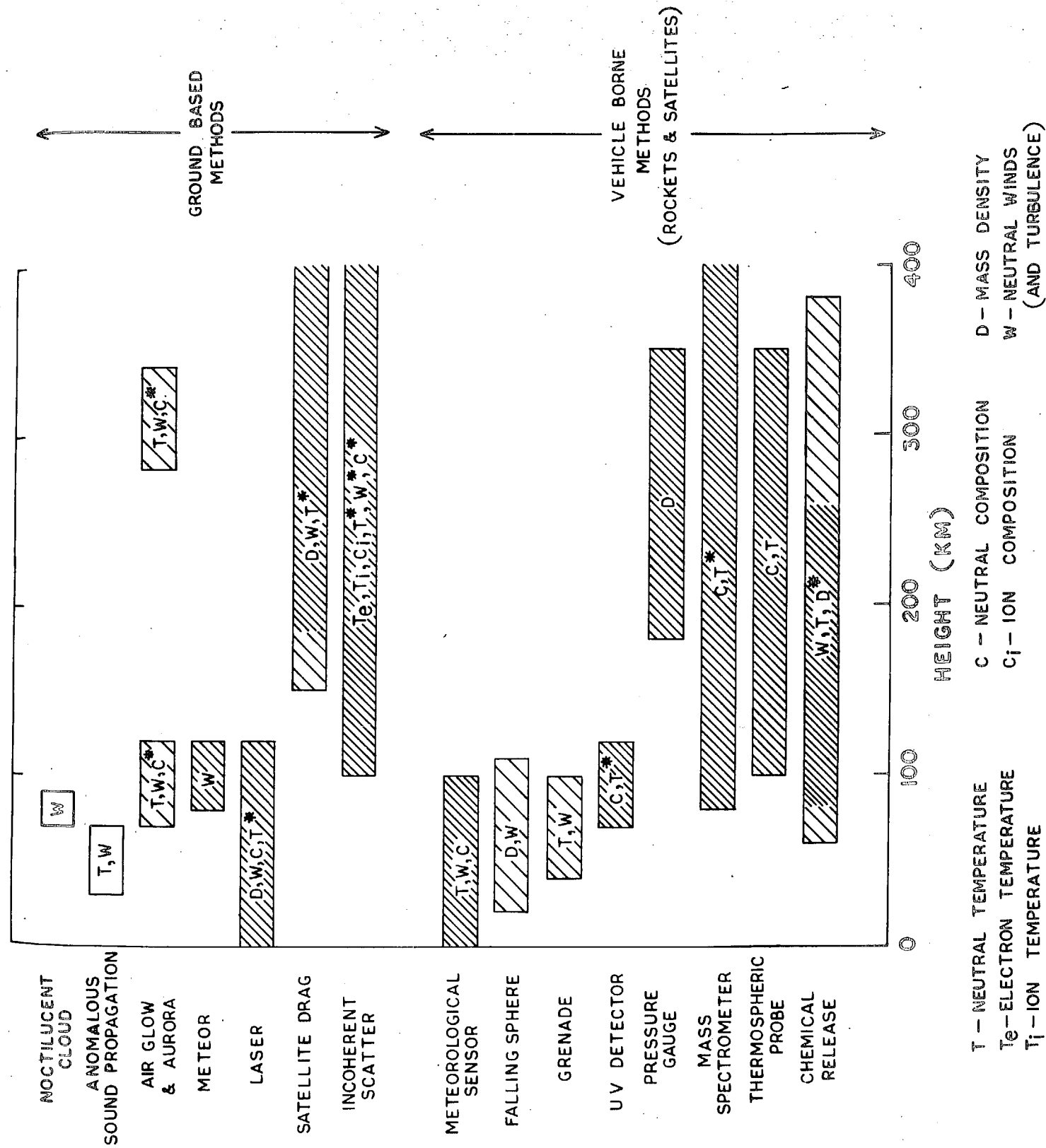


FIG 1-2 EXPERIMENTAL TECHNIQUES FOR THE STUDY OF UPPER ATMOSPHERE STRUCTURE AND DYNAMICS

### 1.2.1 Temperature

Ground-based observations of Doppler line width of 5890 Å and 5896 Å sodium D lines (KASTLER AND BRICARD, 1944), 6300 Å and 5577 Å atomic oxygen emissions by Fabry Perot interferometer technique (KARANDIKAR, 1968; ROBLE ET AL., 1968; HAYS ET AL., 1969, 1970; COGGER ET AL., 1970; FEIBELMAN ET AL., 1972), and rotational band spectra of OH bands from airglow (SHEFOV, 1971) have been made for deducing upper atmospheric temperatures on a regular basis. HUNTEN ET AL. (1963) have reported auroral zone atmospheric temperatures from  $N_2^+$  band spectra.

In these airglow techniques, the measurements are made mostly during night and twilight hours, but dayglow measurements have also been reported by several workers. A brief review of these measurements has been given by SHEPHERD (1969). The various techniques, that have been employed, have been reviewed by JARRETT AND HOEY (1965). Recently HILLARD AND SHEPHERD (1966 A,B) have expanded the scope of atmospheric Doppler temperature measurements by the introduction of Wide Angle Michelson Interferometer (WAMI). Using this technique, ZWICK AND SHEPHERD (1973), by observing 5577 Å and 6300 Å emissions, have estimated auroral electron fluxes and energy spectra, besides vertical temperature profiles, and diurnal variations of exospheric temperatures.

The main disadvantage of the airglow methods is that it is difficult to obtain good altitude resolution and extremely difficult to make accurate temperature measurements during day time. The altitude estimates are particularly important for lower thermospheric measurements where temperature gradients are large.

BLAMONT ET AL. (1962) made a direct determination of temperature at 370 km altitude by releasing a cloud of sodium vapour and measuring the Doppler line-width. They estimated the temperature to be  $1450 \pm 75^{\circ}$  K. Subsequently, quite a number of measurements, using this technique, have been made (LORY, 1965; POLOSKOV ET AL., 1970). Temperature determinations in the upper atmosphere have also been made from the release of various other fluorescent chemicals. AUTHIER (1964), HARANG (1964), REES (1968, 1971 A), GOLOMB ET AL. (1967, 1968), REES ET AL. (1972 A) and LLOYD ET AL. (1972) have each described observations of temperature measurements from the rotational-vibrational spectra of aluminium oxide glow-clouds. The molecular structure of barium oxide has also been used for temperature determination (HARANG AND STOFFREGEN, 1969; REES, 1971 A; GILBERT AND REES, 1971). HARANG (1969) has given a summary of the spectroscopic observations made on vapour releases. LLOYD AND SHEPHERD (1966), and DESAI AND NARAYANAN (1970) have inferred upper atmospheric temperatures from measured diffusion



coefficients of artificial vapour releases. In the vapour cloud technique of temperature measurements, there are a few assumptions involved and the height estimates are also very good. However, stringent visibility conditions, and prohibitive cost are the disadvantageous factors.

Based on 50 direct temperature measurements using the vapour cloud technique, REES (1971 B) has presented, for geomagnetically quiet conditions, a global temperature distribution for altitudes between 150 and 190 km (FIG 1.3). Reviewing the various measurements made by different techniques, he has also pointed out a greater decrease of temperature towards the polar regions than what the model atmospheres have indicated. IVANOVA ET AL. (1969) had also pointed out, in a review of earlier temperature data from several different techniques and at high latitude, that in the altitude region/<sup>of</sup>70-150 km temperatures over Heiss Island ( $81^{\circ}$  N) were lower than those of the appropriate atmospheric models.

In-situ measurements, of the density and temperature of molecular nitrogen, from altitudes of about 140 to 300 km, have been made employing a series of thermosphere probe launchings. The probe consists of an omegatron mass spectrometer (fixed tuned to  $N_2$ ) and an optical aspect instrument. These measurements rely on the interpretation of the vertical gradient of the neutral species to derive temperature. SPENCER



ET AL. (1970) have reviewed in detail these probe measurements. SPENCER AND CARIGNAN (1972) report thermospheric molecular nitrogen temperature variations made on San Marco III satellite in the altitude range 210 to 300 km over the equator. O' NEIL (1972) has reported  $N_2$  vibrational temperatures and  $N_2$  and  $O_2$  molecular density measurements by rocket-borne electron beam induced luminescence between 100 and 150 km altitude.

Temperature measurements made by BLAMONT AND LUTON (1972) from OGO-6, provide the most interesting direct observations to date. A spherical Fabry-Perot Interferometer gives the doppler width of dayglow 6300 Å atomic oxygen line at altitudes between 200 and 350 km. Temperatures, deduced to an accuracy of  $\pm 50^\circ$  K, have been studied as a function of local time, latitude, and solar flux.

Neutral thermospheric temperatures have also been derived from density scale height measurements made on Explorer 32 with density gauges (NEWTON AND PELZ, 1973). Using the densities derived from the measurements of satellite drag (Section 1.2.2), temperatures have been inferred (ROEMER, 1971) and these form the basis of the present day model atmospheres (JACCHIA, 1971). But it is emphasised that this method, essentially is for density determinations.

One of the most powerful ground-based methods of studying thermospheric properties is by incoherent radar scatter observations. This method is currently in use only at three locations, viz., Jicamarca ( $12^{\circ}$  S), Puerto Rico ( $19^{\circ}$  N) and St Nancy ( $45^{\circ}$  N). A detailed study of the technique, important results obtained and limitations of this method have been presented by EVANS (1962) and WALDTEUFEL ET AL. (1971). The power spectra of the back-scattered echoes can be interpreted in terms of electron and ion temperatures. The properties of the neutral atmosphere are deduced, using a non-linear profile of the exospheric temperature, the shape factor in the temperature profile and the atomic oxygen density at a reference altitude in the diffusive equilibrium region. The incoherent scatter measurements brought out for the first time that the observed temperature maximum is not in phase with that derived from satellite drag method (NISBET, 1967; CARRU ET AL., 1967).

WALDTEUFEL (1971) has compared the temperature results from incoherent scatter measurements, rocket probe measurements and satellite drag measurements and concludes that all these results are converging. CHAMPION (1970) and REES (1971 A) have shown that during the geomagnetic storm of November 1968 temperatures derived by satellite drag method, chemical release technique and from  $6300\text{\AA}$ (OI) emission line showed good agreement with one another.

There is, however, a need for exploring the region between 100 and 200 km, which is essentially the extrapolation region for the present model atmospheres, for which the chemical release method and probe measurements are the only answer. There is also the need to establish more incoherent scatter facilities to have a coherent global picture. The airglow methods would be a much cheaper long term thermospheric temperature monitors and would also serve as useful tools for studying latitudinal variations.

### 1.2.2 Density

The equilibrium density distribution in the atmosphere is governed, to a high degree of accuracy, by hydrostatic equation. Density determinations in the thermosphere have, mainly, been made by means of satellite drag measurements. A body of effective cross-section,  $A$ , moving with a velocity,  $V$ , through a gas of density,  $\rho$ , experiences an aero-dynamic drag,  $D$ , given by

$$D = - \frac{1}{2} C_D A \rho V^2$$

where  $C_D$  is the drag coefficient. Knowing the satellite velocity, density is obtained by observing the change in the orbital inclination of the satellite from the ground. The methods and results of these determinations have been discussed by JACCHIA (1963), KING-HELE (1966), PRIESTER ET AL. (1967), and

ROEMER (1971). Accuracies of the order of 10% have been claimed. However, lack of time (about few hours) and spatial ( $30^{\circ}$  latitude zone) resolutions are the chief drawbacks of this method. Besides, satellites with proper geometry, for drag measurements, have only recently been incorporated (DEVRIES, 1971). This technique is not quite applicable in exosphere above about 800 km.

In addition to drag measurements, detailed information on atmospheric density has been obtained in-situ by accelerometers (BROGLIO, 1965; CHAMPION, 1969, 1971; BRUCE, 1971) and by pressure gauges (NEWTON ET AL., 1965; CARTER ET AL., 1969; NEWTON, 1970; ANDERSON AND SHARP, 1971). Pressure gauges in rockets and satellites need calibration, which is different especially for the low pressures encountered by a satellite orbit.

From Molniya 1-F satellite observations, BRIERLEY (1970) has reported two density values at record low altitudes of about 120 km. Following the behaviour of Molniya 1-K which revealed very high and variable air densities near 18 hr L.T., four subsequent Molniya satellites were examined (ALLAN, 1972), which too showed, though to a much less extent, high densities near 18 hr L.T. Profiles of total gas density obtained in the region of 130 - 200 km from orbital drag data, accelerometer measurements and pressure gauge readings of the satellites, Cannon Ball and ATS-2, have been presented by KING-HELE AND WALKER (1969, 1970). CHAMPION ET AL. (1972) and CHAMPION AND MARCOS (1972) have

derived atmospheric densities in the height range of 140 - 800 km from orbital drag and accelerometer measurements on Cannon Ball II and Musket Ball polar satellites. The San Marco III satellite has gathered a large amount of density and composition data on the equatorial neutral atmosphere down to 130 km (BROGLIO, 1972).

Comparison of atmospheric densities, obtained from satellite drag data, gauge measurements and accelerometer results, at satellite altitudes now indicates near agreement, within error limits of  $\pm 20\%$ , of these different techniques (KEATING, 1971). The discrepancies, that were initially there, have since been resolved by taking into account calibration and normalisation (NEWTON, 1969).

Upper-air density has also been derived from the simultaneous measurements of the molecular diffusion coefficient and temperature of chemical cloud, released by rocket. (GOLOMBET AL., 1967, 1968; REES ET AL., 1972; LLOYD ET AL., 1972), assuming ambient molecular weight and collision cross-section of the contaminant-ambient particles. From such measurements over high latitudes, REES (1971 B) has shown that at the equinox, the air density may decrease by about 10% from the equator to  $70^\circ$  latitude, while near the winter-polar cap, a density decrease of the order of 30% may occur. From another such estimate of density from Aladdin II experiment at Eglin, REES ET AL. (1973 B) report that air density at morning twilight was about 50% higher than that during evening twilight between 130 and 160 km.

### 1.2.3 Composition

Composition measurements have primarily been obtained through a variety of mass-spectrometer techniques. As opposed to ambient ionic measurements (NARCISI, 1971), neutral atmospheric constituents are first ionised by an ion source (usually an electron beam with an energy of tens of volts), and the ions from the gaseous mixture, as a function of their charge to mass ratio, are measured in an analyser. The first important mass spectrometer measurements were made by SCHAEFER (1963), POKHUNKOV (1963), NIER ET AL. (1964) etc.

BALSIGER ET AL. (1971) have developed a mass-spectrometer for simultaneous measurement of neutral and ion composition of the upper atmosphere and report two measurements in the altitude range 110 to 220 km over Kiruna. Other important measurements have been reported by SCHAEFER (1969) and SCIALOM (1971). NEWTON ET AL. (1972) report  $O_2$ ,  $N_2$ , He and O measurements on San Marco III satellite over equatorial atmosphere. HEDIN AND MAYR (1972) have constructed a global empirical model for quiet conditions to describe longitudinally averaged OGO-6,  $N_2$  and O densities in the altitude range of 400 to 600 km by spherical harmonic expansions.

Measurements by mass-spectrometer are plagued by vehicle contaminants as well as uncertainties in the effective flight dynamics on gas sampling. Measurement of atomic oxygen concen-



tration has an added problem connected with recombination at the walls of the ion source. It has only recently been possible to make some improvements (BITTERBERG ET AL., 1970; OFFERMAN AND VON ZAHN, 1971). A new mass spectrometer, capable of measuring composition by energy analysis of the sample at vehicle velocity, has been reported by PHILBRICK ET AL. (1972, A).

Measurement of the absorption of solar extreme-ultra-violet radiation at discrete wavelength intervals has been used to determine the number densities of O, O<sub>2</sub> and N<sub>2</sub> (HINTEREGGER 1962; HINTEREGGER AND HALL, 1969; HALL, 1972; SUBBARAYA ET AL., 1972). The molecular oxygen number density distribution in the 100-200 km region has been determined by solar occultation measurements made on Solarad 8 satellite (ROBLE AND NORTON, 1972) and by occultation of stellar ultra-violet light ( $\lambda \sim 1500 \text{ \AA}$ ) monitored on OAO-2 satellite (HAYS AND ROBLE, 1973). The main difficulty in these type of measurements is our insufficient knowledge of some of the important absorption cross sections. These techniques are applicable only to a limited altitude range.

Atomic oxygen profiles have also been measured from the airglow resulting from nitric oxide releases (GOOD AND GOLOMB, 1972). In addition to obtaining density from satellite drag measurements, composition has also been estimated from the vertical distribution of density (JACCHIA AND SLOWEY, 1968).

From the optical and radio observations on meteors entering the earth's atmosphere, densities have been derived, though with uncertainties.

Molecular nitrogen densities in the 90-120 km region, from the shape of the incoherent scatter spectrum (WALDTEUFEL, 1970) and atomic oxygen profiles in the 250-400 km region, where it is the dominant constituent, have been deduced from observations of temperatures and electron densities (BAUER ET AL., 1970; MAHAJAN, 1971).

The study of the ratio,  $O/O_2$ , between the atomic oxygen and molecular oxygen has been one of the most interesting aspects in the composition measurements. Molecular oxygen dissociates at a level of about 90 to 100 km. The  $O/O_2$  ratio increases rapidly upwards reaching a value of about 2 at 115 km and about 10 at 150 km. The various measurements of oxygen by mass spectrometers have shown a varied behaviour of this ratio, ranging from 0.5 to 4, at 120 km. The accurate knowledge of this ratio is essential for developing a model atmosphere. Discrepancies of different measurements have been attributed to instrumentation and calibration difficulties (VON ZAHN, 1967; GIRAUD ET AL., 1972).

There have also been discrepancies in the results of measurements from satellite drag, mass spectrometer observations and extreme ultra-violet absorption techniques. VON ZAHN (1970) has made a comprehensive review of density and composition near 150 km, where he has compared the measurements from various

sources and techniques. He points out that if one assumed that the drag results were high by 10% and those of mass spectrometric measurements of atomic oxygen were low by a factor of 3 to 5 or even more, agreements in these measurements could be obtained. NIER (1971) has re-examined the situation and points out that the relative mass-spectrometer values of atomic oxygen are correct and should not be increased, and instead, proposes that the total density measured by mass-spectrometer be increased by an empirical factor (1.25 to 2.5) to match the satellite drag densities to account for the discrepancies. TAEUSCH AND CARIGNAN (1972) conclude, from an analysis of the composition measurement on OGO-6 for a period of more than one year, that the VON ZAHN (1970) recommendation for the 150 km composition makes the  $O/N_2$  ratio too high at 150 km. More recently, MOE (1973) has made another review on density and composition in the 80-200 km region, emphasising particularly on the results derived from satellite drag observations.

More accurate measurements of the various constituents and from different techniques, as in the Alladin I and II experiments (PHILBRICK ET AL., 1972 B, 73) and an intensive study of the oxygen transport problem (KING, 1964; JOHNSON, 1964; JOHNSON AND GOTTLEIB, 1973) would be necessary for a reasonably firm assessment of the  $O/O_2$  ratio.

Amongst the minor constituent measurements, new results are found from the Illinois Aeronomy Report (SECHRIST AND GELLER, 1972).

### 1.3 TIME VARIATION OF UPPER ATMOSPHERIC PARAMETERS

From studies of the data accumulated from various sources, the following variations in upper atmospheric parameters have been recognised:

#### 1.3.1 Diurnal Variation

The satellite drag and other in-situ measurements show a diurnal variation in density with a maximum around 1400 hr L.T. and minimum around 0400 hr L.T. Model calculations, taking into account only the solar extreme-ultra-violet radiation as input, have shown that the temperature and density maxima are to be expected at 1700 hr L.T. HARRIS AND PRIESTER (1962 A) explained this discrepancy between the observations and theory as due to a second heat source shifted in phase. This hypothesis, however, finds no observational evidence. The incoherent scatter observations show the diurnal temperature maximum at 1600 hr L.T. at low latitudes in all seasons (MCCLURE, 1969; MAHAJAN, 1969; WALDTEUFEL AND COGGER, 1971) and at 1430 hr L.T. in winter and 1900 hr L.T. in summer at mid-latitudes (WALDTEUFEL, 1970). This indicates that diurnal variation is strongly controlled by the length of the day. The incoherent scatter results have also

shown a larger diurnal variation amplitude than derived from drag observations. The phase-lag of 2 to 3 hours between density and temperature maxima from these two techniques, which has come to be known as the 'Diurnal Phase Anomaly', has been investigated on the basis of dynamical models (RISHBETH, 1969; VOLLAND, 1969, 1970).

RISHBETH (1969) and MOFFETT (1969) have pointed out that the effect of vertical neutral motions calculated by DICKINSON AND GEISLER (1968), and RISHBETH ET AL. (1969) are important in determining the density and temperature of the thermosphere. RISHBETH has suggested that horizontal winds may cause a loss of air during the day time at mid-latitudes, which implies either a variation of the lower boundary conditions in the thermosphere (MOFFETT, 1969; VOLLAND, 1970) or a temperature profile in lower thermosphere that makes density and temperature out of phase at greater heights (MOFFETT, 1969; SWARTZ AND NISBET, 1971; BAILEY AND MOFFETT, 1972). MOFFETT has suggested that both vertical winds and a variation of the lower boundary conditions may be important.

STUBBE (1970), from his detailed study, has concluded that the most likely explanation for the diurnal anomaly is to be found in the diurnal variation of density at the lower boundary. CHANDRA AND STUBBE (1970) have extended this work by varying the temperature and density at the lower boundary.

VOLLAND (1970) has contested the above explanation of CHANDRA AND STUBBE as their results are not consistent with observations above 600 km and that variations of conditions at lower boundary demand a large energy input from below.

VOLLAND (1969) has calculated diurnal variation using a superposition of two gravity waves and two heat conduction waves. Some of the boundary conditions then follow, and there remain some adjustable parameters. For the first harmonic of the diurnal variation, both density and temperature peak around 1400 hr L.T. Later, VOLLAND (1970), however, found poor agreement between his theoretical predictions using the second harmonic and the experimental observations. BAILEY AND MOFFETT (1972) have pointed out the neglect of meridional winds in VOLLAND'S calculations.

MAYR AND VOLLAND (1972), considering a two-dimensional time-dependent model, have shown that the wind induced variations in the diurnal component of atomic oxygen dominate over its temperature-induced variations upto 200 km, and thus concept of diffusive equilibrium for atomic oxygen within the lower thermosphere is strictly not valid. The effect of diurnal wind circulations is to redistribute O, so that the maximum in the diurnal variation of O is shifted by one to two hours away from temperature maximum towards noon, and thus contributing to the phase anomaly above 200 km, where O becomes the major constituent. In a further paper, MAYR AND VOLLAND (1973), developing

a self-consistent two-component diffusion model, have shown that phase delays, between density and temperature, depend strongly on the electron density distribution, as it affects thermospheric circulation.

The effects of vertical motion arising from the convergence or divergence of air produced by horizontal winds, diurnal variation of temperature gradient in the lower thermosphere and other dynamical processes together are expected to provide a final answer to the diurnal phase anomaly.

There are several other aspects of diurnal variation, such as, the position and extent of the diurnal bulge, the latitudinal-diurnal variation (NEWTON, 1970; ALCAYDE ET AL., 1972) and the solar wind effect of the diurnal variation amplitude (JACCHIA, 1970 A), which need further study.

### 1.3.2 27-day Variation

Temperature variation in the upper atmosphere showing a 27-day periodicity, has been described by JACCHIA (1971). He gives the empirical relationship

$$T_c = 379^\circ + 3.24 F_{10.7} + 1.3 (F_{10.7} - \bar{F}_{10.7})$$

where  $T_c$  is the global minimum temperature,  $F_{10.7}$  and  $\bar{F}_{10.7}$  are the 10.7 cm solar radiation flux one day prior and the average flux over several solar rotations respectively. JACCHIA (1970 A)

has found that the ratio,  $r$ , of maximum to minimum exospheric temperature on global scale, varies with the solar cycle and lags behind the variation of the 10.7 cm solar flux by more than a year. The variation of  $r$  is, however, in phase with  $\bar{K}_p$ , the average planetary index over a whole year. The 27-day variation is attributed to a similar variation in solar EUV flux.

### 1.3.3 Semi-annual Variation

This variation in density, first pointed out by PAETZOLD AND ZSCHORNER (1961), is characterised by stable maxima in April and October and minima in January and July. COOK (1969 A) has reviewed all observational results upto 1969 and has advanced explanations for the variations. JACCHIA (1971) has concluded that the variation in density cannot be explained in terms of similar variation in exospheric temperature. A variation in the boundary condition near the turbopause may give rise to this effect (COOK, 1969 B).

FATKULIN (1973) has reported ionospheric evidences for the variability of neutral composition at turbopause levels. From incoherent scatter observations, WALDTEUFEL (1970) has identified seasonal variation of atomic oxygen in the lower thermosphere. From a spherical harmonic analysis of meteor trail observations, MAYR AND VOLLAND (1971) have derived two heat sources for the semi-annual variations - one migrating with the sun and the other presumably related to auroral heating



associated with the magnetic storms. The wind circulation, consistent with these sources, has been shown by them to cause a semi-annual distribution of atomic oxygen. From theoretical calculations, RUSTER AND KING (1973) have suggested that the anomaly observed at mid-latitudes at times of large solar activity can be explained by seasonal variations of composition changes. The changes required by them are in agreement with the results obtained from rocket soundings and incoherent scatter observations.

#### 1.3.4 Variation Associated with Geomagnetic Activity

Direct measurements of neutral atmospheric temperatures during a magnetic storm have shown that temperatures increased by  $80^{\circ}\text{K}$  at low latitudes compared to  $300^{\circ}\text{K}$  at high-latitudes (BLAMONT AND LUTON, 1972). During a geomagnetic storm, abnormal variations in equatorial densities have been reported (CHAMPION, 1971). PRAG (1971) has found that for disturbed conditions the models grossly under-estimate the variability of the real atmosphere, particularly below 200 km. Joule heating (COLE, 1962 A,B) and dissipation of energy by hydromagnetic waves (DESSLER, 1958) have been suggested as causative mechanisms for the atmospheric variations during geomagnetic disturbances.

For the temperature variation in the exosphere during a storm ROEMER (1971) has suggested a latitude-dependent expression of the form

$$\Delta T_{\infty} = (21.4 \sin \varphi + 17.9) \bar{K}_p + 0.03 \exp(\bar{K}_p)$$

where  $\bar{K}_p$  is the 0.4 -day mean of the original planetary index  $K_p$ . REES (1971 A) has reported an altitude-dependent correlation between atmospheric temperature and geomagnetic activity in the 130-170 km region.

### 1.3.5 Seasonal-latitudinal Variation

The seasonal-latitudinal density variation (CHAMPION, 1967; JACCHIA AND SLOWEY, 1968) increases rapidly between 90 and 100 km, with a maximum between 105 to 120 km altitude. Above about 150 km there seems to be no appreciable seasonal-latitudinal variation other than that associated with winter helium bulge (KEATING AND PRIOR, 1968).

### 1.3.6 Summary of the Atmospheric Variations

The available data of neutral component of the thermosphere reveal the following general features:

- i) The diurnal component strongly dominates the daily density variation above 200 km with relative amplitudes upto 0.5. The relative amplitude and phase remain roughly constant with altitude above about 300 km. The semi-diurnal component above 200 km is weak though not negligibly small.

- ii) The meridional structure of the diurnal density variation during equinox follows a simple  $\cos \phi$  relation,  $\phi$  being the latitude.
- iii) The annual variation is relatively weak, the density bulge follows the solar zenith angle. On the other hand, the semi-annual variation is strong in the whole thermosphere, mesosphere and stratosphere.
- iv) The average neutral density and the diurnal density amplitude strongly depend on solar activity, indicating the dominant influence of the solar EUV heat input.
- v) During geomagnetic storms the density increases significantly, suggesting additional heating.

#### 1.4 MODEL ATMOSPHERES

Several models of earth's atmosphere, which present temperature, pressure, density and other properties as a function of time, altitude and latitude, have been constructed in recent years. The semi-empirical model of HARRIS AND PRIESTER (1962 A,B) was the first major attempt, after NICOLET (1961) made a beginning, to put the available observational data in a quantitative form to construct a comprehensive model from 120 to 2000 km altitude for various levels of solar

activity, with fixed boundary conditions at the 120 km level and diffusive equilibrium above. JACCHIA (1965) and COSPAR International Reference Atmosphere-CIRA - (1965) models are only modified versions of the same.

With the accumulation of more data, new models have now been constructed. The low altitude model of CIRA for the 25 to 120 km region has been developed by Groves (1971). The high altitude model, for atmosphere above 90 km, has been developed by JACCHIA (1970 B, 1971). It is primarily based on satellite drag results, and the values have been matched at lower heights with mass-spectrometer and other in-situ measurements. In JACCHIA'S model, considerable changes over the models of CIRA (1965) and United States Standard Atmosphere (USSA) Supplement (1966), have been incorporated, particularly in respect of the fixed lower boundary condition (which has been brought down from 120 km to 90 km) and the  $O/O_2$  ratio at 120 km (which has been considerably increased). Mixing is assumed to prevail to a height of 100 km and diffusive equilibrium thereafter. All the recognised variations connected with temporal, solar, geomagnetic, and latitudinal parameters are represented by empirical relations. However, the maximum of temperature, at 1400 hr, as from this model, and at 1600 hr (or later), as derived from incoherent scatter observations, poses a serious problem for this model. JACCHIA'S model is,

however, only a static diffusion model, and unless dynamical aspects are included there are bound to be discrepancies. JACCHIA maintains that the departures of his model from probe measurements, incoherent scatter results, and mass spectrometer values are not serious.

The mean CIRA has been developed for an altitude range 25 to 500 km by CHAMPION AND SCHWEINFURTH (1971), for mean conditions near  $30^{\circ}$  latitude and for a solar flux of  $145 \times 10^{-22}$  watts  $m^{-2}$   $Hz^{-1}$ , based on the models of GROVES (1971) and JACCHIA (1971). JACCHIA'S model has been modified for polar region by BLUM AND HARRIS (1973).

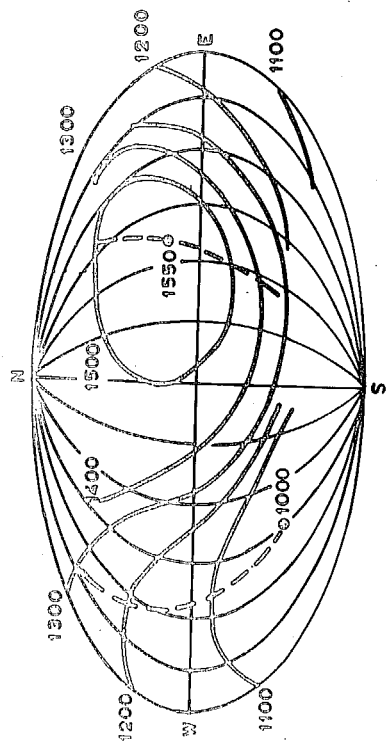
The reliability of the upper atmospheric models are mainly based, as emphasised already, on the turbopause level (assumed constant at 100 km) and the fixed lower boundary conditions. Changes of composition at the base of the thermosphere can have important consequences in several ionospheric phenomena (CHANDRA AND STUBBE, 1970; MAYR AND MAHAJAN, 1971; TAUBENHEIM, 1971; RUSTER AND KING, 1973). The variation of atomic oxygen concentration and the  $O/N_2$  ratio have large influence on the vertical structure of composition in the thermosphere. STUBBE (1972) has shown that because of horizontal transport of air, the  $O/N_2$  ratio in the lower thermosphere is affected, and that there are departures from barometric law.

From the incoherent scatter observations, WALDTEUFEL AND MCCLURE (1969, 1971) and WALDTEUFEL AND COGGAR (1971) have presented global exospheric temperature models. LLOYD ET AL. (1972) have extended WALDTEUFEL AND MCCLURE'S (1969) model to latitudes beyond  $45^{\circ}$ . Two of these incoherent scatter temperature models, as also that of JACCHIA (1971), are shown in FIG 1.4.

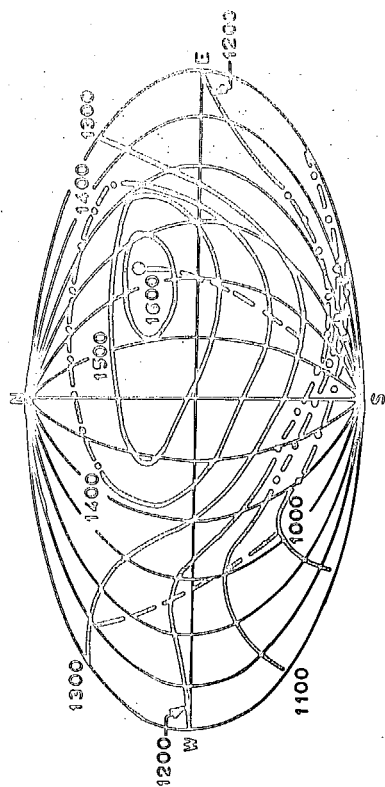
Dynamic diffusion model on theoretical consideration, assuming varying boundary conditions at 120 km, have been proposed by CHANDRA AND STUBBE, (1972). An analytical model, incorporating temperature gradient changes in the region of 125 km, has been proposed by SWARTZ ET AL. (1972), which as claimed, is compatible with both satellite density measurements and the available incoherent scatter measurements. The main feature of this model is that length of the sunlit day is included as a major model parameter.

The temperature measurements of the type made by BLAMONT AND LUTON (1972) alongwith those using coordinated rocket measurements (e.g. the Aladdin experiments of PHILBRICK ET AL., 1972 B, 1973), are expected to fill the gap that now exist between the various models.

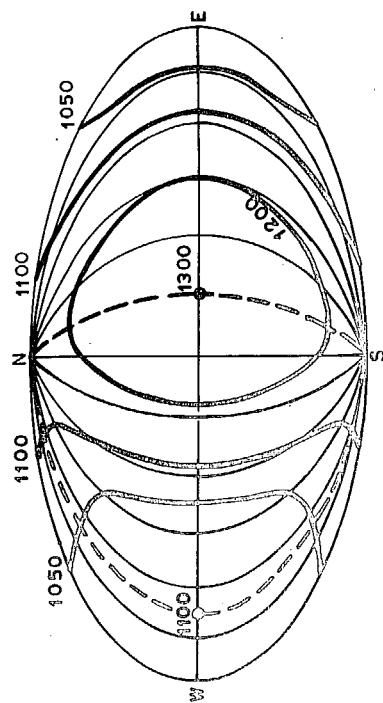
(c) WALDTEUFEL & COGGER (1971)-SUMMER SOLSTICE



(b) WALDTEUFEL AND MCCLURE (1969) SUMMER SOLSTICE  
EXTENSION BY LLOYD ET AL. (1972) SHOWN BY ---



(c) JACCHIA (1971)-EQUINOX



(d) JACCHIA (1971)-SUMMER SOLSTICE

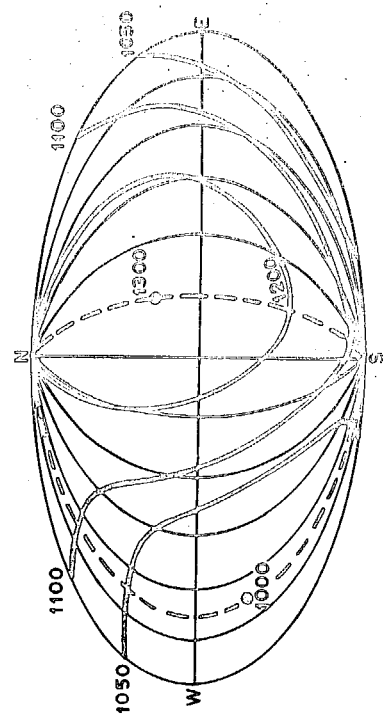


FIG 1-4: EXOSPHERIC TEMPERATURE MODELS. THE LOCAL TIMES OF MAXIMUM AND MINIMUM TEMPERATURES ARE INDICATED BY DASHED LINES.

## 1.5 ENERGY INPUTS IN THE UPPER ATMOSPHERE

Unlike the case of the atmosphere below about 80 km, where solar radiation is the only principal source of energy input, the upper atmosphere derives its energy from various sources. The dynamics, which is largely controlled by hydrodynamic forces at low altitudes, also gets modified significantly at greater heights because of the presence of the ionosphere. Following are the energy sources which play a dominant role in the motions and dynamics of the upper atmosphere.

- i) Absorption of solar ultra-violet radiation and X-radiation, leading to photo-ionisation, photo-dissociation and consequent chemical reactions, liberating heat.
- ii) Dissipation of tidal motions, gravity waves and hydromagnetic waves by molecular viscosity and through turbulence.
- iii) Joule heating by ionospheric current systems, especially equatorial electrojet at low latitudes and auroral electrojet at high latitudes.
- iv) Absorption of energetic charged particles entering the atmosphere.



Part of the heat generated is lost by re-radiation and transport of air. For all re-radiations at wavelengths for which the thermosphere is transparent, which includes visible and infra-red airglow emissions of oxygen, nitrogen and hydroxyl radicals, the heat is lost from the thermosphere.

Following heat transport mechanisms are operative in the upper atmosphere:

- i) Molecular conduction, giving rise to a heat flux which depends on the temperature gradient.
- ii) Eddy transport, which is important around 100 km. This process transfers heat from thermosphere to mesosphere and derives its energy from large-scale wind motions in the mesosphere.
- iii) Transport by large-scale wind, which carries heat horizontally.

Detailed numerical calculations of thermospheric heat sources and sinks in relation to energy balance of the atmosphere have been made by CHANDRA AND SINHA (1973). VOLLAND AND MAYR (1972 A,B,C) have developed a 3-dimensional model of thermospheric dynamics in terms of eigen functions of the atmospheric system, which are excited by solar heating from EUV-radiation, corpuscular heating during geomagnetic storms and from energy due to the dissipation of energy waves generated in the lower atmosphere.

FIG 1.5 is a schematic representation of the various energy sources and their likely effects on the upper atmosphere. A brief account of some of these important energy sources, which cause upper atmospheric motions, is presented in what follows:

#### 1.5.1 Insolation of Solar Radiation

As mentioned earlier, the most important source of thermal energy in the atmosphere is solar radiation. The incoming electro-magnetic radiation from the sun is absorbed by atomic and molecular constituents of the atmosphere in different wavelength regions. The absorption is essentially in two wavelength regions. The radiation in  $\lambda > 7000 \text{ \AA}$  region is absorbed in the lower atmosphere and the shorter wavelengths with  $\lambda < 3500 \text{ \AA}$ , are absorbed in the upper atmosphere.

The most important radiative heating effect is the absorption of solar radiation in the Schumann - Runge (S-R) bands and continuum of molecular oxygen. The S-R heating ranges from less than  $1^\circ \text{ K day}^{-1}$  at 80 km to more than  $20^\circ \text{ K day}^{-1}$  at 105 km. The total energy absorbed between 80 and 105 km is of the order of  $20 \text{ ergs cm}^{-2} \text{ sec}^{-1}$  (DETWILER ET AL., 1961; LEOVY, 1969). In comparison to this, the energy absorbed

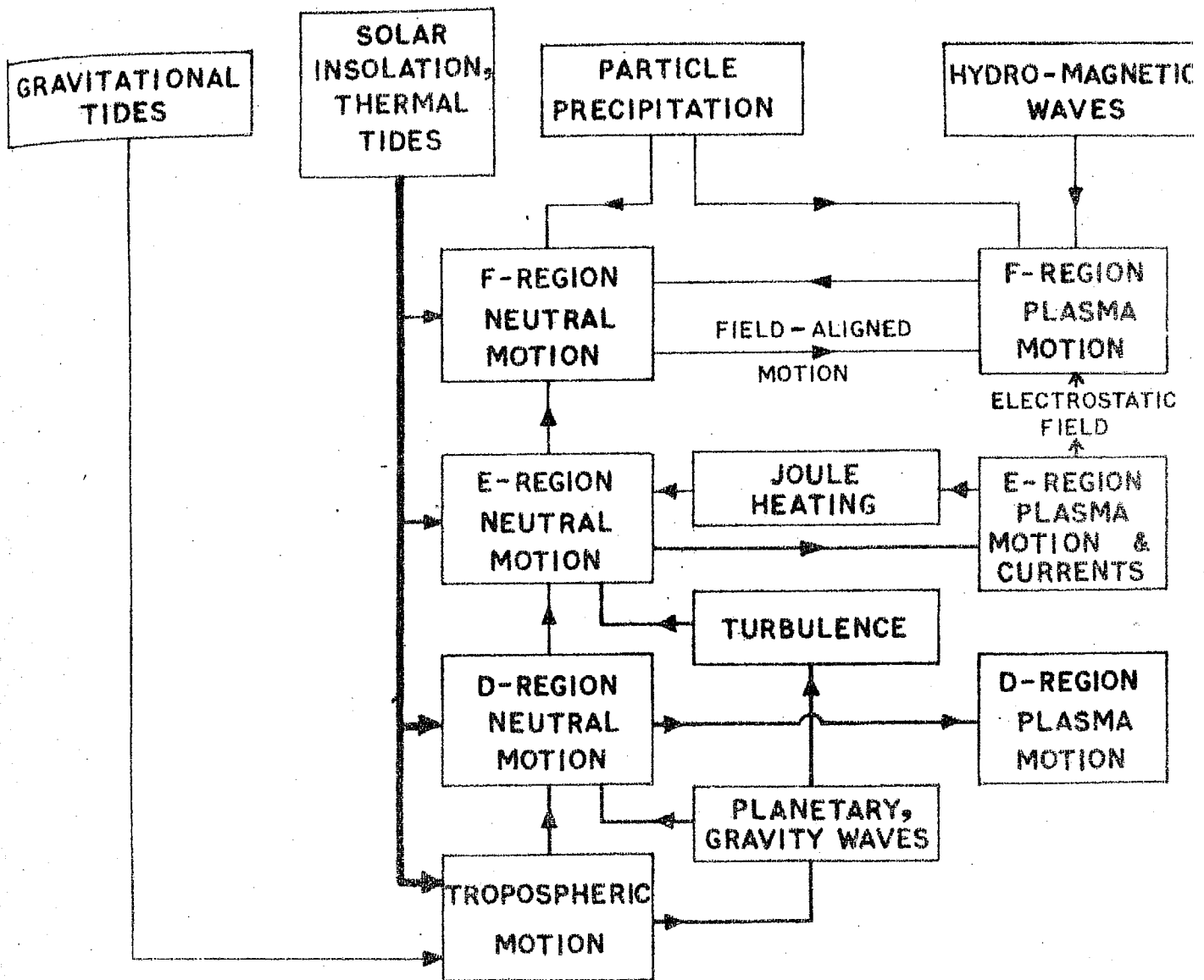


FIG.1-5 ATMOSPHERIC ENERGY SOURCES

in the mesosphere, between 50 to 80 km, is of the order of  $10^2 \text{ ergs cm}^{-2} \text{ sec}^{-1}$ , and in the ozone layer, between 30 and 50 km, is about  $2 \times 10^4 \text{ ergs cm}^{-2} \text{ sec}^{-1}$  for normal incidence of solar radiation (CRAIG, 1965). Solar ultra-violet radiation shorter than  $\lambda = 1000 \text{ \AA}$  deposits about  $3 \text{ ergs cm}^{-2} \text{ sec}^{-1}$  energy at sunspot minimum (ALLAN, 1965; HINTEREGGER, 1965) between 95 and 250 km.

Organised circulations contribute to the heat balance of this region. JOHNSON AND WILKINS (1965) estimate that about  $5 \text{ ergs cm}^{-2} \text{ sec}^{-1}$  energy is transported downwards across 100 km, by thermal conduction and turbulent heat transfer. Vertical transport of atomic oxygen carries down an additional  $3 \text{ ergs cm}^{-2} \text{ sec}^{-1}$ . If all this energy, crossing the 100 km level, were made available for heating the 80 - 100 km region, an average heating of  $10^\circ \text{ K day}^{-1}$  would be estimated. However, most of the atomic oxygen recombines below 80 km, where it makes little contribution to the net heat balance (COLEGROVE ET AL., 1965). Also a large fraction of the energy is radiated away, particularly in the OH bands of night glow, which accounts for about  $2 \text{ ergs cm}^{-2} \text{ sec}^{-1}$ . This corresponds to a cooling rate of  $2^\circ \text{ K day}^{-1}$  at 90 km.

### 1.5.2 Dynamical Energy Sources

At altitudes above 100 km, additional sources of heating, such as propagating waves carrying dynamical energy

upward through the mesosphere, are available (HINES, 1960, 1963, 1965). It has been shown that the heating due to the dissipation of these waves by molecular viscosity and thermal conductivity is sufficient to modify temperatures in the E-region and to account for the very rapid rise of temperature in the lower thermosphere.

HINES (1965), using vertical wind profiles (KOCHANISKY, 1964), estimated that the dissipative heating associated with gravity waves (which have periods of a few minutes to a few hours and spatial scales of a few km to some tens of km in the vertical direction and some hundreds of km in the horizontal direction), is about  $10^{\circ} \text{K day}^{-1}$  at 95 km level, increasing to  $100^{\circ} \text{K day}^{-1}$  near 140 km. More recently, ZIMMERMANN AND ROSENBERG (1971) have calculated the rate of viscous damping from 70 mid-latitude wind profiles, which show large energy contribution near 95 km, tapering-off at higher altitudes. They estimate this source to be four times greater than the S-R continuum absorption in that region.

LINDZEN (1967 A ) has estimated that the upward flux of energy associated with diurnal tide is  $7 \text{ ergs cm}^{-2} \text{ sec}^{-1}$  at the equator, and falls to less than  $1 \text{ erg cm}^{-2} \text{ sec}^{-1}$  outside the tropics. The heating due to this tidal input may be comparable to those of gravity waves. Most of this energy is likely to be dissipated between 80 and 105 km, though its

exact height of deposition is more difficult to assess (HINES, 1965). LINDZEN AND BLAKE (1970) have shown how the thermospheric temperature profile is modified by the tidal energy input in comparison to heating by solar ultra-violet radiation. The gravitational tides of sun and moon, but for their historical importance, are very minor sources of energy input in the upper atmosphere.

HINES (1965) has further discussed another kind of heating associated with these waves, viz., the 'reversible heating'. Until dissipation becomes severe in any given mode, that mode produces reversible, adiabatic heating as one facet of its oscillation. Temperature fluctuations of  $\pm 10^{\circ}$  K in the lower E-region, and  $\pm 30^{\circ}$  K at 110 km can be expected according to his estimates. HOOKE (1969) has advanced the concept of these temperature oscillations to explain some of the anomalous Thomson scatter temperature observations below 130 km. DESAI AND NARAYANAN (1970) have reported negative temperature gradients below 150 km, which could probably find an explanation in terms of reversible heating.

The planetary waves, of global scale and with periods of days, carry an upward flux of about  $1000 \text{ ergs cm}^{-2} \text{ sec}^{-1}$  from troposphere (CHARNEY AND DRAZIN, 1961; DICKINSON, 1968), from which flux at meteor levels of  $1 \text{ erg cm}^{-2} \text{ sec}^{-1}$  is inferred. This implies winds in excess of  $100 \text{ m sec}^{-1}$  at

100 km due to these sources, but the observed values are only about  $10 \text{ m sec}^{-1}$  (GREENHOW AND NEUFELD, 1960). The discrepancy is explained by the reasoning that planetary wave energy resides in modes of smaller horizontal scale and these are severely reflected below mesopause. In middle latitudes, it has a maximum in spring and fall.

The smaller scale gravity wave spectrum reaching altitudes of 90 km or so is thought to be the primary cause for the production of turbulence at these heights. Much of the irregular motion of the upper atmosphere, which was at one time ascribed to turbulence, is now explainable by gravity waves. The power dissipated by turbulence in the 90-100 km region, according to estimates based on direct observational data (GREENHOW, 1959; BLAMONT AND DE JAGER, 1961), is about  $10^{-2} \text{ watts kg}^{-1}$ . There are indications to show that there is little turbulence above 110 km.

The residual energy, due to all these waves, that reaches F-region heights, has been estimated to be about  $1 \text{ erg cm}^{-2} \text{ sec}^{-1}$ . This may contribute to a sizable extent in determining the heat budget at these levels. The propagation of these waves have profound effects in the ionosphere and have been studied by several investigators (eg. DAVIS, 1973).

### 1.5.3 Joule Heating

The currents, that are driven by tidal winds in the dynamo-region of the ionosphere, produce joule heating. COLE (1962 A,B ) estimates a dissipation, due to these currents, of  $0.05 \text{ erg cm}^{-2} \text{ sec}^{-1}$  around 140 km, which is compatible with HINES' (1965) semi-diurnal tidal flux. HINES estimates, though with uncertainty, that these currents produce a heating of about  $25^\circ \text{ K day}^{-1}$ .

The effect of Joule heating for exciting tidal modes and gravity waves has been investigated (BLUEMAN AND HENDL, 1969; STENING, 1970). SASTRY ET AL. (1973) have explained their observations of abnormal electron temperature measurements at equator as due to joule heating. The equatorial electrojet as a source of gravity waves has also been proposed (KNUDSEN, 1969; CHIMONAS, 1970).

### 1.5.4 Auroral Electrojet, Particle Precipitation etc.

In addition to electric currents flowing in the undisturbed ionosphere, large currents flow in the auroral zones at times of magnetic disturbances. The joule heating resulting from the large auroral electric fields during magnetic storms have been estimated as some tens of  $\text{ergs cm}^{-2} \text{ sec}^{-1}$  (KENNEL AND REES, 1972).



Energetic particles, right from auroral to cosmic ray energies, constantly bombard the upper atmosphere. This phenomenon is more pronounced at high and auroral latitudes. Energy deposition associated with these energetic particles in an active aurora can exceed, at times, solar EUV flux by a factor of over a hundred. BELON ET AL. (1966) find a total energy deposition rate of  $380 \text{ ergs cm}^{-2} \text{ sec}^{-1}$  during storms from observations of  $3914 \text{ \AA}$  emission. MOE (1967) has reported heating associated with corpuscular radiation from observations of densities derived from the spin decay of Explorer 6, and finds correlation with the daily planetary magnetic index  $a_p$ .

The large amounts of energy, both particle and field contributions, are deposited in the lower thermosphere and cause large scale dynamic motions that result in the overall global heating associated with magnetic storms (HAYS AND ROBLE, 1971; HAYS ET AL., 1973). COLE (1971), and FEDDER AND BANKS (1972), have studied the thermospheric winds induced by auroral electrojet heating. At times of magnetic storms and active auroral displays, it has been shown (CHIMONAS AND HINES, 1970) that energy might be transported from the auroral zones to lower latitudes by gravity waves and thereby provide excessive heating. SMITH (1968) has presented observational evidences from vapour release experiments of strong thermospheric winds during geomagnetic storm at as low a latitude as Hawaii ( $23^\circ \text{ N}$ ).

Energy releases in the upper atmosphere during some geomagnetic storms have been discussed by KRASSOVSKY (1972).

## 1.6 MOTIONS IN THE UPPER ATMOSPHERE

Motions in the upper atmosphere, as in the lower, occur on space and time scales that range from general circulation to turbulent eddies. Intermediate between these two extremes lie the oscillatory motions (wave motions) induced by tides and the quasi-oscillatory motions of shorter-period internal gravity waves. Thus superimposed on the geostrophic and thermal wind, which constitute the prevailing wind, are the winds caused by various other agencies. The different types of motions at thermospheric levels may be summarised as follows:

- i) Prevailing winds, of global scale, driven by long-lived pressure inequalities, varying with the seasons.
- ii) Thermospheric winds above about 100 km, driven by pressure inequalities due to short-term temperature variations. Though, these can be classified under tidal waves, they are usually not treated so because they can be discussed otherwise without the complicated tidal theory.
- iii) Planetary waves with periods of days.

- iv) Tidal waves, of global scale, with periods of solar and lunar hours, primarily the solar tides.
- v) Internal gravity waves, with periods from a few minutes to a few hours, and scale sizes ranging from a few km in the vertical direction to some hundreds of km in the horizontal direction.
- vi) The turbulent motions, which serve as sinks of energy. Large-scale motions are degraded into small-scale motions and lost as heat. These are, however, not observed above about 105 km.  
(BLAMONT AND BARAT, 1967).

#### 1.6.1 Measurement of Upper Atmospheric Movements

Methods used for determining upper atmospheric movements can be divided into two classes, one concerned with the motion of the neutral atmosphere and the other with the motion of the ionised media. The relation between these two, the relative importance of various components of motion and the comparison of experimental results are the main points of interest in the study of upper atmospheric motions. These studies are complicated by the fact that there is often uncertainty involved as to the nature of the motion that is being measured. Although there are definite diurnal and seasonal trends in motions, there is yet conflict as to the physical interpretation of these.

The principal methods of measuring winds in the neutral atmosphere at ionospheric heights are discussed under two heads:

- i) Methods employing ground-based equipments.
- ii) Methods using sounding rockets and other vehicles.

FIG 1.2 shows the range of heights over which the various methods are used.

#### 1.6.2 Ground-based Methods

##### a) Visual Meteor Method

The high-energy meteors entering the dense regions of the atmosphere - in the 80 to 110 km region-produce a dense ionised trail lasting from a few seconds to even a minute. Meteoric particles of very high energy also produce visible trails in the atmosphere. Such trails become distorted because of winds. Their motion can be photographed and followed from the ground. This method is, however, applicable only during night-hours and when the trails are sufficiently bright. A brief survey of the results obtained by visual-meteor method has been given by LILLER AND WHIPPLE (1954) and MILLMAN (1959). Since 1955 this method has lost importance because of the radio-meteor method.

b.) Radio Meteor Method

The main advantage of this method over the optical method is that, by having sufficiently powerful radars, it can track the fainter trails produced by smaller meteors which are unsuitable for optical observations. This method can be used during all hours of the day to study many more meteor trails. This is, thus, the most powerful method for the resolution of different tidal modes and gravity waves near the 100 km region.

The wind speed is measured through the Doppler shift that the drifting meteor trail produces in the returned electromagnetic signal. ELFORD (1959), GREENHOW AND NEUFELD (1961) and CRAIG (1965) have reviewed the radio-meteor results at Jodrell Bank and Adelaide. Despite being a powerful tool for studying the upper atmosphere in the 80 to 110 km region, this technique has been used only at a few centres.

A new radar has been set up (SPIZZICHINO ET AL., 1965) which employs a continuous wave technique in conjunction with carefully isolated, receiving and transmitting sites. Measurement of Doppler shift and position are made in terms of phase. Greater precision and high echo rates are obtained in this system. Results obtained from this radar have been published by REVAH (1969) and SPIZZICHINO (1969 A ). Theoretical studies, based on these experimental observations, of interaction of different wave components at meteor heights have been reported by SPIZZICHINO (1969 B,C, 1970 A,B).

Besides measurement of winds, the radio-meteor method has been used for the study of turbulence, wind shear and its variation with height (GREENHOW, 1959; GREENHOW AND NEUFELD, 1960; REVAH AND SPIZZICHINO, 1964).

c) Noctilucent Cloud Method

Noctilucent clouds are generally observed during twilight hours in the latitude range of  $50^{\circ}$  to  $65^{\circ}$  and probably consist of small dust and ice particles. These are formed in the altitude range 70 to 90 km but usually around 82 km. Reviews of their properties and behaviour have been given by FOGLE AND HAURWITZ (1966). The observations of their movements have been made by photographing the clouds from the ground (WILT, 1962). The clouds show both bodily movements and wave motions (HAURWITZ, 1961).

d) Airglow Method

From Photometric scans of night sky  $\lambda 5577 \text{ \AA}$  and  $6300 \text{ \AA}$  oxygen (OI) emission lines, the study of irregularities of isophotes on spatial scale have been made. These irregularities have been interpreted as being due to neutral winds (ROACH ET AL., 1958; TOHMATSU AND NAGATA, 1963). This method has not yet proved itself as a useful tool for the measurement of upper atmospheric winds.

e) Satellite Drag Method

One particular perturbation of satellite motion, namely, a progressive change in the inclination of the orbital plane to the earth's equator, has been shown to be due to the prevailing motion of the air (MERSON ET AL., 1959). From the analysis of many satellite orbits, it has been deduced that the neutral air, at heights between 150-400 km, has a net prevailing eastward velocity of the order of  $100 \text{ m sec}^{-1}$ , a phenomenon that has come to be known as "Super Rotation" (KING-HELE, 1964, 1972; KING-HELE AND ALLAN 1966; RISHBETH, 1972 A ). However, this method of determining atmospheric motions from satellite drag gives only the zonal velocity and also suffers from accuracy. Transient phenomena can not be studied by this method.

1.6.3 Vehicle-borne Methods

a) Pilot Tube Method

This method consists of placing pressure gauges at various points on the surface of the sounding rocket. Though mainly used for the measurement of atmospheric density, temperature and pressure, AINSWORTH ET AL. (1961) have demonstrated the potentials of this method for measuring atmospheric winds upto 110 km.

b) Rocket Grenade Method

Detonation of highly explosive grenades in the upper atmosphere and the detection of the resulting acoustic wave has been used for the determination of atmospheric temperature and winds upto an altitude of about 100 km (GROVES, 1963 A; ROSENBERG, 1966). The explosions of grenades at regular intervals along the rocket trajectory are detected by an array of ground-based hot-wire microphones. Comparison of travel times and distances leads to average acoustic velocity over the height interval between the explosions, from which the temperature and horizontal wind velocity are determined. Above about 100 km, the size of the grenades required to produce detectable sound at ground becomes large, but despite these difficulties, PROCUNIER (1967) has made measurements of echoes upto 107 km.

1.6.4 Chemical-release Method

The relative simplicity of this method as compared to most sounding rocket programs, as well as the visual display of this method, has contributed to its widespread use. The motion of controlled chemical releases is observed from the ground (by photographing them against a background of known stars) and interpreted as direct measurements of thermospheric winds. Observations have been made from numerous locations using vapour trails, point-cloud releases and multiple-cloud releases, separated in both space and time. Objectives in these experiments have been

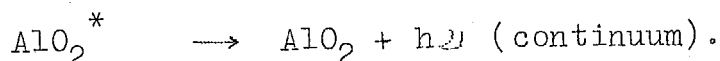


- i) measurements of winds and diffusion from the motion and growth of the cloud respectively,
- ii) determination of temperature, density and other atmospheric parameters from scattered or emitted radiations from the cloud, and
- iii) the relation of neutral and ionised species and the study of electric fields from the drift of neutral and ionised clouds.

Following the suggestion by BATES (1950), who advocated the use of this method for upper atmospheric studies, the first chemical release in the upper atmosphere was a continuous trail of sodium vapour ejected over New Mexico on 12 October 1955 during an evening twilight (EDWARDS ET AL., 1956). Since that time hundreds of releases have been made using sodium and various other chemicals, e.g. Lithium, Potassium, Nitric Oxide, Barium-Strontium etc.

Alkali and alkaline earth-metal releases rely on the resonant scattering of sunlight from the material and are thus useful only during twilight hours for photographic tracking and observation from the ground. The technique itself was greatly advanced by the introduction of trimethyl aluminium as a trace material, which permits the detection of thermospheric motions even during night-times because of its chemiluminescence.

This technique of producing chemi-luminescent trails in the altitude region, 80-150 km for the study of night-time neutral motions by the use of gaseous aluminium compound was suggested by ROSENBERG ET AL. (1963 A, B). The photo-chemical action of atomic oxygen at these heights with trimethyl aluminium gives a luminescent glow, probably according to the following mechanism:



TMA continuum emission is in the wavelength range  $\lambda$  4500 - 6500 Å. Canisters and payloads for producing TMA trails have been discussed in detail by CORMAN AND GUARINO (1965). The use of this technique has been markedly enhanced by the introduction of gun-launched vehicles to lay the trails (MURPHY ET AL., 1966); with their accuracy and reproducibility of trajectory, and their relatively high repetition rate and modest cost, they have introduced the realistic possibility of a synoptic study of sequential wind profiles.

The Ba-Sr vapour release technique was developed first at the Max Plank Institute (FOPPL ET AL., 1965, 1967). A mixture of Ba and CuO, with an excess of Ba is evaporated, resulting in vaporised barium. The vaporised barium, released

in the upper atmosphere gets ionised by the action of solar ultra-violet rays and this could be identified as a cigar-shaped cloud, stretched along the magnetic field lines. The ionised Ba cloud and the barium which combines with the oxygen of the atmosphere (generally below 150 km) and forms BaO, are visible by resonant scattering and can be used to study ionospheric electric fields and neutral atmospheric motions. Strontium is always present as an impurity in the Ba metal, and because of its good evaporation efficiency, a neutral Sr cloud is also formed. The emissions from the ionised barium and neutral Ba-Sr clouds have been discussed in detail by HASER (1967), and BABER ET AL. (1971). Some of the principal lines of emission are

Ba I	5535 Å
Ba II	455.4 Å, 4934 Å
Sr I	4607 Å

The BaO has a band spectrum with band heads between 5200 Å to 5300 Å for the sequence  $\Delta v = 5$ .

Chemical trail release is an unique method for obtaining a highly accurate and detailed vertical profile of the horizontal wind over a large altitude range. Sunlit alkali and TMA releases during twilight have been used for the measurement of atmospheric movements at altitudes between 80 and 250 km; chemi-luminescent trails allow measurements from

in the upper atmosphere gets ionised by the action of solar ultra-violet rays and this could be identified as a cigar-shaped cloud, stretched along the magnetic field lines. The ionised Ba cloud and the barium which combines with the oxygen of the atmosphere (generally below 150 km) and forms BaO, are visible by resonant scattering and can be used to study ionospheric electric fields and neutral atmospheric motions. Strontium is always present as an impurity in the Ba metal, and because of its good evaporation efficiency, a neutral Sr cloud is also formed. The emissions from the ionised barium and neutral Ba-Sr clouds have been discussed in detail by HASER (1967), and BABER ET AL. (1971). Some of the principal lines of emission are

Ba I	5535 Å
Ba II	455.4 Å, 4934 Å
Sr I	4607 Å

The BaO has a band spectrum with band heads between 5200 Å to 5300 Å for the sequence  $\Delta v = 5$ .

Chemical trail release is an unique method for obtaining a highly accurate and detailed vertical profile of the horizontal wind over a large altitude range. Sunlit alkali and TMA releases during twilight have been used for the measurement of atmospheric movements at altitudes between 80 and 250 km; chemi-luminescent trails allow measurements from

90 to about 150 km altitude during the night. Height resolutions ranging from a fraction of a km at 100 km to a few kms around 200 km can be achieved. Accuracy of wind measurements ranges from a few  $\text{m sec}^{-1}$  to about ten  $\text{m sec}^{-1}$  in the above altitude ranges.

Serious limitations of the vapour trail method are that observations from atleast two known sites are required to determine the space-position of the release by triangulation, and that the atmospheric seeing conditions have to be perfect, as it is an optical method. Besides, this technique is applicable only during twilight and night hours (in a narrower altitude range), though recently new techniques for tracking lithium trails during day-time with a differential photometer employing narrow-band interference filters have been developed (BEDINGER, 1970 A; BEST, 1970; REES ET AL., 1972 B). BEDINGER (1973) reports photography of vapour clouds during day-time, taken from aircraft flying at 40,000' altitude and using 10 Å band-width filters. The above techniques are expected to fulfil the great need for knowing the day-time winds in the thermosphere, and also to extend the usability of the vapour cloud method as an all weather method.

#### 1.6.5 Methods for Determining Plasma Motions in the Ionosphere

KENT (1970) has described exhaustively the various methods, their limitations etc., for measuring the ionisation

movements. A few of the important methods are described in brief in the following.

a) Spaced Receiver Method

The diffraction pattern observed on the ground from the radio waves reflected from the ionosphere is interpreted in terms of motions of irregularities (MITRA, 1949). This radio method has been used extensively to measure apparent motions of large scale ionospheric irregularities in the E- and F-regions (KENT AND WRIGHT, 1968; BRIGGS, 1972). Despite the vast data gathered, the relation of the measured drifts of the irregularities to the neutral wind motions at the same height is still on a doubtful premise (HINES AND RAGHAVA RAO, 1968). This method also suffers from the disadvantage that it is extremely difficult to locate accurately the height at which the motion is being measured.

b) High-frequency Doppler and Phase-path Method

These two related techniques are very useful for studying short-period perturbations in the thermosphere, such as internal and acoustic gravity waves and infrasonic waves. The observed iso-ionic contours are interpreted as closely corresponding to the causative wind-oscillations in the neutral medium. High time-resolution studies on the structure of short-period disturbances are possible with these techniques (VINCENT, 1972).

c) Incoherent Scatter Method

This technique, which is one of the most powerful tools for studying the ionosphere to high altitudes, has been developed during the past 15 years (GORDON, 1958; EVANS, 1969). Precise measurements of the frequency spectra of signals incoherently scattered by individual electrons reveal shifts caused by macroscopic motions of the ions. The chief merit of this system is that many parameters, such as, electron and ion temperatures, ion velocity, electron density etc. can be simultaneously measured and the needed information on dynamical effects can be obtained.

This method can be used to derive neutral winds at altitudes of 90 km and above. Above 140 km, however, only the meridional component (along the magnetic meridian) can be obtained with this technique. A recent review of ionospheric movements by this technique has been given by EVANS (1972). This method has a good time-resolution (10-30 mins) and height-resolution ( $\sim 10$  km) and shows great promise for the future.

1.7 OBSERVATIONAL RESULTS OF WINDS IN THE UPPER ATMOSPHERE

In the thermosphere, from about 100 to 200 km, data on winds are very meagre, and till today the information on atmospheric movements is not adequate for its full understanding. Turbulence is less evident at heights beyond about 105 km and it seems likely that atmospheric motions can be interpreted

in terms of the three main components - a general circulation, tidal movements and internal gravity waves.

Most of the results in this region have been obtained through the vapour release method. The experiments conducted so far are insufficient in number for a clear dissemination of the motion into the various components. Many workers have reviewed and compiled bibliographies of wind results by this technique (BEDINGER 1966, 1971; SWIDER, 1971). Most of the observations are from northern mid-latitude stations and below 150 km altitude, with Wallops Island ( $38^{\circ}$  N), Eglin ( $31^{\circ}$  N) and Woomera ( $32^{\circ}$  S) providing the bulk of the data.

Speeds of over  $100 \text{ m sec}^{-1}$  and large vertical shears in wind velocities below 140 km have been reported from the study of vapour trail releases. Space- and time-correlations of winds in the 100-150 km altitude region, by sequential trail releases, have been reported (ROSENBERG AND JUSTUS, 1966). ROSENBERG (1968 A,B,C) analysed over 70 mid-latitude trails and found an rms wind speed of  $45\text{-}70 \text{ msec}^{-1}$ , rms shear of  $0.004\text{-}0.02 \text{ sec}^{-1}$  and a transition from turbulent to laminar flow between 100 and 115 km. Wind shears upto  $0.1 \text{ sec}^{-1}$  have also been reported. Above some 140 km, the wind profiles have been shown to be more regular.



### 1.7.1 Periodic Components and Waves

Meteor data from Adelaide and Jodrell Bank (HAURWITZ, 1964) have provided unambiguous resolution of the observed winds into the various tidal components at the 100 km level. Using an altitude scale,  $\eta$ , normalised with respect to the neutral scale height,  $H$ , defined in the form (as suggested by MACLEOD)

$$\eta = \int_{80}^z \frac{dz}{H}$$

the vertical variation of neutral wind profiles have been studied from vapour cloud data (ROSENBERG AND JUSTUS, 1966; REES ET AL., 1972 A; LLOYD ET AL., 1972). This has been shown to be a convenient method of studying the regular and random components of any wind profile. The auto-correlation of the profile permits an estimate of the dominant vertical wavelength, which in turn is interpreted in terms of the dominant propagating wave. The cross-correlation of the zonal and meridional profiles can be used for inferring the phase advance of one over the other, which is in essence the rotation of the wind vector due to a propagating tidal mode (ROSENBERG AND EDWARDS,

1964). LLOYD ET AL. (1972) report dominance of (1,1) mode\* in the morning and (2,4) mode\* in the evening from auto-correlation studies of vapour trail releases over Woomera.

HINES (1966) has suggested yet another method for extracting the tidal components, primarily diurnal, from the dawn and dusk wind profiles, and has shown the (1,1) mode to be important up to 120 km altitude. Following this method, and the one suggested by GROVES (1959) for meteor winds, WOODRUM AND JUSTUS (1968 A) and WOODRUM ET AL. (1969) have calculated the vertical wavelengths and phases of various components in the 90 to 130 km altitude region from the vapour cloud data. Specific identifications of (2,4) and (2,6) modes have also been claimed (ZIMMERMANN AND MARKOS, 1966). Incoherent scatter observations of ion drifts have been analysed to study the height structure of meridional tidal winds in the ionosphere (AMAYENC AND REDDY, 1972; AMAYENC ET AL., 1973).

KATO (1966 A,B) and LINDZEN (1966 A) independently, and almost simultaneously, theoretically predicted the existence of diurnal negative modes which are evanescent in the vertical direction. These studies are now able to explain the contrasting dominance of diurnal and semi-diurnal tides in

---

\* In (n,m) mode, n denotes the latitudinal, and m, the longitudinal structure of the wave pattern; eg. the (2,4) mode denotes semi-diurnal tide with (m-n) i.e.  $4-2 = 2$  nodes between pole to pole in the oscillation.

the middle (Adelaide  $35^{\circ}$  S) and high-latitudes (Jodrell Bank  $52^{\circ}$  N), which were inferred from meteor observations (HAURWITZ, 1964). KATO, further showed that these could well explain the geomagnetic  $s_q$  variations. These results have aroused interest for a renewed study of the diurnal tide, which had hitherto been considered insignificant compared to the semi-diurnal.

The observed profile often has the form of a large spiral in which the sense of rotation, when viewed from above, is clockwise in the northern hemisphere, and in the opposite sense in the southern hemisphere. ROSENBERG AND JUSTUS (1966) have emphasised this feature in experiments conducted from Eglin ( $30^{\circ}$  N). Results from equatorial- and low-latitude locations (BHAVSAR AND RAMANUJA RAO, 1968; SHAFI AHMAD, 1967) have shown a mixed behaviour.

The spiral structures have often reversals in direction and the profiles appear to be highly stratified such that directional changes occur in small height intervals which are separated by regions of little change. BEDINGER ET AL. (1968) have shown, from the study of Wallops Island ( $38^{\circ}$  N) observations, that smooth spiral patterns are associated with large wind speeds, and irregular patterns with low speeds. Similar studies have been reported from Yuma ( $33^{\circ}$  N) and Barbados ( $12^{\circ}$  N) observations (MURPHY AND BULL, 1968; MURPHY, 1969).

Studies of temporal variations of winds are severely restricted by the inability to observe winds during day time. However, several series of observations have been made through the night in the 80 to 150 km altitude region (ROSENBERG AND EDWARDS, 1964; ROSENBERG ET AL., 1964; MURPHY AND BULL, 1967, 1968) to study these variations. Sequences of TMA trails have revealed sinuous patterns of wind structure moving downward in time and have been interpreted as manifestation of tides (SMITH, 1972). Winds measured at tropical latitudes (MURPHY AND BULL, 1967, 1968; MURPHY, 1969) have been shown to exhibit a rotating wind vector pattern, with meridional wind vector contour descending during the night in contrast to zonal wind contour. The rate of descent could be used to infer the dominant wave motion.

ROSENBERG AND JUSTUS (1966), from simultaneous spatially separated observations, have deduced horizontal wavelengths of the order of a few thousand km. From up-and-down trails, lower limits for horizontal wavelengths have been inferred (BHAVSAR AND RAMANUJA RAO, 1965; BEDINGER ET AL., 1968). BLAMONT (1963) has reported the observation, during the same twilight, of two nearly identical profiles separated by about 650 km.

#### 1.7.2 Irregular Winds

The irregular wind structure, revealed by vapour trails above 80 km, have been attributed to internal gravity

waves (HINES 1960, 1963) and have been analysed in detail (KOCHANISKY, 1964, 1965, 1966) to estimate the gravity wave contribution. The smallest vertical wavelengths present in the data have been identified by ZIMMERMANN (1964) and shown by HINES (1964 A) to be consistent with the small scale cut-off of the gravity wave spectrum. WOODRUM AND JUSTUS (1968 B) determined an rms irregular wind maximum of  $60-70 \text{ m sec}^{-1}$  near 102 km with a characteristic vertical wavelength of 16 km (JUSTUS, 1970). Analysis of a number of trails has revealed that vertical wavelengths exceeding 5 km contain by far the greater portion of the energy in the 90-140 km region (NOEL, 1966). LINDZEN (1969) has discussed the necessary information vital to a proper description of tides and gravity waves from the vapour cloud observations.

The globular structure of the vapour trails below about 105 km has been attributed to turbulence. BLAMONT AND BARAT (1967) report a sandwich structure of turbulence in the 80 to 100 km region, with alternate layers of turbulence and its absence. Eddy diffusion coefficients have been estimated from many vapour trails (ZIMMERMANN AND CHAMPION, 1963; COTE, 1965, 1967). LAYZER AND BEDINGER (1969) strongly maintain that the vapour trail structure observed in the lower region is not an indication of turbulence and that the irregular noise-like component of the horizontal wind cannot be described adequately by linear theories involving turbulence and gravity waves.

They suggest an alternative explanation ascribing the irregular component to the non-linear response of the upper atmosphere and holding that tidal energy alone is needed to explain the observed behaviour.

### 1.7.3 Vertical Winds

Vertical winds are considered to be much smaller in magnitude than the horizontal ones, and their determination needs a careful examination of the profiles. Spherical clouds and point-releases would allow easier measurements of vertical motions. EDWARDS ET AL. (1963) have deduced vertical velocities upto  $13 \text{ m sec}^{-1}$  in the 97 to 111 km region from motion of identifiable globular structures. MACLEOD (1969) has reported vertical wavelength of 9 km in vertical winds and that vertical shear of vertical wind is comparable to vertical shear of horizontal wind. REES (1969) from a study of 17 wind profiles reports rms velocity and wavelength of  $10 \text{ m sec}^{-1}$  and 7 km respectively near 100 km, increasing to  $30 \text{ m sec}^{-1}$  and 40 km near 180 km.

### 1.7.4 Observations During Storms and Disturbances

Individual magnetic sub-storms have been observed to produce neutral wind speeds of over  $500 \text{ m sec}^{-1}$  in the height range of 130 to 150 km (REES, 1972 B). FEES (1971), from LOGCAS measurements, has reported wind velocities in excess of  $1000 \text{ m sec}^{-1}$  at high latitudes during magnetic storms.

A strong correlation between east-west wind,  $V_E$ , and the mean local ground magnetic perturbation of the previous two hours,  $\Delta x$ , has been established by REES (1972), from his auroral zone measurements, of the form

$$V_E = - 2.5 \Delta x .$$

It has been shown that the wind disturbances can propagate to mid-latitudes in the night-hemisphere and can produce large neutral wind speeds on a global scale. Thomson scatter observations of F-region, during strong magnetic storms, have been interpreted as internal gravity waves originating from auroral zone (VASSEUR AND WALDTEUFEL, 1969; THOME 1968). SMITH (1968) has reported strong thermospheric winds at Hawaii ( $23^\circ \text{N}$ ) during a geomagnetic storm. REES (1972) has compiled the observations available for winds during disturbances and has proposed a model for these conditions.

HICKS AND JUSTUS (1970), from a correlation study of winds in the 90-140 km region with  $K_p$ , sunspot number and solar flux, suggest a dynamo type of interaction below 110 km, in which atmospheric circulation variations cause changes in the geomagnetic field strength, and a motor type of interaction between the solar corpuscular radiation and the winds above 110 km.

## 1.8 INTERACTION OF NEUTRAL AND IONISED ATMOSPHERES

It has long been appreciated that the ionospheric plasma and neutral air exert forces on each other as a result of collisions between charged particles and neutral atoms. The drift of ions with neutral air takes place till  $\omega_{in}$ , the ion-neutral collision frequency, is greater than  $\omega_i$ , the ion gyro frequency, which holds upto about 140 km in the upper atmosphere. The influence of neutrals on electrons is lost at altitudes as low as 70 km, because of the latter's small mass and the consequent large gyro frequency. At altitudes above 150 km, neutral winds in the magnetic meridian move the plasma up and down the field lines with velocities comparable to those due to ambipolar diffusion and electric fields, thus affecting the ionisation distribution.

Ionisation drags the neutral particles with it at the F-region heights, and this is an important force in the consideration of atmospheric wind systems at these heights, particularly during day time. Because of the much larger neutral to-ion density ratio below 200 km, the influence of ions on neutrals is inappreciable in this region.

There are many situations in which interaction between charged particles and neutrals takes place depending on the height. The more important ones among them are, the Mid-latitude Sporadic E, the Dynamo Currents and the F-region Wind

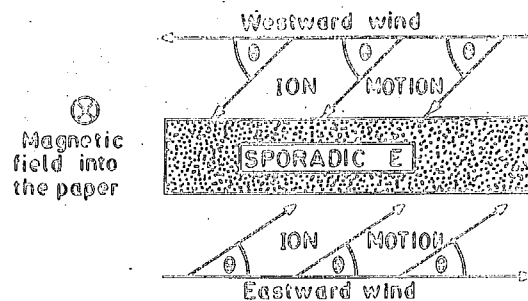


System. FIG 1.6 schematically illustrates these three phenomena and in the sub-sections to follow, a brief account of them is given.

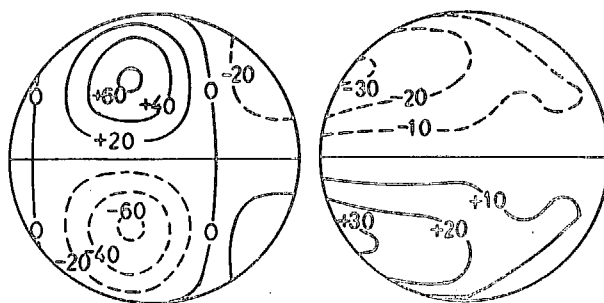
### 1.8.1 Sporadic E

Ionosonde often detects dense layers or patches of ionisation in the E-region at heights around 100 to 120 km, which do not seem to be related to the normal day-time E-layer. Such patches of ion-electron clouds are called sporadic E or  $E_s$  because of their irregular behaviour. Sporadic E has been studied with ground-based ionosondes and backscatter methods. General reviews of  $E_s$  formation, its morphology and other properties have been discussed by SMITH AND MATSUSHITA (1962, 1966), WHITEHEAD (1970) and MATSUSHITA AND SMITH (1972).

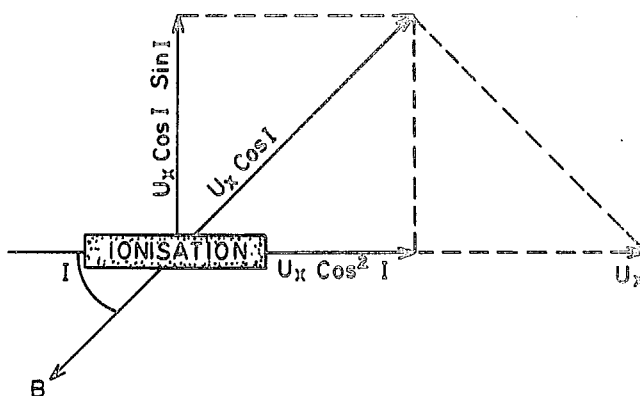
The observations of horizontal winds in the neutral air in the E-region suggest that large vertical shears are often present. WHITEHEAD (1961, 1967) has shown that the shears can redistribute the E-region ionisation and lead to the formation of dense layers. FIG 1.6 (a) illustrates a situation in which a vertical shear of east-west wind produces an  $E_s$  layer. The wind drags with it the positive ions for which collision frequency with neutrals,  $\nu_{in}$ , is greater than its gyro-frequency,  $\omega_i$ . The ions experience a Lorentz force ( $\mathbf{v} \times \mathbf{B}$ ) and are driven at an angle to the wind velocity so that they accumulate within the shear. The electrons, unaffected



(a) WIND SHEAR & SPORADIC E



(b) THE DYNAMO  $S_q$  CURRENT SYSTEM AT E-REGION DUE TO NEUTRAL WINDS (VESTINE, 1960)



(c) MERIDIONAL WINDS AND F-REGION IONISATION

FIG. 1.6 INTERACTION OF NEUTRAL & IONISED ATMOSPHERES

by the wind are, however, constrained to move along the field lines in such a way as to neutralise the space charge set up by the ion motion and the accumulated layer thus consists of neutral ionisation.

It has been shown (WHITEHEAD, 1961; HINES, 1964 B) that the vertical component of ion motion is

$$v_z = u_y \frac{\omega_i}{\omega_{in}} \cos I$$

where  $I$  is the dip of the field lines to the horizontal and  $u_y$  is the eastward wind blowing normal to  $\underline{B}$ .

An earlier suggestion by DUNGEY (1956) depended on the vertical motion produced by a north-south wind. The resulting vertical drift can be shown to be dependent on the small ratio  $\omega_i^2/\omega_{in}^2$ , as compared to  $\omega_i/\omega_{in}$  for the east-west shears. At F-region heights, this drag will be more effective, but large wind shears are not known to be present/at these heights.

MURPHY ET AL. (1966) and WRIGHT ET AL. (1967) have shown many instances of correlation of E-region shears observed by chemical releases and sporadic E seen on ionosonde records.

### 1.8.2 Ionospheric Dynamo Currents

Tidal wind motions at E-region levels can give rise to electric currents because the electrons and ions, embedded in the neutral gas, have different mobilities. The currents, in turn, give rise to space-charge distributions in such a way

that the resulting electrostatic fields maintain a divergence-free current system on a global scale (MAEDA AND KATO, 1966; MATSUSHITA AND CHAMBELL, 1967). In FIG 1.6 (b) the global current system is shown; the one on the left represents the day-side current system and the one on the right corresponds to the night-side. Between two neighbouring streamlines  $2 \times 10^4$  amperes of current is flowing.

The magnitude and distribution of the currents, and the associated electric fields are primarily determined by the global distribution of neutral winds. Many of the apparent anomalies, in the geomagnetic daily-variations, may find an explanation in terms of the complex wind motions at dynamo-region heights. From the observed geomagnetic daily-variation at ground, MAEDA (1955, 1957) and KATO (1956, 1957) have derived the diurnal and semi-diurnal tidal wind systems at E-region heights on a global scale.

The electric fields at E-region levels are communicated to F-region heights along the highly-conducting magnetic field lines. The ions and electrons drift together with a velocity  $E/B$  where  $E$  is the electric field. These F-region electric fields, communicated from E-region, have been invoked to explain some of the F-region behaviours, e.g. F-region vertical and horizontal drifts (WOODMAN, 1970; BALSLEY, 1973), the equatorial anomaly (MARTYN, 1947, 1955), etc. REES ET AL. (1973 A), from simultaneous measurements of F-region drifts,

determined by spaced receiver method and barium ion cloud movements, and from a study of ground-based magnetograms, report rather poor agreement between the electric fields derived from these two methods.

### 1.8.3 F-region Plasma Motions

KING AND KOHL (1965) showed for the first time that large winds exist at F-region heights, and that the meridional component of these winds can lift the ionisation up and down the magnetic field lines and also cause an air-drag on the ionisation movements. FIG 1.6 (c) illustrates the situation, where meridional neutral wind of magnitude  $u_x$ , imparts velocities of  $u_x \cos^2 I$  and  $u_x \cos I \sin I$  to the ionisation along the meridional and vertical directions respectively. Here,  $I$ , the dip angle, is the angle made by  $u_x$  with the magnetic field  $B$ . These meridional neutral winds have profound effects on the maintenance of night-time F-region (discussed in detail in Chapter IV), and are also thought to be the cause for the asymmetry in the equatorial anomaly (THOMAS, 1968).

## 1.9 SCOPE OF THE PRESENT THESIS

The study of the neutral upper atmospheric parameters, with the help of rocket-released chemical vapour clouds, was initiated by the Physical Research Laboratory in 1963. The purpose was to study the neutral upper atmospheric winds,

turbulence, density, temperature and interaction of the neutral and ionised upper atmospheres. The work was started by BHAVSAR AND RAMANUJA RAO (1965, 1968) by releasing sodium vapour at twilight hours for the determination of winds in the height region of 80 to 200 km.

Initial observations, confined to wind measurements by means of sodium trails, were limited to twilight hours. Later, TMA release technique was established, which permitted wind measurements during night hours as well, thus giving a better coverage in time for the measurements. The first results of such a study, from three TMA releases, are presented and discussed in detail in Chapter II. Twilight wind measurements, made from Barium-Strontium releases, and observational evidences of interactions of neutral and ionised atmospheres are also discussed in this chapter.

The winds observed at any one particular station form part of the global general circulation, which in turn determines the upper atmospheric dynamics. To get an overview of general circulation, synoptic launchings of vapour cloud releases were organised by COSPAR in 1964. The experimental results obtained during these synoptic studies were, however, inadequate to draw any definite conclusions. In the present thesis the author has made an attempt to put together, the results of some 200 vapour cloud experiments conducted, from different locations over the globe, during the last 1½ decades,

and has shown that prevailing winds flow with some regularity in the upper atmosphere. Seasonal effects above 150 km, and diurnal effects above 180 km, have also been derived. These studies are also presented in Chapter II.

In addition to the determination of winds, the vapour-release technique also permits determination of temperature and density of the atmosphere. In earlier attempts of direct temperature measurements, by line-width determination of the resonant scattered radiation by vapour clouds, large optical thickness of the cloud had vitiated reliable temperature estimates. The author, during the Ba-Sr cloud release experiments, resorted to another technique which was an indirect method. In this technique the diffusion coefficients at different heights were first determined for the neutral clouds. A new analytical method was evolved to derive atmospheric temperatures from the measured diffusion profiles. A more accurate procedure for sky back-ground correction in the diffusion measurements was also developed to take account of the bright and variable twilight sky. These results, and the methods of measurement form Chapter III.

Because of the paucity of a sufficient number of rockets, for the study of dynamics of the atmosphere, theoretical studies, to derive winds were also resorted to and the study of winds at F-region heights was undertaken. From the study of winds at F-region heights, it has also been possible to investigate

the dynamics of the ionosphere and the maintenance of the night-time ionosphere. A detailed discussion of the interaction of the neutral and the ionised atmospheres from these investigations, form the subject matter of Chapter IV.

The present study, thus, provides useful and reliable observational and theoretical material for purposes of understanding the neutral atmosphere and F-region ionosphere.



## CHAPTER II

### WINDS IN THE NEUTRAL UPPER ATMOSPHERE

THE Space Research Programme of India was started in 1963, with the first rocket launch from the International Thumba Equatorial Rocket Launching Station (TERLS) carrying a sodium vapour payload. Since then 15 rocket experiments have successfully been carried out by means of sodium vapour, trimethyl aluminium (TMA) and barium-strontium releases. These vapour cloud experiments at Thumba have been a part of an extensive programme, undertaken by the Physical Research Laboratory, Ahmedabad, for the study of the equatorial upper atmosphere, including the ionosphere and the electrojet, by using rocket-borne and ground-based instruments and by theoretical investigations.

The results obtained from the first six vapour cloud experiments in the altitude region above 80 km carried out during 1963-64, for the study of neutral upper atmosphere, with sodium releases at twilight have been presented earlier in detail (BHAVSAR AND RAMNUJA RAO, 1968). In the present chapter, the first results of the measurements carried out from Thumba, of the night-time winds at the equator in the height region 90 to 125 km are presented and discussed.

The measurements of winds, during both morning and evening twilights carried out at Thumba since 1964 are also presented and compared with the earlier results.

Neutral upper atmospheric winds have been measured in many parts of the world, using vapour cloud techniques from widely spaced rocket stations. From the results of over 200 such rocket experiments, which have hitherto been available, a global neutral atmospheric circulation pattern, for the height region 100 to 180 km has been derived and presented in this chapter. Prevailing average winds have been estimated and related to the observed global temperature models at these heights.

## 2.1 EXPERIMENTAL DETAILS

### 2.1.1 Ground Equipment and Observation Sites

The method of observations followed for the present experiments was the camera technique, involving simultaneous photography of the cloud, against a star background, from two or more widely separated ground stations. The Cameras used were Kodak model, K-24, aerial reconnaissance cameras, having a field of view of  $40^\circ \times 40^\circ$  and equipped with F/2.5 lenses of focal length 17.8 cm. The cloud pictures were registered on a 12 cm x 12 cm format. To ensure the success of the observations, two cameras were installed at each camera station. The film used was the Kodak recording film no.2475. This film has almost a constant wavelength response, between  $3800 \text{ \AA}$  to  $6800 \text{ \AA}$ , with a sharp cut-off on the red-side. The characteristic curve for this film is discussed in detail in Chapter III, Section 3.3.

For the TMA releases no filter was used, the brightness of the sky background during night-time being inappreciable. For the Ba-Sr releases during twilight hours, however, Kodak Wratten series blue filters, no.44 and no.45, were used, one for each of the cameras at every camera station. These filters have maximum transmissions in the wavelength region  $4800 \text{ \AA}$  to  $4900 \text{ \AA}$ . Filter no.45 has a narrower band pass. The half transmissions lie at about  $700 \text{ \AA}$  for filter no.44 and at about  $45 \text{ \AA}$  for filter no.45, on either side of the peak transmissions.

FIG 2.1 is a Map of South India giving the relative positions of the rocket launch site and the camera stations. The magnetic equator, which is just north of Thumba, is also shown in this figure. Table 2.1, given below, lists the geographic co-ordinates (GULATTEE, 1956) and heights above mean sea level, of the sites.

Table 2.1

Coordinates of Launch Site and Camera Sites

<u>Site</u>	<u>Latitude</u>	<u>Longitude</u>	<u>Height(meters)</u>
<u>Launch Site</u>			
Thumba	$8^{\circ} 32' 28'' \text{ N}$	$76^{\circ} 51' 38'' \text{ E}$	000
<u>Camera Sites</u>			
Kottayam	$9^{\circ} 34' 05'' \text{ N}$	$76^{\circ} 31' 55'' \text{ E}$	035
Palayamcottai	$8^{\circ} 43' 00'' \text{ N}$	$77^{\circ} 44' 04'' \text{ E}$	057
Cape Comorin	$8^{\circ} 04' 44'' \text{ N}$	$77^{\circ} 32' 50'' \text{ E}$	050

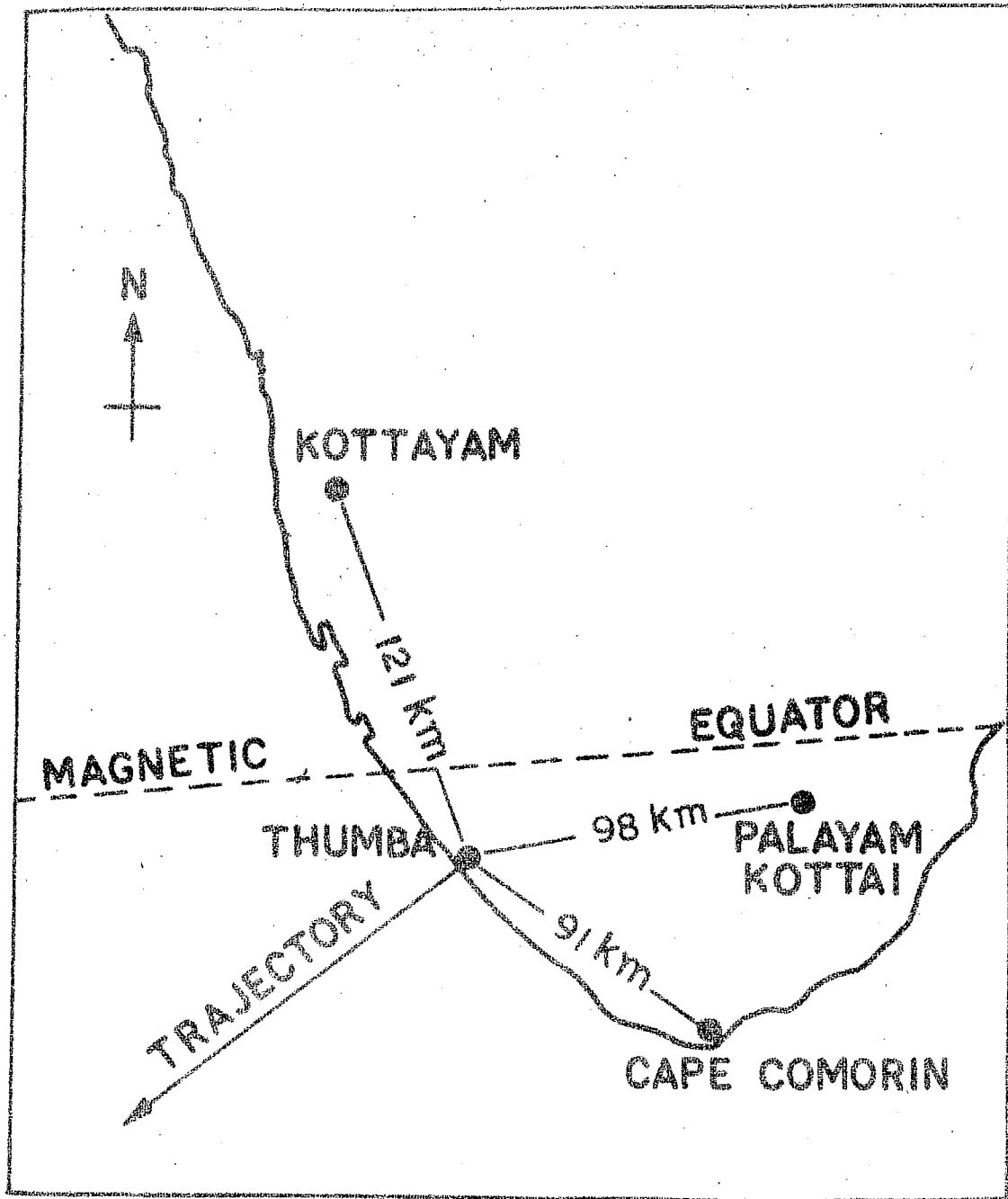


FIG 2.1 MAP OF SOUTH INDIA SHOWING LAUNCH SITE AND CAMERA SITES

The criterion for the selection of camera sites in relation to the launch site and launch direction, the details of photographic sequences, the choice of launch timings (for twilight releases), the operational procedures etc. have all been discussed in detail by MANRING AND LEVY (1961), and by RAMANUJA RAO (1966). A guide to 'Rocket Luminous Vapour Experiments', giving details of this and data reduction procedure, has been published by the COSPAR (DUBIN, 1964).

#### 2.1.2 Data Reduction

In the vapour cloud method, winds are determined from the motion of the released cloud. This requires accurate determination of the space positions of different portions of the released cloud at selected intervals of time. Several procedures have been discussed in the literature for triangulation of vapour clouds (GROVES AND OWEN, 1960; ALBRITTON ET AL., 1962; JARRETT ET AL., 1963; EDWARDS, 1963; SMITH, 1963). A numerical method combining that of JUSTUS ET AL. (1963) and SMITH (1963) was adopted by the author for the present study. The calculations were performed with the help of IBM 1620 computer.

In the method used, the first step was the calculation of the orientation of the camera axis at each station. This was obtained with the help of the positions of the known stars registered on the photograph containing the cloud picture

(JUSTUS ET AL., 1963). For star identification, NORTAN'S STAR ATLAS (1969) was used. The positions of the stars for the times of observation were taken from the Indian Ephemeris and Nautical Almanac.

Next, assuming a cylindrical shape for the vapour cloud trails appearing on the photograph, a visual central line along its axis was drawn on each photograph, and the data points on this central line were read very closely on an x-y coordinate-measuring microscope. For the Ba-Sr releases, the centre points of the clouds were determined from the densitometric scans (Chapter III). The image plate-coordinates of these points, relative to the fiducial marks on each plate, were then transformed with the help of camera axes calculated earlier to azimuth and elevation corresponding to the observation station.

The geometry shown in FIG 2.2 illustrates the triangulation method. The azimuth and elevation angles of the vapour points calculated as above, would be relative to planes parallel to the earth's surface at the respective stations, A, and B, in the figure. To correct for the earth's curvature, the azimuth and elevation angles are converted to a plane parallel to the earth's surface at a point P, on the earth, approximately below the cloud. The position of P can be estimated from a preliminary space triangulation. The conversion is easily achieved by using the latitude and longitude

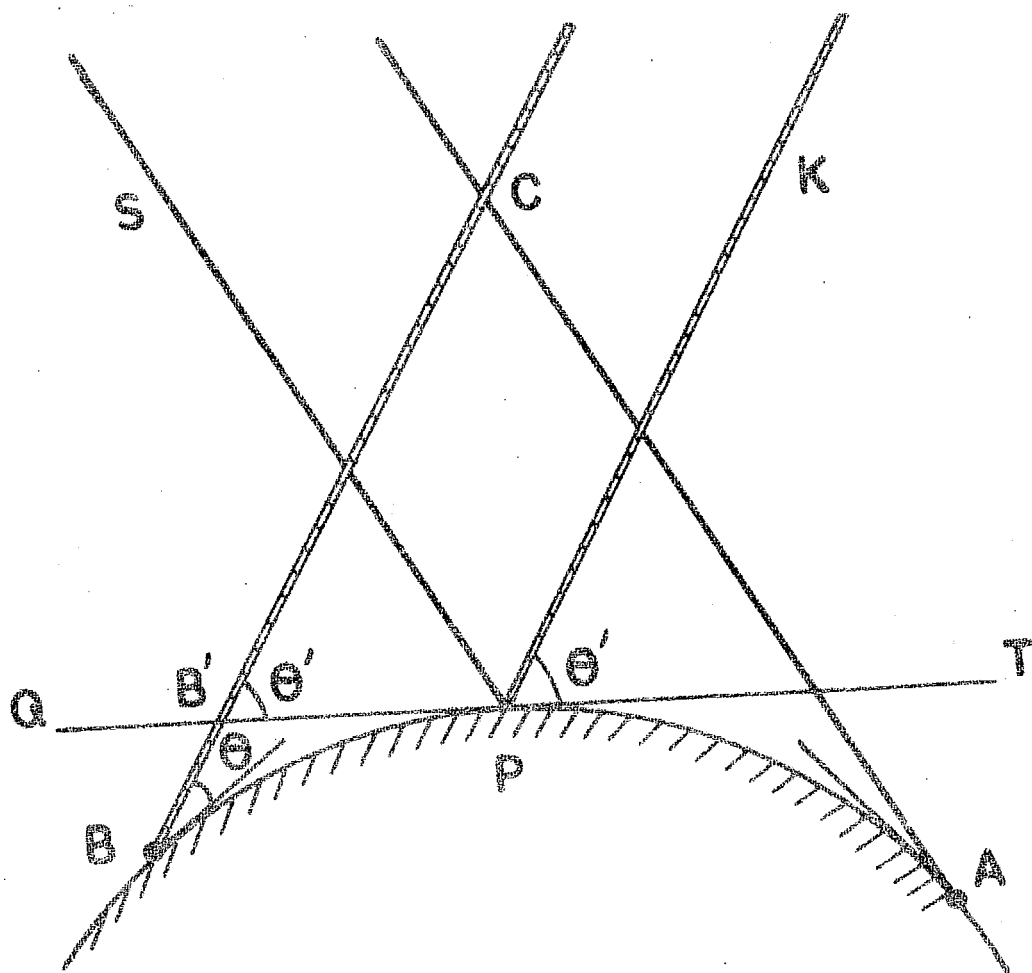


FIG 2.2 : Geometry illustrating triangulation procedure and the effect of curvature of the earth's surface.

of P, instead of those of A and B, for calculating the camera axes.

Choosing a right-handed cartesian coordinate system with x,y,z axes pointing towards south, east and zenith respectively at P, the cartesian coordinates of the camera stations A and B relative to P are worked out from a knowledge of the latitude and longitude of the three places.

If  $(x_1, y_1, z_1)$  and  $(x_2, y_2, z_2)$  be the coordinates of A and B respectively and  $(x, y, z)$  be those of a cloud point, C, and if  $(a_1, e_1)$  and  $(a_2, e_2)$  be the azimuths and elevations of C with respect to A and B respectively, relative to the plane through P, the equation of the line AC would be

$$\frac{x-x_1}{l_1} = \frac{y-y_1}{m_1} = \frac{z-z_1}{p_1} \quad (2.1)$$

where  $l_1, m_1, p_1$  are the direction cosines of the line AC. A similar equation can be written for BC.

In general, AC and BC may be skew lines and may not intersect. The minimum perpendicular distance between the two lines is given by

$$F_{12} = \begin{vmatrix} x_1 & x_2 & l_1 & l_2 \\ y_1 & y_2 & m_1 & m_2 \\ z_1 & z_2 & p_1 & p_2 \\ 1 & 1 & 0 & 0 \end{vmatrix} \times K \quad (2.2)$$



where  $K = [\sum (m_1 p_2 - m_2 p_1)^2]^{-\frac{1}{2}}$

If  $C_1$  and  $C_2$  are the ends of this perpendicular, the former on the line from A, and the latter on that from B, the sign of  $F_{12}$  depends on whether  $C_1 C_2$  makes a right-handed or left-handed frame of reference with  $C_1 A$  and  $C_2 B$ . Ideally  $F_{12} = 0$ ; in practice, however, due to many experimental and numerical limitations, this is not so. The best approximation for C is the mid-point of  $C_1 C_2$ . The vector position,  $\underline{R}$ , of the point C is, then given by (SMITH, 1963)

$$\begin{aligned} \underline{R} = & \frac{1}{2} (\underline{r}_1 + \underline{r}_2) \\ & + \frac{1}{2 |\hat{n}_1 \times \hat{n}_2|^2} \{ \hat{n}_1 (\underline{r}_2 - \underline{r}_1) \cdot [\hat{n}_1 - \hat{n}_2 (\hat{n}_1 \cdot \hat{n}_2)] \\ & + \hat{n}_2 (\underline{r}_1 - \underline{r}_2) \cdot [\hat{n}_2 - \hat{n}_1 (\hat{n}_2 \cdot \hat{n}_1)] \} \quad (2.3) \end{aligned}$$

where  $\underline{r}_1$  and  $\underline{r}_2$  are the vector positions of A and B, and  $\hat{n}_1$  and  $\hat{n}_2$  are the unit vectors from A to  $C_1$  and B to  $C_2$  respectively. The height of C relative to the plane through P is finally converted to that with respect to the surface of the earth by calculating the horizontal distance of the perpendicular from C on the plane through P.

For the spherical clouds and for those parts of the trails which are clearly identifiable as corresponding points on the photographs from the two camera stations, the above procedure is easily applied to determine the cloud position.

In the case of smooth portions of trails, the corresponding points are found by keeping the line of sight from one camera station fixed and searching for two adjacent points on the photograph from the other station which give a change of sign in the minimum perpendicular distance with the line of sight from the first station.

## 2.2 ERRORS IN CLOUD POSITIONS

### 2.2.1 Systematic Errors

#### a) Earth's Curvature

The neglect of earth's curvature introduces an error equivalent to the difference between the angles  $\theta$  and  $\theta'$  of FIG 2.2. The effect of this is principally an error  $\Delta z$  in  $z$  (height) given approximately by

$$\Delta z = - z^2/R$$

where  $R$  is the earth's radius. This effect has been appropriately considered by choosing a plane on the surface of the earth, approximately below the cloud, as discussed earlier.

#### b) Refraction Through the Glass Plate

The glass plate in the camera, against which the photographic film is pressed, causes refraction of the light rays from the object being photographed before they form image on the film. This error has been analytically worked out by

JUSTUS ET AL. (1963) and has been shown to be about 0.001 cm at a distance of 9 cm from the centre. The accuracy of the travelling microscope used for plate measurements being of the same order, this error has not been considered significant.

c) Film-shrinkage, Photographic-paper Expansion, Contraction etc.

To estimate the error due to change in the distances between the fiducial marks on different photographic films and prints used for data reduction, it was examined for one particular launch very carefully. It was found that this error was smaller than the error of measurements. Hence this error has not been taken into account.

d) Camera Tilt

This is determined in the process of determination of camera axis with the help of background stars (JUSTUS ET AL., 1963). The tilt in the present experiment, was upto  $2^{\circ}$  in some cases, and has been duly accounted for in the reductions as described by JUSTUS ET AL.

e) Atmospheric Refraction

The effect of this is to displace the objects towards the observer's zenith, and is larger for larger zenith distances. Following the procedure of JUSTUS ET AL. (1963), this correction for different elevations, atmospheric pressures, temperatures etc., was calculated. Even at zenith distances

of  $60^\circ$ , the correction due to this amounted to only about two minutes of arc, amounting to a positional error of about 0.1 km at a range of 200 km. This has again been considered insignificant in the present analysis.

#### f) Distortion of the Camera Lens

A thorough analysis was carried out for ascertaining distortion of all cameras, which could be expected to be significant at the periphery of the field of view. Assuming little or no distortion within a radius of 1.5 cm from the camera axis, from the known group of stars photographed all over the field of view, the stars within the 1.5 cm radius from the format centre were used to calculate the positions of stars beyond this radius. The difference between the observed and calculated positions of the stars was attributed to distortions. FIG 2.3 shows the plot of distortion vs observed positions of all the stars including those within 1.5 cm radius. The scatter plot shows no significant tendency for departures even at greater distances from the centre. Even near the centre, departures of about 0.01 cm from the calculated positions are discerned. This clearly shows distortion to be insignificant compared to reading errors.

### 2.2.2 Accidental Errors

#### a) Camera Station Coordinates

The errors in the coordinates of the camera stations would contribute to an error in the base line, which is

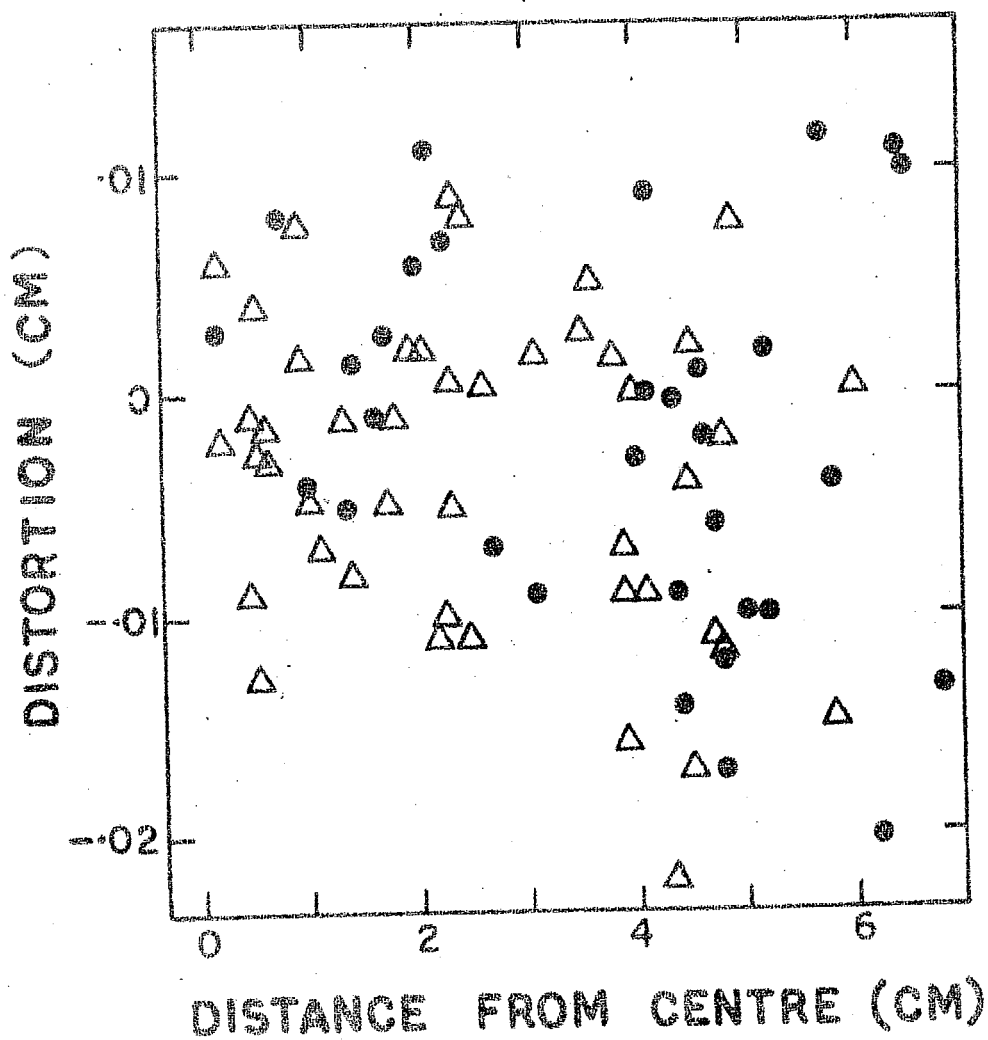


FIG 2.3 : Camera Distortion. The marks ● and △ show the distortion calculated for two different cameras.

expected to be not more than about 50 meters (Survey of India-Private Communication). This would introduce an error of about the same order in the cloud positions.

b) Trail and Camera Station Orientation

The limitations on accuracy and resolution are determined essentially by physical considerations pertaining to the trail and not by the method of data reduction. Comparison of the results of various triangulation combinations from all the observing sites would be a valuable check. WHITEHEAD (1972), commenting on the triangulation techniques, concludes that an increase in the number of the observing sites is the only way of determining detailed structure of complicated clouds, however good the camera resolution may be. It is also important from the accuracy point of view that the observing sites and launch sites are properly chosen, particularly in relation to the solar illumination, for twilight releases.

Although three camera stations were established for the present experiment, weather stood in the way of simultaneous observations from all the three camera stations excepting on one or two occasions. To cater for the weather, additional camera stations would have been of advantage. Successful simultaneous observations from three or more camera stations would have the further advantage that the cloud can be photographed from different orientations and that its correct profile can be ascertained. This is

especially so, in the case of long trails and where trails are released both in the up-and down-leg of the rocket trajectory. However, in the present study the profiles of the releases did not present any major problem, since the TMA releases were at altitudes below 130 km and the Ba-Sr clouds were only point releases.

### c) Centering and Reading Errors

The major source of error in the analysis is in drawing the central line of the trail. Uncertainties, in drawing the central line, result from distortion due to wind shear, uneven illumination by solar rays (in case of twilight releases), smearing of the image due to large winds, diffusion (particularly at high altitudes), irregular trail structure and camera orientation.

A large number of stars (a minimum of 8 to 10) were read on the film for fixing the camera axis, and it was found that each combination of two stars gave values of azimuth, elevation and tilt of camera differing by not more than 0.5' of arc, and values of focal length differing by not more than 0.01 cm. It is thus considered that errors in reading star positions are considerably smaller compared to the central line drawing.

The error in drawing the central line is generally small at lower altitudes where the edges are usually sharp.

This error becomes larger at greater heights - beyond 130-140 km. The minimum perpendicular distance,  $F_{12}$  (expression 2.2), might provide a fair check on the accuracy of measurements. In the present analysis,  $F_{12}$  ranged from 50 to 200 meters. As the TMA trails were observed only below 130 km, the centering error was taken as not more than 0.05 cm. The centering error for Ba-Sr point clouds was assumed less. An error of 0.05 cm was assumed for the 200 km Barium cloud and the error in position determined. The error estimates due to centering, on azimuth and elevation were made, and thence the error in x,y,z coordinates of the vapour trail, by differentiating the expression 2.3 for  $R$  and these are listed below:

<u>Range of the cloud (km)</u>	<u>Total positional error in x,y,z (km)</u>
300 km	4 km
150 km	2 km
100 km	1 km

### 2.2.3 Errors in Wind Velocities

A major contribution to the error in determining wind velocity comes from the inaccurate location of the centre of the cloud on the photograph and hence of its position in space. If two photographs separated by time  $t$  are used in determining the wind velocity at any height, and if horizontal positional errors be  $\Delta x_1$  and  $\Delta x_2$ , the wind velocity,  $v$ , and the



corresponding error,  $\Delta v$ , will be given by

$$v \pm \Delta v = \frac{(x_1 \pm \Delta x_1) - (x_2 \pm \Delta x_2)}{t}.$$

Maximum error in velocity,  $\Delta v$ , is then

$$\Delta v = \frac{\Delta x_1 + \Delta x_2}{t}.$$

For positional errors of 2 km and time intervals between two photographs of the order of 600 secs, the error would amount to about  $7-8 \text{ m sec}^{-1}$ . It will thus be seen that, if the time interval between two photographs chosen for wind determination is large enough, the error would be smaller. Wind fluctuations, if any, of a smaller scale, would, however, be suppressed by such large time separations.

## 2.3 RESULTS AND DISCUSSIONS

### 2.3.1 Chronology of the Experiments

Table 2.2 lists the dates and times of the rocket launchings conducted from Thumba for vapour cloud releases reported in the present thesis. All the experiments were conducted on magnetically quiet days except the one of 31st March 1968 morning twilight. This is evident from the 3-hourly  $K_p$  indices listed in the last coloumn of the table. The barium-strontium release experiments were a part of a collaborative programme with the Max Planck Institute, West Germany for

TABLE 2.2

Vapour Cloud Experiments Conducted from Thumba Equatorial Rocket Launching Station  
(TEKLS) for Upper Atmospheric Studies during 1966 to 1971.

THUMBA: Geographic Latitude 8.5°N, Longitude 76.9° E, Magnetic Latitude 0.8° S

	Time of launching (IST)*	Rocket	Payload	Height Range (km)	Three hourly K <sub>p</sub>	Remarks
24-3-1966	2215	Centaure	TMA	105-125	0 <sub>+</sub>	First Night-time launch over Thumba.
25-3-1966	0230	Centaure	TMA	105-125	2 <sub>+</sub>	
12-3-1967	2230	Centaure	TMA	90-120	1 <sub>-</sub>	
28-3-1968	1855	Nike Apache	Ba-Sr	135-205	2 <sub>o</sub>	Cloudy weather. Observa- tions at 200 km cloud and 135 km cloud vitiated.
30-3-1968	1855	Nike Apache	Ba-Sr	105-205	3 <sub>-</sub>	
31-3-1968	0537	Nike Apache	Ba-Sr	150-175	4 <sub>+</sub>	
** 31-3-1968	1745	Nike Apache	Ba-Sr	150	2 <sub>-</sub>	
** 19-4-1971	1855	Nike Apache	Na	90-150	1 <sub>o</sub>	

Note: \* IST = 82.5° East Meridian Time (Indian Standard Time) = U.T. + 5.5 hr

\*\* The results from these two launchings have not been included in the present study, except for broadly corroborating some other inferences.

the study of electric fields in the equatorial ionosphere over Thumba. Only the wind results, obtained by tracking the neutral strontium clouds in those experiments, are presented here. The ion drifts obtained by tracking the barium cloud, are mentioned only for the sake of comparison of motions of neutral and ionised clouds in the upper atmosphere.

The neutral atmospheric wind velocities were determined by photographic tracking and subsequent triangulation of the vapour trails and clouds as described earlier. For night-time wind studies, the TMA releases produced chemi-luminescent trails only at heights below 125 km. Thus, the neutral atmospheric winds at night-time were measured in this first study, in the equatorial upper atmosphere, between the height region 90 to 125 km only. The winds at twilight were measured by tracking the neutral strontium clouds upto 200 km altitude.

In the figures and discussions that follow the under-mentioned conventions have been adopted for designating the direction of the wind motion:

- i) westerly, or eastward, wind to mean wind blowing from west to east, designated positive.
- ii) easterly, or westward, wind to mean wind blowing from east to west, designated negative.

iii)\* southerly, or northward wind to mean wind blowing from south to north, designated positive.

iv)\* northerly, or southward, wind to mean wind blowing from north to south, designated negative.

### 2.3.2 Earlier Results Near the Equator from Studies Conducted at Thumba

Six sodium vapour release experiments had been conducted during northern hemispheric winter months in 1963-64 from Thumba (BHAVSAR AND RAMANUJA RAO, 1968). These experiments, three during morning twilight and three during evening twilight hours, gave important information about the character of the winds near the equator for the first time. Following are some of the important findings of this earlier study:

- i) The wind maximum occurs between 100 and 110 km, the average height where this maximum occurs being around 107 km, and the average wind speed at the maximum is about  $106 \text{ m sec}^{-1}$ .

---

\*Note: The designation of positive winds, in the meridional direction, is winds blowing from north to south in Chapter IV. This has been done to keep consistency with the designation of other workers.

- ii) Two minima are seen in all the wind profiles, one around 112 km and the other between 135 and 150 km.
- iii) In the 100-110 km region, large wind shears are observed, similar to those observed at other latitudes.
- iv) The zonal winds at Thumba are towards the east in the height region of 115-140 km and towards the west in the height region of 140-180 km.
- v) The meridional component of winds shows irregular variations with height upto about 150 km and thereafter it is mostly towards the north.
- vi) The winds show a diurnal variation between 130-170 km, the evening twilight winds being stronger than those of the morning twilight.
- vii) The rotation of the wind vector with height does not show any regular pattern.

### 2.3.3 Night-time Neutral Atmospheric Winds Over Thumba

The three TMA releases experiments conducted over Thumba, two during the same night on March 1966, and the third, an year later, during the same month as the first two, have yielded useful results. These first results of night-time winds near the equator are presented and compared with

winds at evening and morning twilights. All the three night-time wind profiles, which were confined to 90 to 125 km height region, showed typical characteristics of winds in this height region, namely, wind shears and wave like structures, and smaller irregular-structures superimposed on them. In the discussions that follow, the three TMA releases have been designated as under:-

24-3-1966,	2215	IST	TMA-I
25-3-1966,	0230	IST	TMA-II
12-3-1967,	2230	IST	TMA-III

#### a) Meridional Winds

The north and south components of the wind velocities at different heights, as observed from TMA-I, II and III, are shown in FIG 2.4. The average winds observed at twilight are also plotted for comparison. The two releases, TMA-I and II, which were conducted during the same night, but separated by about 4 hours, show completely opposite behaviour in the whole altitude region under observation. TMA-III, however, shows a behaviour similar to that of TMA-I from about 115 km upwards, the winds having a prominent southward component. It is significant to note that TMA-I and TMA-III experiments were conducted at the same local time one year apart. The large shears which are so commonly observed in the individual

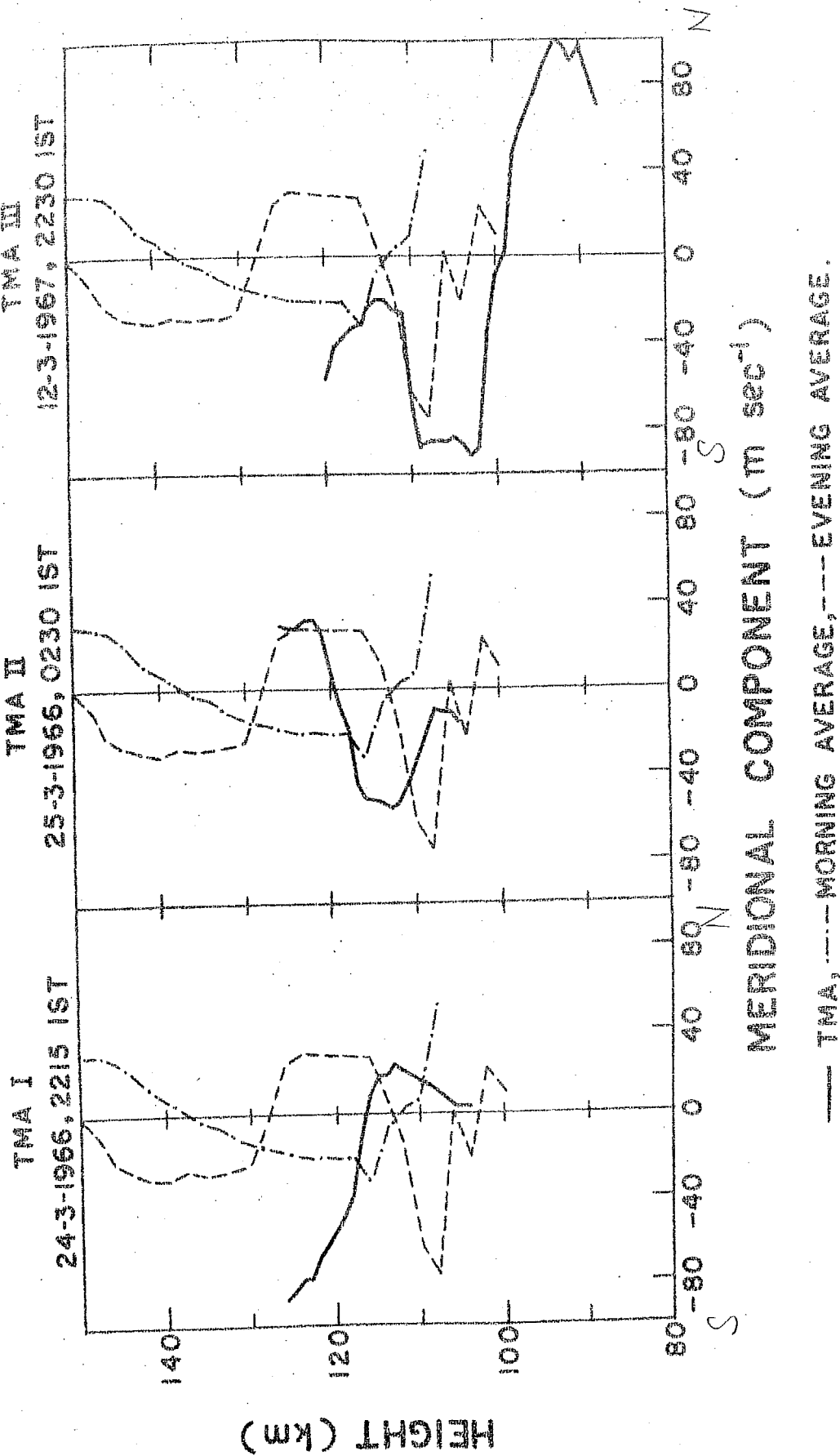


FIG 2.4 : Meridional component of winds over Tamba from the three night-time TMA releases.

profiles during twilight releases at all latitudes are less prominent in these night-time releases. However, wind shears are not totally absent. TMA-III shows a north to south (N to S) shear of  $0.02 \text{ sec}^{-1}$  between 93-103 km. Shears, in the meridional component, observed during twilight, averaged to about  $0.025 \text{ sec}^{-1}$  N to S, and about  $0.015 \text{ sec}^{-1}$  S to N over Thumba, though on one occasion a N to S shear as high as  $0.08 \text{ sec}^{-1}$  was observed.

#### b) Zonal Winds

FIG 2.5 shows the zonal wind components observed at night during TMA-I, II and III releases alongwith the average morning and evening zonal wind profiles. The TMA-I and III show almost a similar behaviour, except for the altitude difference for the major characteristics. The maximum of wind velocity at 110 km for TMA-I continues to be evident in TMA-II, though of a reduced magnitude. The shears are smaller for TMA-III, the W to E shear being  $0.015 \text{ sec}^{-1}$  at 92 km. The W to E shears were more often observed than the E to W shears during the twilight observations.

The twilight winds, as mentioned in Section 2.3.2, have shown regular eastward winds in the height region 115 to 140 km. For TMA-I and III, the winds in the region 115 to 120 km are towards west while for TMA-II they show an eastward component.



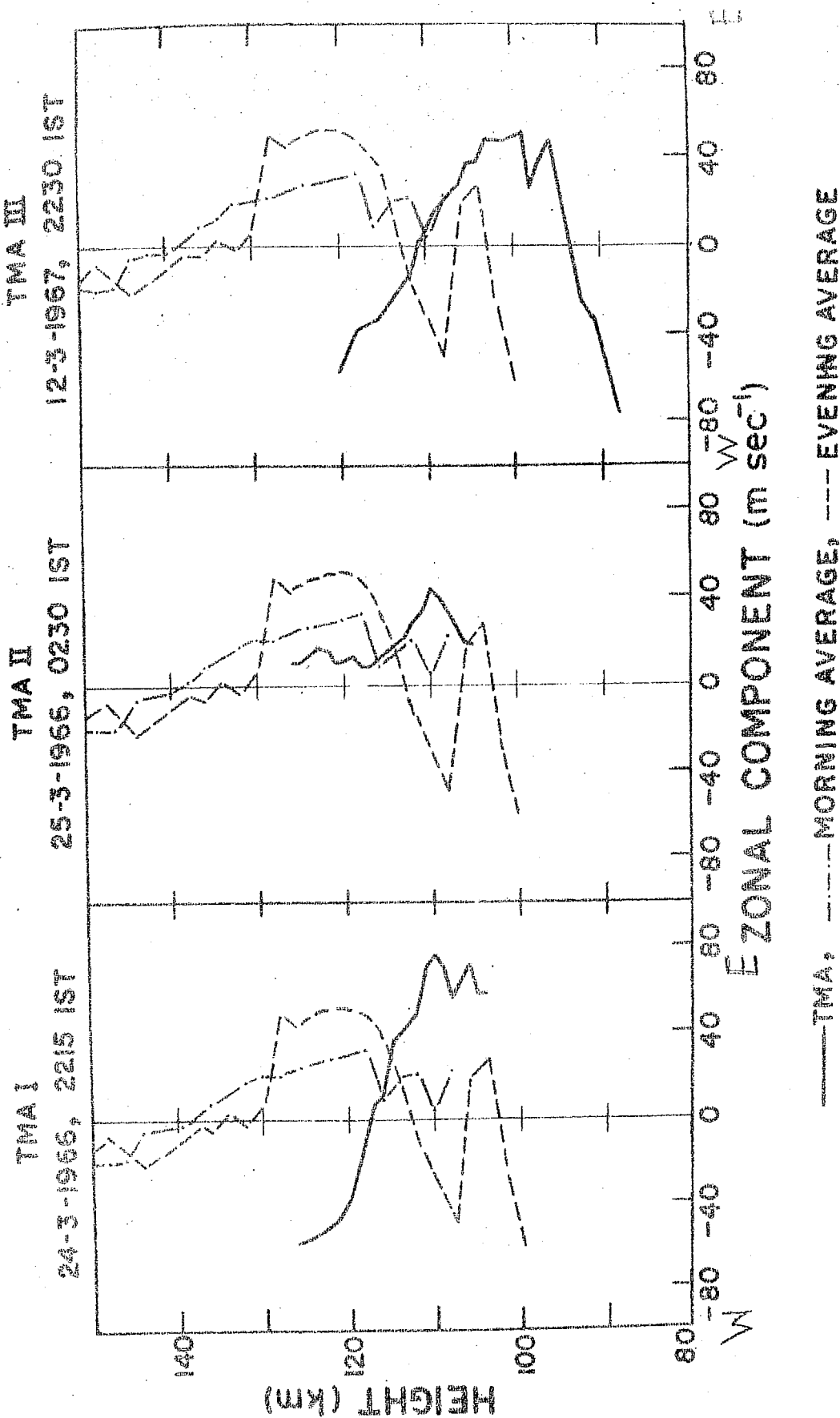


FIG 2.5 : Zonal component of winds over Thumba from the three night-time TMA releases.

### c) Speed Profiles

The variation of wind speed with height, for the three TMA releases are shown in FIG 2.6. The average speeds for the twilights have also been shown. The results of TMA-I and III, which relate to times prior to mid-night, show a behaviour of increasing wind speed above 115 km, whereas those of TMA-II, which relates to a time after mid-night, appears to follow the morning twilight average behaviour. The results of TMA-I and II together show an upward shift of the characteristic features in 4 hours, yielding an average upward velocity of  $0.5 \text{ m sec}^{-1}$ . It may be noted that this result is in disagreement with the findings of BHAVSAR AND RAMANUJA RAO (1968), who from a study of two sodium releases, one on the evening twilight of 9th November 1964 and the next on the succeeding morning twilight of 10th November 1964, had reported that there was a downward movement of some observable features.

The present result does not conform either to the tidal hypothesis (downward phase motion) or to the thermal expansion. Between the two TMA releases, the atmosphere can only be expected to be still in the process of cooling down, and hence, only downward movements due to this cause should be observed.

Because of the limited altitude-coverage of the present wind profiles, it is likely that erroneous identification of similar features might have been made to interpret the

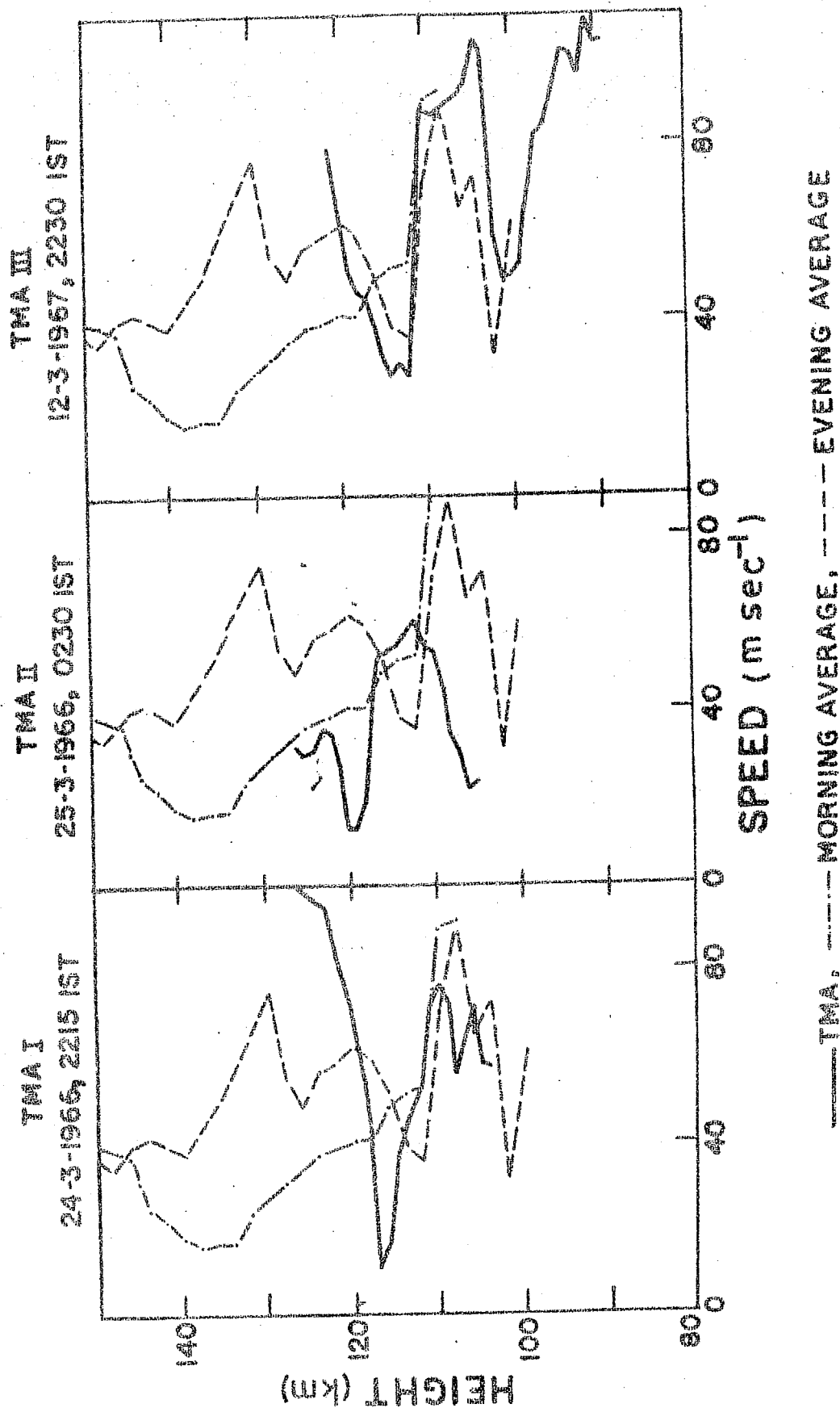


FIG 2.6 : Wind speeds over Thumba from the three night-time TMA releases.

features as progressing upwards. A series of four to five launchings, spread over the night only can resolve such ambiguities.

#### d) Rotation of the Wind Vectors

The wind velocity hod-ographs for the three experiments are shown in FIG 2.7. TMA-I and II profiles show no large variations of wind direction over the altitude range of observation. The sense of rotation of wind vector is different in the two cases. TMA-III shows a smooth clockwise rotation behaviour. These results, together with the twilight results at Thumba, show a mixed behaviour of the wind vector rotation with altitude. The results from Barbados ( $13^{\circ}$  N) (MURPHY AND BULL, 1967), Hawaii ( $22^{\circ}$  N) (BEDINGER, 1966) and Sonmiani ( $25^{\circ}$  N) (SHAFI AHMAD, 1966, 1967) confirm the contention of a transition zone for the tidal behaviour of winds over low latitudes (on either side of the equator), sometimes extending to the latitude of Sonmiani.

BEDINGER ET AL. (1968) have concluded, from the Wallops Island observations, that the spiral pattern of the hodograph is associated with large wind speeds, whereas irregular hodograph pattern is associated with low wind speeds. The three TMA results have shown no large wind speeds, nor has any irregular pattern been observed in the hodographs. The earlier twilight observations at Thumba (RAMANUJA RAO,

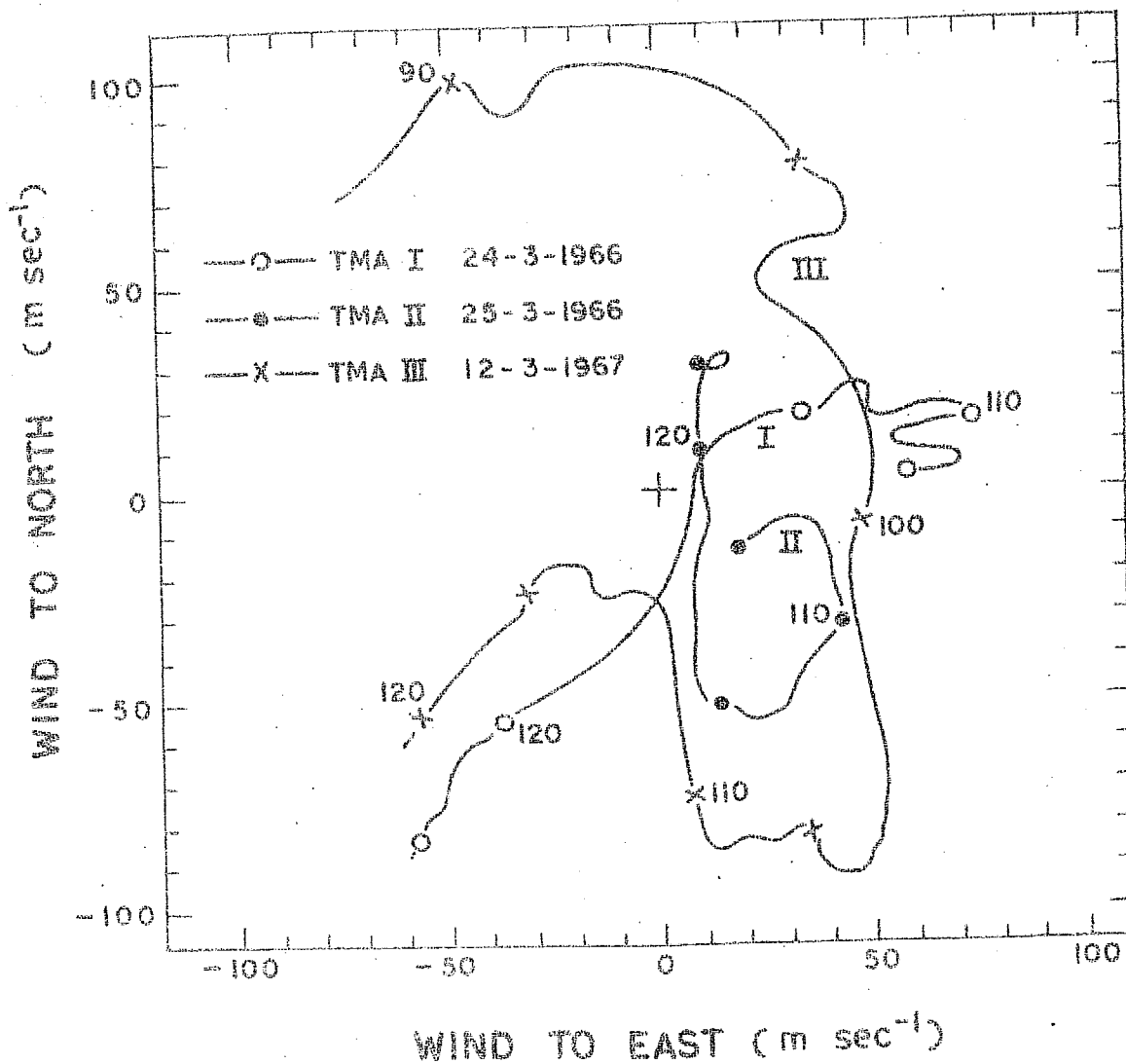


FIG 2.7 : Hodograph of wind vectors over Thumba during the three night-time TMA releases. o, ●, and x show 5 km marks on the curves.

1966) do, however, support to some extent such conclusions of BEDINGER ET AL.

#### 2.3.4 Results obtained from Ba-Sr Releases at Twilight from Thumba

As the Ba-Sr experiments were point releases made at discrete heights, 20 to 30 km apart in the vertical direction covering the altitude region of 100 to 200 km, complete vertical profiles of the winds could not be obtained. Hence, shears as well as vertical structure, of winds could not be studied. However, being point releases, they served as good tracers for studying vertical motions and growth rates. The morning release of 31st March 1968 was only partially successful due to bad weather, thus rendering measurements only on two clouds.

The results from these experiments are presented in Table 2.3, and in FIG 2.8. The ion motions are also shown. It is seen that, in general, the two evening observations correspond well with one another, in both meridional and zonal components and in other general behaviour. For comparison, the average evening and morning velocity profiles, obtained from earlier sodium releases, are also shown in FIG 2.8.

##### a) Meridional Component of Winds

The evening twilight release of 28th March, vide FIG 2.8 (a), shows that the meridional wind over Thumba, around 135 km, is towards the north which decreases to a

Table 2.3

## Ba-Sr Releases - Neutral and Ion Velocities

Height (km)	Neutral velocities ( $\text{m sec}^{-1}$ )		Ion velocities ( $\text{m sec}^{-1}$ )					
	To East	To North	Speed	Direction	To East	To North	Vertical	Horizontal
28-3-1968, 1855 IST								
205	0	-35	35	180°	-80	-35	-25	86
174	-55	-25	60	250°	-90	-30	-25	92
152	-50 to -100	+ 5	50 to 100	270°	-100	-15	-25	100
133	-30	+40	50	320°				
30-3-1968, 1855 IST								
204	+10	-12	16	140°	-75	- 8	-35	76
180	-40	+15 to -10	42	270°	-80	0	-35	80
152	-70	+ 5	70	270°	-80	+ 5	-25	80
106	+55	-20	58	110°				
31-3-1968, 0537 IST								
175	-10	+50	51	350°	+58	+70	+74	91
148	-48	-60	75	215°				

\* Note : Direction of wind vector from north through east.

## Ba - Sr CLOUD

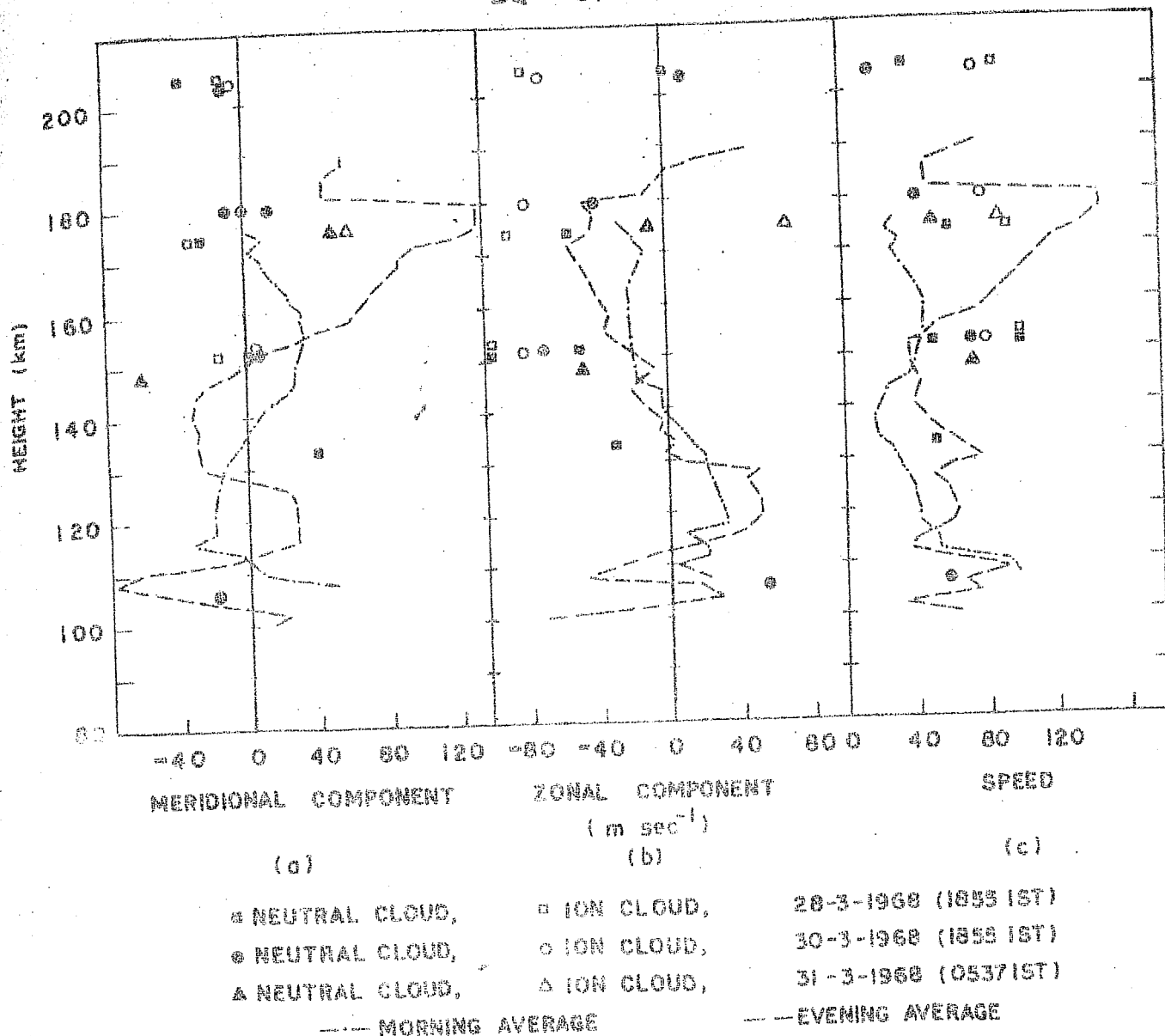


FIG 2.8 : Meridional and zonal components and wind speeds at discrete heights over Thumba from the three twilight Ba-Sr point releases. Both neutral and ionised cloud drifts are shown and are compared with earlier results of morning and evening winds obtained from sodium releases.



very small magnitude around 150 km and then changes direction to the south at higher altitudes. The evening twilight release of 30th March shows that this changeover from north to south takes place at a great height. The morning twilight release of 31st March shows, however, that the wind which is southward below 150 km changes northward above this height.

Earlier twilight observations over Thumba have shown that during the northern hemisphere winter (November-January), the wind in the evening has northward meridional component continuously increasing with height in the 150 to 190 km altitude region. The morning observations have shown that the northward component decreases with height, suggesting that it would reverse in the height range 170-180 km.

The present results suggest that the meridional flow is opposite in direction in summer from what it is in winter, the changeover probably occurring during the equinox. This behaviour is shown in more detail in the general global circulation pattern, vide Section 2.4.4.

#### b) Zonal Component of Winds

The zonal wind component, observed by tracking the neutral strontium clouds during Ba-Sr releases, is shown in FIG 2.8 (b). The evening observations, of the 28th and 30th March, 1968, as well as the morning observation of the 31st March, all show predominantly westward wind, with a maximum

around an altitude of 150 km, decreasing thereafter to a small magnitude, and ultimately reversing its direction to eastward wind above 200 km. The zonal flow seems to be in general agreement with that observed by BHAVSAR AND RAMANUJA RAO. They had shown that over Thumba, above 140 km, the zonal winds were mostly towards the west and on three occasions the winds exhibited a tendency to reverse above 180 km.

The present results seem to confirm the super-rotation hypothesis advocated by KING-HELE (1964). This is discussed in greater detail in Section 2.4.3.

#### c) Wind Speed at Different Altitudes

From FIG 2.8 (c), where the speeds for the three releases are shown, a tendency of almost constant wind over the whole altitude region will be evident. These results fall under the morning twilight category of winds reported by BHAVSAR AND RAMANUJA RAO and shown to be decreasing with height. From earlier wind measurements, a wind minimum was reported at around 150 km over Thumba. Such a behaviour is, however, not discerned from the present results.

#### 2.3.5 Propagating Waves

The highest cloud release (205 km) of 28th March 1968 descended, after about 12 minutes of observation, by as much as 15 km in 8 minutes. This gave a vertical downward velocity of about  $30 \text{ m sec}^{-1}$ . In the first 12 minutes it had, however,

maintained a constant height. The 152 km cloud release, on the same day, had also shown a vertical motion, revealed about 20 minutes after the release, but the motion in this case was upwards by about 6 km in 6 minutes. This yielded a vertical upward velocity of about  $16 \text{ m sec}^{-1}$ . The 135 km and 175 km releases, on the other hand, did not show any vertical motion. (The vertical motions of the 205 km and 152 km releases are not shown in FIG 2.8, in order to maintain the clarity of the figure. Only the heights, which these two clouds maintained for a major period of observation, are indicated in the figure).

On 28th March the 152 km release, and on 30th March the 180 km release, showed horizontal wind velocity variations during the observation period. In the former case, it was the zonal velocity, and in the latter case, it was the meridional velocity, that changed.

In FIG 2.9 the movements, as a function of time, of the clouds which had shown a vertical motion, as well as of those which had shown varying horizontal winds, have been presented.

The Ba-Sr releases of 28th March seem to manifest a propagating wave phenomena, as seen from the height-time plot of FIG 2.9 (a). Vertical wavelength of the order of 80 km can be discerned in the vertical velocity. It is also

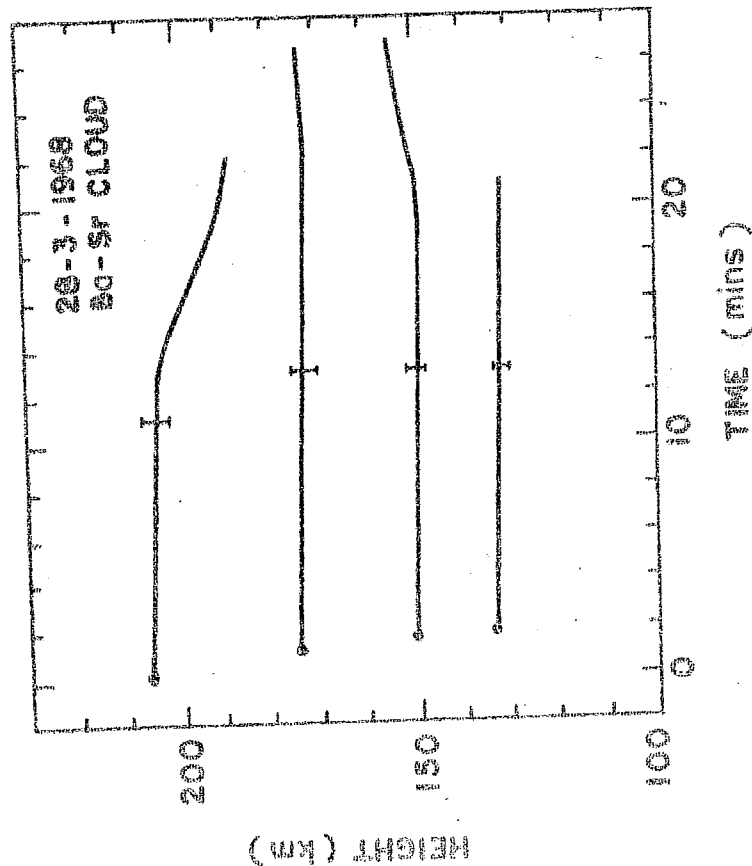
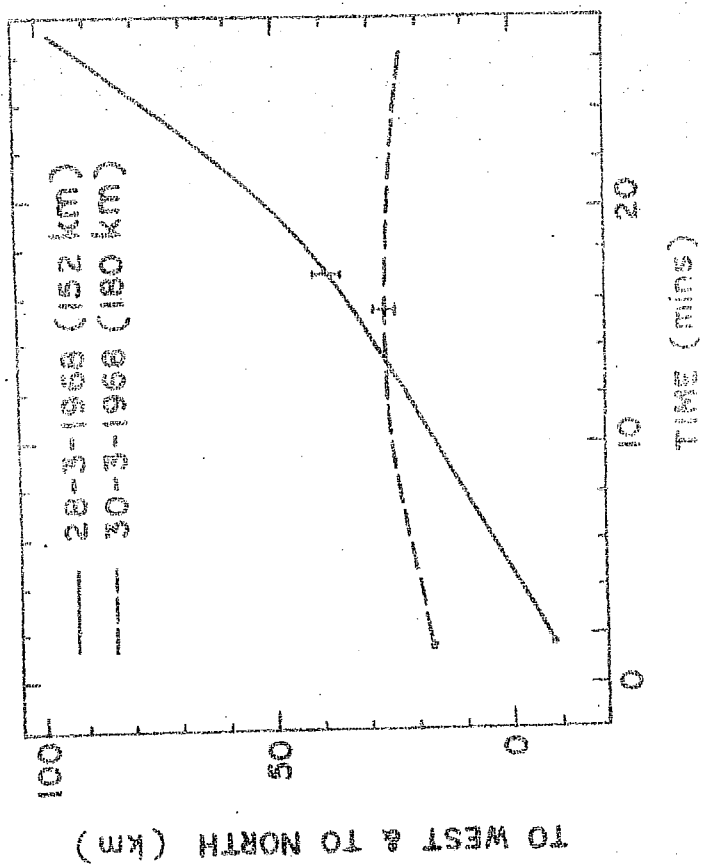


FIG 2.9 : (a) Heights of the four neutral Ba-Sr clouds released over Thumba on 28-3-1968, as a function of time.



(b) Horizontal motions of neutral Ba-Sr clouds released at 152 km on 28-3-68, and at 180 km on 30-3-1968 as a function of time.

seen that this wavelength is increasing in the upward direction, and that the amplitude of the wave is also increasing with altitude.

It is presumed that a similar horizontally propagating wave would have caused the horizontal wind velocity changes, as seen from FIG 2.9 (b), on the 152 km cloud of 28th and to a lesser extent on the 180 km cloud of the 30th.

Minimum periods of about 1 hour for the horizontal waves could be estimated at these heights, if the total observation period is considered to be the half-period of the wave-pattern. The vertical wavelength derived for the vertical winds is in good agreement with the theoretical estimates and the period derived for horizontal winds is also not inconsistent.

The other possibility for the cause of varying horizontal winds could be that, as the 152 km cloud changed its height, horizontal velocity changes have also taken place corresponding to its new height. DESAI (Private Communication) also reports such velocity variation from change in height of cloud position from the analysis of Ba-Sr clouds released at 130 km altitude over Thumba during January 1972. However, the large velocity variations, of the order of  $50 \text{ m sec}^{-1}$  in about 5 to 10 km altitude change, which were observed on 28th March, are normally not expected at this height.

### 2.3.6 Turbulence

A remarkable feature, observed on the vapour trails released in the upper atmosphere, is the apparently sudden cessation of turbulence at about 100 km level. Whereas the trail picture below this altitude shows a patchy and uneven structure, the portion above is smooth. In general, this has been accepted as an evidence for the existence of sharp turbo-pause level, separating turbulent region of atmosphere below, from the non-turbulent region above. There has, however, been a different view also, held by LAYZER AND BEDINGER (1969), who consider the observed patchiness of the trail to be due to instabilities generated because of the release of energy by the rocket ascending into the region of decreasing gas density.

*Campan*

These authors compare the photographs of the trails in the up- and down-leg portions of the releases and show that it is only the up-leg portions which show the patchy structure below 100 km. Down-leg releases, on the other hand, have been, according to them, difficult to classify, but, yet, they maintain that these show no distortion, and therefore no turbulence.

Only BLAMONT AND DE JAGER (1961) have, so far, shown evidence of turbulence features on the simultaneous up- and down-legs of the trail release. Recently LLOYD ET AL. (1973)

have shown clear evidences of turbulence in the down-leg release of a vapour cloud released from 150 down to 92 km.

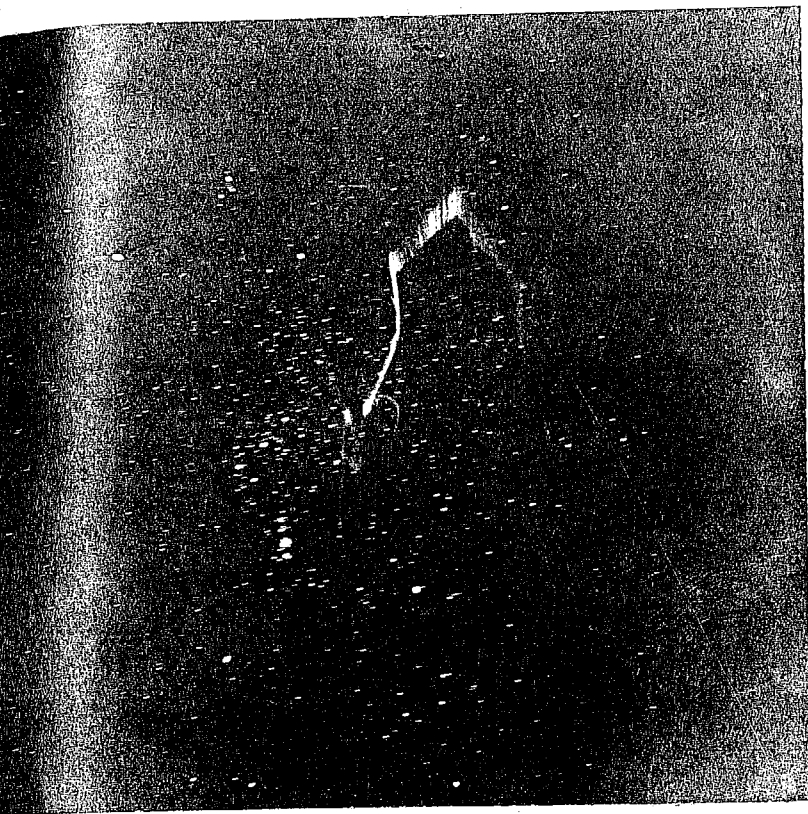
A photograph of the sodium cloud, released on the up-leg on 19 April 1971 from Thumba, indicating turbulence features, is shown on page 114. The turbopause was located at around 100 km. The TMA III release of 12 March 1967, has also shown some evidence of turbulence. This release was carried out during the down-leg of the rocket trajectory. A photograph of this cloud is also shown on page 114. The turbopause height was located at 96 km in this photograph.

A major difficulty in explaining turbulence at around 100 km is the rarity of observance of large wind shears to generate turbulence. The shear that is necessary to produce turbulence, from Richardson number criterion at mesopause height, is about  $0.10 \text{ sec}^{-1}$ . This value for the shear has also been estimated by HODGES (1967). Such strong shears have rarely been observed from any location including Thumba. However, on two occasions during twilights at Thumba, shears of magnitude 0.08 and  $0.10 \text{ sec}^{-1}$  happened to be observed at 107 km and 110 km altitudes respectively, and on the latter occasion (12 January 1964 morning twilight) some turbulence features were also seen. The cloud was released on the up-leg of the rocket trajectory. Because of cloudy weather the turbulence features were not sufficiently clear to warrant further investigation.



Sodium up-leg release on 19-4-1971

(evening twilight), photographed about  
3 minutes after the release; exposure  
duration 10 secs.



TMA-III down-leg release on 12-3-1967

(night-time), photographed about  
10 minutes after the release; exposure  
duration 10 secs.



With propagating gravity waves available to initiate turbulence the shear necessary to maintain the generated turbulence is, as suggested by HODGES (1967), very small, being about  $0.02 \text{ sec}^{-1}$ . These shears are very commonly observed. BLAMONT and his group (BALMONT AND BARAT, 1967) have laid stress on the Reynold number criterion, and find the critical value of this number

$$R_{ec} = \frac{1}{\lambda} \frac{\partial u}{\partial z}$$

to be about 600, where  $\lambda$  is the kinematic viscosity and  $\partial u / \partial z$  is the velocity gradient with altitude. In the two examples, where they observed turbulence,  $\partial u / \partial z$  have been shown to be  $0.02 \text{ sec}^{-1}$  and  $0.03 \text{ sec}^{-1}$ , which are much smaller than the requirements of LAYZER AND BEDINGER. The shears observed in the TMA-III release over Thumba were also quite small, being only  $0.03 \text{ sec}^{-1}$ . Detailed turbulence study on this cloud could not be made, because only ordinary K-24 cameras, and not larger ones, were used for the photography.

REES ET AL. (1972, A) have studied the time delay for the onset of turbulence at 100 km and have compared this time, for different levels, with a characteristic time constant related to the Kolmogoroff microscale and kinematic viscosity. They show that with the plausible assumptions regarding rate of dissipation of turbulence energy, the observed delays in the onset of turbulence agree fairly well with this

time scale. They conclude that at the altitude of turbopause the Kolmogoroff microscale of turbulence increases very rapidly with altitude. According to them, turbulence exists above the turbopause also, but its efficacy in transport processes, relative to molecular diffusion, decreases with altitude.

However, if one compares the lateral dimension of the trail just below the turbopause level with that just above, it is seen (for the TMA-III down-leg release from Thumba) that the overall growth rate is faster for the lower portion. Thus, the present author would prefer to interpret the trail evidence as specifically indicating cessation of turbulence rather than the time scale effect, for in the latter situation growth rate of trail should have been at any rate faster for the higher levels.

### 2.3.7 Interaction of Neutral and Ionised Atmospheres

The TMA-III release of 12th March 1967 was accompanied by a Langmuir Probe for the measurement of electron density. The latter acquired data on the up-leg (SATYA PRAKASH ET AL., 1968) and the TMA was released during the down-leg of the rocket trajectory. From FIG 2.10, where electron density and TMA-III wind profiles are plotted, no relationship is apparent between them.

In the middle latitudes, as well as at low latitudes (Barbados 12° N), strong correlations between vertical wind

TMA III 12-3-1967, 2230 IST

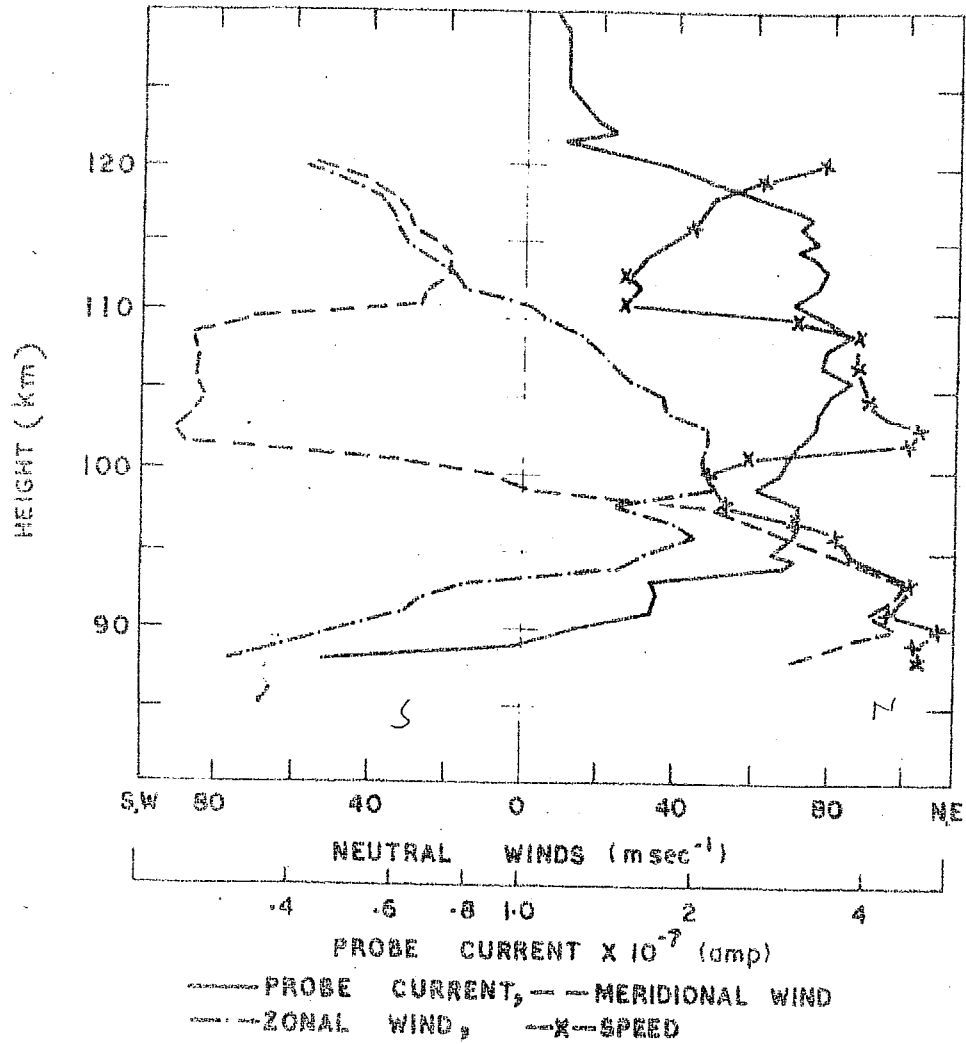


FIG 2.10 : Electron Density profile (up-leg) and Zonal, Meridional and Speed profiles of Neutral Wind (down-leg) from the experiment conducted on 12th March 1967 (2230 IST).

shear and sporadic E have been observed on many occasions (BOWEN ET AL., 1964; SMITH, 1966; WRIGHT ET AL., 1967) supporting WHITEHEAD'S (1961) hypothesis. Such a phenomenon is ruled out at the equator because magnetic lines of force are horizontal. However, REDDY AND DEVASIA (1973) have, recently, shown that blanketing type  $E_s$  at the magnetic equator can be formed due to horizontal shear of horizontal neutral winds.

The interaction of neutral and ionised atmospheres is manifested very clearly by the Ba-Sr releases. Referring to FIG 2.8, it is seen that the ion motions and neutral motions are close to each other in the meridional direction. The neutral and ion motions are different in the east-west direction. At around 150 km, however, from the available two observations, the zonal components also seem to be in agreement. This gives support to the expectation that the ion motion will follow the neutral, below 150 km and that above this height, neutral motions will not have significant influence on the ions, above 150 km neutral gas can drive the ionisation only along the field lines.

Over Yuma, Barbados and Eglin, about 100 radio spaced-receiver Kinesonde measurements were compared with 40 neutral wind measurements made by gun- and rocket-launched TMA trails in the night-time E-region. Good agreement between the drifts and neutral winds have been reported (WRIGHT, 1968).

An ionospheric drift recorder, measuring ionospheric drifts at E and F-regions by the spaced-receiver method, is operative at Thumba. General pattern of drifts has been presented by RASTOGI ET AL. (1972). The equipment, due to its low transmitting power, was unable to detect the E-region ionisation, during the times of the vapour releases, i.e. during twilight and night-time. Hence no comparison of winds with drifts for the times of vapour cloud launch has been possible.

Recently, MISRA AND RASTOGI (1971) have presented results of diurnal variation of E- and F-region drifts over Thumba, obtained by means of a more powerful transmitter. By observing the  $E_s$ -echoes at night-times, they have shown that the drifts at these levels are entirely westward during day-time and are mainly eastward during the night. The hours of reversal have been quoted, on an average, as 0530 hr and 2000 hr. All the three TMA results, in the 95-115 km region show an eastward velocity and are thus in good agreement with the drift results. The TMA-II, in particular, has shown an eastward wind all through its height coverage. The meridional drifts, by spaced-receiver technique, are difficult to identify at the magnetic equator. Hence no comparison of meridional winds with drifts has been made here, though some mention of it will be made in Section 2.5.

## 2.4 GENERAL CIRCULATION IN THE UPPER ATMOSPHERE

The wind pattern and temperature distribution, with altitude and latitude, in the lower atmosphere, below about 100 km is now fairly well understood from the observations of instrumented balloons, meteorological rockets, etc. Mean circulation patterns have been presented as contour diagrams by MURGATROYD (1957, 1965), BATTEN (1961), KOCHANSKI (1963), CRAIG (1965), WEBB (1968) and others. The winds have been shown to be essentially geostrophic and zonal. In stratosphere and mesosphere, meridional circulation is more difficult to analyse observationally on account of smaller velocities. Using the thermal wind equation,

$$g \frac{\partial T}{\partial x} = 2 T^2 \Omega \cos \theta \frac{\partial}{\partial z} \left( \frac{u}{T} \right)$$

where  $x$  = meridional direction, positive southwards

$T = T(x, z)$ , the temperature

$\Omega$  = earth's angular velocity

$\theta$  = colatitude of the place

$g$  = acceleration due to gravity

$u = u(y, z)$  the zonal velocity, measured positive eastward

MURGATROYD (1957, 1965) has shown that the zonal winds are reasonably consistent with the direct measurements of latitudinal temperature distribution. The derived temperature

distribution has been shown to be consistent with the hypothesis that the heat balance is maintained largely by radiative processes (MURGATROYD AND GOODY, 1958).

Between 80 and 120 km, the radio-meteor method has been used to obtain information about prevailing and periodic components. Harmonic components for different latitudes and for different seasons have been analysed (HAURWITZ, 1964; AREFYEVA ET AL., 1966; MULLER, 1968; REVAH, 1969; SPIZZICHINO, 1969 A). Despite the small number of observation stations, general patterns have emerged. Prevailing winds of the order of  $20 \text{ m sec}^{-1}$ , and meridional winds of the same order as zonal winds, have been reported. From these studies, it has emerged that the amplitude of the diurnal component is dependent on latitude, and this has provided a renewed fillip to the study of diurnal tide.

Above 200 km, zonal velocities of the order of  $100 \text{ m sec}^{-1}$  have been derived by the satellite drag method. It has not been possible to study the diurnal, seasonal or latitudinal variations by this method. Meridional winds at these altitudes have been deduced by the incoherent scatter technique (VASSEUR, 1969; AMAYENC AND VASSEUR, 1972; EVANS, 1972). There has yet been no attempt to couple the two measurements and obtain a mean circulation pattern at these levels. Theoretical computations of F-region winds have, however, been

made, on the basis of model atmospheric temperature distribution, by many workers (KOHL AND KING, 1967; GEISLER, 1967 A; CHALLINOR, 1969).

In the thermosphere, above about 120 km, very little information on prevailing wind systems is available. Profiles of artificial chemical trails are characterised by their oscillatory nature, and require extensive averaging to obtain prevailing component and to provide any clear picture of the general circulation pattern. Some attempts in this regard have been made in the past, at mid-latitudes, by RAGSDALE AND WASKO (1963), KOCHANISKI (1964, 1965, 1966) and KANTOR AND COLE (1964). BHAVSAR ET AL. (1969), for the first time, from the available observations over the globe, have presented a mean circulation pattern above 100 km.

In the following sections, the observational data on winds, hitherto obtained, in the 100 to 200 km height region is presented, and regularities in the mean flow, derived from this data, are discussed. In the light of the paucity of data it is not possible to distinguish between the various kinds of motions prevailing at these levels, nor is it possible to discern clearly the diurnal and seasonal trends. However, attempts at these are also made.



#### 2.4.1 The Data and Grouping of Stations

Most of the observational wind data, available from the vapour release technique is limited to altitudes below 140 km. It has been shown, from a number of studies and from individual profiles, that winds are quite irregular below this altitude, and for studying the circulation below this level, a very large sample has to be dealt with. The discussions to follow will, thus, mainly concern with observations available above 140 km.

From many of the observation-sites only a few launchings have been made, and this fact has to be taken into account in the conclusions to be drawn from this analysis. Table 2.4. gives the launch sites, their geographical coordinates, the number of observations from each station and the last date of observation from that station included in this study. A total of nearly 210 launchings were available for this analysis. The sources of these data are given in Appendix I.

The available data has been subjected to three different types of analysis, and thus to different grouping systems. For assessing a very general atmospheric flow, only two groupings were made, i.e., of stations below and above 30° latitude. For the study of diurnal and seasonal behaviour from individual launchings, the stations have been grouped into three belts, viz., those below 30°, those between 30° and 35° and those above 35° latitude.

# Wind Data Available from Various Stations over the Globe.

Sl.No.	Station	Latitude	Longitude	No. of observations	Last observation
1.	Thumba	8° N	77° E	12	31-3-1968
2.	Barbados	13° N	60° W	16	23-9-1965
3.	Hawaii	22° N	160° W	30	2-6-1967
4.	Sonmiani	26° N	67° E	3	25-2-1966
5.	Reggan	27° N	0°	6	21-5-1963
6.	Eglin	30° N	87° W	35	14-12-1967
7.	Hammaguir	31° N	3° W	13	12-6-1963
8.	Woomera	31° S	137° E	18	17-10-1969
9.	Kagoshima	31° N	130° E	2	2-11-1964
10.	Chamical	32° N	66° W	2	30-11-1962
11.	New Mexico	33° N	107° W	2	26-11-1957
12.	Wallops Island	38° N	76° W	56	16-7-1966
13.	Sardinia	40° N	10° E	7	21-5-1963
14.	Ile du Levant	43° N	6° E	2	21-5-1963
15.	Ft.Churchill	58° N	94° W	8	15-9-1966

Further classification was considered not desirable, because of the meagre observational data. In the zone below  $30^\circ$  latitude, only Thumba and Hawaii provide a fair amount of data. The whole of the data from Barbados is limited to altitudes below 140 km. For Reggan and Sonmiani, only one observation profile each, above 140 km, was available. It may also be mentioned that all the observation-sites included in the present study, except Woomera and Chamical, belong to the northern hemisphere.

#### 2.4.2 The Average Flow Above 100 km

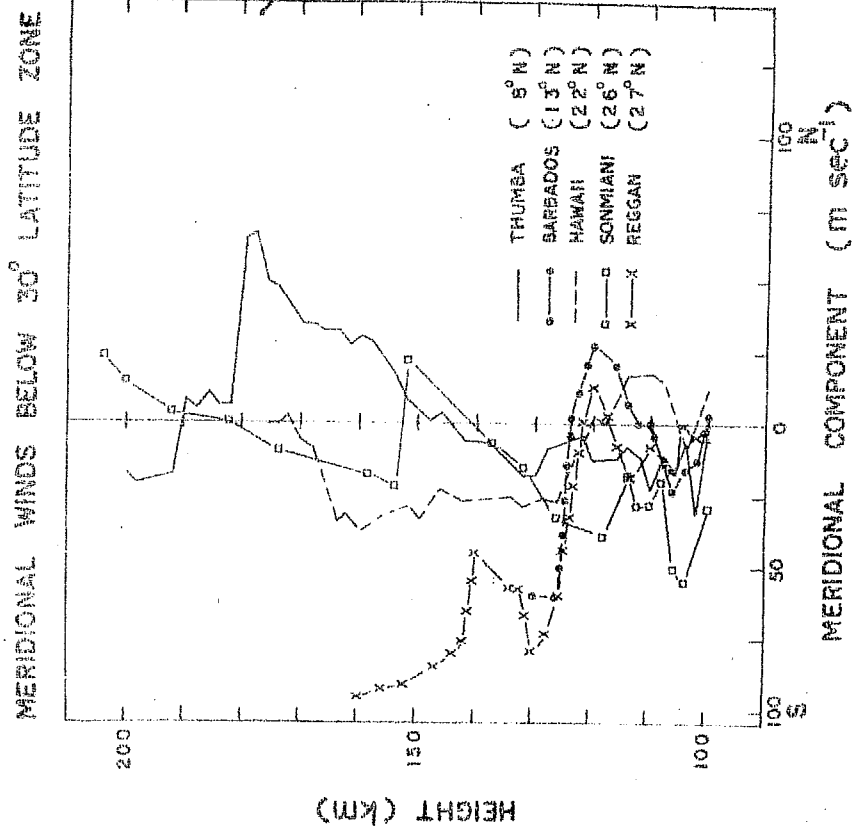
To determine the average flow at a station, all the available wind velocity-height profiles relating to that station were superimposed one over another and an average profile for the purpose was found. In this process, the presumption has been that the gravity wave contribution will be annulled; tidal contribution, however, may remain. In most of the cases, the evening twilight observations have very much outnumbered the morning observations and the night-time results. So the results derived in the present section may have a bias towards evening average flow. This can not be overcome unless a good, and almost equal, number of morning and evening twilight observations are available.

The meridional, zonal and speed profiles in the two zones, one above and the other below  $30^\circ$  latitude, determined

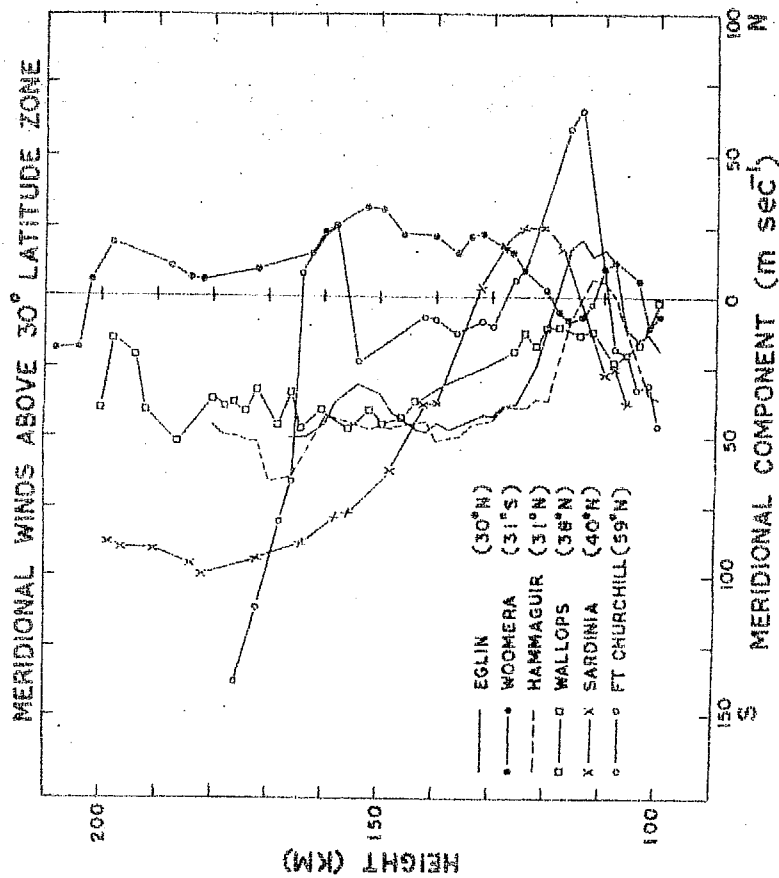
by the above procedure for the different stations, are plotted in FIGs 2.11 (a), (b) , and 2.12 (a), (b) and 2.13 (a), (b) respectively. The meridional flow shows some seasonal trends. This is, thus, separately discussed in Section 2.4.4. The results obtained at Chamical, Kagoshima, Ile du Levant and New Mexico are not shown in the above figures, firstly because of want of clarity and secondly because these stations provided only two observations each.

From these figures the following broad conclusions about winds in the 100 to 180 km region emerge:

- i) The average flow in the equatorial and low latitude regions is different from the average flow at higher latitudes (above  $30^\circ$ ).
- ii) In the height region 100 to 120 km, no regularity is seen except a wind maximum (more so from individual profiles, which is suppressed because of averaging) in both the groups.
- iii) Above 120 km altitude, the average wind speed decreases, (or, at best, remains constant) with height for latitudes below  $30^\circ$ , and increases with height for latitudes above  $30^\circ$ . The results from Ft.Churchill ( $58^\circ$  N) show this behaviour most prominently.

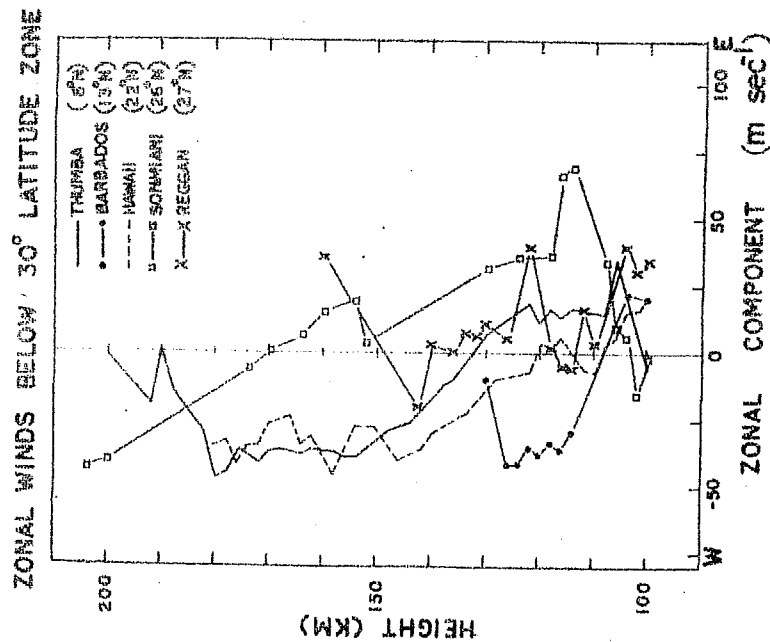


(a)

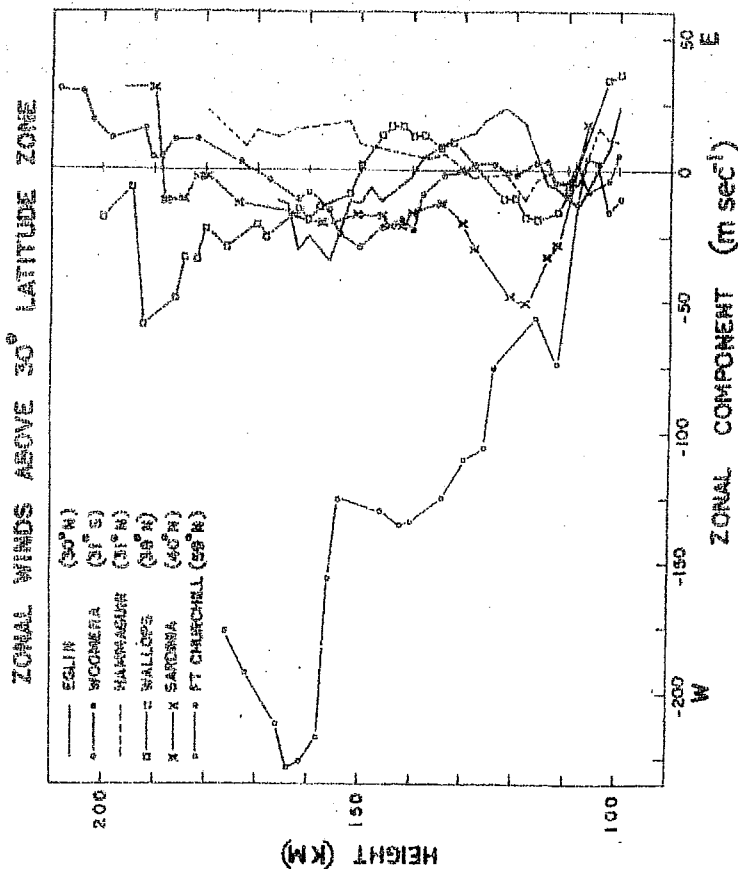


(b)

FIG 2.11 : Average meridional winds at different stations in the two latitude zones.

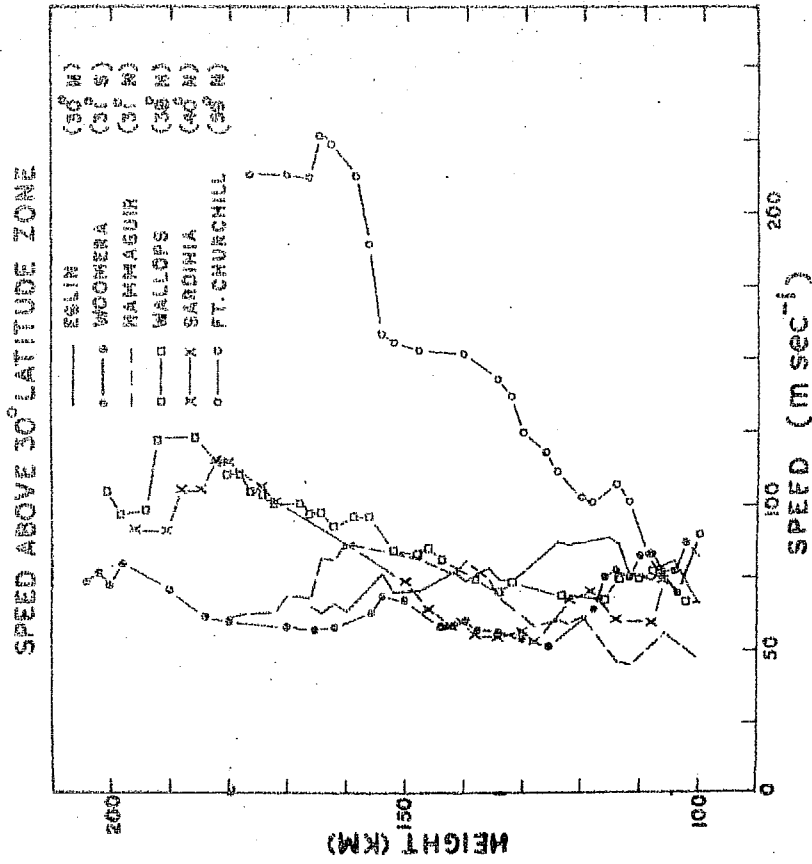


(a)

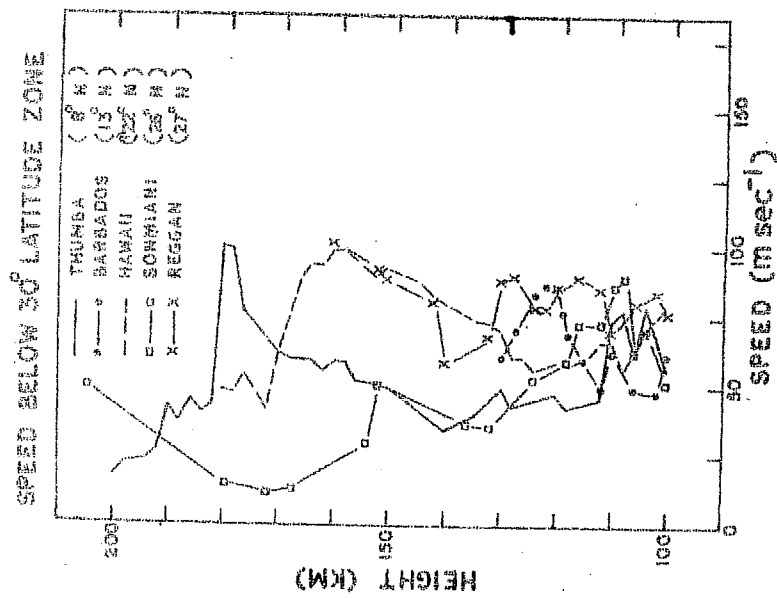


(b)

FIG 2.12 : Average zonal winds at different stations in the two latitude zones.



(b)



(a)

FIG 2.13 : Average wind speeds at different stations in the two latitude zones.

iv) In the equatorial region, below  $30^\circ$  latitude, there is a regular zonal circulation, with a westerly flow in the region 120 to 140 km and an easterly flow in the 140 to 180 km region.

v) At latitudes higher than  $30^\circ$ , the zonal flow in the height range 120 to 180 km seems to be easterly all the time, though two of the mid-latitude stations show an eastward flow behaviour, particularly above 160 km.

#### 2.4.3 Super Rotation of the Upper Atmosphere

Since the time the eastward rotation of the atmosphere above 180 km was revealed by orbiting satellites, it has been of interest to see if the high altitude observations of the drifts of vapour clouds also show this behaviour (BEDINGER, 1970 B). That the two evening Ba-Sr releases over Thumba, reported in the present study, have shown an eastward wind component above 190 km, has already been discussed in Section 2.3.4.

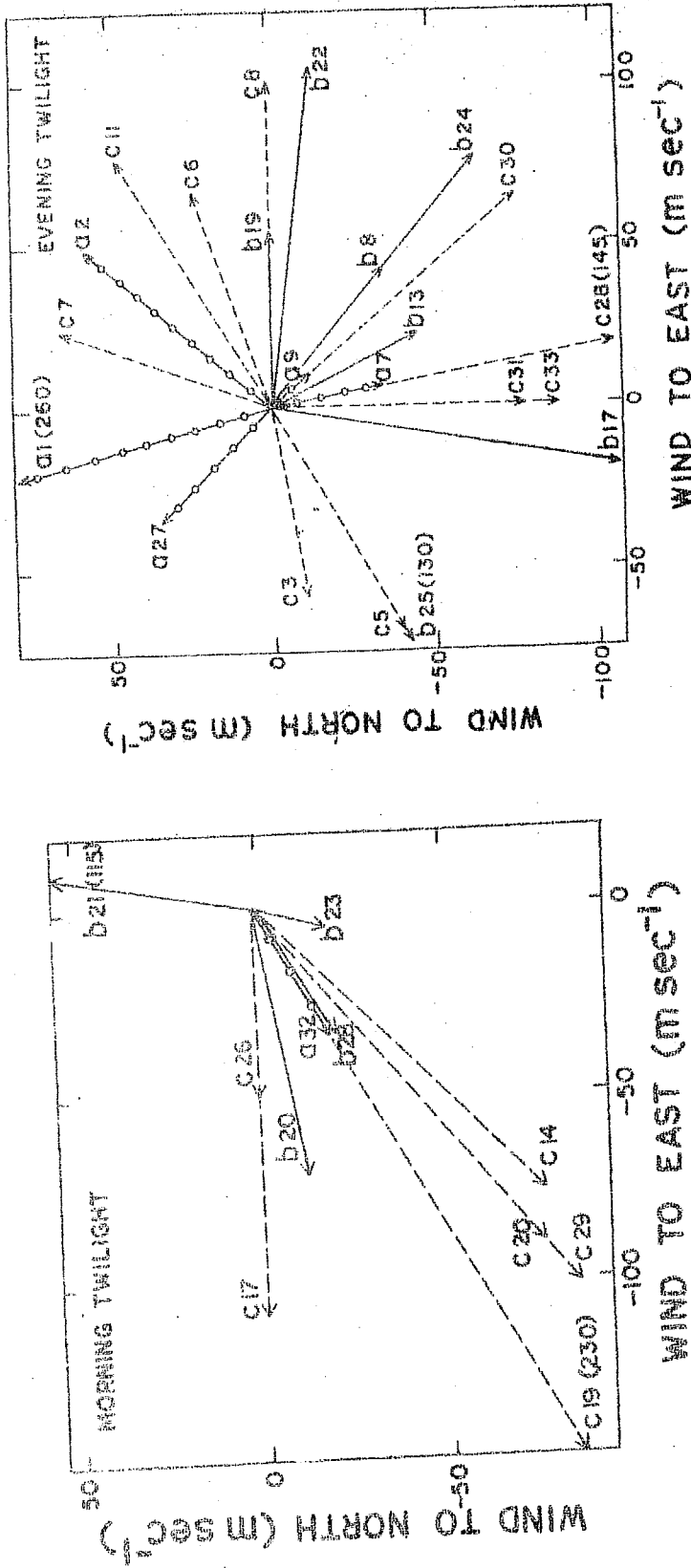
Recent results of KING-HELE (1972) show that the highest mean eastward speed occurs near 350-380 km altitude. Values of about 1.5 for  $\lambda$ , corresponding to an eastward velocity of  $200 \text{ m sec}^{-1}$  at mid-latitudes have been inferred ( $\lambda$  being the rotation of the atmosphere in revolutions  $\text{day}^{-1}$ ). It has also been shown that  $\lambda$  apparently decreases to unity



near the altitudes of 150 and 450 km. Earlier results (KING-HELE AND SCOTT, 1967) had indicated a probable maximum eastward wind around 1800 hr L.T. Later results have shown no such time-dependence. Individual satellite results show large changes of the mean rotation rate with time. Whether, and how, the satellite data reflect wind structure variation with latitude, local time, season, and geomagnetic activity is still an open question. KING-HELE'S analyses provide the most comprehensive survey of neutral wind behaviour near 200 km altitude.

In Appendix II all the available observational data on winds at the highest altitude above 180 km, are presented in three latitude zones with a view to examining the super rotation behaviour. Also presented in this table are data on mean wind flow above 150 km at various stations for individual days. These are, however, discussed in Section 2.4.4. FIGs 2.14 (a) and (b) show plots, as observed in northern hemisphere, of these winds above 180 km. The southern hemisphere observations are shown with the sign of their meridional component reversed. The two wind observations, reported by ACKERMAN AND VAN HEMELRIJCK (1971), have not been included here, because they corresponded to a very high altitude, i.e. 275 km.

The following is a summary of the results of zonal winds, at the highest altitude of observation above 180 km, in the three latitude zones:



(a)

(b)

FIG 2.14 : Wind vectors at the highest altitudes of observation, above 180 km. (The figures, given within brackets in certain cases, refer to wind speeds extending beyond the limits of the above diagrams).

---→  $a_i$  - latitudes below 30°, ---→  $b_i$  - latitudes between 30° and 35°,  
 .....→  $c_i$  - latitudes above 35°.

Table 2.5

Summary of Winds above 180 km

<u>Latitude Zone</u>	<u>Twilight</u>	<u>Total Observs</u>	<u>Eastward velocity</u>	<u>Westward velocity</u>	<u>No zonal component</u>
Low ( $< 30^\circ$ )	Morning	1	-	1	-
Middle ( $30^\circ$ - $35^\circ$ )		4	1 (but low)	3 (in one case low)	-
High ( $> 35^\circ$ )		6	-	6	-
Low ( $< 30^\circ$ )	Evening	5	3 (in 2 cases low)	2	-
Middle ( $30^\circ$ - $35^\circ$ )		7	5	2 (in one case very low)	-
High ( $> 35^\circ$ )		10	6 (in one case very low)	2	2

It is apparent from FIGs 2.14 (a) and (b) and the above table that, during morning twilight, the velocities are almost definitely westward (south westward most of the time), with no eastward component ever observed except on one occasion for a mid-latitude station.

For the evening twilight periods it is also apparent that the mid-latitude observations show a more pronounced eastward behaviour of winds than the low or high-latitude observations. From Sardinia, which is the highest latitude

station for which observations are available, only one out of four observations, shows a convincing eastward flow behaviour. However, no westward flow is also discernible in the other three cases. In general, it is noted that the eastward motion trend is more pronounced during winter evenings than during summer, but observations are too scanty to draw firm conclusions.

It is, thus, seen that there is a tapering off of the nett eastward component on either side of mid-latitude. From Ft Churchill, which is situated at as high a latitude as  $58^{\circ}$ , large westward winds have been observed, though only below 160 km. It is, thus, probable that the super-rotation behaviour veers round at high latitudes.

At first sight, the wind measurements, which show almost opposite behaviour in the morning and evening, suggest that there might not be a nett eastward flow averaged over the day, thus, conflicting with KING-HELE's observations. This discrepancy is partially resolved if we take into account the fact that the afternoon and evening (14-20 hr) air densities are about 20% greater than that in the morning. Hence when expressed as air-flux, a nett average eastward flow may be obtained.

#### 2.4.4 Comparison with Global Pressure Models

REES (1971 B) has proposed a global pressure model (FIG 2.15) for equinox-conditions between 150 and 190 km,

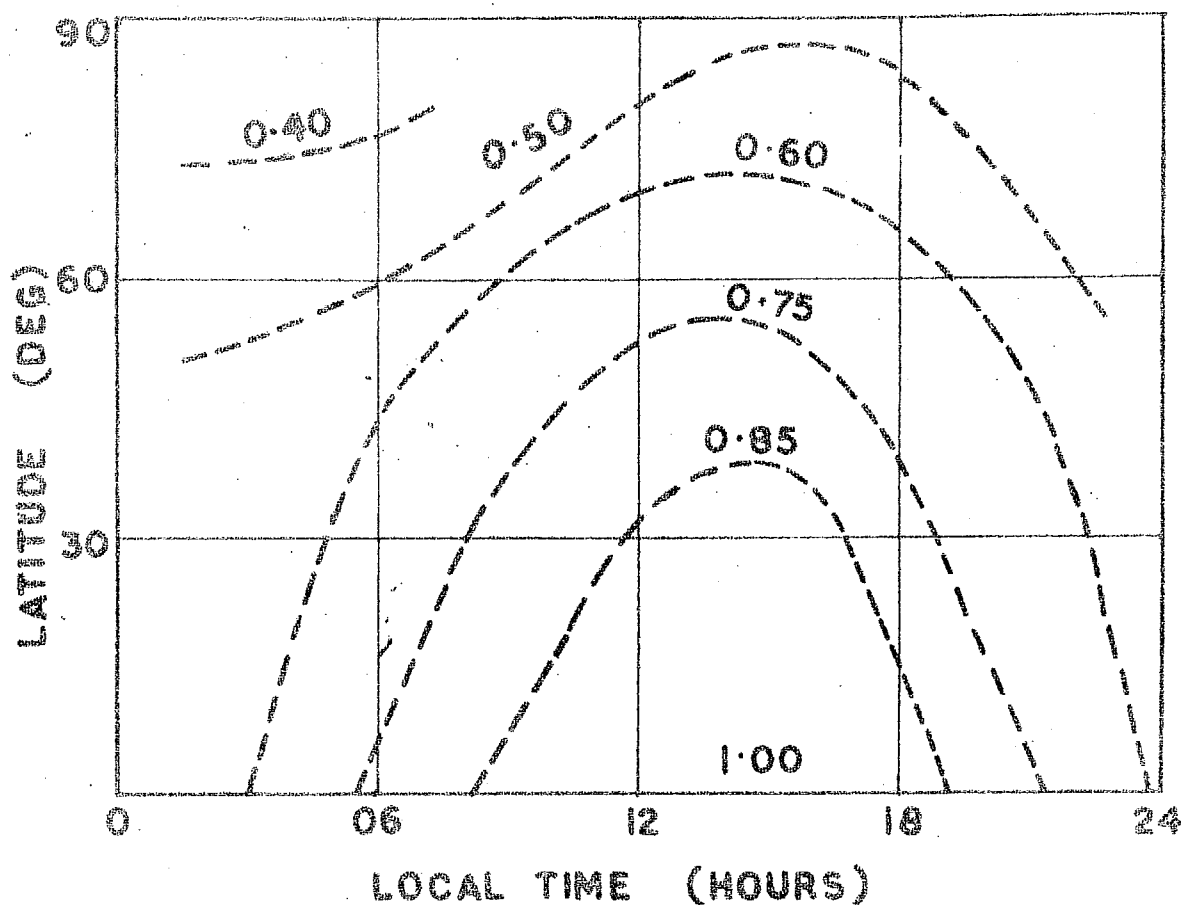


FIG 2.15 : REES' (1971 B) global pressure model for the  
 150-190 km region, relative to unit values:  
 at 150 km =  $4.58 \times 10^{-3}$  dynes  $\text{cm}^{-2}$   
 at 170 km =  $2.34 \times 10^{-3}$  dynes  $\text{cm}^{-2}$   
 at 190 km =  $1.39 \times 10^{-3}$  dynes  $\text{cm}^{-2}$

based on temperatures and densities derived from vapour trail releases. LLOYD ET AL. (1972) have suggested a temperature and thence a pressure model for solstice-conditions, based on an extension of WLDTEUFEL AND MCCLURE'S (1969) temperature model (FIG 1.4).

These new models show larger day-time meridional pressure gradients than those of JACCHIA (1971), whereas the night-time gradients at equinoxes and the winter solstice are lower and have a reversed direction to that of JACCHIA. The night gradients at summer solstice in these two models have the same sense as those of JACCHIA (1971).

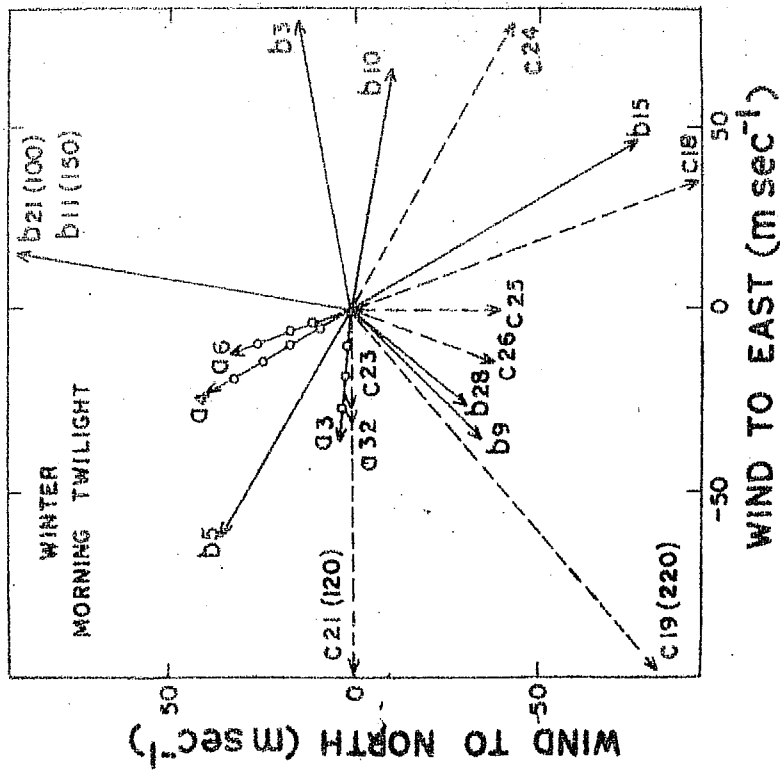
This pressure system, during day-time, near equinox and winter conditions, will drive a geostrophic wind in the eastward direction giving a velocity of the order of  $150 \text{ m sec}^{-1}$  at 200 km. This is at least 5 times larger than the mean eastward winds observed during evening twilight. The effects of ion drag and viscosity would, however, modify the winds produced by these pressure gradients, but this large discrepancy can not be accounted for by them.

RISHBETH (1972 A) has reviewed the various possible suggestions for explaining the eastward rotation. The pressure model of REES suggests that the super-rotation could be because of a pseudo-geostrophic wind due to the mean global pressure gradients which are predominantly equatorward.

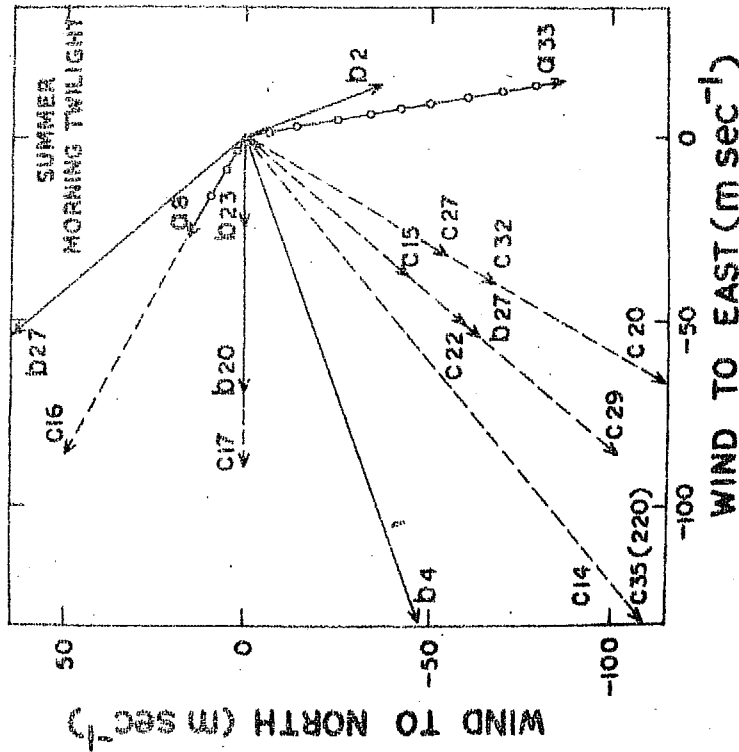
CHALLINOR (1969) has computed winds resulting from an asymmetric global pressure system and hydro-magnetic forces. In mid-latitudes, the predicted flow is eastward during evening twilight, in accordance with KING-HELE'S observations. This result is supported to a good extent by the vapour trail data from mid-latitudes, as shown in Table 2.5 and FIG 2.14 (b). The model predicts southwestward winds during morning twilight at mid-latitudes in the northern hemisphere, which is confirmed by FIG 2.14 (a).

The tapering off of the mean eastward wind towards high latitudes, is also inferable from the calculations of ILL ET AL. (1973), who used a pressure model derived from the temperature model of WALDTEUFEL (1971) and density model of BARLIER ET AL. (1972). Their calculations however, show only a slight diminution of the super-rotation near the equator. In order to reconcile their results with the present values observed at low latitudes from vapour cloud releases, smaller pressure gradients than those of ILL ET AL. AND REES have to be resorted to.

The meridional component of wind in the 150 to 200 km region shows a strong tendency of flow away from the summer pole to the winter pole, as shown in FIGS 2.16 (a), (b) and 2.17 (a), (b). In these figures the mean winds above 150 km as tabulated in Appendix II, have been plotted on a polar



(a)



(b)

FIG 2.16 : Mean wind vectors above 150 km for Morning Twilight. (The figures, given within brackets in certain cases, refer to wind speeds extending beyond the limits of the above diagrams).

—  $\rightarrow$   $a_i$ -latitudes below 30°,  $\rightarrow$   $b_i$ -latitudes between 30 and 35°,  
 ---  $\rightarrow$   $c_i$ -latitudes beyond 35°.





graph. The flow from the winter to the summer hemisphere is more prominently noticed in the evening twilight plots. Though summer morning also shows this feature to some extent, winter morning shows no particular trend. Applying, again, the air-flux criterion it can be seen that there is a nett transfer of flow from the summer to the winter hemisphere. This flow might serve as the source for inter-hemispherical energy transfer, and provide the mechanism to refrigerate the summer pole and warm the winter pole.

From the several wind measurements over Kiruna ( $60^{\circ}$  N), close to mid-night, during mid-April (summer pole conditions), strong equatorward winds were reported by REES (1972) at and above 150 km. These have been associated by him with the winds observed at mid-latitudes. Thus, there seems to be a general equatorward flow, of the order of  $100 \text{ m sec}^{-1}$ , throughout night-time in the summer hemisphere. However, only night-time measurements over mid- and low-latitudes will be able to confirm the continuity of air motion over the equator.

The meridional winds may not be caused by the pressure model of REES (1971 B), unless systematic asymmetries are introduced. Asymmetries could arise, as suggested by REES, by a combination of low winter polar densities (inferred by him from Heiss Island and Secor 6 satellite data), and the seasonal migration, in latitude, of the diurnal density and

temperature bulge at equator (KEATING, 1969; WALDTEUFEL AND MCCLURE, 1969; JACCHIA ET AL., 1967).

Though the mean eastward flow of the upper atmosphere above 180 km is, more or less, in consonance with the models, the zonal winds below 180 km, as observed from FIG 2.12 (a), (b) are quite different. From 140 to 180 km the winds are westward all through, i.e., just opposite to the super-rotation behaviour. This could call for a re-thinking on the models below 180 km.

The incoherent scatter and satellite drag models are based essentially on exospheric temperatures, and the model of REES (1971 B), based on the scanty data from vapour trail releases, is for heights in the region 150 km to 190 km.

GROVES (1971), in his neutral atmosphere model upto 120 km, has shown that the maximum temperatures are found, as in the mesosphere, in the vicinity of the winter pole. To reconcile GROVES' model with the present data, high temperature gradients between 110 and 150 km, or even upto 180 km, are required near the summer pole and lower gradients at the winter pole. REES.(1971 B) speculates that the large polar summer-time temperature gradients between 90 and 130 km should mean that atmosphere is more stable in summer than in winter in that region. He quotes, to substantiate this, that TMA trails released in late April over Kiruna were non-turbulent between

90 to 130 km whereas similar trails during winter at high latitude were irregular.

RAGSDALE AND WASKO (1963), who constructed the mean wind model upto 200 km for the  $30^{\circ}$  to  $40^{\circ}$  N latitude, from the sparse measurements then available, had shown that zonal components show a decrease between 120-140 km with height, which might suggest a reversal of thermal gradient. Though this behaviour is not seen from the general wind pattern presented here, either for low or high latitudes, some individual wind profiles do show such a behaviour. BHAVSAR AND RAMANUJA RAO (1968) had found this behaviour in the Thumba profiles. Temperature measurements in the 100-150 km region are still very scanty, and many anomalies too have been observed in this region (Chapter III). The importance of tidal components has also to be established to resolve the discrepancy.

Pressure models based on independent temperature and density measurements, between 100 and 200 km region, are required to explain the uncertainties that still remain. Temperature measurements, particularly between 100 and 150 km, the region of steep temperature rise, over a wide latitude zone are the first necessity towards understanding the global circulation system above 100 km.

## 2.5 ASYMMETRY IN EQUATORIAL ANOMALY

The equatorial anomaly in the  $F_2$ -region of the ionosphere has been studied in detail (RASTOGI, 1959; LYON AND THOMAS, 1963). These studies have been concentrated for the equinox periods, in which the latitudinal variation of peak electron density  $N_m F_2$  shows a minimum near the magnetic equator and crests of similar magnitude to the north and south, at about  $30^\circ$  dip latitude. Theoretical studies by BRAMLEY AND PEART (1964, 1965), MOFFETT AND HANSON (1965), and HANSON AND MOFFETT (1966) have shown that an upward electromagnetic drift, operating with electron production, loss and ambipolar diffusion in the  $F_2$ -region, can adequately account for the equatorial anomaly.

LYON (1963), LYON AND THOMAS (1963) and THOMAS (1968), from studies of  $f_o F_2$  ( $F_2$  layer critical frequency) data, have indicated marked asymmetries in the equatorial anomaly about the magnetic equator during solistices. They have shown that the day-time  $f_o F_2$  crest is larger on the winter-side than on the summer-side, and  $h_m F_2$  (height of the peak electron density) is about 100 km lower at the winter crest than at the summer crest. THOMAS (1966) has shown that differences in neutral gas temperature will produce an insignificant effect on the  $N_m F_2$  distribution. BRAMLEY AND YOUNG (1968) have demonstrated

that asymmetrical photo-ionisation rates will also not produce any gross asymmetries.

HANSON AND MOFFETT (1966) and THOMAS (1968) have pointed out that these asymmetries could be produced by horizontal winds, with speeds of about  $50 \text{ m sec}^{-1}$ , blowing across the trough of the anomaly from the summer to the winter hemisphere. ABUR ROBB AND WINDLE (1969), solving the time-varying continuity equation for electrons in the  $F_2$ -region, have demonstrated that neutral winds can produce distributions similar to day-time and night-time asymmetrical distributions, indicating that ionisation is transported from one hemisphere to the other by neutral winds.

No observations of the F-region neutral winds are as yet available to confirm or contradict the above hypothesis. But, it is pointed out here that even the lower F-region neutral winds could be contributing factor to the asymmetry in the anomaly. Ionisation, if carried along by the meridional neutral wind while it is moving upwards under the influence of the  $\mathbf{E} \times \mathbf{B}$  force, could cause an asymmetry.

The polar plots of FIGS 2.16 (a), (b) and 2.17 (a), (b) do show that in the 150 km to 200 km height region there is a preferential meridional flow from the summer to the winter hemisphere. This is particularly evident for the evening twilight periods.

Direct evidences of ionisation being carried along by neutral winds in the north-south direction has been found in the present study. From Table 2.3 and FIG 2.8 where the velocities obtained from neutral and ionised Barium clouds over Thumba are summarised, it is seen that the north-south component of the ion motion has been following the neutral motion which was southwards, i.e. towards the winter hemisphere.

During the Barium cloud experiments over Thumba, one of the rockets released 15 kg of Barium at a height of 150 km, and 75 km west and 15 km north of Thumba, on 31st March 1968 at 1745 IST ( + 12° solar depression). The results from this launch have not been included in this study. However, it was seen that the barium cloud released at 1745 IST, had drifted far south when it could be first photographed at 1915 IST. No observation was possible before that time because the sun was above the horizon. Both neutral and ion clouds were found to be well separated and their new positions, at 1915 IST, showed that the neutral cloud had moved nearly 320 km west and 375 km south of the release-position giving a velocity of about  $60 \text{ m sec}^{-1}$  and  $70 \text{ m sec}^{-1}$  in the westward and southward directions respectively. The neutral velocities derived for this experiment were, however, not accurate. The ion cloud had moved to a new position, to a height of about 190 km, and 205 km west and 180 km south of the release-position,

yielding average speeds of  $8 \text{ m sec}^{-1}$ ,  $40 \text{ m sec}^{-1}$  and  $35 \text{ m sec}^{-1}$  in the upward, westward and southward directions respectively.

The large southward velocities i.e. from summer to winter hemisphere observed on almost all the three occasions from Thumba, alongwith a simultaneous movement of ionisation in the same direction while it was moving upwards, gives credence to the argument that the meridional winds could be the contributing factor for the asymmetry in the anomaly. The earlier sodium cloud launchings from Thumba, which were conducted during winter months, have also shown unambiguously that the meridional flow is from the summer to the winter hemisphere over the equator.

The north-south ionospheric drifts are difficult to measure at the equator by the spaced receiver technique, because of the alignment of irregularities along the field lines. However, DESHPANDE AND RASTOGI (1968) have been able to show that the day-time drifts at Thumba, during winter show slight northward movement, while during summer, considerable southward movements are observed. BAMGBOYE AND LYONS' (1968) drift observations over another equatorial station, Ibadan, corroborate DESHPANDE AND RASTOGI'S results.

These observational evidences, as also the general behaviour of the meridional winds on a global scale, showing



a preferential flow from the summer to the winter hemisphere, strongly support the hypothesis put forth by HANSON AND MOFFETT (1966), BRAMLEY AND YOUNG (1968) and THOMAS (1968), that it is the neutral winds that cause the asymmetry in the anomaly.

### CHAPTER III

#### UPPER ATMOSPHERIC STRUCTURE FROM DIFFUSION OF ROCKET-RELEASED VAPOUR CLOUDS

WHEN chemical vapour clouds are released in the upper atmosphere with the help of rockets, they mix with the air by the process of diffusion. This diffusive transfer of mass from the point of release to the ambient atmosphere takes place mainly because of the gradient caused in the mass concentration. Some initial diffusion also takes place due to pressure and temperature gradients. However, as the released vapour clouds reach ambient conditions soon after the release, the subsequent mixing is entirely due to the gradient in the mass concentration.

Though a majority of the artificial vapour release experiments have been conducted for the determination of winds in the upper atmosphere, diffusion and temperature measurements have also been made by several investigators. GOLOMB ET AL. (1967, 1968, 1969), REES (1968), REES ET AL. (1972 A), LLOYD ET AL. (1972), etc. have reported simultaneous diffusion and temperature measurements in the 120-250 km altitude region from the vapour releases, from which atmospheric densities at different heights have been inferred.

Barium-Strontium point releases, made from Thumba during evening twilight hours on 28th and 30th March 1968

in the height range 130 to 200 km, have already been described in Chapter II in connection with the measurement of neutral wind velocities. These releases have been also used for studying neutral upper atmospheric structure by observing their growth rates and thus determining the molecular diffusion coefficients. This study forms the subject matter of the present chapter.

### 3.1 DIFFUSION EQUATION

If chemical vapour is released at a point in the atmosphere, the resulting cloud grows radially. The initial expansion occurs with nearly the velocity of sound, as the initial pressure at release is higher than the ambient. In order to enable equilibrium to be established and the subsequent expansion to be controlled by diffusion, the following conditions have to be met :

- (i) After the release, the cloud must expand atleast to a dimension equal to the equilibrium size, equivalent to a sphere of radius  $r_0$ , when the number density of the released material inside the sphere is equal to the number density of the ambient,
- (ii) If the temperature of the released material is higher than the ambient, the minimum

equilibrium radius must be such that energy density inside and that of the ambient are the same, and

- (iii) Sufficient collisions between the atoms of the released material and the ambient molecules must take place before the equilibrium size is reached.

The above conditions can be summarised by the following expressions (MANRING ET AL., 1961) :

$$\frac{4\pi N}{3} r_0^3 \leq n_A$$

$$\frac{4\pi N}{3} r_0^3 T_R \leq n_A T_A$$

$$r_0 \geq M L \quad (M \sim 5)$$

where  $N$  = total number of atoms of the released material  
 $T_R$  = temperature of the material  
 $n_A$  = the ambient number density  
 $T_A$  = the ambient temperature  
 $L$  = mean free path  
 $r_0$  = minimum equilibrium radius.

After the initial expansion has occurred and the released cloud is in equilibrium with the ambient, further

expansion occurs by diffusion process. In the upper atmosphere, this is the case for vapour clouds released above a height of about 110 km where there is no turbulence or the scale of turbulence is large compared to the cloud dimensions.

For vapour cloud releases below a height of about 110 km, turbulent (eddy) diffusion is an important process of expansion. In the turbulent part of the cloud small globules originate, which increase in diameter rapidly at first and slowly later. Turbulent diffusion studies have been made by BLAMONT AND DE JAGER (1961), COTE (1965), etc. The expansion velocity in these cases is a complicated function of atmospheric parameters, and the cloud radius, unlike in the case of molecular diffusion, does not vary as the square-root of the time after release.

The differential equation describing the behaviour of a diffusing spherical cloud which is being depleted at a rate  $Kn$  at a point, having the contaminant - particle's number density  $n$ , is :

$$\frac{\partial n}{\partial t} = D_{12} \left( \frac{\partial^2 n}{\partial r^2} + \frac{2}{r} \frac{\partial n}{\partial r} \right) - Kn \quad (3.1)$$

where  $r$  is the distance from the cloud centre,  $t$  the time after release and  $D_{12}$  (designated as  $D$  hereafter) the molecular diffusion coefficient for the inter-diffusion of two dissimilar species (CRANK, 1956; JOHNSON AND LLOYD, 1963). With the initial Gaussian distribution of the cloud given by

$$n(r, 0) = n(0, 0) \exp\left(-\frac{r^2}{r_0^2}\right) \quad (3.2)$$

the solution of equation 3.1 is

$$n(r, t) = n(0, 0) \exp(-Kt) b^3 \exp\left(-\frac{r^2}{r_e^2}\right) \quad (3.3)$$

where  $r_0$  = the initial effective radius (minimum equilibrium radius) of the cloud

$n(0, 0)$  = the initial peak number density

$r_e^2 = r_0^2 + 4Dt$ , the effective radius of the cloud at time  $t$

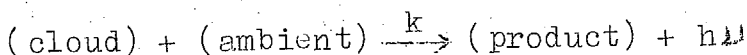
$b = r_0/r_e$ , a dimensionless time-dependent parameter.

In the following analysis, the zero for time is taken at the first observation on the cloud, and  $r_0$  refers to this time. Critical calculations for initial cloud radius at the time of release have been made by GROVES (1963 B), JOHNSON AND LLOYD (1963), LLOYD AND SHEPPARD (1966), etc.

Equation 3.3 shows that at any point the decrease in number density is due to two factors, viz.,

- (i) the  $\exp(-Kt)$  factor, which accounts for the depletion of the contaminant due to reaction with the ambient, and
- (ii)  $b^3 \exp(-r^2/r_e^2)$ , which accounts for molecular diffusion.

A reaction of the form



results in a loss of cloud particles at a rate  $k n_R n_A$ , where  $k$  is the reaction rate constant,  $n_R$  the reacting cloud particle number density and  $n_A$  the ambient atmosphere number density.

Expressions for  $n(o, t) = n(o, 0) \exp(-Kt)$  in equation 3.3, for certain limiting cases, have been obtained by LLOYD (1965).

### 3.2 RADIANCE OF THE CLOUD<sup>x</sup>

For an optically thin cloud, rendered visible by resonance scattering of sunlight, the apparent surface brightness of the cloud is proportional to the number of atoms in a column of unit area along the line of sight. The surface brightness is, thus, given by

$$B = \frac{q}{4\pi} \int_0^{\infty} n(r, t) ds \quad \text{photons cm}^{-2} \text{ sec}^{-1} \text{ str}^{-1} \quad (3.4)$$

where  $q$  is the number of photons scattered, per atom per second, into  $4\pi$  steradians and  $ds$  is the differential path length along the line of sight.

Writing the column density  $\int_0^{\infty} n(r, t) ds$  as equal to  $\eta$ , for a spherical cloud with a Gaussian distribution of contaminants,

$$\eta(a, t) = n(o, 0) \exp(-Kt) b^2 \exp\left(-\frac{a^2}{r_e^2}\right), \quad (3.5)$$

'a' being the perpendicular distance from the cloud centre to the line of sight in question. The brightness distribution can similarly be written as

$$B(a, t) = B(o, o) \exp(-Kt) b^2 \exp\left(-\frac{a^2}{r_e^2}\right), \quad (3.6)$$

$B(o, o)$  being the brightness along the line of sight through the cloud centre corresponding to zero time.

If a sunlit glow cloud is not very far above the earth's shadow, the intensity of the sunlight incident on the glow is diminished by absorption and scattering in the lower layers of the earth's atmosphere. Since the height of the earth's shadow does not remain constant, the intensity of the sunlight falling on the cloud will change with time. If the time dependence of the incident solar flux in such cases is given by  $F(t)$ , equation 3.6 can be replaced by the more general expression

$$B(a, t) = B(o, o) f(t) b^2 \exp\left(-\frac{a^2}{r_e^2}\right) \quad (3.7)$$

where  $f(t) = F(t) \exp(-Kt)$ . The centre point radiance at any instant is given by

$$B(o, t) = B(o, o) f(t) b^2 \quad (3.8)$$

In cases where  $\eta$  is of the order of, or larger than, the reciprocal of the atomic scattering cross section  $\sigma$ ,



the surface brightness is no longer proportional to  $\eta$ . For such regions of the cloud, the surface brightness is proportional to the solar flux times the absorption line width. For regions in which  $\eta$  represents several optical thicknesses (one optical thickness =  $1/\sigma$ ), the brightness becomes independent of  $\eta$ . Radiance of chemi-luminescent and sunlit glow clouds for cases of

(i) emission with no absorption

(ii) emission and absorption, with and without re-emission of absorbed radiation

etc., has been studied theoretically by LLOYD (1965).

### 3.3 FILM CALIBRATION

An understanding of the photographic image formation is necessary to interpret the measurements of the vapour cloud expansion from the photographs of the cloud taken at fixed time intervals.

The total intensity of energy per sq cm incident upon the film determines the degree of darkening of the film negative, which is called the photographic density,  $\rho$ . The law of darkening of each film is represented by what are known as 'characteristic curves' of the film, i.e., curves of  $\rho$  vs logarithm of Exposure (i.e.,  $\ln$  Exposure). This 'Exposure' is defined as the product of the intensity incident on the film

and the duration of exposure. Over the linear portion of the curves, the relation between the density,  $\rho$ , and exposure,  $E$ , may be written as

$$\rho = \gamma \ln E + C \quad (3.9)$$

where  $\gamma$  represents the contrast of the film and is given by

$$\gamma = \frac{d\rho}{d(\ln E)}$$

The region of constant  $\gamma$  is the region of sharpest contrast (film darkening) for a given change in  $\ln E$ .

The determination of  $\gamma$  requires a proper calibration of the film. The Kodak no. 2475 film, which was used in the present study to photograph the vapour releases, was calibrated using a 6-step standard neutral wedge. Wedge impressions were obtained on the unexposed portions of the same film-roll containing the cloud images, to keep the conditions of film development the same for the calibration and for the cloud photography. These impressions were got on the film for 1-sec, 3-sec and 10-sec exposures which were the same exposure times used for cloud photography. This was to ensure that the proper value of  $\gamma$  was used for each exposure.

The photographic densities of these wedge impressions were then determined by scanning them on a Zeiss Densitometer and the output was recorded on a chart recorder. The densities

of wedge impressions on the film, as obtained from the densitometric records, were then plotted against the logarithm of wedge transmissions (proportional to  $\ln E$ ) for all exposure times that were used for the cloud photography.

The characteristic curve derived by the calibration procedure described above, for the film used (Kodak 2475) for 1-sec and 3-sec exposures for the 30th March 1968 cloud releases, are shown in FIG 3.1, where the zero of  $\ln E$  scale is arbitrary. Source brightness, for calibration with different exposures, were not identical. It was observed that there was little change in the value of  $\gamma$  for the different exposures of wedge impressions, which implied that reciprocity relation was holding good for all the exposure times of the experiment.

### 3.4 MEASUREMENT OF CLOUD DENSITIES

The relationship between the cloud image as represented by film density  $f'$ , and the number density,  $n$ , in cloud can be summarised as follows: As shown earlier, the column density over the line of sight distance is given by

$$\eta = \int_0^{\infty} n \, ds \quad \text{particles cm}^{-2}$$

and the brightness by

$$B = \frac{q\eta}{4\pi r^2}$$

It then follows from Sections 3.2 and 3.3 that

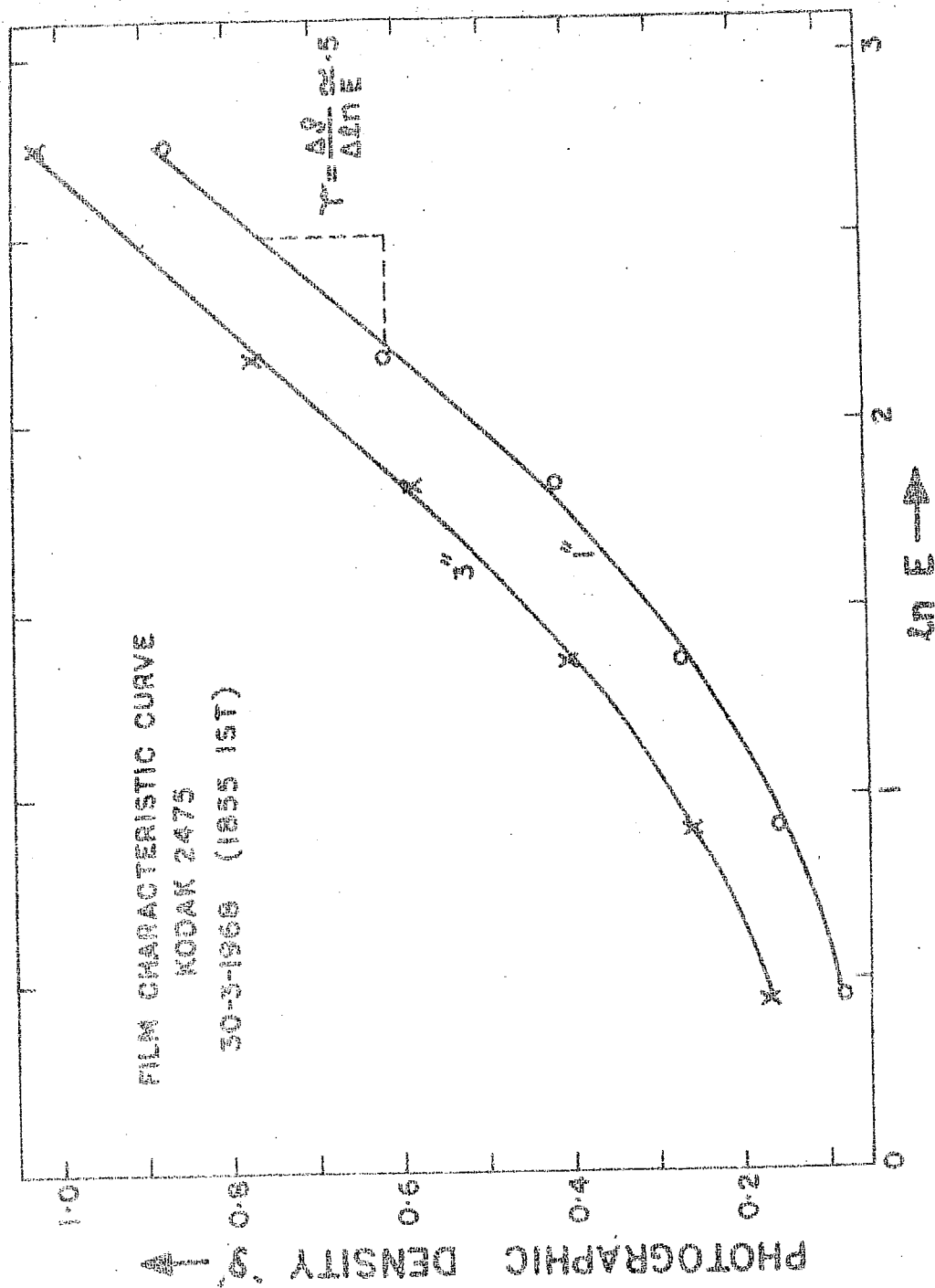


FIG 3.1 : Characteristic Curve for Kodak Film no. 2475

$$\frac{d\mathcal{F}}{r} = d(\ln E) = d(\ln B e^{-k}) = d(\ln q \eta e^{-k}) \quad (3.10)$$

where attenuation and other factors are included in  $k$ . The exposure,  $E$ , is considered proportional to brightness  $B$ .

If  $\eta, \mathcal{F}$  and  $E$  represent the respective quantities along the line of sight at a distance 'a' from the cloud centre, and  $\eta_0, \mathcal{F}_0$  and  $E_0$  represent the same quantities along the line of sight through the cloud centre, then for an optically thin cloud equation 3.9 can be written as :

$$\frac{\mathcal{F} - \mathcal{F}_0}{r} = \ln \frac{E}{E_0} = \ln \frac{B}{B_0} = \ln \frac{\eta}{\eta_0} \quad (3.11)$$

Equations 3.10 and 3.11 are valid if the range of exposure,  $E$ , associated with the vapour cloud, remains within the region where  $r$  is constant.

Micro-densitometry was performed for the Ba-Sr clouds (avoiding the overlap of ionised Barium) released on the 28th and 30th March 1968 to obtain photographic densities. At least 15-20 photographs taken during the cloud growth were examined for each case in this study. A typical micro-densitometric scan for one of the clouds is shown in FIG 3.2 (a). For each cloud, two scans were made at right angles to one another to ensure the sphericity of the cloud. The variation in radiance across the cloud could be found from the micro-densit-ometric scan with the help of the characteristic curve, and from this

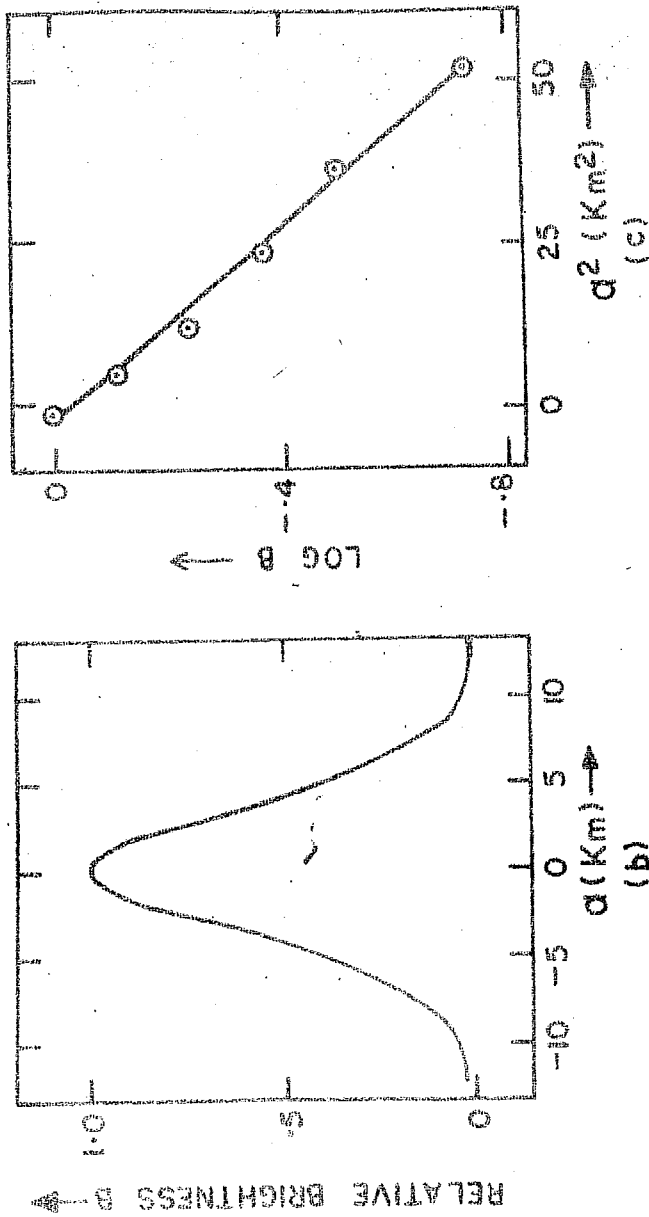


FIG 3.2 : (a) Micro-densitometer scan, about 10 minutes after the release, for the neutral cloud released at altitude 174 km on 28th March 1968.

(b) the brightness profile for the scan (a).

(c) Plot of (log Brightness) against (square of the distance from cloud centre) for the scan (a); the plot shows that the brightness across the cloud is Gaussian.

the effective radius could be determined. The detailed procedure is described in Section 3.5 where the procedure for the background sky-brightness correction is also discussed.

The brightness distribution across the cloud diameter for the scan relating to FIG 3.2 (a), is shown in FIG 3.2(b). That this brightness distribution is Gaussian is obvious from the straight line nature of (log B vs  $a^2$ ) plot shown in FIG 3.2 (c).

The distance on the negative of any point of the cloud from its centre is converted to its actual distance in space by multiplying it with the ratio of the range of the cloud from the camera to the focal length of the lens. For clouds which show a non-Gaussian behaviour, the effective radius can be calculated from the slope of the straight line segment of the plot of log B against  $a^2$ , although the analysis of the glow cloud in terms of Gaussian model is strictly not valid for such cases. However, provided that the non-Gaussian part of the cross section is relatively insignificant,  $r'_e$ s may be inferred, but with caution.

The non-Gaussian shape is more marked during the early development of the glow clouds, especially at the lower altitudes. FIG 3.3, reproduced from LLOYD AND SHEPPARD (1966), summarises the conditions under which the radiance distribution is substantially Gaussian, as a function of altitude.

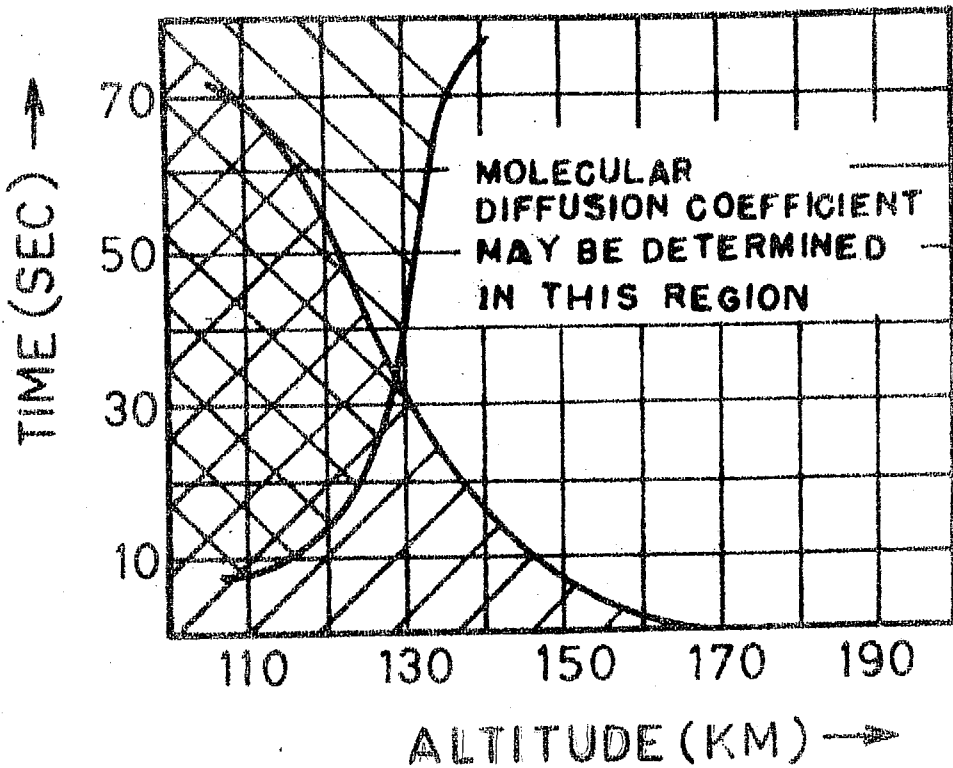


FIG 3.3 : \\\ Regions where turbulent diffusion dominates the expansion, /// Regions where brightness distribution across the cloud is markedly non-Gaussian. Molecular diffusion coefficient may be determined using vapour release techniques over the remaining regions (Reproduced from Lloyd and Sheppard, 1966).



The Gaussian nature of the profile for the clouds at selected intervals was ensured for making reliable measurements of diffusion from the photographs.

### 3.5 DETERMINATION OF DIFFUSION COEFFICIENTS

Several investigators have used different methods for measuring the expansion of a chemical release and deriving the diffusion coefficient in the upper atmosphere from these measurements (MANRING ET AL., 1961; COTE, 1965; LLOYD AND SHEPPARD, 1966; REES, 1967). The method used by the author is described in detail below. A brief account is also given of other methods, the conditions of the vapour cloud in which they are used, their limitations, the errors involved and the procedures for applying corrections.

#### 3.5.1 Effective Radius Method

This method is what has been used to analyse the data presented in this thesis. This method has the advantage that depletion of the contaminant due to reaction with the ambient or due to diffusion does not affect the results.

For an optically thin cloud, the brightness distribution across the cloud is, as shown in Section 3.2 given by;

$$B(a,t) = B(o,t) \exp \left( -\frac{a^2}{r_e^2} \right) \quad (3.12)$$

The effective radius of the cloud,  $r_e$ , at any time,  $t$ , is the radius of the contour of brightness, which is  $1/e$  times the peak brightness at the centre of the cloud, and, as already defined, is given for a spherical cloud by:

$$r_e^2 = r_o^2 + 4 Dt$$

The slope of the plot  $r_e^2$  vs  $t$  gives the diffusion coefficient.

Over the linear portion of the characteristic curve of the film emulsion, the photographic image density at any point of the cloud corresponding to a brightness  $B$  is, from equation 3.9, given by

$$\rho = \gamma \ln B + C'$$

where  $C'$  is a new constant which includes the proportionality constant between brightness  $B$  and exposure  $E$ . Corresponding to cloud brightness  $B_o$  at the centre of cloud and  $B_e$  at the effective radius

$$\rho_o = \gamma \ln B_o + C'$$

$$\rho_e = \gamma \ln \frac{B_o}{e} + C'$$

and hence

$$\rho_e = \rho_o - \gamma \quad (3.13)$$

Thus a measurement of the radius of the cloud on the density trace at a point  $\rho_e = \rho_o - \gamma$  gives the effective radius of the cloud.

### 3.5.2 Correction for the Sky Background Brightness

The presence of bright and variable sky background vitiates the accurate measurements of the cloud densities unless proper correction is applied. Sky background results in a background photographic density over a region outside the cloud image and also modifies the density over the cloud image.

Depending on whether the background photographic density, say  $\rho_b$ , corresponds to the linear portion of the characteristic curve, or to the toe region, two different procedures have been adopted for the background correction:-

#### a) When $\rho_b$ Corresponds to the Linear Region

The relation between image density and brightness for background, background plus cloud central brightness and background plus brightness at effective radius point, can be written respectively as

$$\rho_b = \gamma \ln B_b + C'$$

and

$$\rho_o = \gamma \ln (B_b + B_o) + C' \quad (3.14)$$

$$\rho_e = \gamma \ln \left( B_b + \frac{B_o}{e} \right) + C'$$

The first step here is to calculate the ratio  $X$  of the true central brightness of the cloud to the brightness of the sky background, by eliminating the constant  $C'$  from the first two expressions of equation 3.14. The result is:

$$\rho_o - \rho_b = \gamma \ln (1+X) \quad (3.15)$$

The density  $\rho_e$  appropriate to the contour of brightness  $1/e$  times central brightness is given by :

$$\rho_e = \rho_o - \gamma \ln \left( \frac{1+X}{1+X/e} \right) \quad (3.16)$$

From a comparison of equations 3.13 and 3.16 one can define an effective  $\gamma$  for the film for different X values as :

$$\gamma_{\text{eff}} = \gamma \ln \left( \frac{1+X}{1+X/e} \right) \quad (3.17)$$

The ratio of X is, in general, a smoothly varying function of time. The variation with time of X and of the resulting  $\gamma_{\text{eff}}$  for the highest cloud release on 30-3-1968 over Thumba is shown in FIG 3.4.

b) When  $\rho_b$  Corresponds to the Toe Region

In this case, the values  $\ln E_o$  and  $\ln E_b$  are read along the  $\ln E$  scale appropriate to the densities  $\rho_o$  and  $\rho_b$  from the characteristic curve. The ratio X is calculated from

$$\ln (1+X) = \ln E_o - \ln E_b$$

The value  $\rho_e$  is now read on the characteristic curve corresponding to the brightness  $E_e$  given by :

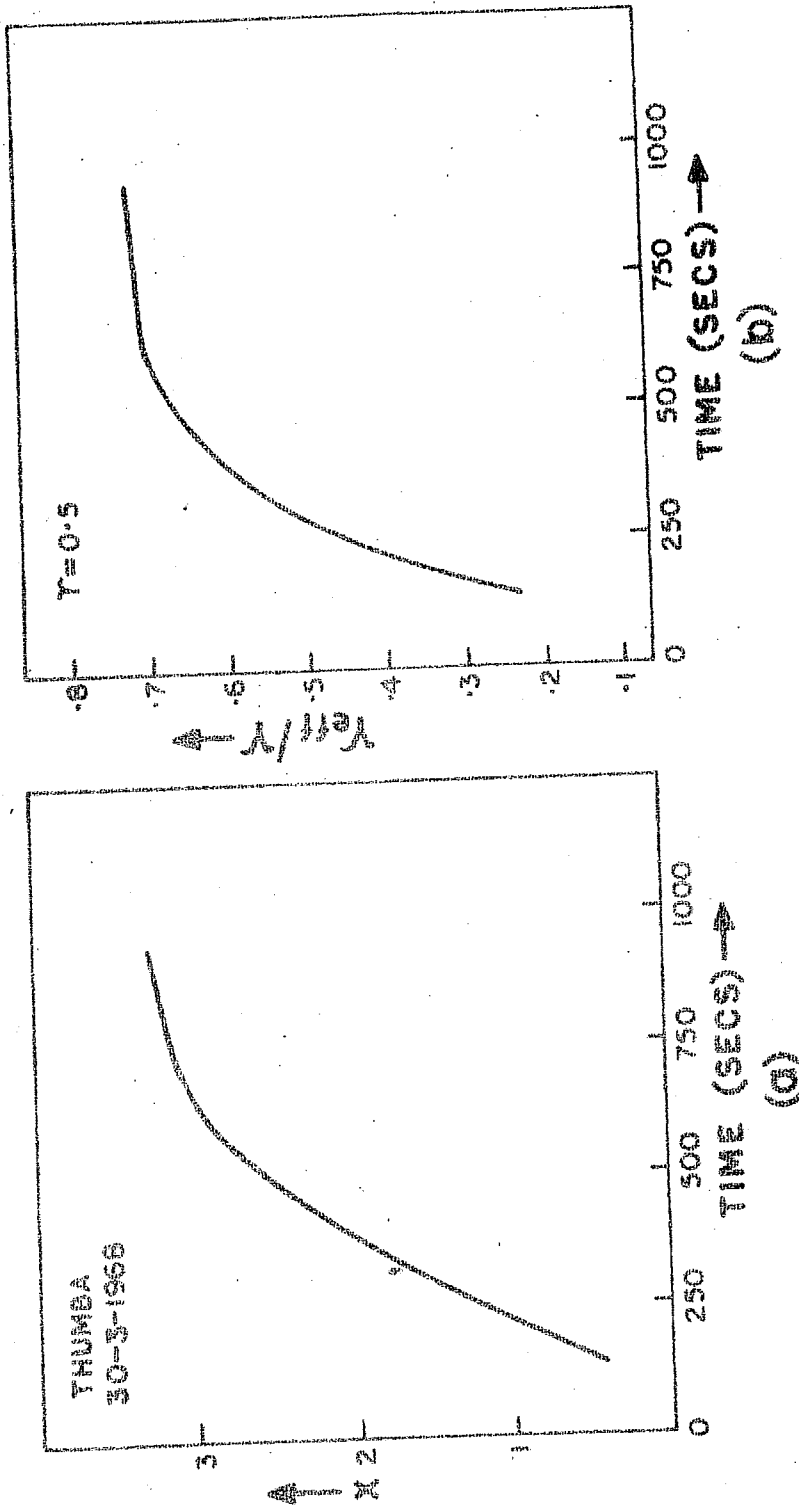


FIG 3.4 : (a) Variation of  $Y$ , the ratio of central peak brightness of the cloud to the sky background brightness, as a function of time for the cloud release at 204 km on 30th March 1968.

(b) Variation of the ratio between the effective  $Y$  and the true  $Y$  of the film, determined from (a), as a function of time.

$$\ln E_e = \ln E_o - \ln \left( \frac{1+X}{1+X/e} \right) \quad (3.18)$$

Once the radius of the contour of photographic density  $\rho_e$  is determined from the densitometer scans, the effective radius can be calculated, knowing the distance of the cloud from the camera station and the focal length of the camera lens.

### 3.5.3 Other Methods

When the brightness distribution is non-Gaussian, or the cloud is optically thick, or when the effective radius of the cloud is not easily measured, variants of the above method, as outlined below, may be employed for the determination of the diffusion coefficient.

#### a) Maximum Radius Method

This method is used when the cloud is optically thick, and the other methods with their requirement for a Gaussian profile are not acceptable. The assumption implicit in this method is that, in terms of surface brightness, the sky background brightness remains constant. Thus the visual edge of the cloud is defined at all times by a constant value of  $B$ , say  $B_{ed}$ , with corresponding radius,  $a_{ed}$ .

From equation 3.12, with  $\frac{\partial B_{ed}}{\partial t} = 0$ ,

$$\frac{d}{dt} (a_{ed}^2) = \frac{d}{dt} (r_e^2) \left( \frac{a_{ed}^2}{r_e^2} - 1 \right) \quad (3.19)$$

As the cloud expands,  $a_{ed}$  reaches a maximum and then starts to contract. If this radius is denoted by  $a_{max}$ , then at this time  $r_e^2 = a_{max}^2$ . Equation 3.12 then reduces to :

$$\frac{B_{ed}}{B_o} = \frac{r_o^2}{e a_{max}^2} \quad (3.20)$$

As  $B_{ed}/B_o$  is a constant, equations 3.12 and 3.20 yield

$$\frac{1}{e a_{max}^2} = \frac{1}{r_e^2} \exp - \frac{a_{ed}^2}{r_e^2}$$

i.e.,

$$\frac{r_e^2}{a_{ed}^2} = \ln \frac{a_{max}^2}{r_e^2} + 1. \quad (3.21)$$

This equation can be solved, for obtaining  $r_e^2$ , by knowing  $a_{ed}$  and  $a_{max}$ . The slope of the plot of  $r_e^2$  vs  $t$  gives 4 D.

The method is feasible only if the total integrated intensity of the cloud and the sky background do not change during the observation period.

#### b) Gradient (ln B) Method

The diffusion coefficient can also be found from a plot of

$$\frac{1}{\frac{\partial}{\partial a^2} (\ln B)} \text{ vs } t$$

which has a gradient of 4 D. As with all the methods, for the measurement to be exact, the cloud profile has to be Gaussian. The additional condition for accurate measurements is that the total integrated intensity of the cloud,  $P(t)$ , has to be constant with time. REES (1967) has shown, from his glow cloud measurements, that  $P(t)$  is, in general, not constant, though a correction factor,

$$\ln \int_0^{\infty} B(a) a^2 da / \ln \int_0^{\infty} B(a) a^2 da \text{ (maximum)} \quad (3.22)$$

where  $\ln \int_0^{\infty} B(a) a^2 da \text{ (maximum)}$  is the peak total output of the cloud, can be used to correct the gradient measurements. This depends on the accuracy of the integration of the total intensity of the cloud.

### c) Central Intensity Method

The central intensity of the (optically thin) cloud at any time  $t$  is given by :

$$B(o, t) = B(o, o) \frac{r_o^2}{r_o^2 + 4 Dt}$$

From this

$$\frac{B(o, o)}{B(o, t)} = 1 + \frac{4 Dt}{r_o^2}$$



and thus

$$\frac{\partial}{\partial t} \frac{B(o,o)}{B(o,t)} = \frac{4 D}{r_o^2} \quad (3.23)$$

which yields diffusion coefficient.

The requirements of this method are most likely to be found in small spherical puffs, as those of rocket grenades. However, when the total intensity of the cloud changes with time the method suffers from the same limitations as described in (a) and (b) above.

#### d) Measurements of Faint and Irregular Features

In the lower regions of the trail releases, below 110 km or so, the cloud breaks up into globules and eddies. Also the wind distorts these clouds to such an extent that portions of the trail from different altitude levels are seen along the same line of sight. Under these conditions, the usual methods of determination of cloud expansion are difficult, and the following method is used (REES, 1967).

A brightness level  $B_1$  corresponding to density  $\rho_1$  is chosen that is clear of interference from other parts of trail or the film noise level. This intensity contour has a radius  $a_1$  which is measured along with  $B_1$  and the peak intensity  $B_0$ . The effective radius  $r_e$  can then be calculated from:

$$B_1 = B_0 \exp \left( - \frac{a_1^2}{r_e^2} \right)$$

hence

$$\frac{r_e^2}{a_1^2} = \ln \frac{B_1}{B_0} \quad (3.24)$$

The plot of  $r_e^2$  vs  $t$  gives a straight line, the slope of which is again  $4D$ . This method is a more exact version of the Maximum Radius Method, since, in this case, the ratio of the two brightnesses can be directly measured with better accuracy, and the measurement of  $a_1$  is more precise, as it can be a level which is distinct from the extreme edge of the cloud image and is thus not susceptible to film grain size etc.

### 3.6 SOURCES OF ERRORS IN THE MEASUREMENT OF $r_e$ AND $D$ et

The sources of error in the measurement of the effective radius,  $r_e$ , leading to error in the resulting diffusion coefficient,  $D$ , lie in quantities involving grain size, non-uniformity of film emulsion, development process, and signal-to-noise ratio of the image. Besides these, factors such as the error in measurement of range of the cloud from the camera, discussed in Chapter II, are also to be considered. In addition, the instrumental errors of the micro-densitometer and camera, and dispersive atmospheric effects also contribute to inaccuracies.

#### 3.6.1 Film Effects

A great deal of care is to be exercised in the correct

choice of film, its calibration, development, etc., for the diffusion measurements. Film grain size is a limiting factor if small scale features of the cloud, such as turbulence, are to be studied. In the molecular diffusion measurements, the grain size contributes to the background noise level, and this in turn contributes to an uncertainty in the brightness profile determination. In the present study, the root-mean-square base level fluctuations of the micro-densitometry profile varied differently, and on an average it was estimated to contribute to an error of about 3% in the image density and brightness determinations.

### 3.6.2 Instrumental Errors

The micro-densitometer used for the density traces was the Zeiss Micro-densitometer, coupled to the Zeiss Recorder. The error of tracing, and measurement from chart, of the density and the effective radius was estimated to be not more than 2%.

The effects of camera distortion (Section 2.5) and vignetting are considered too small to necessitate any correction to the measured effective radius.

### 3.6.3 Non-central Scanning

The equation for the brightness trace can be written as (REES, 1967)

$$B(a) = B_0 \exp \left( - \frac{a'^2 + x^2}{r_e^2} \right)$$

$$= B_0 K' \exp \left( - \frac{a^2}{r_e^2} \right)$$

where  $x$  is the shift from the cloud centre at which the scan has been made, and  $K' = \exp(-x^2/r_e^2)$ . It will be seen that only the maximum signal will be affected, with no change in the value of  $r_e$ . It must be mentioned that  $x$  also corresponds to an altitude shift (of not more than about half km) of scanning and this could mean an actual change in the diffusion coefficient. This error will reflect as a scatter around the mean, but for small values of  $x$  the error will be negligible.

#### 3.6.4 Uncertainty in the Range of the Cloud

As will be evident from Section 3.4, the accuracy of determination of the effective radius,  $r_e$ , is dependent on the range of the cloud from the camera. The uncertainty in the range of the cloud has been discussed in Section 2.5. An error of about 3 to 4% is estimated in  $r_e$  due to this uncertainty.

### 3.6.5 Atmospheric Effects

In the theory of diffusion (Section 3.2) it has been assumed that the release of contaminant vapour does not alter <sup>(Change)</sup> the ambient atmospheric properties. This assumption may not strictly be correct. Again, excessive contaminant would result in self-absorption and/or large surface brightness, leading to photographic densities in the shoulder region of the characteristic curve, which would vitiate the measurements. Further, the features themselves become distorted by the combined effects of turbulence (50 m to a few km on a microscopic scale) and wind shear ( a few km to some tens of km on a macroscopic scale). Finite photographic exposure time and mass motion of the cloud are factors which have also to be taken into account for obtaining correct results.

#### a) Turbulence

In the present study, it has been assumed that there is no turbulence above about 110 km, and besides, all the measurements were carried out above 130 km. The effects of turbulence would be that the brightness profile does not remain strictly Gaussian throughout and the value of D

obtained is larger than what can be expected from molecular diffusion. The departure from straight line of the plot of  $r_e^2$  vs  $t$  may reflect to some extent the effect of this.

b) Wind Shear

If a velocity gradient exists across the cloud, the cloud shape would become elliptical. If  $v_x$  be the velocity along the  $x$  direction and has a gradient along the  $y$  direction (perpendicular to  $x$ ),  $v_y$  being zero, the axis of the elliptical cloud will be at an angle  $\theta$  to  $y$  axis, given by (REES, 1967)

$$\tan 2\theta = \frac{\partial v_x}{\partial y} \cdot \frac{t}{2}$$

which is proportional to  $\frac{\partial v_x}{\partial y}$  for small  $\theta$ s. Here  $t$  refers to the time after the release of the cloud.

A densitometer trace along  $y = 0$  will still give the correct radius. An estimate of the shear effect could be assessed, if the cloud radius is determined from central scanning on two mutually perpendicular directions. In the present study, as the clouds were released above 130 km, where shears are usually small (the actual shears could not be measured, because these were point releases), no noticeable difference was observed in the perpendicular scannings.

BEDINGER AND CONSTANTINIDES (1968) and QUESADA AND MACLEOD (1972) have discussed diffusion coefficient determinations in the shear regions.

c) Finite Exposure and Wind Velocity

For a finite photographic exposure time, the micro-photometer study of the cloud photograph will not give the true instantaneous brightness profile because of the proper motion of the cloud due to winds, which results in a smearing of the cloud image. The observed effective radius,  $r'_e$ , will in such cases be larger than the true effective radius  $r_e$ . It has been suggested (REES, 1967) that a correction can be applied as  $r_e = r'_e - \frac{1}{2} vT$  when  $v$  is the wind velocity and  $T$  is the exposure time.

This problem has been investigated analytically in the present study, and it is found that the correction suggested above is not appropriate and is too large. The brightness  $B(P)$  of a spherically symmetric cloud along the line of sight through a point  $P$  at distance  $a$ , from the cloud centre is given by

$$B(P) = B(0) \exp \left( - \frac{a^2}{r_e^2} \right)$$

where  $B(0)$ , the peak central brightness, is assumed to remain constant during the short time interval of exposure. The line of sight through  $P$  (fixed in space) which is at a

distance 'a' from the cloud centre at the beginning of exposure ( $t=0$ ), will be at a distance  $(a-vt)$  after a time 't', 'a' being reckoned positive in the direction of  $v$ . For an exposure time  $T$ , the integrated brightness along this line of sight would, therefore, be

$$\overline{B(P)} = \overline{B(0)} \int_0^T \exp \left[ - \left( \frac{a-vt}{r_e} \right)^2 \right] dt$$

or

$$\overline{B(P)} = \overline{B(0)} \cdot \frac{r_e}{v} \left[ \operatorname{erf} \left( \frac{a}{r_e} \right) - \operatorname{erf} \left( \frac{a-vT}{r_e} \right) \right] \quad (3.25)$$

"erf" being the error function.

The brightness profile measured from the micro-photometer study of the cloud photograph will correspond to  $\overline{B(P)}$  and its effective radius will be  $r'_e$ . It can be shown that  $r'_e$  is a function of  $vT/r_e$  only; hence the correction applicable due to finite  $vT$  can be presented, as in FIG 3.5(a), as a curve of percentage increase in  $r_e$  vs  $vT/r_e$ . The figure also shows that even for  $vT = 2 r_e$  the ratio  $r'_e/r_e = 1.34$ , whereas according to the correction suggested by REES, this ratio should be two, amounting to 100% error when  $vT$  is neglected.

FIG 3.5 (b) shows the profile of  $\overline{B(P)}$  for  $vT = 2 r_e$ , compared with the brightness profile  $B(P)$  for  $vT = 0$ . It is seen that except for increased effective radius  $r'_e$ , the Gaussian nature of the profile is not measurably distorted.



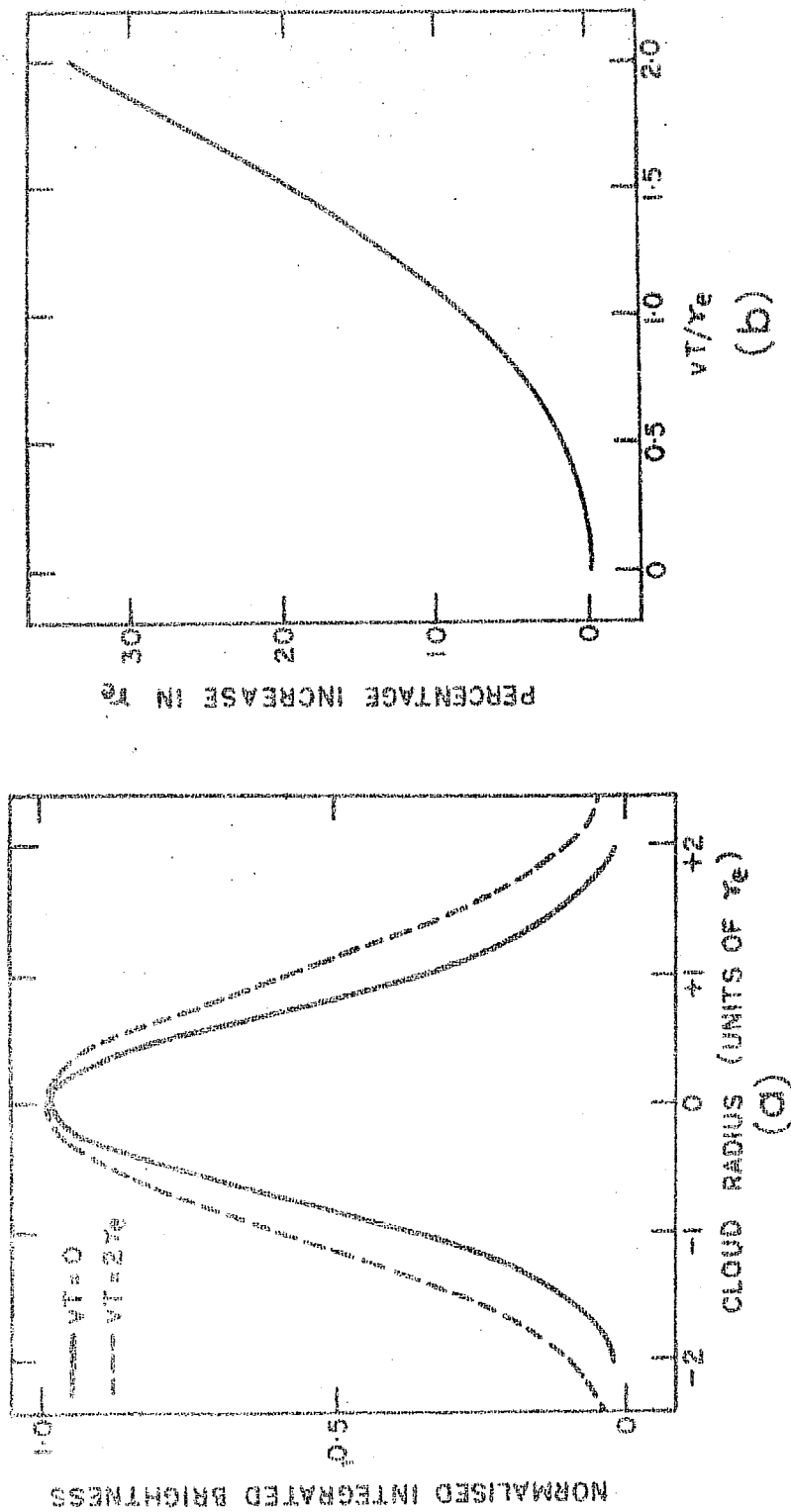


FIG 3.5 : (a) Brightness distribution across the cloud. —  $vt=0$ ,  
 ---  $vt = 2 r_e$ .

(b) Percentage increase in the effective radius, as a function of  $vt/r_e$ .

One feature not shown in the diagram is the shift of the position of central peak brightness by  $\frac{1}{2} vT$ .

To get a closer insight into the process leading to increased effective radius, the effect of finite exposure and finite wind velocity on the measured brightness distribution can also be looked upon in the following way. When plotted in units of  $r_e$ , the instantaneous brightness profile (assumed Gaussian) is a normal curve with effective radius equal to unity. The effect of finite  $v$  and  $T$  can now be considered as the scanning of this normal curve with a rectangular window  $vT/r_e$ . This also explains why percentage increase in  $r_e$  is function of  $vT/r_e$  only.

It may finally be concluded that for usual photographic exposures of about 10 seconds and for atmospheric winds upto  $100 \text{ m sec}^{-1}$ , the correction to the effective radius is quite small, except for the very early parts of observations (where, however, one does not use exposures as long as 10 seconds). In any case FIG 3.5 (b) may be used to correct for the effects of wind and exposure.

### 3.6.6 Probable Errors

While the atmospheric effects can duly be dealt with in the measurement of  $r_e$ , the same is not possible in respect of the accidental errors described in Sections 3.6.1 to 3.6.4. As a result of these, the probable error in a particular measurement of the effective radius  $r_e$  is estimated to be

about 8%. The probable error in the determination of the diffusion coefficient  $D$  will then be  $\frac{2}{\sqrt{n}}$  times the probable error in  $r_e$ , where  $n$  is the number of  $r_e$  measurements. In the present study, atleast 15 to 20 pictures were analysed for the  $r_e$  measurements for each cloud release, and thus the mean probable error in  $D$  is estimated to be around 4% due to these effects. At lower heights, more number of photographs (about 25 to 30) were analysed, and consequently, the error is expected to be only about 3%. The probable error due to these sources can be obtained from the  $(r_e^2 \text{ vs } t)$  plot and this has been computed for each cloud release.

### 3.7 DIFFUSION COEFFICIENT RESULTS

Using the effective radius method described in Section 3.5, the diffusion coefficients for the Ba-Sr point releases at 133 km, 152 km, 174 km and 205 km of 28th March 1968, and at 152 km, 180 km and 204 km of 30th March 1968, were determined. On 28th March 1968, the cloud releases at 205 km and 152 km showed vertical velocities after about 12 minutes and 20 minutes after release respectively. The diffusion measurements on these two clouds reported here, were made when they had maintained the constant height.

Typical plots of  $r_e^2$  vs  $t$  for two cloud releases are shown in FIG 3.6. The probable error in  $D$  was assessed for each cloud release and did not exceed 6%, except for the

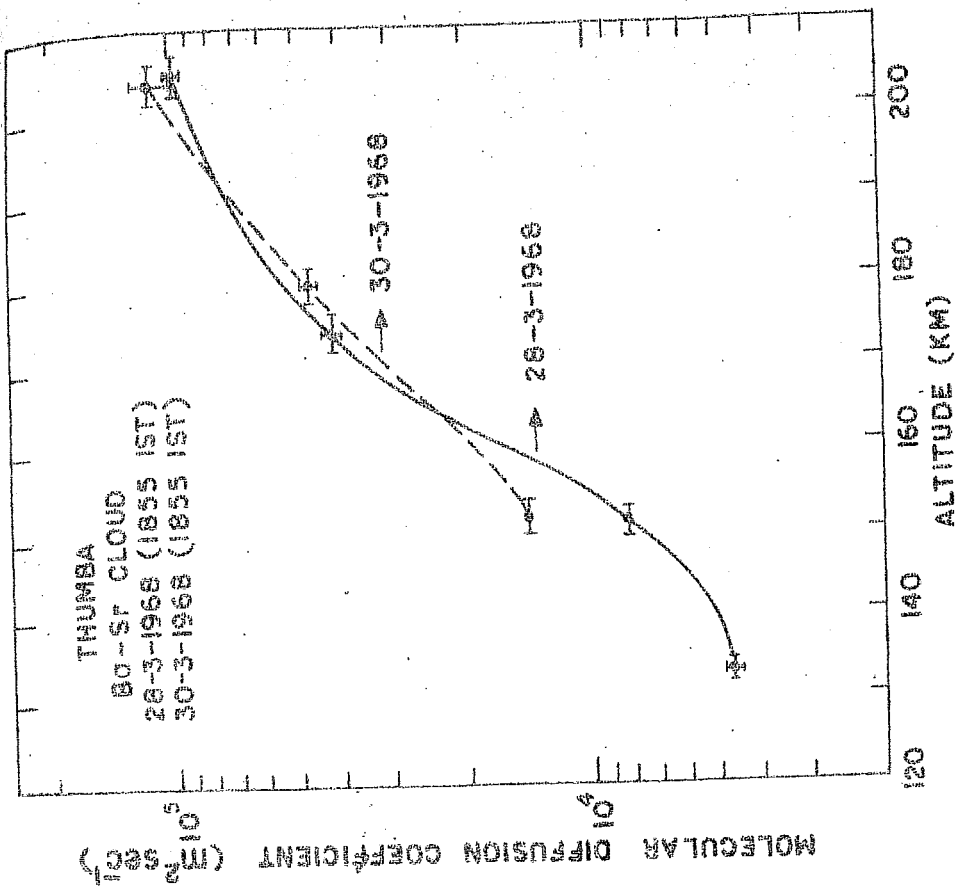


FIG 3.6 : Plot of the square of effective radius vs time, for clouds collected over Thumba on 30th March 1968.

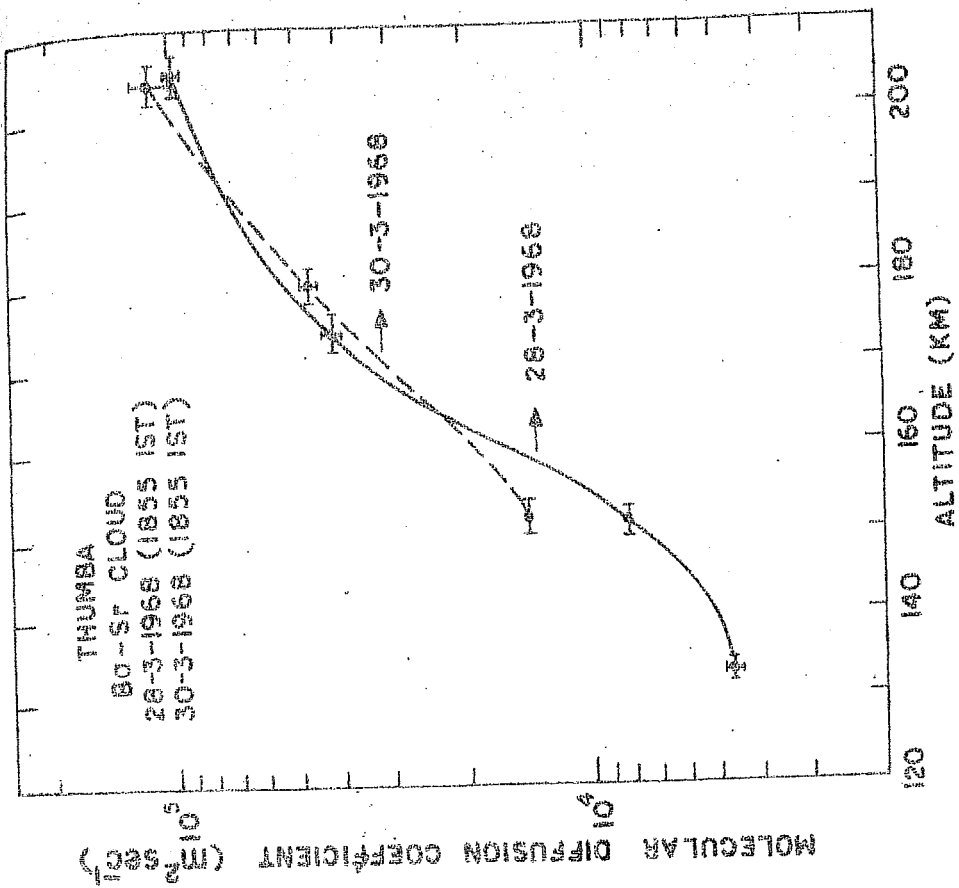


FIG 3.7 : Diffusion profiles over Thumba, as observed, during evening twilight on 28th and 30th March 1968.

204 km cloud release of 30th March 1968, for which the probable error was around 12%. Table 3.1 lists the measured diffusion coefficients with the corresponding probable errors for the different clouds on the two days. FIG 3.7 shows the plot of D vs altitude.

Table 3.1

Date and Time of Experiment.	Altitude of release (km)	Diffusion coefficient ( $\times 10^{-4} \text{ m}^2 \text{ sec}^{-1}$ )
28th March 1968 1855 IST	205	$9.65 \pm .58$
	174	$4.07 \pm .18$
	152	$0.79 \pm .03$
	133	$0.46 \pm .02$
30th March 1968 1855 IST	204	$10.80 \pm 1.30$
	180	$4.50 \pm .23$
	152	$1.38 \pm .04$

### 3.8 ATMOSPHERIC STRUCTURE FROM MEASURED DIFFUSION COEFFICIENTS

The molecular diffusion coefficient for inter-diffusion of two dissimilar species (denoted by the subscripts 1 and 2) is given by the expression (CHAPMAN AND COWLING, 1960; HIRSCHFELDER ET AL., 1954)

$$D_{12} = \frac{2.628 \times 10^{-7}}{P_{012}} (T^3/2\mu_{12})^{\frac{1}{2}} \text{ m}^2 \text{ sec}^{-1} \quad (3.26)$$

where P and T are respectively pressure in atmospheres and temperature in degrees Kelvin,  $\mu_{12}$  is the reduced molecular weight given by  $M_1 M_2 / (M_1 + M_2)$ ,  $M_1$ ,  $M_2$  being the molecular weights of the two species, and  $\sigma_{12}$  is the temperature-dependent collision cross-section between the two species.

One can write  $\sigma_{12}^2 = \sigma_0^2 \Omega(T^*)$  where  $\sigma_0$  is the temperature-independent collision cross-section, and  $\Omega(T^*)$  is the temperature-dependent part of  $\sigma_{12}$ . The factor  $\Omega(T^*)$  is a tabulated function of  $T^* = Tk/\epsilon$ , where k is the Boltzman constant and  $\epsilon$  is the force constant in the inter-molecular interaction. Numerical tables of  $\Omega(T^*)$  vs  $T^*$  exist for several assumed analytical forms for the inter-molecular potential functions (HIRSHFELDER ET AL., 1954). In the present calculations, Lennard-Jones (6-12) potential function (FIG 3.8) has been used for the calculation of  $\Omega(T^*)$ .

LLOYD AND SHEPPARD (1966) have proposed a method for the calculation of the atmospheric temperatures from the diffusion measurements. To outline their method briefly, the ratio  $H_P^{-1} / H_D^{-1}$  is first calculated for a relevant model atmosphere for different heights, where  $H_P^{-1}$  and  $H_D^{-1}$  are  $-\frac{1}{P} \frac{dP}{dz}$  and  $-\frac{1}{D} \frac{dD}{dz}$  respectively. The observed values of  $H_D^{-1}$  are then multiplied by the value of this ratio at the corresponding heights to obtain  $H_P^{-1}$  and hence the temperatures. As is obvious, the method relies to a considerable

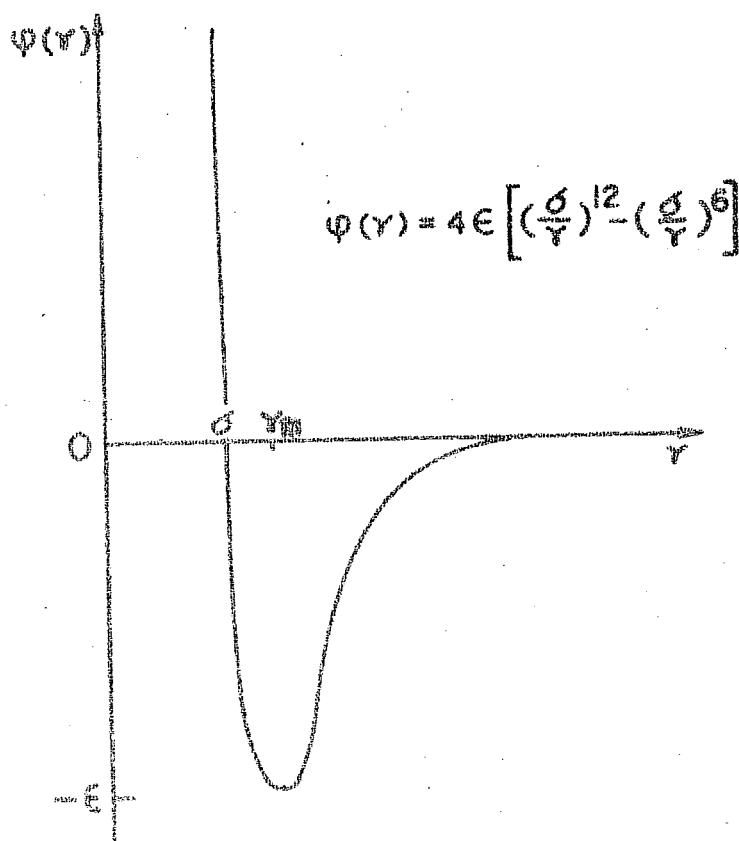


FIG 3.8 : Lennard-Jones (6-12) inter-molecular interaction potential.

extent on the particular model atmosphere chosen to calculate  $H_P^{-1}/H_D^{-1}$ . Temperature profiles calculated by this method show large deviations compared with the model atmospheric profiles.

An alternative method has been developed in this study, which appears to work much better and does not depend upon assumption of any model atmosphere parameters except that it makes use of the temperature and number densities at a single height, preferably the highest height at which the diffusion coefficient is determined.

Above 100 km altitude, different atmospheric species undergo diffusive separation (JACCHIA, 1971), and consequently their number density distribution can be represented by:

$$n_i = n_i^0 \cdot \frac{T_0}{T_z} \exp \left( - \int_{z_0}^z \frac{m_i g}{kT} dz \right) \quad (3.27)$$

where  $T_0$  and  $T_z$  are the temperatures at heights  $z_0$  and  $z$  respectively and  $n_i^0$  and  $n_i$  the corresponding number densities for the molecular species of mass  $m_i$ . Atomic oxygen (O), molecular oxygen ( $O_2$ ) and molecular nitrogen ( $N_2$ ) have been assumed to be the major constituents above 100 km.

Differentiation of equation 3.26 and incorporation of the relation 3.27 give:

$$\frac{dT}{dz} = \frac{\frac{1}{D} \frac{dD}{dz} - \frac{M_A g}{RT} + \frac{M_R}{2 M_A (M_R + M_A)} \frac{dM_A}{dz}}{\frac{3}{2T} - G(T)} \quad (3.28)$$



Equation 3.28 can be used for the calculation of the atmospheric temperatures from the observed  $H_D^{-1}$ . In the above equation,  $M_R$  and  $M_A$  are respectively the molecular weight of the contaminant vapour molecules and the mean molecular weight of the ambient atmospheric species, and  $R$  is the gas constant. The mean molecular weight of the ambient atmosphere at any height is obtained from the relation

$$M_A = \frac{\sum n_i M_i}{\sum n_i},$$

$M_i$  being the molecular weight of an individual atmospheric constituent. The term  $G(T)$  in the denominator of equation 3.28 takes account of the temperature variation of the collision cross-section. It is given by

$$G(T) = \frac{1}{T_c} \frac{1}{\Omega} \frac{d\Omega}{dT^*}$$

where  $T_c = \frac{\epsilon}{k}$  and  $T^* = \frac{T}{T_c}$ , and can be calculated as a numerical function of  $T$  from tables of  $\Omega$  vs  $T^*$  (HIRSHFELDER ET AL., 1954) if the force constant term  $\epsilon$  in the interaction potential of the contaminant - ambient interaction is known. At present, data regarding force constants for the interaction between dissimilar molecules are practically non-existent. HIRSHFELDER ET AL. (1954) suggest, however, the use of a combining law,  $\epsilon_{ij} = \sqrt{\epsilon_i \epsilon_j}$ , to calculate such force constants from the force constants of interactions between similar

molecules. BIRD ET AL. (1960) have suggested empirical expressions for the estimation of force constants and collision cross-sections from the properties of, the fluid at the critical point, c, liquid at boiling point, b, or the solid at the melting point, m, by the following relations:

$$\frac{\epsilon}{k} = 0.77 T_c, \quad \sigma = 0.841 V_c^{1/3} \quad \text{or} \quad 2.44 \left( \frac{T_c}{P_c} \right)^{1/3}$$

$$\frac{\epsilon}{k} = 1.15 T_b, \quad \sigma = 1.166 V_{b, \text{liq}}^{1/3}$$

$$\frac{\epsilon}{k} = 1.92 T_m, \quad \sigma = 1.222 V_{m, \text{sol}}^{1/3}$$

where  $\epsilon/k$  is in  $^{\circ}\text{K}$ ,  $\sigma$  in Angstroms,  $V$  in  $\text{cm}^3 \text{ g-mole}^{-1}$ , and  $P_c$  in atmospheres.

The value  $410^{\circ}\text{K}$  for  $\epsilon/k$  was used for interactions of Ba-Sr atoms with atmospheric constituents. For interactions involving aluminium oxide-air molecules, the value  $120^{\circ}\text{K}$  for  $\epsilon/k$  has been used, after LLOYD AND SHEPPARD (1966), who have inferred this value appropriate to the molecular weight of  $\text{AlO}$  from the values of  $\epsilon/k$  for other substances tabulated by HIRSHFELDER ET AL. (1954).

Temperatures were determined by integrating equation 3.28 in steps of 1 km. Upward integration, with assumed values of temperature and number densities of  $\text{O}$ ,  $\text{O}_2$  and  $\text{N}_2$ , as taken from the model atmosphere (JACCHIA 1971), for the lowest

altitude of measurement, led to negative temperature gradients between 120 to 150 km, which made further upward integration difficult. Hence downward integration, starting from model atmosphere values for temperature and number densities appropriate to the highest altitude for which D was measured, was resorted to. This led to more satisfactory results. Cause for the failure of the upward integration procedure is discussed in Section 3.10. The present method simultaneously calculates the number density profiles, molecular weight profile etc., besides the temperature profile, and thus these need not be taken from the model atmosphere for every height.

### 3.9 DERIVED TEMPERATURE RESULTS

Temperatures were calculated by the method outlined above from the diffusion measurements on Ba-Sr neutral clouds released over Thumba. FIG 3.9 shows the temperatures calculated and also the model temperature profile for comparison. It will be seen that the temperatures calculated for 30th March 1968 agree closely with the model atmosphere temperatures, but those calculated from 28th March 1968 data show departure, particularly below 150 km.

REES ET AL. (1969) have reported upper atmosphere temperatures calculated from their diffusion measurements on aluminium oxide vapour clouds, using the technique described by LLOYD AND SHEPPARD (1966). They have also reported direct spectroscopic measurements of the temperatures. FIG 3.10 shows

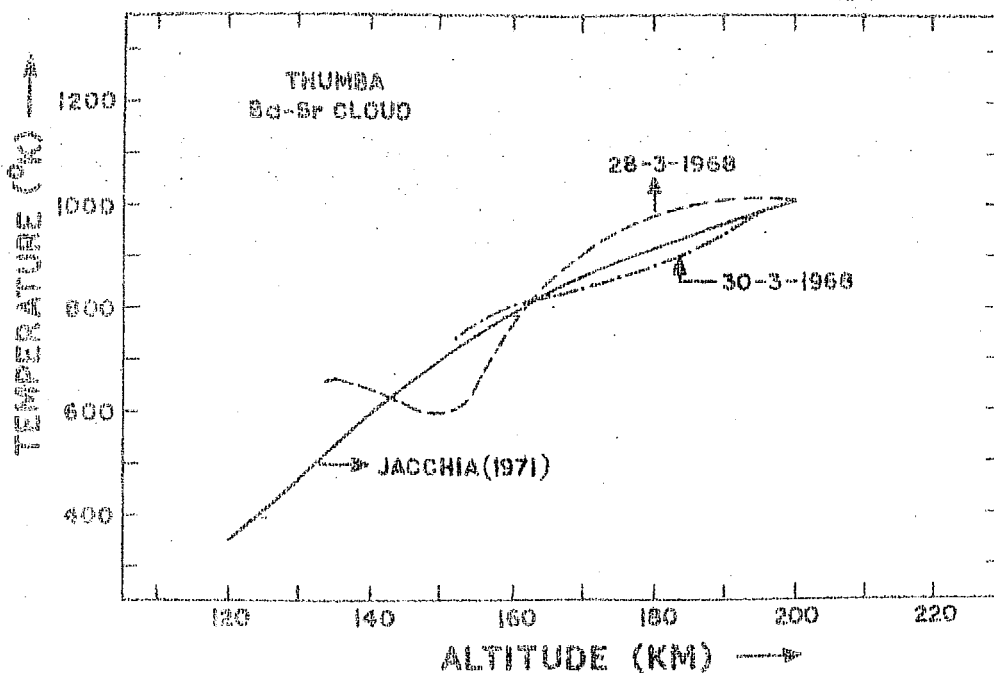


FIG 3.9 : Temperature profiles over Thumba, calculated from the diffusion profiles of FIG 3.7.

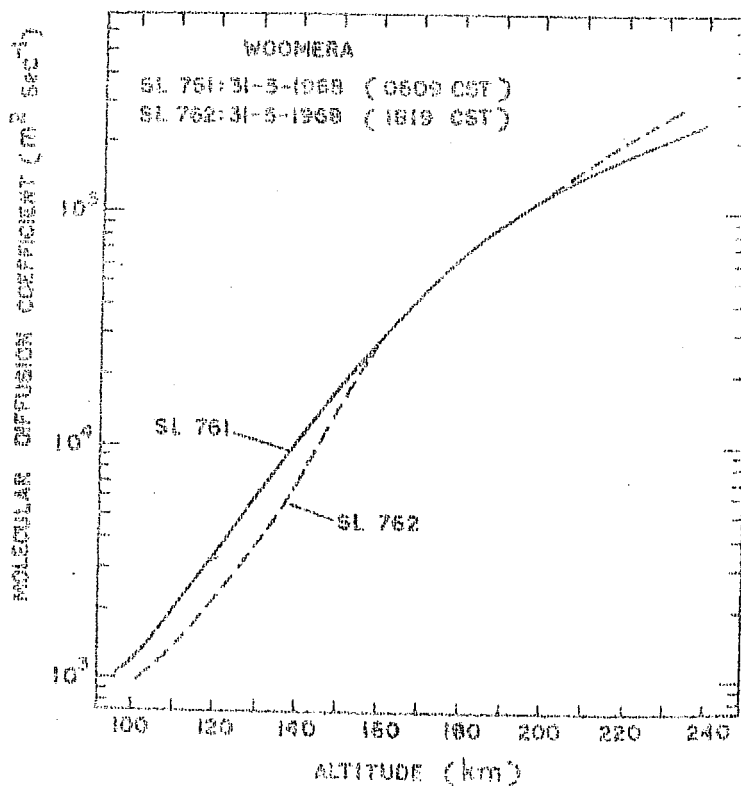


FIG 3.10 : Diffusion profiles observed for AlO vapour clouds released over Woomera (Reproduced from Rees et al., 1969).

the two diffusion profiles that have been measured by them. This diffusion data has also been used in the present study to calculate temperatures. FIGs 3.11 and 3.12 show the temperature profiles as calculated by the author using the method described in Section 3.8, and as calculated by REES ET AL. using LLOYD AND SHEPPARD'S method. These figures also show, for comparison, the model atmospheric temperatures and the spectroscopic direct measurements.

It will be seen from FIG 3.12 that there is good agreement between the results obtained from the present method and the model atmosphere temperatures. Direct temperature measurements are much lower. Temperatures calculated by REES ET AL. by LLOYD AND SHEPPARD'S method show poor agreement with both direct measurements and the model atmosphere temperatures. FIG 3.11 shows that spectroscopically measured temperatures and model temperatures agree closely and temperatures calculated by the present method are some what higher. Those calculated by REES ET AL. are again very much in disagreement.

It will thus be seen that the present method, besides being much less dependent on the model atmosphere than the LLOYD AND SHEPPARD'S method, is also superior to the latter in the final temperature results.

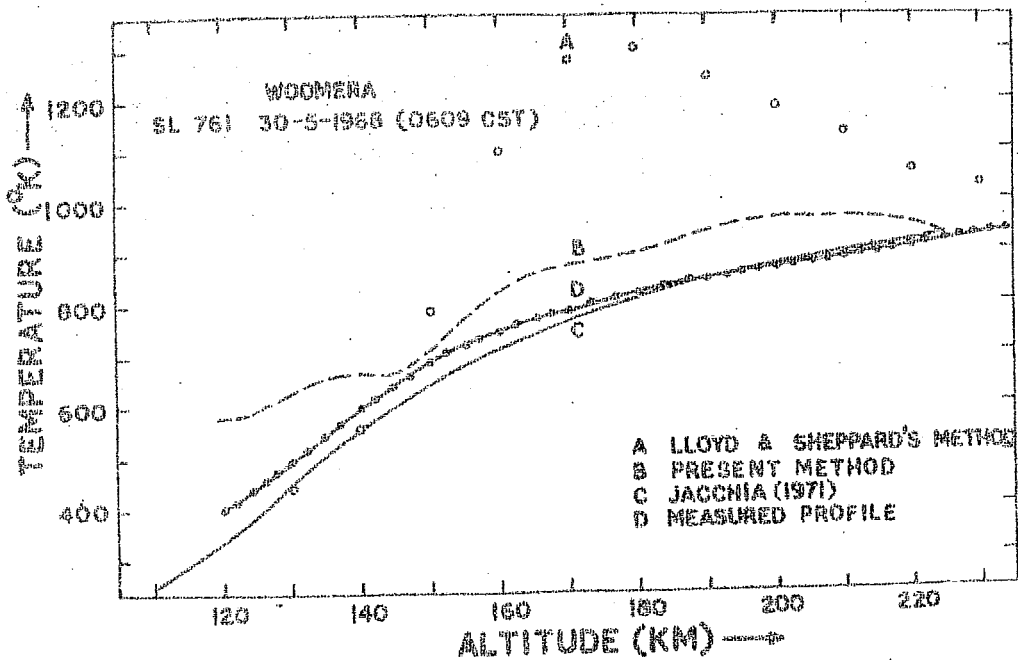


FIG 3.11 : Temperatures over Woomera, calculated from the diffusion profile of FIG 3.10 for flights SL 761, 31-5-1968, 0609 CST.

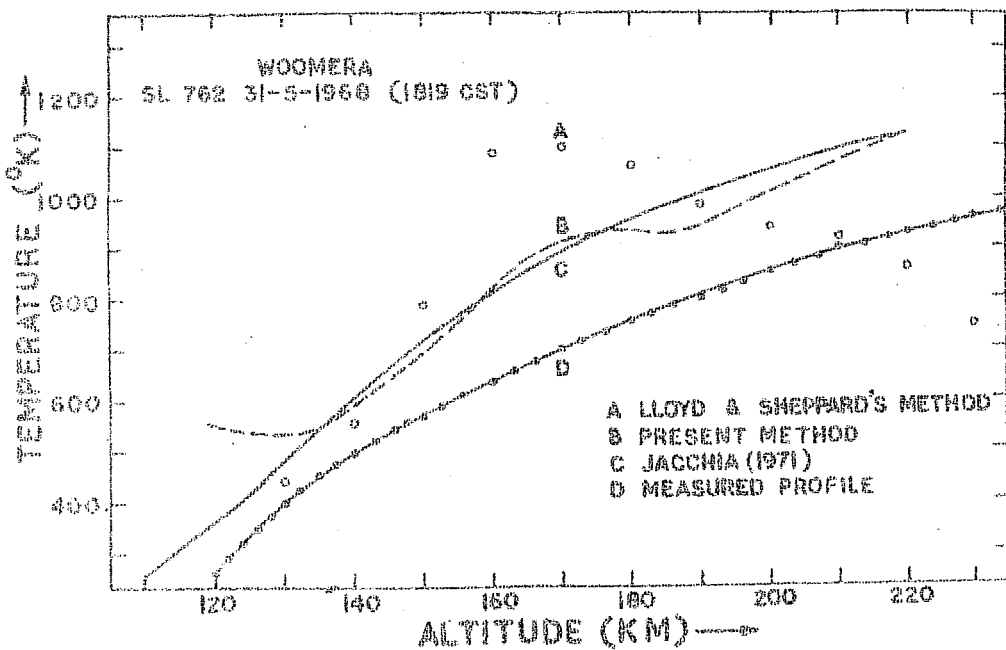


FIG 3.12 : Same as FIG 3.11 for flight SL 762, 31-5-1968, 1819 CST.

### 3.9.1 Accuracy in Temperatures

The actual error in diffusion measurements was, in most cases, less than 10%, but even assuming a 10% error, the inaccuracy in the calculated temperature at any height has been estimated, from actual computations, to be not more than 7%.

There are two further sources of error that require study. These are the uncertainties in the mean molecular weight (derived from the number densities of ambient constituents) and the temperature assumed at the highest altitude. To assess the resulting inaccuracies in the temperature profiles due to these two sources, equation 3.28 has been integrated for REES ET AL.'s profiles (because of their larger altitude coverage), assuming the atmospheric mean molecular weight to be 5% above and 5% below the assumed JACCHIA (1971) value. Similarly the profiles have also been obtained assuming the temperature at the highest altitude to be 50 °K above and 50 °K below the model value. The following conclusions emerge from these calculations:

Changes of 5% in the mean molecular weight at 220 km result in about 3% change in the calculated temperature profile around 120 km, the difference being progressively smaller for the higher altitudes. The temperature profiles calculated with different starting temperatures at 220 km tend to converge at lower altitudes, their contribution to

the uncertainty in the calculated temperatures being consequently smaller. This convergence has been used to advantage in integrating equation 3.28 downwards. The error in temperature determinations due to uncertainty in the value of  $\epsilon/k$  has been estimated to be less than 2%.

The overall inaccuracy consequent on these sources can be estimated at any height to be not more than 10%.

### 3.10 ANOMALOUS TEMPERATURE PROFILE BELOW 150 KM

It is seen from FIGs 3.9, 3.11 and 3.12 that the temperature gradient below 150 km assumes negative values. This was one of the main reasons why upward integration of equation 3.28 could not be carried out for deriving the temperature profile from the observed diffusion profile.

The indications of anomalous temperature profiles below 150 km have also come from the analysis of many other diffusion profiles of other investigators (results not presented here), and also from mass-spectrometer composition profile (SHIRKE ET AL., 1969), incoherent scatter results etc. Various possibilities for such temperature inversions are discussed below, with special reference to the results of the experiment carried out on 28th March 1968 over Thumba.

#### 3.10.1 Additional Diffusion

The various terms important in determining the temperature gradient for the above experiment at some heights are



given below:

<u>Height</u>	$\frac{1}{D} \frac{dD}{dh}$	$\frac{M_A g}{RT}$	<u>GL</u>	$\frac{3}{2T}$	<u>G (T)</u>
200	0.02	0.02	-0.0008	0.0015	-0.0003
175	0.04	0.03	-0.0009	0.0016	-0.0003
150	0.04	0.04	-0.0013	0.0032	-0.0007
140	0.03	0.04	-0.0015	0.0030	-0.0006

(GL represents the third term in the numerator of the right hand side of equation 3.28).

The diffusion coefficient derived for 28th March 1968, at 150 km, is about half of that derived for 30th March 1968. The diffusion profile below 160 km on 28th March gives values of  $\frac{1}{D} \frac{dD}{dh}$  which are rather too low, contributing to negative temperature gradients. This suggests additional diffusion, besides molecular diffusion, below 150 km. If this process could be turbulent diffusion, the plot of the square of the effective radius vs time should have also shown up large departures from a straight line plot. This, however, was not the case.

### 3.10.2 O/O<sub>2</sub> Ratio

An explanation in terms of mean molecular weights, taking recourse to the controversy, of the ratio between

$O$  and  $O_2$ , is also ruled out. An  $O/O_2$  ratio, of atleast about 30-40 at 150 km, is required to offset the negative temperature gradients, whereas the present-day model atmospheres may allow a ratio upto a maximum of about 15 at this height.

### 3.10.3 Wave Propagation

Many investigators (ROSENBERG AND JUSTUS, 1966; WOODRUM ET AL., 1969) have considered viscous energy dissipation of winds at these levels. The role of joule heating by atmospheric current systems is also an important source of heat in this region. SPENCER ET AL. (1970) from probe measurements have also pointed out the importance at 150 km altitude, of other energy sources. But, because of the short time for heat conduction at these levels, any localised heat-input would make the temperature profile smooth in a very short time. However, the reversible heating, that has been advocated by HINES (1965), has shown some promise in explaining some of the temperature anomalies at E-region heights observed by incoherent scatter method (HOOKE, 1969). Gauging from the rather sinusoidal nature of the temperature profile of 28th March (though derived with the help of releases made only at four heights), it looks plausible to invoke the atmospheric waves for explaining the anomalies. It has already been discussed (Section 2.3) that vertical winds, and varying horizontal winds were observed on this day. The estimated vertical wavelength of the temperature profile (about 60 km at 170 km) is compatible with a

similar wavelength deduced for vertical winds. It would have been worth the while if it was possible to make diffusion measurement the succeeding morning, to test if a downward phase progression was observable, which would have unambiguously proved or disproved the propagating wave phenomena.

However, from the two profiles of REES ET AL. (1969) it appears that such plausibility is verified. If, in the derived temperature profiles (FIGs 3.11 and 3.12) the features at 145 km (in the morning profile) and at 130 km (in the evening profile of the same day) are to be identified as similar ones, one has then phase progression downwards corresponding to energy propagation upwards. REES ET AL. (1972 A), from an auto-correlation study of horizontal wind profiles of these two experiments, have reported vertical wavelengths of the wind profiles which are in agreement with those derived from the temperature profiles.

REES ET AL. (1972 A) and LLOYD ET AL. (1972) have also reported temperature and density anomalies, but at greater heights. GOLOMB ET AL. (1969), making simultaneous diffusion and temperature measurements, report that a wave-like structure is evident in some diffusion curves, and that these cannot be explained in terms of corresponding temperature changes, and that compression-rarefaction waves are probably involved. BERNARD AND SPIZZICHINO (1971) report semi-diurnal temperature oscillations in the 100-140 km region with vertical wavelengths of the order of 50 km.

Thus, there seems to be strong evidence for wave propagation being a major contributor to these atmospheric structural anomalies.

#### 3.10.4 Departures from Barometric Law

MAYR AND VOLLAND (1972), STUBBE (1972), and several other investigators have shown that large departures from barometric law for the distribution of atmospheric species above 100 km are possible, and that atomic oxygen may not be in diffusive equilibrium because of the convergence and divergence of air due to horizontal neutral motions. The vertical velocities, have great consequences on the vertical distribution of the constituents. It is important to note that on 28th March 1968, vertical velocities were observed, but, however, only during the later part of the experiment. The assumption that is implicit in the derivation of equation 3.28 is that barometric law holds good at all heights and that all the constituents are in diffusive equilibrium. How far the effects of these departures would affect the temperature profile is, however, open to question, but this does seem to be another possibility for, atleast, partially explaining the anomaly.

#### 3.10.5 Desirability of Further Experiments

From ALADDIN II experiment, REES ET AL. (1973 B) have reported a variation in the morning and evening values

of density by as much as a factor of two. From this, as well as from what has been stated in the foregoing sections, it would be clear that the region between 100 to 150 km is most complex, and that more co-ordinated experiments, using a variety of techniques and measurements, should be conducted to resolve the various discrepancies that exist. Four to five, rocket experiments, spread over the night, may be necessary to obtain a satisfactory indication of the role played by the various agencies in the 100-150 km region.

NEUTRAL UPPER ATMOSPHERIC WINDS AND MID-LATITUDE  
NIGHT-TIME IONOSPHERE

FEW problems in ionospheric physics have consistently aroused as much interest as the behaviour and structure of the F-layer. Many reviews on this subject (SHIMAZAKI, 1959; DUNCAN, 1960; RISHBETH, 1964, 1967 A, 1968 B; YONEZAWA, 1966; FARLEY ET AL., 1967; GOLDBERG, 1969; EVANS, 1971; etc. to mention a few) have been presented at regular intervals to explain the many observed phenomena.

By experimental means, such as bottomside and topside sounders, incoherent backscatter radar, etc., a vast amount of data, on a global scale, on altitude distribution of electron density,  $N(z,t)$ , at F-region heights, have been gathered over the years. Electron and ion temperatures have also been studied widely, particularly after the establishment of the incoherent scatter technique (BANKS, 1967; MCCLURE, 1969; WILLMORE, 1970; EVANS, 1973).

#### 4.1. THEORETICAL STUDY OF THE IONOSPHERE

Although the variations in electron density may be regarded as reasonably well-known, physical explanations are not possible without a great deal of information about other atmospheric properties, viz. the density, temperature and composition of the neutral atmosphere, the flux of the ionising radiation, the chemical reactions, etc.

Unlike at lower levels, the distribution of ionisation with altitude at F-region is affected not only by chemical mechanisms but also by transport processes. For example, the role of ambipolar diffusion as the cause of formation of  $F_2$ -peak (RATCLIFF, 1956), and the electric fields originating at lower levels of the atmosphere by dynamo effect (MARTYN, 1947, 1953) which play an important role in the  $F_2$ -layer structure, have been recognised for a long time now. The work of KING AND KOHL (1965) first drew attention to the importance of winds in the movements of  $F_2$ -layer height. The probable importance of neutral winds in maintaining night-time ionosphere was first construed as a possibility by HANSON AND PATTERSON (1964).

There have principally been two approaches by which the F-region has been investigated theoretically, the synthetic and the analytic approaches. In the synthetic approach, idealised forms of the continuity equation for the electron density are solved with suitable numerical values of the parameters, and the results compared with the actual F-region behaviour. This approach usually does not lead to accurate determination of the parameters but, nevertheless provides a feel for the effects that different physical processes could produce in the ionosphere. This has been the method followed by many investigators (RISHBETH, 1964, 1967 B, 1968 B; KING ET AL., 1967; KOHL ET AL., 1968; STUBBE, 1968 A, 1970; BAILEY ET AL., 1969; STUBBE AND CHANDRA, 1970; FALKULIN AND MURADOV, 1971).

In the analytic approach, the continuity equation is written to include all the processes which are being considered, and the experimental  $N(z,t)$  data are inserted. The best fitting values of the physical parameters are thus derived. This method has been followed by NISBET AND QUINN (1963), SHIMAZAKI (1966), CHUNG-MING-HUANG (1966), and to some extent by STUBBE (1968 A).

A combination of the analytic and synthetic approaches has been used in the present study. The F-region monthly mean electron density profiles for each hour of the day, at Puerto Rico (geographic co-ordinates,  $18^\circ$  N and  $67^\circ$  W; geomagnetic latitude  $29^\circ$  N; dip  $51^\circ$ ) for the year 1960, published by CRPL (1960, 1961), have been used to derive, by the analytic approach, parameters affecting the night-time F-region. Using the synthetic approach, the effect of the various parameters on the electron density distribution at night has also been studied. The purpose is to understand and estimate the importance of the different mechanisms which affect the F-region during night-time hours.

In Section 4.2, the basic theory of F-region and the various processes which affect it are described. Section 4.3 deals with various propositions putforth to explain the maintenance of night-time F-region. The mathematical formulation of the present problem is discussed in Section 4.4. The numerical procedure, that has been employed for solving the various equations, is described in Section 4.5. The limitations of the



present calculations are discussed in Section 4.6. Sections 4.7 to 4.9 discuss the results obtained from the observed electron density profiles over Puerto Rico. The results obtained by studying the night-time behaviour of F-region for equinox conditions by the synthetic approach are presented in Section 4.10.

#### 4.2 PHYSICAL THEORY OF THE F-REGION

Most of the theoretical discussions of the F-region have been conducted in terms of the continuity equation for electron density,  $N(z,t)$ , as a function of altitude  $z$  and time  $t$ . If  $q$  and  $l$ , denote the rate of production and loss of electrons per unit volume respectively, and  $\underline{v}$ , is the transport velocity, the continuity equation may be written as

$$\frac{\partial N}{\partial t} = q - l - \text{div} (N\underline{v})$$

The F-region is electrically neutral; positive and negative charge densities are not likely to differ more than about 1 in  $10^{12}$  (JOHNSON AND HULBURT, 1950); also negative ions are likely to be very small in number; and thus, the above equation applies equally for electrons and ions. The individual terms contributing to the continuity equation, are described below.

##### 4.2.1 Production (q)

The ionisation in the  $F_2$ -layer is produced mainly by photo-ionisation of atomic oxygen. Solar ultra-violet radiation

in the 170-911 Å range, with 304 Å and 584 Å Helium lines as the principal radiations, is the main ionising mechanism in the F-region during day-time. Electrons, with energies less than 2 keV, have also been thought to be the agents responsible for ionising the constituents at F-layer heights to some extent.

The main ionic constituents in the lower F-region are  $\text{NO}^+$  and  $\text{O}_2^+$ ; they are  $\text{O}^+$  between 200 and 800 km altitude, and  $\text{He}^+$  and  $\text{H}^+$  beyond the altitude of about 800 km. The peak production during the day occurs at a height of about 170-180 km, though the maximum ionisation is found to occur at a height of about 250 km with electron densities typically of the order of  $10^6 \text{ cm}^{-3}$ . The electron density decreases by about a factor of five during night-time, with the height of maximum ionisation correspondingly raised by about 50 to 100 km over its day-time value.

#### 4.2.2 Loss (1)

The resulting  $\text{O}^+$  ions in the F-region are lost by the formation of molecular ions by ion-atom interchange followed by dissociative recombination (BATES, 1955). These processes lead to a loss of electrons at a rate,  $l$ , approximately given by  $l = \alpha N^2$  in the lower F-region, and  $l = \beta N$  above it, where  $\beta$  and  $\alpha$  are termed the linear loss coefficient and dissociative recombination coefficient respectively. These coefficients depend on the rates of the reaction. Coefficient  $\beta$  depends,

besides, on the number densities of atmospheric molecular constituents. The transition of the loss rate from the form  $\alpha N^2$  to  $\beta N$  gives rise to the formation of the day-time F-layer ledge, termed the  $F_1$ -layer.

#### 4.2.3 Transport Term ( $\text{div}[N_y]$ )

The lower F-region, where production and loss are the main contributions to the continuity equation, is termed the photo-chemical regime. The region above 200 km, where the transportation processes become important is known as the transport-dominated region.

The transport-velocities are obtained from the equations of motion for the electrons and ions, which depend on various forces acting on them, one of which is the interaction with neutral air.

#### 4.2.4 F-region Parameters and Their Relationships

In addition to the above, many of the F-region processes depend on the temperatures of electron, ion and neutral components, each of which is again subject to a heat balance or thermal continuity equation. Simple relations, relating to the  $F_2$ -peak, based on earlier theoretical investigations (RISHBETH, 1966) are summarised below (RISHBETH AND GARRIOT, 1969):

Day equilibrium conditions:

Height of peak electron density  $\beta_m \sim D_m / H_i^2$

$-h_m$  at which height-

Maximum electron density-  $N_m \sim q_m / \beta_m$

Night decay coefficient-  $\beta' \sim \beta_m$

In the above,

$D$  = ambipolar diffusion coefficient

and  $H_i$  = the ion scale height.

The subscript  $m$  denotes the parameters at the peak of ionisation and  $h_m$  and  $N_m$  denote the height of the peak and the corresponding maximum value of electron density respectively.

If a vertical drift  $v$  is imposed on the plasma, the height of the peak is shifted by an amount

$$\Delta h_m \sim \frac{v H_i^2}{D_m}.$$

Below and above the  $F_2$ -peak the electron density approximately assumes the alpha-Chapman distribution

$$N(z) = N_m \exp \frac{1}{2} \left( 1 - \frac{z - h_m}{H_i} - \exp - \frac{z - h_m}{H_i} \right).$$

Well above the  $F_2$ -peak the plasma assumes a diffusive equilibrium distribution given by:

$$N(z) = N_m \exp \left( - \frac{z - h_m}{H_p} \right)$$

where  $H_p = 2kT_p/m_i g$ , is the plasma scale height, assumed to be independent of altitude

$k$  = Boltzmann constant

$g$  = acceleration due to gravity

$T_p = (T_e + T_i)/2$ , is the plasma temperature

$T_e$  = electron temperature

$T_i$  = ion temperature

$m_i$  = ion mass

#### 4.3 THE NIGHT-TIME IONOSPHERE

The behaviour of the night-time F-region is mainly a problem of the maintenance of the night-time F-layer in the absence of production by solar ultra-violet radiation. The maintenance of the mid-latitude night-time ionosphere has been the subject of active debate in the past decade (HANSON AND PATTERSON, 1964; YONEZAWA, 1965; GEISLER AND BOWHILL, 1965; STUBBE, 1968 A). In mid-latitudes, during equinox and winter months, only for a few hours after sunset does the decay of the  $F_2$ -layer resemble that of the idealised night-time stationary layer. Afterwards, the electron densities are found either to decay very slowly, or maintain a constant level until sunrise with minor fluctuations, or even, on some nights, reverse before sunrise. The total electron content appears to behave similarly (EVANS AND TAYLOR, 1961; TITHERIDGE, 1968). This suggests that some processes act to maintain a 'base level' ionisation of about  $10^5 \text{ cm}^{-3}$ .

This behaviour can be explained either in terms of a change in the effective recombination coefficient for the layer or in terms of a night-time source of ions, or both. A brief resume, of the various processes under the above two mechanisms, is given below.

#### 4.3.1 Change in the Recombination Coefficient

Such a change can arise from an actual change in the chemical composition of the atmosphere or by a vertical translation of the F-layer into a region of lower atmospheric density. Composition changes of the type postulated as the cause for F-region seasonal anomaly (RISHBETH AND SETTY, 1961; STROBEL AND MCELROY, 1970; RUSTER AND KING, 1973), can be ruled out because they necessitate changes in the atomic to molecular number density ratio at the base of the thermosphere. Time constants preclude such diurnal changes, though they may allow such seasonal changes. The loss rate can also reduce because of temperature decrease during night, but to explain the maintenance of ionisation, from the available data on temperature dependence of loss rates, a temperature decrease from day-to-night by a factor of two to three will be required which is scarcely likely.

MAYR AND VOLLAND (1972), while discussing the problem of diurnal phase anomaly, have pointed out that the diurnal wind circulation might distribute the atomic oxygen concentration such that the diurnal variations in the  $O/N_2$  and  $O/O_2$

ratios get damped by about 20%. This, according to them, could contribute to the maintenance.

The mechanism, of vertical translation of F-layer into regions of lower atmospheric density, could, however, produce large changes in the actual loss rate. HANSON AND PATTERSON (1964) first advocated that equatorward winds could produce vertical translation efficiently.

After KING AND KOHL (1965) first drew attention to the important fact that large atmospheric winds exist at F-region heights and that large vertical drifts of ionisation could be caused by them at these heights in mid-latitudes, much work has gone in this direction for explaining many of the ionospheric F-region variations. KING ET AL. (1967), KOHL ET AL. (1968, 1969), ECCLES ET AL. (1971) and many other investigators have studied the influence of neutral winds at F-region heights in detail. A complete bibliography can be found in the review by RISHBETH (1972 B). These studies have brought out the important fact that winds are equatorward during the night and, in mid-latitudes, can raise the layer by about a scale height. This height change could reduce  $\beta_m$  by a factor of nearly five which would certainly help preserving the night-time ionisation.

The drifts computed from meridional winds at these heights are generally downward by day, changing to upward around sunset. The time of change is crucial to the above explanation, since should a downward drift persist after

sunset, the plasma would be rapidly destroyed, and a subsequent upward drift would bring no recovery, unless a strong nocturnal source were postulated.

STUBBE (1968 A), without invoking neutral winds, explains the night-time maintenance by horizontal electric fields of the order of 5-10 mv. However, the required field, besides being large, is in the opposite sense to what it is normally assumed to be.

#### 4.3.2 Sources of Ionisation

The wind does not, by itself, preserve the layer, as is evident from the foregoing discussions. By reducing the effective loss rate it cannot halt the decay completely and hence some source of ionisation has to be sought. Some possible sources are discussed below.

##### a) Ionisation from Conjugate Point

Some of the pre-sunrise phenomena have been attributed to an influx of photoelectrons along the geomagnetic field-lines when the conjugate point is illuminated by the sun (EVANS, 1965; CARLSON, 1966). These photoelectrons could raise the electron temperature and also the airglow intensity (COLT, 1965), but do not possess sufficient energy to produce required new ionisation (NAGY AND BANKS, 1970; NAGY ET AL., 1973).

##### b) Corpuscular Ionisation

During recent years, several investigators have suggested



energetic particles to be a cause of various F-layer phenomena, particularly those associated with disturbances and those at high latitudes (IVANOV-KHOLODNY, 1965; TORR AND TORR, 1970). The part played by corpuscular ionisation in the F<sub>2</sub>-region maintenance is, however, still on a doubtful premise (KRASSOVSKY ET AL., 1965). Particles capable of producing ionisation at these heights would be electrons or protons of energy less than 2 kev. An average columnar production rate of a few times  $10^8$  ion-electron pairs  $\text{cm}^{-2} \text{sec}^{-1}$  throughout the night would be required to maintain the night-time F-layer (RISHBETH, 1968 A; STROBEL AND MCELROY, 1970) which amounts to an energy input of  $10^{-2} \text{ erg cm}^{-2} \text{sec}^{-1}$ .

Calculations of ionisation, caused by electrons of various incident energies, have been made by several workers (REES M.H. 1963, 1968; MAEDA, 1965; OSIPOV AND PIVAVORAVA, 1971 A,B,C), although for very low energies the estimates are only a few. TORR AND TORR (1970), in particular, have examined in detail, in conjunction with neutral winds, the effect of corpuscular radiation as the source of night-time F-region for a high-latitude station.

A serious handicap in such studies is the lack of observational data concerning electrons in this low energy range. Most of the available observations are for the auroral latitudes. However, WILLMORE (1964) has estimated, from measurements by Ariel I satellite, that the electron temperature

distributions during the night between 400 and 1200 km could be accounted for as a result of heating due to electrons with energies of 2-3 kev and in fluxes of  $\sim 8-9 \times 10^9 \text{ cm}^{-2} \text{ sec}^{-1}$ . SAVENKO ET AL. (1963), and KNUDSEN (1968) have also reported measurements of soft particle fluxes at F-region heights.

There are still only a few satellite or rocket measurements to speculate diurnal variations of the flux. An indication of particle precipitation into the atmosphere is the detection of  $3914 \text{ \AA}$  emission (the first negative band of  $\text{N}_2^+$ ) in the nightglow. From the study of  $3914 \text{ \AA}$  and  $4278 \text{ \AA}$  airglow emissions, TORR AND TORR (1970) have estimated the diurnal variations of electron flux for their calculations.

In the absence of reasonably known values of fluxes and their variations at mid-latitudes, the effect of corpuscular radiation has not been included in the present calculation. This omission, however, will not be significant for the present investigation of mid-latitude quiet-time ionosphere, since the object is only to see, if the ionosphere would be maintained with the better known parameters.

### c) Plasma Flux from the Protonosphere

Since the magnetosphere contains a great deal of plasma, it can in principle, act as a reservoir from which night-time F-region can be maintained. The coupling between the ionosphere and the protonosphere (which is situated above a level of about 1000 km) is complicated by the domination of the two

regimes by different ions and by the presence of the diffusive barrier (HANSON AND ORTENBURGER, 1961) that hinders free exchange of ionisation between the two regions. This diffusive barrier effectively de-couples the two regions, so that, though large diurnal changes are observed in the ionosphere, changes in the protonosphere are only to the tune of 30%.

As the  $F_2$ -layer decays after sunset, the oxygen ion concentration at high altitudes is reduced, and the layer of hydrogen ions in the protonosphere, which effectively floats on the oxygen ions, tends to be lowered into the region where charge exchange with atomic oxygen takes place efficiently. This process replenishes the oxygen ion supply, and when a steady state is reached, enough hydrogen ions are converted to oxygen ions which move downward along field lines (diffusion) or drift downwards due to electric fields, to balance the losses taking place lower below.

Different values of the protonospheric flux, ranging from  $5 \times 10^7$  electrons  $\text{cm}^{-2} \text{sec}^{-1}$  (YONEZAVA, 1965) to  $2$  to  $3 \times 10^8$  electrons  $\text{cm}^{-2} \text{sec}^{-1}$  (HANSON AND PATTERSON, 1964; GEISLER AND BOWHILL, 1965), have been quoted for the maintenance of a peak electron density of about  $10^5$  electrons  $\text{cm}^{-3}$ . HANSON AND PATTERSON (1964) and GEISLER (1967 B) have computed an upper limit of about  $2 \times 10^7$  electrons  $\text{cm}^{-2} \text{sec}^{-1}$  for the upward flux of plasma into the protonosphere by day, to which the downward night-time flux must be comparable. RISHBETH (1963,

1968 B) has shown that a flux of  $2 \times 10^7 \text{ cm}^{-2} \text{ sec}^{-1}$  would contribute only to the extent of maintaining the base level  $N_m$  at  $3 \times 10^4 \text{ electrons cm}^{-3}$ , with  $h_m$  already raised higher by winds. This, therefore, does not represent a significant enough contribution to the night-time  $F_2$ -region.

From the above calculations, it can be seen that the day-time upward flux to the protonosphere is about one order less than the downward flux necessary to maintain the F-layer. From these it has frequently been inferred that the protonosphere does not function as a significant reservoir of ionisation. The calculations of maximum possible flux, however, involve several parameters which are not well known, and hence the above conclusions are subject to revision.

BANKS AND HOLZER (1969) have calculated polar wind fluxes of 2 to  $7 \times 10^8 \text{ protons cm}^{-2} \text{ sec}^{-1}$  based on atmospheric models. PARK (1970), from whistler studies, has observed that under quiet geomagnetic conditions the observed rate of increase in day-time magnetospheric content gives an upward flux of about  $3 \times 10^8 \text{ electrons cm}^{-2} \text{ sec}^{-1}$  across the 1000 km level into the protonosphere, and a downward flux of about  $1.5 \times 10^8 \text{ electrons cm}^{-2} \text{ sec}^{-1}$  at night, an amount sufficient to maintain the nocturnal ionosphere according to the previous studies. He has also proposed (PARK, 1971) a mechanism, by which westward electric field enhances downward flux from the protonosphere during substorms, to explain the night-time ionisation changes during storm times.

#### 4.4 MATHEMATICAL FORMULATION OF THE PROBLEM

Theoretical exploration of the upper atmosphere or ionosphere requires simultaneous solving of a number of time-dependent equations, viz., continuity equation and the equations of motion and heat conduction. These equations relate to individual neutral and charged particle species, which are considered to be influencing the physical behaviour of the region.

In a most comprehensive investigation of steady state solutions of coupled differential equations for  $N$ ,  $T_e$ ,  $T_i$  and  $T_n$  (electron concentration, electron, ion and neutral temperatures respectively), HERMAN AND CHANDRA (1969) initiated rigorous numerical methods for atmospheric studies. Steady state solutions are reasonable when the time necessary for the solutions to become independent of the initial profile is short, as compared to a characteristic time for the change of typical ionospheric parameters. This is the case for electron- and ion-densities and temperatures. It is, however, not so for neutral wind velocity and neutral temperature, which have a transient time of the order of a few days. Time dependent solutions are, therefore, necessary. STUBBE'S (1970) is the only exhaustive work in this connection to date.

In the present calculations, time-dependent equations of motion for neutrals have been solved for day and night, and time-dependent continuity equation for electron density has

been solved for night-time, after estimating the parameters influencing the electron density profiles during night-time. Continuity equation for neutral air has not been solved and JACCHIA'S (1971) static diffusion model has been adopted instead. The following processes have been considered to be operative during night-time at F-region heights in the present study.

- i) Losses due to recombinations
- ii) Neutral winds
- iii) Plasma flux from the protonosphere, divesting itself into ambipolar diffusion and electric field drifts.

#### 4.4.1 Definitions and Assumptions

##### a) Coordinate System

A cartesian coordinate system, with the x,y and z axes pointing respectively along south, east and zenith, is adopted. The geographic and geomagnetic-axes are assumed to coincide, implying that declination is zero. Time and east-west coordinates are assumed to be inter-changeable, i.e.

$$\frac{\partial}{\partial y} = \frac{1}{R \Omega \sin \theta} \frac{\partial}{\partial t}$$

where  $\Omega$  is the angular velocity of the earth, R the radius of the earth and  $\theta$  the colatitude of the place.

b) Horizontal Derivatives

The usual simplifying assumption, that the different dependent variables are functions only of height and time, has been made, viz.,

$$\frac{\partial}{\partial x} = \frac{\partial}{\partial y} = 0.$$

This assumption, however, applies only to individual calculations relating to a particular location, and does not mean that the variables do not change either with latitude or longitude (and time). Specifically, vertical gradients are considered more important than the horizontal ones. This assumption is not applied to neutral atmospheric pressure which is the driving force for the neutral winds. The assumption is specifically made for the divergence term,  $\text{div}(\underline{N}\underline{y})$  in the electron continuity equation.

Although quite rapid horizontal motions may exist, they do not necessarily contribute much to the divergence term, because the horizontal gradients of  $N$  and  $\underline{y}$  are usually much smaller than their vertical gradients. Horizontal gradients generally involve scale distances of hundreds or thousands of km, but vertical scales are only tens of km, though the horizontal gradients in  $N$  during sunrise and sunset times would be important.

c) Model Atmosphere

Calculations have been performed in the height region of 90 to 800 km. Static diffusion model of JACCHIA (1971), appropriate to the 10.7 cm solar flux, has been used to derive neutral atmospheric temperature, pressure and constituents, as functions of altitude and time. All known variations of temperature and density described by JACCHIA have been included.

The neutral, electron and ion temperatures, are assumed to be equal for all times and for all heights. It is assumed that neutral atmosphere consists of O, O<sub>2</sub>, N<sub>2</sub> and He, and that, above 100 km, these are in diffusive equilibrium. Hydrogen is considered only from 500 to 800 km, where it is also assumed to be in diffusive equilibrium.

Ionic constituents are assumed to be O<sup>+</sup>, NO<sup>+</sup> and O<sub>2</sub><sup>+</sup> upto 400 km, and above this altitude O<sup>+</sup> only is considered as constituting the ionisation. H<sup>+</sup> ions are usually considered important only above 800 km during medium and high sunspot activities and hence they have not been included in the calculations.

d) Transport Velocities

All neutral and ionic constituents are assumed to move with velocities, u and v respectively.



#### 4.4.2 The Equations to be solved

The electron continuity equation and the equations of motion for ions and neutrals are the ones which are to be solved. With the assumptions enunciated in Section 4.4.1, these equations, with requisite simplifications, are written as follows.

##### a) Continuity Equation

The continuity equation for the electron density is,

$$\frac{\partial N}{\partial t} = q - 1 - \text{div} (N \underline{v}). \quad (4.1)$$

For solving this equation for night-time, it is assumed that there is no production due to any source, i.e.  $q = 0$ . With the further assumption that only vertical gradients are important in the divergence term, the continuity equation is written in the simplified form as

$$\frac{\partial N}{\partial t} = -1 - \frac{\partial}{\partial z} (N v_z) \quad (4.2)$$

where  $v_z$  is the upward drift velocity of the ionisation.

##### b) Equations of Motion for the Ions and Electrons

It is assumed that all ions move with the same velocity  $\underline{v}$ . The ion motion can be written as (DOUGHERTY, 1961)

$$\begin{aligned} m_i N \frac{d\underline{v}}{dt} = & -k \nabla (N T_i) + m_i N \underline{g} + eN (\underline{E} + \underline{v} \times \underline{B}) \\ & - NF (\underline{v} - \underline{u}) \end{aligned} \quad (4.3)$$

where  $\underline{v} = (v_x, v_y, v_z)$ , the ion velocity  
 $\underline{u} = (u_x, u_y, u_z)$ , the neutral velocity\*  
 $\underline{g}$  = acceleration due to gravity  
 $\underline{E} = (E_x, E_y, E_z)$ , the electric field  
 $\underline{B}$  = the magnetic induction  
 $e$  = electron charge  
 $F$  = Frictional coefficient which depends on  
collision frequencies (STUBBE, 1968 B).

The frictional coefficient in equation 4.3 for collision between ions and neutrals is given by

$$F = 2 m_{in} \nu_{in}$$

where  $m_{in}$  is the ion-neutral reduced mass and  $\nu_{in}$  is the collision frequency of the ions with the neutrals. The frictional force between the different ionic species is neglected, as it is small compared with that between the ions and neutral particles. It has been shown (DOUGHERTY, 1961), that the inertial term in the above equation can be neglected.

Expression 4.3 applies also for electrons. Neglecting small terms, including electron mass and inertial terms, its motion can be written as (DOUGHERTY, 1961)

---

\* Note : Positive meridional component is towards south and not to the north, as in Chapter II. This has been done to maintain the notation followed by others workers, and to facilitate comparison and discussion.

$$k \nabla_{\parallel} (N T_e) + eN (\underline{E} + \underline{v}_e \times \underline{B}) = 0 \quad (4.4)$$

where  $\underline{v}_e$  is the electron velocity.

At F-region heights,  $\nu_{in}/\omega_i \sin I \ll 1$  ( $\omega_i$  being the gyro frequency of the ions). Setting the inertial term to zero in equation 4.3, and neglecting the declination effect and also assuming that electron, ion and neutral temperatures are equal, the three components of ion motion can be analytically obtained from equations 4.3 and 4.4 as

$$v_x = -\frac{E_y}{B} \sin I + v_D \cos I + u_x \cos^2 I + u_z \sin I \cos I \quad (4.5)$$

$$v_y = \frac{E_x}{B} \operatorname{cosec} I \quad (4.6)$$

$$v_z = v_D + \frac{E_y}{B} \cos I + u_x \sin I \cos I + u_z \sin^2 I \quad (4.7)$$

or 
$$v_z = v_D + W$$

where

$$v_D = -\frac{2kT \sin^2 I}{m_i \nu_{in}} \left( \frac{1}{N} \frac{\partial N}{\partial z} + \frac{1}{T} \frac{\partial T}{\partial z} + \frac{m_i g}{2kT} \right) \quad (4.8)$$

and

$$W = \frac{E_y}{B} \cos I + u_x \sin I \cos I + u_z \sin^2 I. \quad (4.9)$$

Here  $T$  is the particle temperature and  $I$  is the magnetic dip angle.

The vertical ion velocity can be written as :

$$v_z = v_D + v_E + v_N + v_T \quad (4.10)$$

where  $v_D$  = ambipolar diffusion velocity as defined in equation 4.8

$v_E = \frac{E}{B} \cos I$ , drift due to the electric field

$v_N = u_x \sin I \cos I$ , drift due to the meridional neutral motion

$v_T = u_z \sin^2 I$ , drift due to thermal motions. This is comparatively a very small term.

The terms  $u_x$  and  $u_z$  are obtained by solving the equation of motion for the neutral particles.

#### c) Equation of Motion for Neutral Particles

The equation of motion for the neutral gas can be written as (DOUGHERTY, 1961)

$$\rho \frac{d\mathbf{u}}{dt} = -\nabla p + 2\rho (\mathbf{u} \times \boldsymbol{\Omega}) + \mu \nabla^2 \mathbf{u} + \rho \mathbf{g} - N\mathbf{F}(\mathbf{u}-\mathbf{v}) \quad (4.11)$$

where  $\rho$  = neutral mass density  
 $p$  = neutral air pressure  
 $\mu$  = coefficient of viscosity.

The expression for the acceleration, used in the equation of motion, is important for neutral particles, unlike in the case of ions, and consists of two parts. It can be written as

$$\frac{du}{dt} = \frac{\partial u}{\partial t} + (\underline{u} \cdot \nabla) \underline{u}. \quad (4.12)$$

The first term is the partial time derivative and the second is the non-linear term; it is very difficult to include the second term in the calculations of motion, because, then, the number of independent variables increases from two to four.

In almost all previous works in this field, the non-linear term has been assumed to be negligible compared with the other terms in the equations of motion, though some tentative rough estimates of its magnitude have been made (KOHL AND KING, 1967; BAILEY ET AL., 1969; STROBEL AND MCELROY, 1970). CHALLINOR (1969) is the only one who included the non-linear term in his calculations, but he simplified the equations otherwise by neglecting viscosity.

KOHL (1971) and RUSTER AND DUDENEY (1972), particularly the latter authors, in detailed discussions of the non-linear term in the equation of motion for the neutrals, have emphasised that this term would be quite important during early morning hours.

In the present calculations also, the non-linear term has not been included. However, some estimates of its magnitude have been made and discussed under the head 'Limitations of the Present Calculations' in Section 4.6.

Hydrostatic equilibrium for the neutral atmosphere is assumed in the vertical direction. A temporal change in temperature would move the whole gas up or down. The resulting vertical velocity can be written as (SHIMAZAKI, 1959)

$$u_z = T \int_{z_0}^z \frac{1}{T^2} \frac{\partial T}{\partial t} dz. \quad (4.13)$$

The equation 4.11 thus needs to be solved only for the x and y components. Neglecting the non-linear term, the two components of motion for the neutral air are thus written as

$$\frac{\partial u_x}{\partial t} = \mu \frac{\partial^2 u_x}{\partial z^2} - \frac{1}{\rho} \frac{\partial p}{\partial x} + 2 \Omega \cos \theta u_y - \frac{N \nu_{in}}{n} (u_x - v_x) \quad (4.14)$$

$$\frac{\partial u_y}{\partial t} = \mu \frac{\partial^2 u_y}{\partial z^2} - \frac{1}{\rho} \frac{\partial p}{\partial y} - 2 \Omega \cos \theta u_x - \frac{N \nu_{in}}{n} (u_y - v_y) \quad (4.15)$$

Here n denotes the number density of neutral species.

#### 4.4.3 The Data and Calculation of Parameters

Monthly mean values of electron density for each hour of the day for the months of January, April, July and October (typically representing the seasons) for Puerto Rico for the year 1960 are the data that have been used for the present analysis. These data are available in tabular form at 10 km interval, from about 100 km during day and 200 km during night, to the level of  $h_m$ , the height of maximum electron density. Above the height  $h_m$ , and upto 800 km the electron densities

were calculated by assuming a Chapman distribution, with atomic oxygen scale height.

An atmospheric model, corresponding to the 10.7 cm solar flux and appropriate to the conditions of the above months was chosen to plug-in the proper atmospheric parameters in the various equations.

The other quantities that occur in the equations were derived as under:-

#### a) Pressure Gradients

The pressure gradients, which are the driving forces for the neutral particles, are given by

$$-\frac{1}{\rho} \frac{\partial p}{\partial x} = -T \int_{z_0}^z \frac{g}{T^2} \cdot \frac{\partial T}{\partial x} dz \quad (4.16)$$

and

$$-\frac{1}{\rho} \frac{\partial p}{\partial y} = \frac{2.16 \times 10^{-5}}{\sin \theta} T \int_{z_0}^z \frac{g}{T^2} \frac{\partial T}{\partial t} dz \quad (4.17)$$

which can be evaluated from the model atmosphere.

#### b) Viscosity and Collision Frequency

The value used for the coefficient of viscosity is that given by DALGARNO AND SMITH (1962), viz.

$$\mu = 3.34 \times 10^{-6} \text{ gm cm}^{-1} \text{ sec}^{-1}$$

The collision frequency for momentum transfer has been discussed by many investigators (BANKS, 1966; STUBBE, 1968 B;

FATKULIN AND MURADOV, 1970; HOROWITZ AND BANKS, 1973). The following relation has been used in the present calculations,

$$\nu_{in} = 8.0 \times 10^{-10} (T/1000)^{0.5} \text{ cm}^{-3} \text{ sec}^{-1}$$

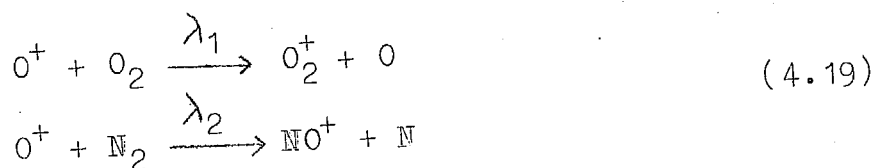
### c) Rate Constants

The loss term (1) occurring in equation 4.1 is given by (SHIMAZAKI, 1965)

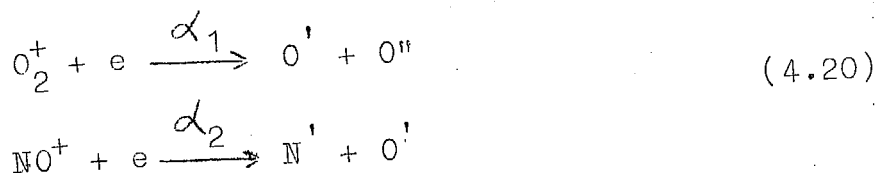
$$1 = \frac{\lambda_1 [O_2] + \lambda_2 [N_2]}{\frac{\lambda_1}{\alpha_1} [O_2] + \frac{\lambda_2}{\alpha_2} [N_2] + N} N^2 \quad (4.18)$$

where  $\lambda$ 's and  $\alpha$ 's are the rate coefficients for the following reactions:

charge exchange:



dissociative recombination:



In the expression 4.18,  $[O_2]$  and  $[N_2]$  are the number densities of molecular oxygen and nitrogen respectively. In general, above 300 km altitude, 1 can be approximated by



The continuity equation 4.1 is written, expanding the divergence term to include all the parameters, in a form as follows (STUBBE, 1968 A):

$$\begin{aligned} \frac{\partial N}{\partial t} = & q - \beta N - N \frac{\partial W}{\partial z} - W \frac{\partial N}{\partial z} + D_a \left[ \frac{\partial^2 N}{\partial z^2} + \frac{\partial N}{\partial z} \left( \frac{0.5 + p}{H_i} + \frac{3}{T} \frac{\partial T}{\partial z} \right) \right. \\ & \left. + \frac{N}{H_i} \left( \frac{p}{2 H_i} + \frac{0.5 + p}{T} \frac{\partial T}{\partial z} - \frac{1}{R_0 + z} \right) \right] \quad (4.21) \end{aligned}$$

where

$$p = \frac{1 + 2.5 [N_2] / [O_2]}{1 + 1.4 [N_2] / [O_2]}, \text{ takes into account the}$$

the relative collision frequencies of  $N_2$  and  $O$  with  $O^+$ .

$$D_a = \frac{2 kT \sin^2 I}{m_i \nu_{in}}, \text{ the ambipolar diffusion coefficient}$$

$R_0 =$  radius of the earth.

The three partial differential equations, viz., the electron continuity equation, and the equations of the x component and y component of the neutral motion, can now be expressed in the following form:

$$\frac{\partial N}{\partial t} = f_1 \frac{\partial^2 N}{\partial z^2} + f_2 \frac{\partial N}{\partial z} + f_3 N + f_4 \quad (4.22)$$

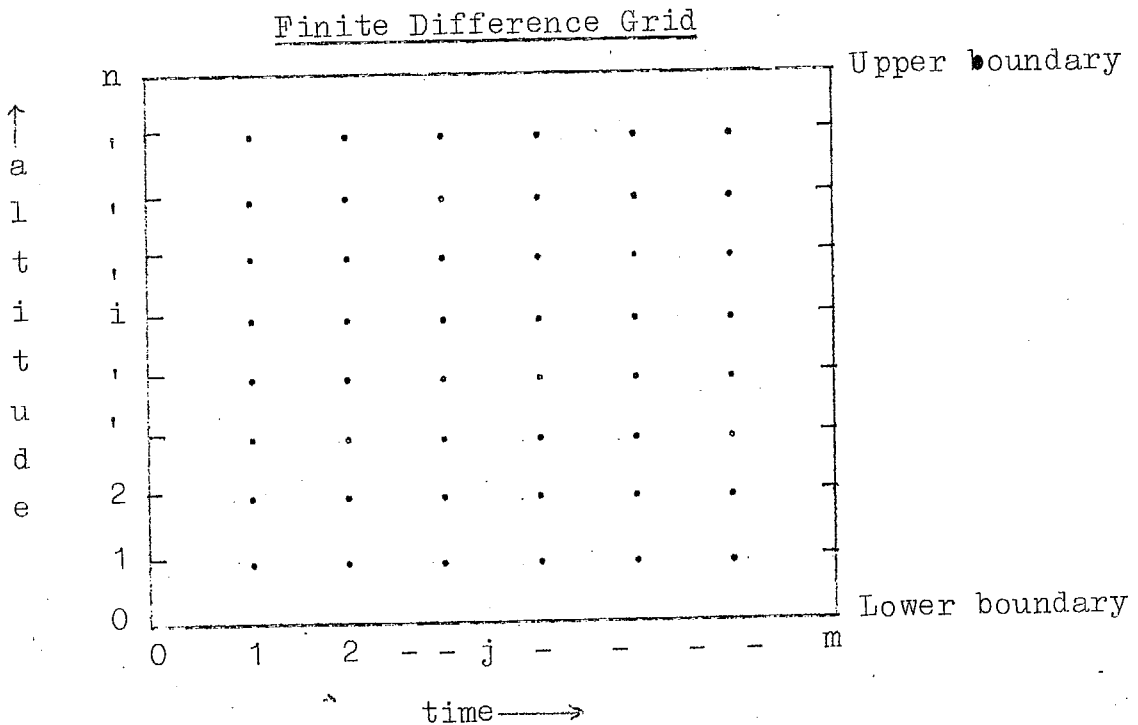
$$\frac{\partial u_x}{\partial t} = f_5 \frac{\partial^2 u_x}{\partial z^2} + f_6 \frac{\partial u_x}{\partial z} + f_7 u_x + f_8 \quad (4.23)$$

$$\frac{\partial u_y}{\partial t} = f_9 \frac{\partial^2 u_y}{\partial z^2} + f_{10} \frac{\partial u_y}{\partial z} + f_{11} u_y + f_{12} \quad (4.24)$$

where  $f_i$  ( $i = 1$  to  $12$ ) are functions of height, time, model atmosphere parameters and initial values of  $N$ ,  $u_x$  and  $u_y$ .

#### 4.5.1 The Finite Difference Method

All the above three equations are of first order in time and of second order in altitude. Thus, this is an initial value problem in time and a boundary value problem in height. For the solution of these equations, they are first transformed into a system of finite difference equations, which are solved numerically. The finite difference grid is schematically represented in the following diagram.



In expressing equations of motion for the neutral air, in finite difference form, the following scheme was employed:

$$\frac{\partial u}{\partial t} = \frac{u(i, j+1) - u(i, j)}{\Delta t} \quad (4.25)$$

$$\frac{\partial u}{\partial z} = \frac{u(i+1, j+1) - u(i-1, j+1)}{2 \Delta z} \quad (4.26)$$

$$\frac{\partial^2 u}{\partial z^2} = \frac{u(i+1, j+1) - 2u(i, j+1) + u(i-1, j+1)}{(\Delta z)^2} \quad (4.27)$$

where  $u(i, j)$  denotes  $u(i \cdot \Delta z, t_0 + j \cdot \Delta t)$ ,  $t_0$  being the initial time. Similar expressions have been used for electron density, but the form

$$\frac{\partial N}{\partial z} = \frac{N(i+1, j+1) - N(i, j+1)}{\Delta z} \quad (4.28)$$

was used for the first altitude derivative of  $N$ .

Incorporation of this scheme in equations 4.22 to 4.24 would yield

$$A_i u_x(i-1, j+1) + B_i u_x(i, j+1) + A_i u_x(i+1, j+1) = C_i \quad (4.29)$$

$$A_i u_y(i-1, j+1) + B_i u_y(i, j+1) + A_i u_y(i+1, j+1) = D_i \quad (4.30)$$

$$E_i N(i-1, j+1) + F_i N(i, j+1) + G_i N(i+1, j+1) = R_i \quad (4.31)$$

where

$$A_i = - \frac{\mu}{\rho (\Delta z)^2}$$

$$B_i = \frac{1}{\Delta t} + \frac{2\mu}{\rho} \frac{1}{(\Delta z)^2}$$

$$C_i = \frac{u_x(i,j)}{\Delta t} - \frac{1}{\rho} \frac{\partial p}{\partial x} + 2 \Omega \cos \theta \cdot u_y(i,j)$$

$$- \frac{N v_{in}}{n} (u_x - v_x)$$

$$D_i = \frac{u_y(i,j)}{\Delta t} - \frac{1}{\rho} \frac{\partial p}{\partial y} - 2 \Omega \cos \theta u_x(i,j) - \frac{N v_{in}}{n} (u_y - v_y)$$

$$E_i = \frac{D_a \Delta t}{\Delta z^2}$$

$$F_i = -1 - \beta \Delta t + E_i \left[ -2 - \frac{\Delta z}{H_i} (0.5 + p) + \frac{3}{T} \Delta T + \frac{p \Delta z^2}{2 H_i^2} + \frac{0.5 + p}{H_i T} \Delta T \Delta z - \frac{\Delta z^2}{H_i (R_0 + z)} \right] + \frac{\Delta t}{\Delta z} W$$

$$G_i = E_i \left[ 1 + \frac{z}{H_i} (0.5 + p) + \frac{3}{T} \Delta T \right] - \frac{\Delta t}{\Delta z} W$$

$$R_i = -N(i,j) - \Delta t \cdot q$$

$$\Delta T = \frac{T(i+1, j+1) - T(i-1, j+1)}{2}$$

All the model atmosphere parameters used correspond to time (j+1).

#### 4.5.2 Boundary Conditions

For boundaries of the height axis, the lower bound was fixed at 90 km and the upper at 800 km. The boundary conditions

as stated in the following sub-sections were imposed for solving the equations 4.29 to 4.31.

a) Boundary conditions for Neutral Winds

The velocity fields  $u_x$  and  $u_y$  were arbitrarily set equal to zero at the lower boundary, because pressure gradients from JACCHIA model are always zero at this height. LINDZEN (1966 B, 1967 B) has shown that the effects of a finite velocity at the lower boundary are attenuated within about a scale height.

At the upper boundary, a stress-free boundary condition for the velocity fields was imposed, viz.

$$\frac{\partial \underline{u}}{\partial z} \rightarrow 0 \text{ as } z \rightarrow \infty.$$

The justification for this assumption stems from the argument that  $\partial^2 \underline{u} / \partial z^2$  should tend to zero when the coefficient of viscosity,  $\mu$ , increases exponentially with increasing altitude. This amounts to saying that  $\partial \underline{u} / \partial z = \text{constant}$  for  $z \rightarrow \infty$ . This constant must also be zero, because otherwise  $\underline{u}$  itself would tend to infinity with increasing height (KOHL AND KING, 1967). This condition implies an absence of momentum exchange with the exterior. KOHL (1971), imposing various kinds of upper boundary conditions, has shown that the derived results, for altitudes less than  $z = 500$  km, are not very sensitive to these conditions.

b) Boundary Conditions for Electron Density

At the lower boundary,  $N$  is constrained by the photochemical equilibrium value, i.e.

$$N = \frac{q}{\beta N}.$$

At night, the following arbitrary condition

$$N(0, j+1) = N(1, j+1)^2 / N(2, j+1)$$

was employed. Even  $N(0, j+1) = 0$  would give satisfactory results. Exponential decay with time of  $N$  at the lower boundary may also be assumed.

At the upper boundary, many workers have employed different conditions (BAILEY ET AL., 1969; STROBEL AND MCELROY, 1970). In the present calculation, the flux from protonosphere was equated to  $Nv_z$ .

c) Initial Values for Neutral Winds and Electron Density

Arbitrary altitude profiles for  $u_x$ ,  $u_y$  and  $N$  were chosen for the initial time 0800 hr, and the equations were solved, choosing production in such a way that for the time around 1900 hr, the solutions were the same as the observed values of  $N_m$  and  $h_m$ . It has been observed that if calculations are started from the observed values of  $N$  profile and the calculated values of  $u_x$  and  $u_y$  profiles (vide Section 4.8) for 1900 hr, stability is not achieved. It is necessary that the calculations

are made using an initial time during the day so that the solutions become stable by 1900 hr and studies of the effect of various parameters are made thereafter.

#### 4.5.3 Tri-diagonal System

The numerical solutions converge as  $(\Delta t)$  and  $(\Delta z)^2$ . It was established, after trial calculations, that the optimum altitude step-width,  $\Delta z$ , and time step-width,  $\Delta t$ , should be 5 km and 5 minutes respectively. From 90 km to 800 km, there are, thus, 141 height-steps and consequently 142 equations to be solved for 144 unknowns at any time, knowing the values of  $u_x$ ,  $u_y$  and  $N$  at the previous time-step at all heights. The boundary conditions enunciated earlier enables one to do away with the lower and upper values of  $u_x$ ,  $u_y$  and  $N$  at all times as shown below:

##### i) Lower Boundary

$$u(0, j+1) = 0$$

$$\text{Day-time : } N(0, j+1) = \frac{q(0, j+1)}{\beta(0, j+1)}$$

$$\text{Night-time: } N(0, j+1) = \frac{N(1, j+1)^2}{N(2, j+1)}$$

##### ii) Upper Boundary

$$u(n+1, j+1) = u(n, j+1)$$

$$N(n+1, j+1) = \frac{\text{Flux}}{v_z(n+1, j+1)}$$

Here, zero in the altitude axis denotes the lower boundary and  $n$ , the upper boundary.

With the imposition of these boundary conditions the equations reduce to a tri-diagonal form, which, in the matrix notation for  $u_x$ , may be represented as

$$\begin{bmatrix} B_1 & A_1 & 0 & 0 & - & - & - & - & 0 & 0 & 0 \\ A_2 & B_2 & A_2 & 0 & - & - & - & - & 0 & 0 & 0 \\ 0 & A_3 & B_3 & A_3 & 0 & - & - & - & 0 & 0 & 0 \\ - & & - & & - & & - & & - & & - \\ - & & - & & - & & - & & - & & - \\ 0 & 0 & 0 & 0 & - & - & - & - & A_{n-1} & B_{n-1} & A_{n-1} \\ 0 & 0 & 0 & 0 & - & - & - & - & 0 & A_n & (B_n + A_n) \end{bmatrix} = \begin{bmatrix} C_1 \\ C_2 \\ C_3 \\ ' \\ ' \\ C_{n-1} \\ C_n \end{bmatrix}$$

Similar tri-diagonal systems can be formed for  $u_y$  and  $\Pi$ .

These tri-diagonal systems were solved by the methods described by National Physical Laboratory (1960) and CONTE (1969) on IBM 360. The time taken for a 36-hr calculation was around 25 minutes, two-thirds of this time being consumed for the calculation of model parameters.

The above procedure of solving the equations is continued in the time axis at steps of  $\Delta t$ , and profiles of



$u_x$ ,  $u_y$  and  $N$  are thence obtained. The value and height of the maximum in the  $N$  profile were designated  $N_m$  and  $h_m$  respectively.

As the constants  $A_i$  to  $G_i$  and  $R_i$  involve the variables  $u_x$ ,  $u_y$  and  $N$ , it is necessary to evaluate these also for the time  $(j+1)$ . For achieving this, iterations are carried out. Normally two iterations are adequate.

The procedure for calculating neutral winds with the observed electron density profiles (vide Section 4.8) is also the same as described above, except that the continuity equation for electron density is not solved in this case, the observed values of electron density profiles are used instead. For calculating only neutral winds, stable solutions are obtained by proceeding in the time axis for more than 36 hours, yielding 6 to 8 hours of overlap values.

#### 4.5.4 The Stability and Accuracy of the Numerical Method

The following tests were performed to see what effects they had on the results.

- i) The starting hour was varied between 0600 hr and 1000 hr. The solutions did not vary by more than 1%.
- ii) The step-width,  $\Delta t$  and  $\Delta z$ , were halved. The departure was only around 3%.

- iii) The lower boundary values of  $u_x$ ,  $u_y$  and  $N$  were changed by arbitrary amounts, i.e.  $u_x$ ,  $u_y$  were made  $10 \text{ m sec}^{-1}$  and  $N$  set to five times its ordinary value. The departures were less than 1%, above 200 km altitude.
- iv) The upper boundary was varied between 700 km and 900 km, and this produced less than 1% variation in the result.
- v) Iterations for evaluating the constants  $A_i$  to  $G_i$  and  $R_i$  at time  $(j+1)$  was carried out successively three times. The result differed from that obtained from two successive iterations by not more than 2%.

Thus, in all cases the departures were only a small percentage of the values of  $N_m$  and  $h_m$  and in the values of  $u_x$  and  $u_y$  at  $h_m$ .

#### 4.6 LIMITATIONS OF THE PRESENT CALCULATIONS

The many assumptions that have been enunciated in the preceeding sections pose some limitations on the results. The implications of some of them are discussed below:

##### 4.6.1 Model Atmosphere

The exospheric temperature and density profiles have been adopted from the JACCHIA (1971) model. Backscatter measurements show many dissimilarities between the observed profiles

and the JACCHIA model - the important among them are the differences in the phase of daily temperature maximum and the ratios of day-time maximum to night-time minimum temperatures. A comprehensive dynamical model, of the type suggested by SWARTZ ET AL. (1972), or the one which includes density from JACCHIA and temperature from incoherent scatter would be an ideal choice. Solving neutral continuity equation together with the equations of motion of charged particles and neutrals and the continuity equation of charged particles is the most appropriate one. From the calculations performed with WALDTEUFEL'S (1971) incoherent scatter model for July (vide Section 4.8), it is seen that the wind values are nearly twice as large as that obtained by using the JACCHIA model. Phase shifts of 2-3 hours of both density and temperature show almost similar shifts in the phase of wind maxima. These will have a bearing on the derived electron densities.

#### 4.6.2 Non-linear Term

The non-linear term  $(\underline{u} \cdot \nabla) \underline{u}$  has been omitted in the equations of motion for neutrals. This term can be neglected (STROBEL AND MCELROY, 1970), if

$$\left| \frac{\underline{u} \cdot (\nabla_h \underline{u})}{\frac{1}{\rho} \nabla_h p} \right| \ll 1.$$

where  $\nabla_h$  is the horizontal gradient. Taking the characteristic

scale of the horizontal motions equivalent to earth's radius,  $R_0$ , the equivalent of the above expression may be written as :

$$\left| \frac{\beta u^2}{R_0 \nabla_h p} \right| \ll 1.$$

Under day-time conditions, when velocities are small due to ion-drag, this inequality is very well satisfied. The comparative figures at  $F_2$ -peak, based on the present calculations, for different hours are listed below:

PUERTO RICO, APRIL 1960

<u>Time</u>	<u><math>\frac{1}{\beta} \nabla_h p</math></u>	<u>u</u>	<u><math>\frac{\beta u^2}{R_0 \nabla_h p}</math></u>
1200 hr	2.3	20	.03
2100 hr	4.0	65	.16
0600 hr	3.5	130	.75

It is, thus, seen that in the morning hours the non-linear term becomes quite important. Also at lower heights, below about 150 km, this term is important. Future calculations must include this term, atleast in some simplified form, though its inclusion makes the method of calculations rather difficult.

#### 4.6.3 Electron Density

The protonospheric fluxes that have been obtained in Section 4.7, were calculated from hourly-spaced electron density profiles, and monthly mean values. For day-to-day variability and better accuracy, individual day's electron density profiles, closely spaced in time, should be used.

#### 4.6.4 Temperatures

The neutral, electron and ion temperatures have been assumed to be equal. This is essentially so under night-time conditions. If these differ, the diffusion coefficient and the loss terms will also be modified. But changes in diffusion coefficient and loss term are more susceptible to changes in neutral constituents and hence the assumption, that all temperatures are equal, is within the limits of present uncertainty in the neutral number densities.

#### 4.6.5 Magnetic Declination

The effect of magnetic declination has been excluded in the present calculations. The east-west component of neutral motion will also contribute to vertical drifts of ionisation if this effect is included. The declination of Puerto Rico is only  $8^\circ$ , and for looking at gross features, this effect will not be significant.

#### 4.6.6 Electric Field

Arbitrary electric field drifts, based on some

reasonable theoretical estimates have been assumed, in the absence of other information. This again, has been shown as not significant enough to produce much discrepancy.

#### 4.6.7 Coefficients

The rate coefficients, collision frequencies, coefficient of viscosity, etc. have been assumed, on the basis of the work of various researchers. The implications of variations of these quantities have been discussed at appropriate places. Though the effect of  $\mu$  is not important, the uncertainties in  $\lambda_s$  and  $\mathcal{U}$  are significant. The values for these coefficients are based on laboratory measurements and are beset with some uncertainties. This will have an effect on the derived results.

#### 4.6.8 Numerical Method

The finite difference scheme that has been employed for the present calculations is reasonably satisfactory. But, some of the boundary conditions that have been employed, are rather arbitrary. Nevertheless, the solutions and results at  $F_2$ -peak have been shown to be not very sensitive to the boundary conditions, except the upper boundary condition for  $N$ , in which the protonospheric flux has been equated to  $Nv_z$ .

## 4.7 PLASMA FLUX FROM THE PROTONOSPHERE

When the horizontal gradients of the electron density  $N$  and the electron velocity  $v$  are negligibly small in comparison with the corresponding vertical gradients, the night-time electron continuity equation can be written as:

$$\text{div} (N v_z) = \left( -1 - \frac{dN}{dt} \right) = P \quad (\text{say}) \quad (4.32)$$

Integrating

$$v_z = \frac{N_0 v_0}{N} + \frac{1}{N} \int_{z_0}^z P dz \quad (4.33)$$

where  $N_0$  and  $v_0$  are the electron density and vertical velocity respectively at the reference height  $z_0$ . The value of  $v_z$  at any height may be estimated if the velocity height distribution or the velocity at some reference height is assumed. MITRA ET AL. (1964, 1967) have estimated the velocity, and also the loss coefficient, for the period around mid-night by assuming height profiles of  $v_z$  and  $l$ .

KRISHNA MURTHY AND SEN GUPTA (1972) have shown that if  $N$  and  $P$  are linear, atleast down to a height where  $N$  and  $P$  are small - and this is so during night-time conditions when low lying ionisation is negligible - the velocity can be written as

$$v_z = \frac{2P \frac{dN}{dz} - N \frac{dP}{dz}}{2 \frac{dN}{dz}} \quad (4.34)$$

From the night-time profiles, in the lowest height region, where  $N$  and  $P$  are linear,  $dN/dz$  and  $dP/dz$  are evaluated, from which the velocity  $v_0$  corresponding to that height (lower boundary) is determined. Velocities at higher heights are then estimated using the relation 4.33. Using this procedure, KRISHNA MURTHY AND SEN GUPTA (1972) have determined vertical velocities over Thumba, for some hours during night-time upto  $h_m$ .

Night-time hourly electron density profiles from 1800 hr to 0600 hr that were available for Puerto Rico for the months of January, April, July and October, 1960 were used for calculating the vertical velocities by the above method.

The term  $\frac{dN}{dt}$  was estimated for all heights from successive hourly values of  $N$ . The loss term was calculated by the procedure described in Section 4.4.3. Using the electron density values at the lowest two heights of observation the lower boundary velocity  $v_0$  was calculated from the relation 4.34. For calculating the velocities at subsequent higher heights,  $P$  was calculated for each height, and numerical evaluation was made of  $\int_{z_0}^z P dz$  from the lower boundary to the height in question. Thus, velocities were determined from about 200 km (which is usually the lower boundary during night-time) to 800 km.

It is necessary to mention in this connection that only hourly electron density profiles were available for the



present calculations. It has been assumed that the electron density variations are linear between any two hourly intervals. Thus, the velocities derived are the average velocities applicable between the hourly intervals.

#### 4.7.1 Vertical Velocities

FIG 4.1 shows the total vertical velocities at  $h_m$ , from 2000 hr to 0600 hr, calculated by the above method for night-time conditions for the months January, April, July and October typically representing the seasons of the year, 1960. Shown in this figure are also the ambipolar diffusion velocity,  $v_D$ , near  $h_m$ . A good correspondence of  $h_m$  variation with that of  $v_D$  and an anti-correspondence with that of  $v_z$  is discernible from these curves.

From the results, it is apparent that the velocities are always downward. At the upper boundary, i.e. at 800 km, the term  $Nv_z$  is interpreted as the flux entering the ionosphere from the protonosphere.

FIG 4.2 shows the fluxes entering the ionosphere at the 800 km level. FIGs 4.1 and 4.2 also show the night-time variations of  $h_m$  and  $N_m$ .

Table 4.1 summarises the fluxes that were derived for the different hours, pertaining to night-time, for the four months. The  $h_m$  and  $N_m$  values are also given for comparison. The calculated large fluxes, particularly during 1800 hr to

## PUERTO RICO 1960

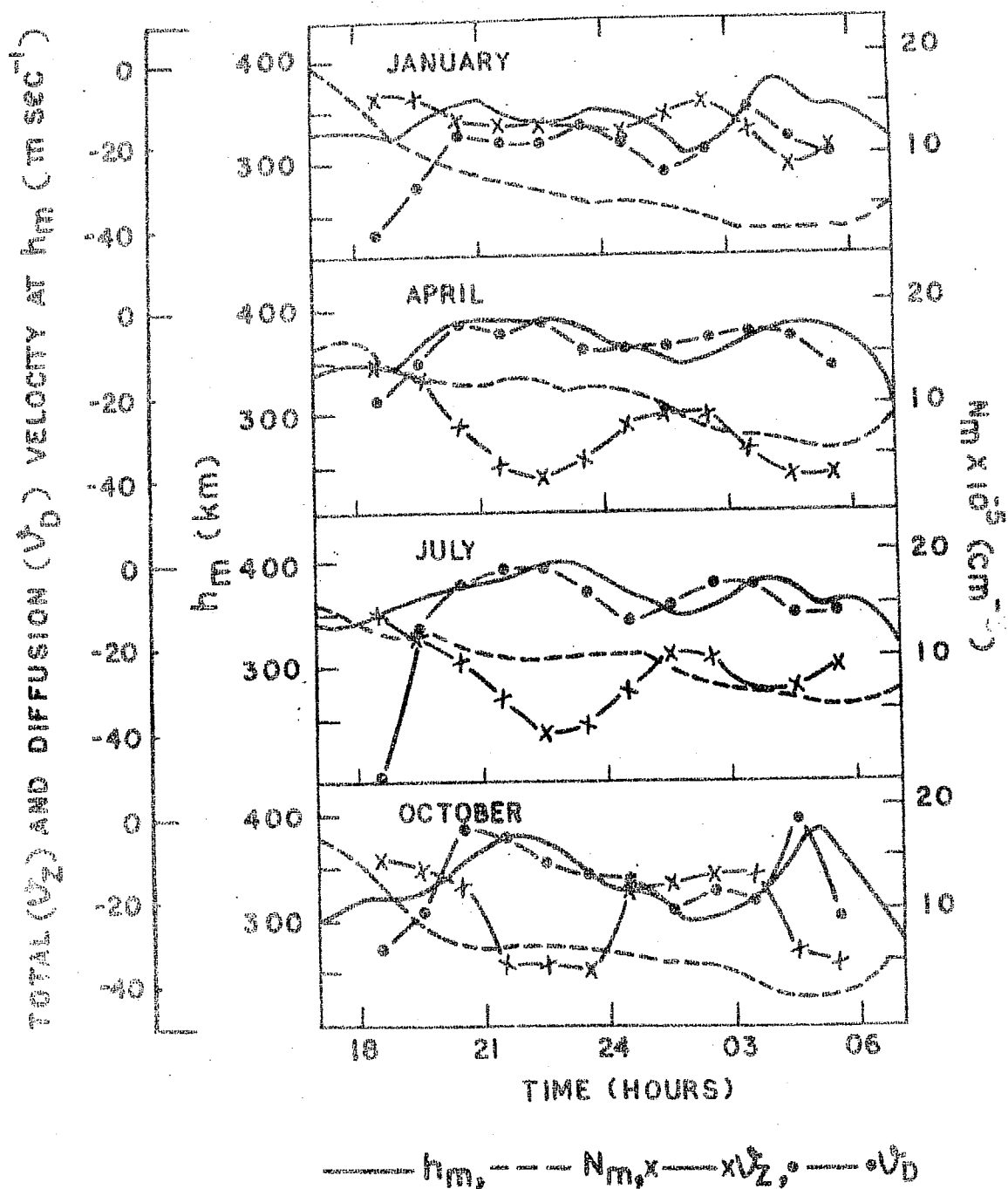


FIG 4.1 : Night-time total vertical drift and vertical component of diffusion velocity at  $h_m$ .

## PUERTO RICO 1960

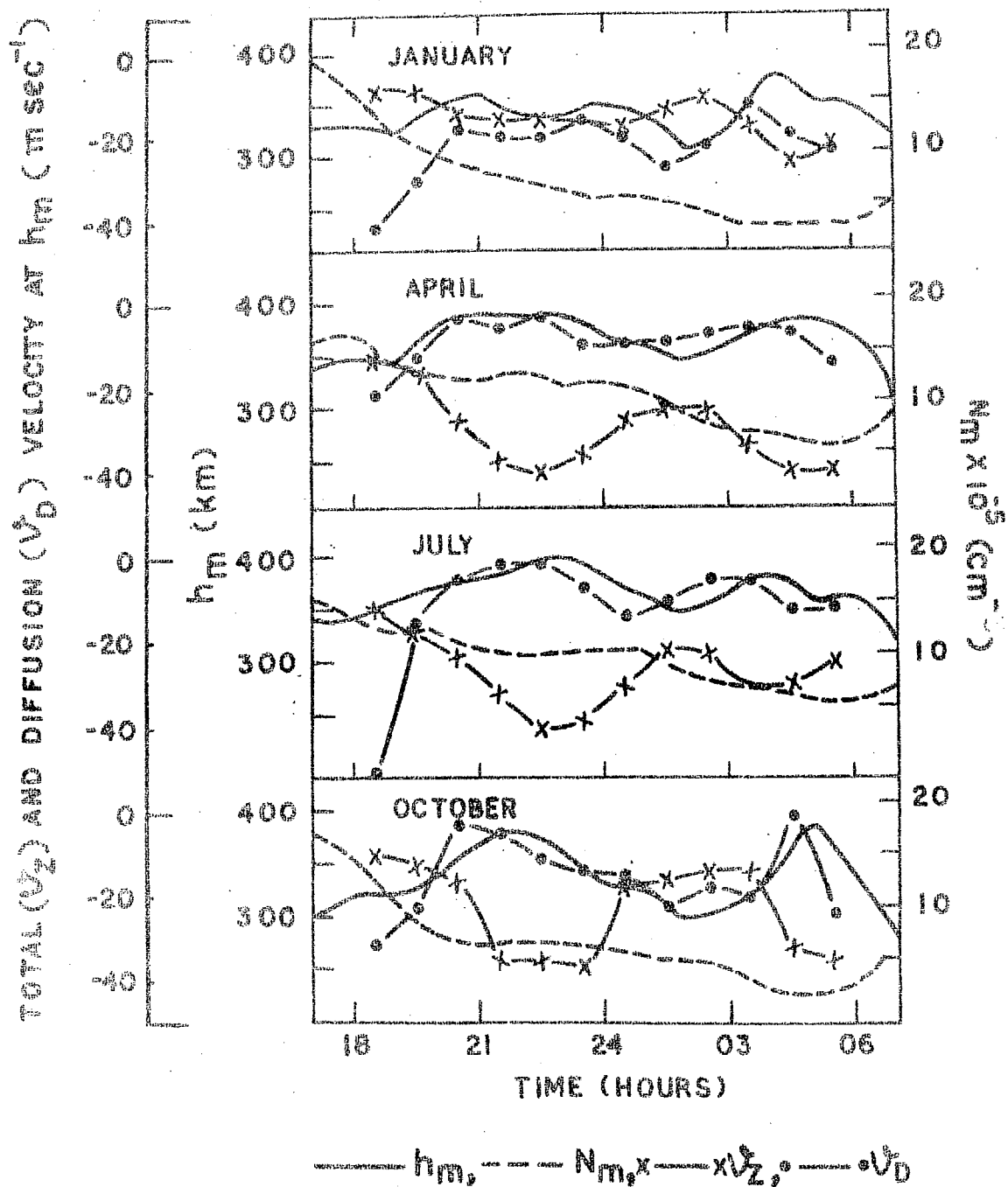


FIG 4.1 : Night-time total vertical drift and vertical component of diffusion velocity at  $h_m$ .

## PUERTO RICO 1960

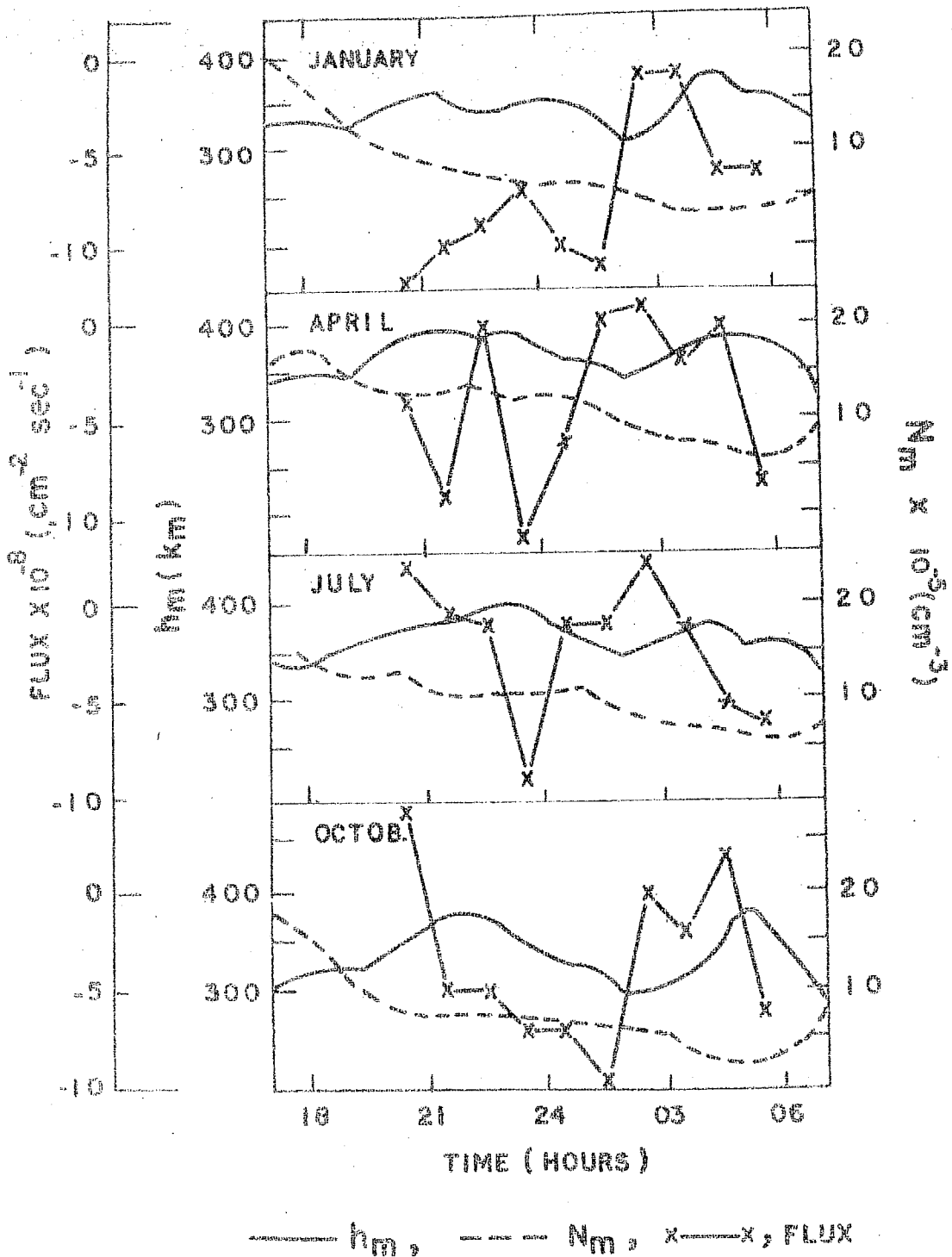


FIG 4.2 : Night-time protonospheric flux at the top of the ionosphere (800 km) as calculated from  $N(z,t)$  profiles.

Table 4.1

$h_m$ ,  $N_m$  and average Fluxes for the night-time calculated over Puerto Rico: 1960

Hour	JANUARY			APRIL			JULY			OCTOBER		
	$h_m$	$N_m$	Flux	$h_m$	$N_m$	Flux	$h_m$	$N_m$	Flux	$h_m$	$N_m$	Flux
1830	330	1334	-3.5	350	1470	-2.0	350	1212	-5.8	320	1242	-2.3
1930	340	1000	-2.2	365	1280	-0.9	365	1173	-2.2	330	0888	-0.8
2030	355	0854	-1.2	385	1205	-0.4	375	1110	+0.2	355	0687	+0.4
2130	350	0755	-1.0	390	1216	-0.9	385	1011	0.0	375	0645	-0.5
2230	340	0650	-0.9	390	1198	0.0	395	0984	-0.1	370	0638	-0.5
2330	345	0567	-0.7	380	1155	-1.1	390	0985	-0.9	345	0606	-0.7
2430	345	0522	-1.0	365	1108	-0.6	370	0996	-0.1	325	0573	-0.7
0130	325	0486	-1.1	355	0950	0.0	355	0903	-0.1	310	0535	-1.0
0230	320	0381	-0.1	360	0767	+0.1	360	0744	+0.2	305	0421	0.0
0330	355	0280	-0.1	375	0668	-0.2	375	0648	-0.1	325	0279	-0.2
0430	370	0266	-0.6	385	0596	0.0	370	0588	-0.5	365	0219	+0.2
0530	355	0266	-0.6	380	0559	-0.8	360	0551	-0.6	365	0211	-0.6
Average from 2030 hr to 0530 hr												
	346	0503	-0.7	376	0942	-0.4	373	0852	-0.2	344	0481	-0.36

Units:  $h_m$  - km;  $N_m$  - electrons  $\text{cm}^{-3} \times 10^{-3}$ ; Flux - particles  $\text{cm}^{-2} \text{sec}^{-1} \times 10^{-9}$ .

2000 hr, and on some occasions between 0500 hr to 0600 hr, may be accounted for as due to the neglect of possible production by solar uv radiation during those times.

It may be of interest to mention that the values of the flux between 0100 hr to 0300 hr are very small. It may also be observed that despite the larger differences in the mean  $h_m$  between the two equinox months - April and October and a large difference in mean  $N_m$  by as much as a factor of two, the mean flux during those two months are nearly the same, being about  $3.8 \times 10^8$  particles  $\text{cm}^{-2} \text{sec}^{-1}$ . In contrast, the January-October and April-July pairs, despite having almost identical  $h_m$  and  $N_m$  values, show large variations in the calculated fluxes between themselves.

#### 4.7.2 Accuracies

KRISHNA MURTHY AND SEN GUPTA (1972) have discussed the errors involved in these velocity estimates. They emphasise on the linearity assumption of N and P at the lowest height. As the electron density data was available only at 10 km height interval,  $dN/dz$  determination is likely to be in some error. However, from the present calculations it has emerged that the variations of the lower boundary velocity  $v_0$  by a factor of two, either way, did not affect the velocity, and hence the flux, at other heights by more than 5%. At the upper boundary the flux changed by less than 4% for changes of  $v_0$  by a factor of two.

About 20% change in the rate constants,  $\lambda_1$  and  $\lambda_2$  reveal changes of about 25 to 30% in the flux values. The variation in the calculated flux due to inaccuracy in the height determinations of the  $N(z,t)$  profile (with the heights assumed to be in error by 5 km) amounts to less than 5%. The height error can also be looked upon as an uncertainty in the value of the rate constants.

Assuming that observed  $\frac{dN}{dt} = 0$  at all hours and at all heights, the average incoming flux, calculated for maintaining constant  $N_m$ , was about 10% more than when  $N_m$  variation was taken into account for the calculation of the flux.

From the above calculations it is seen that in equation 4.33 the term under the integral, and particularly the term 1, is the most dominant in the evaluation of the flux. The calculations, thus, mainly depend on the proper choice of the rate constants.

#### 4.7.3 Discussion

PARK (1970), as pointed out already, has shown from his whistler observations that a flux of about  $2$  to  $4 \times 10^8$  electrons  $\text{cm}^{-2} \text{sec}^{-1}$  is observed to be crossing the protonosphere-ionosphere boundary. The present estimates are in good agreement with his results. The limiting flux calculations of  $1.5 \times 10^7$  electrons  $\text{cm}^{-2} \text{sec}^{-1}$  by GEISLER (1967 B) have to be modified in the light of observations by PARK (1970)

and EVANS ET AL. (1970). The latter investigators have inferred from Thomson scatter observations that fluxes through the exosphere can exceed  $10^8$  electrons  $\text{cm}^{-2} \text{sec}^{-1}$ . DESHPANDE (1972), suggests from a different theoretical estimate that a flux of about  $3.8 \times 10^8$  electrons  $\text{cm}^{-2} \text{sec}^{-1}$  at 500 km altitude is required for maintaining  $N_m$  of the order of  $3.5 \times 10^5$  electrons  $\text{cm}^{-3}$ . In view of the uncertainties in the rate constants, the agreement between the various estimates can be regarded as reasonably good.

For an explanation of the large flux in January, as compared to the other three periods it appears unlikely that corpuscular radiation, which was neglected in the calculation of the flux, would have been the contributing factor. This is because, the trend of protonosphere flux from January to October has not been in a continuously decreasing direction, the flux in October showing higher values than in July. If the corpuscular radiation had been the cause of a gradually decreasing trend, corresponding to the decreasing trend in solar activity during this period, would have been noticed.

It also appears unlikely that variations in the values of  $h_m$  and  $N_m$  during the different periods would have been the cause for the high value of the flux in January. For a higher  $h_m$  or for a lower  $N_m$  the required flux would be smaller. Higher values of  $h_m$  have been associated, as would be expected, with higher values of  $N_m$  and vice versa in all the data treated in



this study. Nevertheless, the April-July and January-October pairs reveal different fluxes, despite same values for  $h_m$  and  $N_m$ .

It is necessary, in the estimation of fluxes, to specify the base values of  $N_m$  that the flux would maintain, as well as the corresponding height. As has been calculated by the author a vertical translation of the whole profile by 20 km either up or down, substantially (to more than 50%) alters the flux values. This fact is borne out very clearly from Table 4.1, where mean  $h_m$ ,  $N_m$  and flux values for the four months are shown.

#### 4.8 NEUTRAL WINDS AND ELECTRIC FIELD DRIFTS

Besides the total vertical velocities and the fluxes, the other parameters that have been estimated from the  $N(z, t)$  data, are the neutral winds for day and night and electric field drifts for the night hours.

In order to get stable and self-consistent solutions of equations 4.14 and 4.15 for neutral winds, the procedure that is normally adopted is that arbitrary altitude profiles for  $u_x$  and  $u_y$  are assumed for the starting time - usually early morning, around 0800 hr-and the equations are solved for the next 24 hours to obtain solutions for the starting hour again. This process in time is continued until the results at any time are within a few percent of those for the same hour of the previous day. As the ion drag is the dominant

force during day-time, solutions become quite stable by about 1400 hr on the first day itself, so that if the equations are solved from 0800 hr of one day to 1500 hr of the next day, stable solutions for full 24 hours are obtained. This kind of iterative procedure is not necessary for solving ion motions, for, in their case the inertial forces are negligible. The ion drag term occurring in equations 4.14 and 4.15 are obtained at any time using the electron density profile corresponding to that time.

For calculating the neutral wind motions, it is necessary to know the ion motions as well, since the two are coupled. For calculating the horizontal components of ion motion, one needs additional information about the ambipolar diffusion velocity and the electric field components  $E_x$  and  $E_y$ . The diffusion velocity is easily calculated from the expression 4.8 with the given electron density profile.

For estimating the electric field contribution, the following iterative process was employed in a chronological order.

- i) It was assumed that  $E_x = 0$ . This would only affect the y-component (eastward) of ion motion, and hence the east-west neutral motion, i.e.,  $u_y$ . This  $u_y$ , however, is coupled to  $u_x$  by the coriolis term. The geographic latitude of Puerto Rico is  $18^\circ$  N, and thus the coriolis

force term is quite small. This essentially means that no large changes will occur in  $u_x$  corresponding to changes in  $u_y$ , and vice versa.

- ii) At the start of the iterative process,  $E_y$  was also set to zero, and equations 4.5 to 4.7, 4.14 and 4.15 were solved simultaneously to derive, by the procedure outlined earlier in this section, stable altitude profiles of  $u_x$  and  $u_y$  for 24 hours.
- iii) From the total vertical ion velocities that were calculated for night-time, from 2000 hr to 0500 hr, vide Section 4.7, the following expression was used to calculate the electric field drift:

$$v_E = \frac{E_y}{B} \cos I = v_z - (v_D + u_x \cos I \sin I + u_z \sin^2 I)$$

This expression is only a rearrangement of equation 4.7. Using this expression for heights below  $h_m$ , the drift due to the  $E_y$  field was estimated for the night-time. Further, the usual assumption that the electric field is constant with height was also made.

- iv) From the electric field drift due to  $E_y$ , calculated for different hours during night-time,

an average value was estimated and this was assumed to be holding good from 1800 hr to 0600 hr. A reversed electric field from 0600 hr to 1800 hr was also assumed.

v) Now, using this value of the electric field as derived for night-time and thence for day-time, neutral winds were again calculated.

The procedure (ii) to (v) was repeated till reasonably stable solutions were obtained. Only two iterations were carried out in the present case and an accuracy of 5% was easily obtained particularly during night-hours. More than two iterations were not necessary because during night-time the ion drag is fairly small and the effect of ion motion is thus little reflected in neutral motion during these times. The driving force, viz., pressure gradient, is the dominant term during these times.

#### 4.8.1 Results of Neutral Wind Velocities

The average electric field drift for the night hours calculated, as detailed above, ranged from  $15-25 \text{ m sec}^{-1}$  in the downward direction for the different months. The above values resulted from the first iteration of neutral wind equations. For the second iteration of the neutral wind equations, these downward drifts were used for night-time and same values with reversed sign (i.e. upward drift) were used for day-time.

FIG 4.3 shows the plots of neutral wind components  $u_x$  and  $u_y$  at  $h_m$ , for the four months for a 24-hour period from 0600 hr to 0600 hr. The values of  $u_x$  and  $u_y$  for these plots were obtained by solving equations 4.14 and 4.15 using JACCHIA'S (1971) model atmosphere and the  $N(z,t)$  profiles of Puerto Rico appropriate to these months. The monthly mean  $h_m$  and  $N_m$  variations for these months have also been shown in the same figure.

The general behaviour of the neutral winds derived by the author in this study is similar to that of the winds derived by earlier investigators (e.g. BAILEY ET AL., 1969). One feature of special notice is the smaller velocities in the winds now derived, even for night-hours. This is explainable as being due to the larger electron densities and hence greater ion drag in the present case.

The zonal motion reveals reversals at 0400 hr and 1300 hr for all the four periods closely corresponding to the times of temperature minimum and maximum. Besides, the maximum westward winds observed during early morning hours are in agreement with the direct measurements made by vapour release experiments (vide Chapter II, Section 2.4). There has often been difficulty in relating the diurnal east-west motion of winds to the super-rotation phenomenon (KING-HELE AND SCOTT, 1967; KING-HELE, 1972). The results of BAILEY ET AL. (1969) show almost equal eastward and westward motions over 24 hours, with the result

## PUERTO RICO 1960

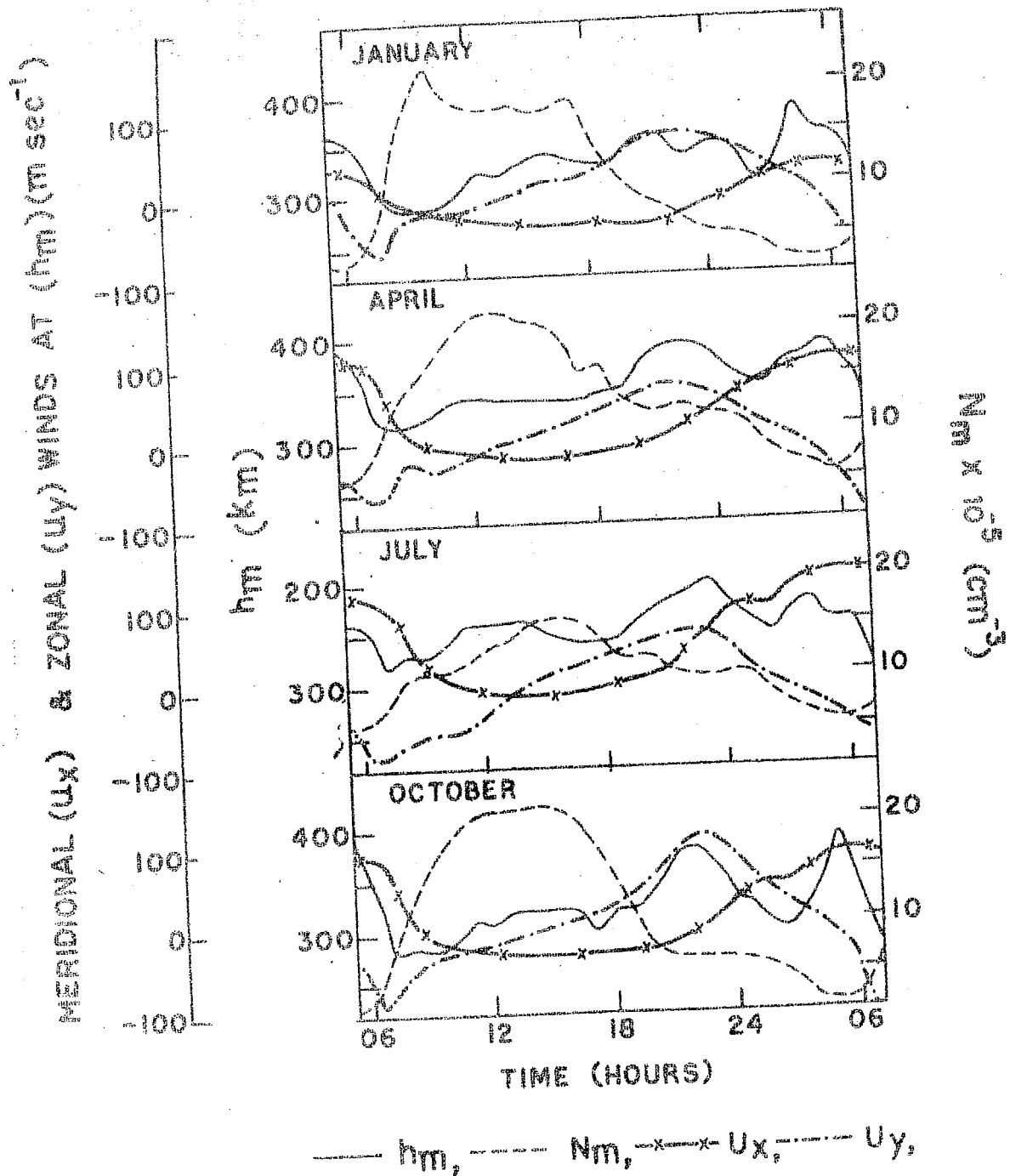


FIG 4.3 : 24-hr variation of meridional and zonal neutral wind velocities at  $h_m$ .

that an average over a whole day would be very nearly zero. They have, however, interpreted their results, in terms of an average  $u_y$ , as  $\bar{\rho} u_y / \bar{\rho}$ , where the bars denote the diurnal average and  $\bar{\rho}$  the neutral mass density. The afternoon and evening (1400 hr to 2000 hr) air densities are about 20% greater than the morning values, and so, when expressed in terms of air flux, for comparison with the satellite drag measurements, the mean global zonal wind has a nett eastward component, though quite small, according to their estimates, being only about  $5 \text{ m sec}^{-1}$ .

In the present results, eastward motions for all months are, in general, seen to be stronger than the westward motions, except for July, where both are nearly of equal magnitude. The larger eastward velocities between 1300 to 0400 hr, are because of the comparatively reduced ion drag during these times. Eastward velocities occur for about 14 hours a day and westward velocities for the remaining 10 hours. Thus, this clearly indicates that there is a nett annual global eastward flow, around 300 km altitude, of the order of  $30 \text{ m sec}^{-1}$ . If the air-flux criterion is adopted this amounts to eastward winds of  $35 \text{ to } 40 \text{ m sec}^{-1}$  magnitude. Though these eastward wind velocities are still lower when compared with the super-rotation value obtained by KING-HELE (1972) from satellite drag results, the agreement is better when compared with similar derivations by other workers.

As for the behaviour of meridional winds, these are poleward during day-time reversing to equatorward during night hours. As already emphasised, the change to equatorward direction is crucial for explaining the preservation of night-time ionisation in terms of neutral winds. In general, the night-time equatorward flow is much stronger, except during January (winter). A discussion as to how these winds would affect the ionisation, is given in the next section.

The effect of variation of coefficient of drag and viscosity are shown in FIG 4.4. Even doubling the coefficient of viscosity does not affect the winds at  $h_m$ . Some workers (CHALLINOR, 1969; ILL ET AL., 1973) have omitted this term in the equation of motion. However, BAILEY ET AL. (1969) find this term to be important at night-times, but this is due to the fact that their  $N_m$  values are lower than  $1 \times 10^5 \text{ cm}^{-3}$  at those times. The ion-drag produces considerable change in the magnitude of the neutral velocities as is shown in FIG 4.4.

FIG 4.5 shows the comparative winds derived from the model atmospheres of JACCHIA (1971), based on satellite drag data, and WALDTEUFEL (1971), based on incoherent scatter observations, for the period July. The calculated winds are nearly twice as large for the latter model as compared to the former.



# PUERTO RICO : APRIL, 1960

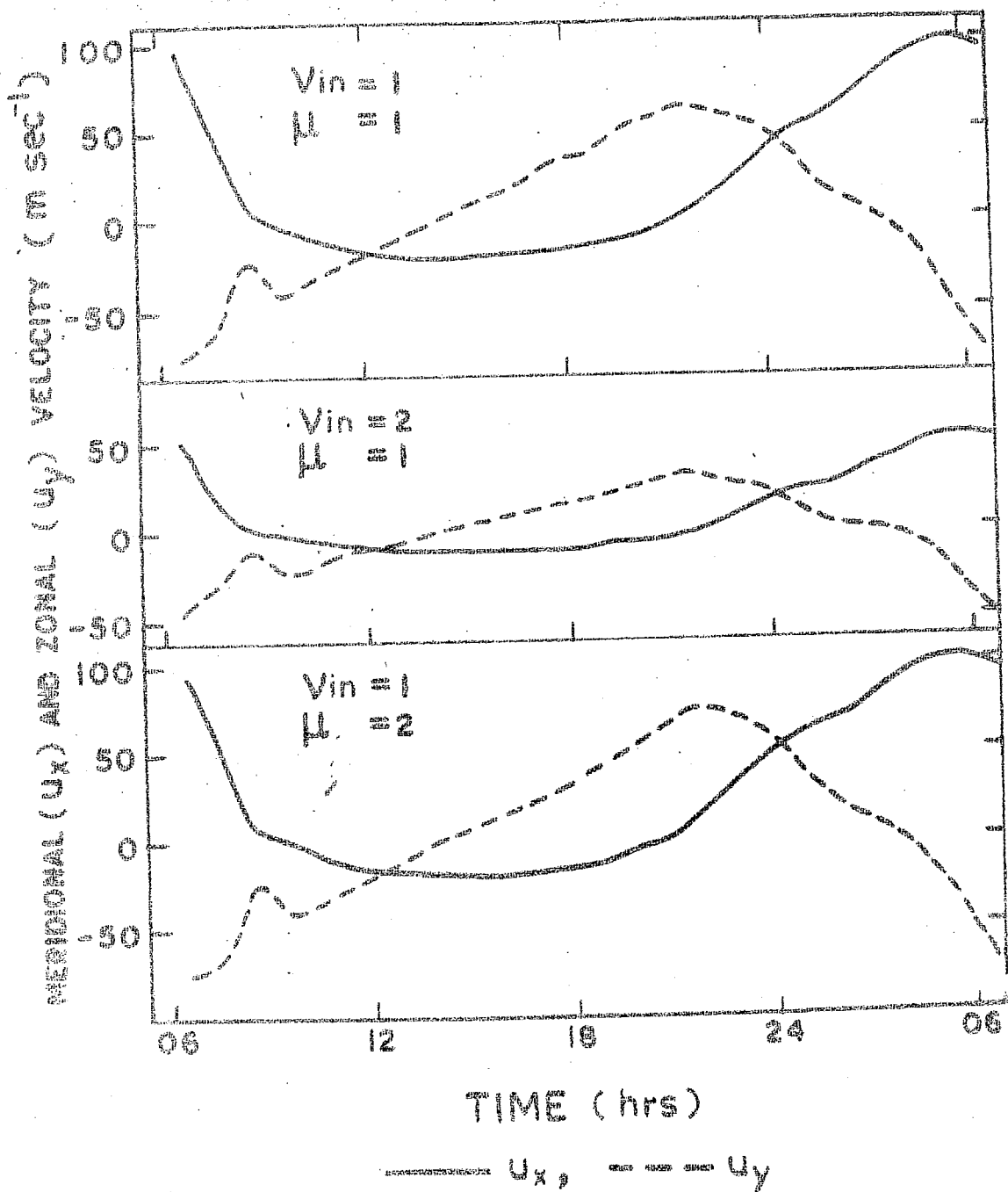


FIG 4.4 : Effects of variation of collision frequency ( $\nu_{in}$ ) and coefficient of viscosity ( $\mu$ ) on neutral wind velocities.

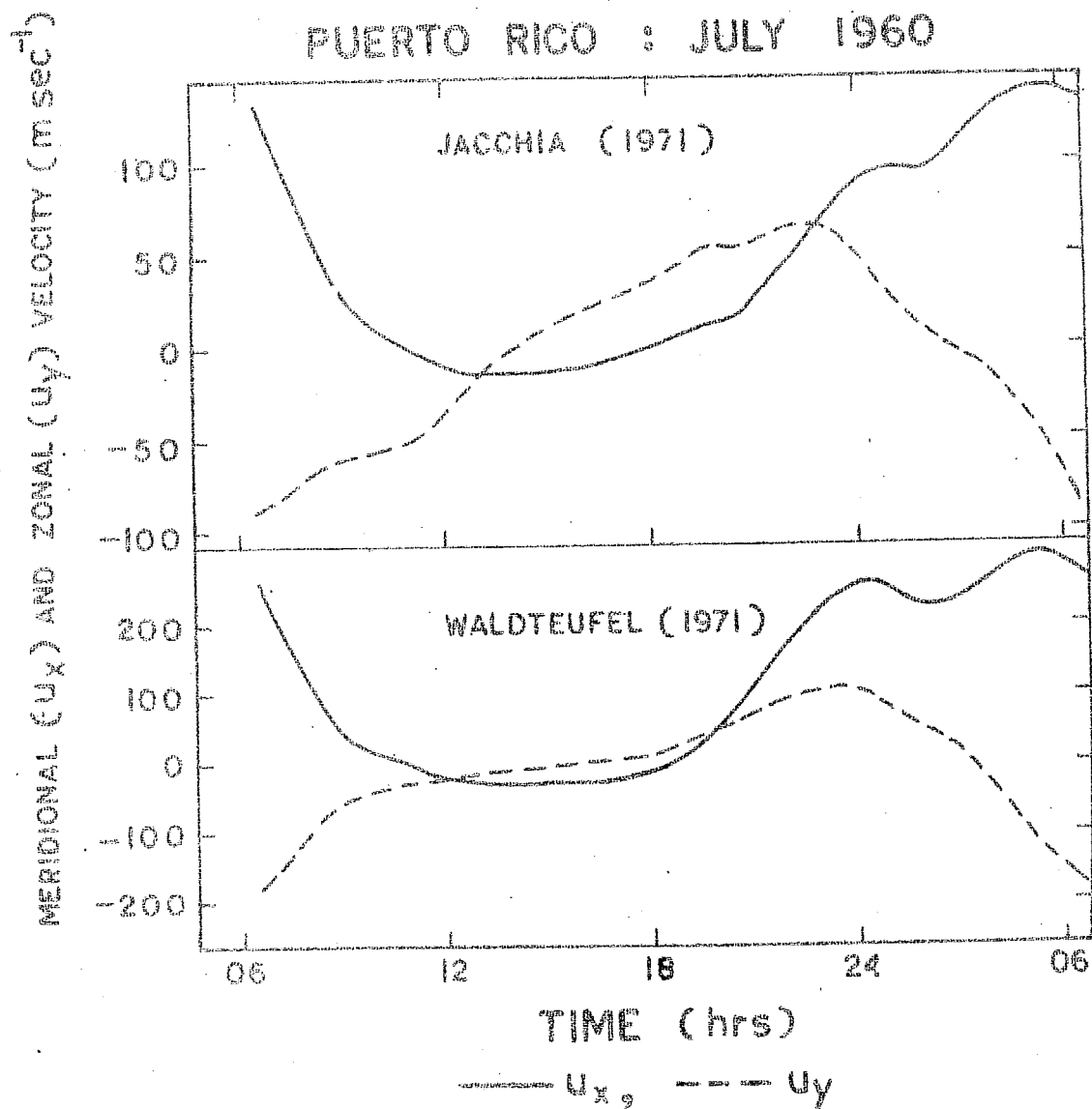


FIG 4.5 : Wind velocities as derived from Jacchia's Model and Waldteufel's Model.

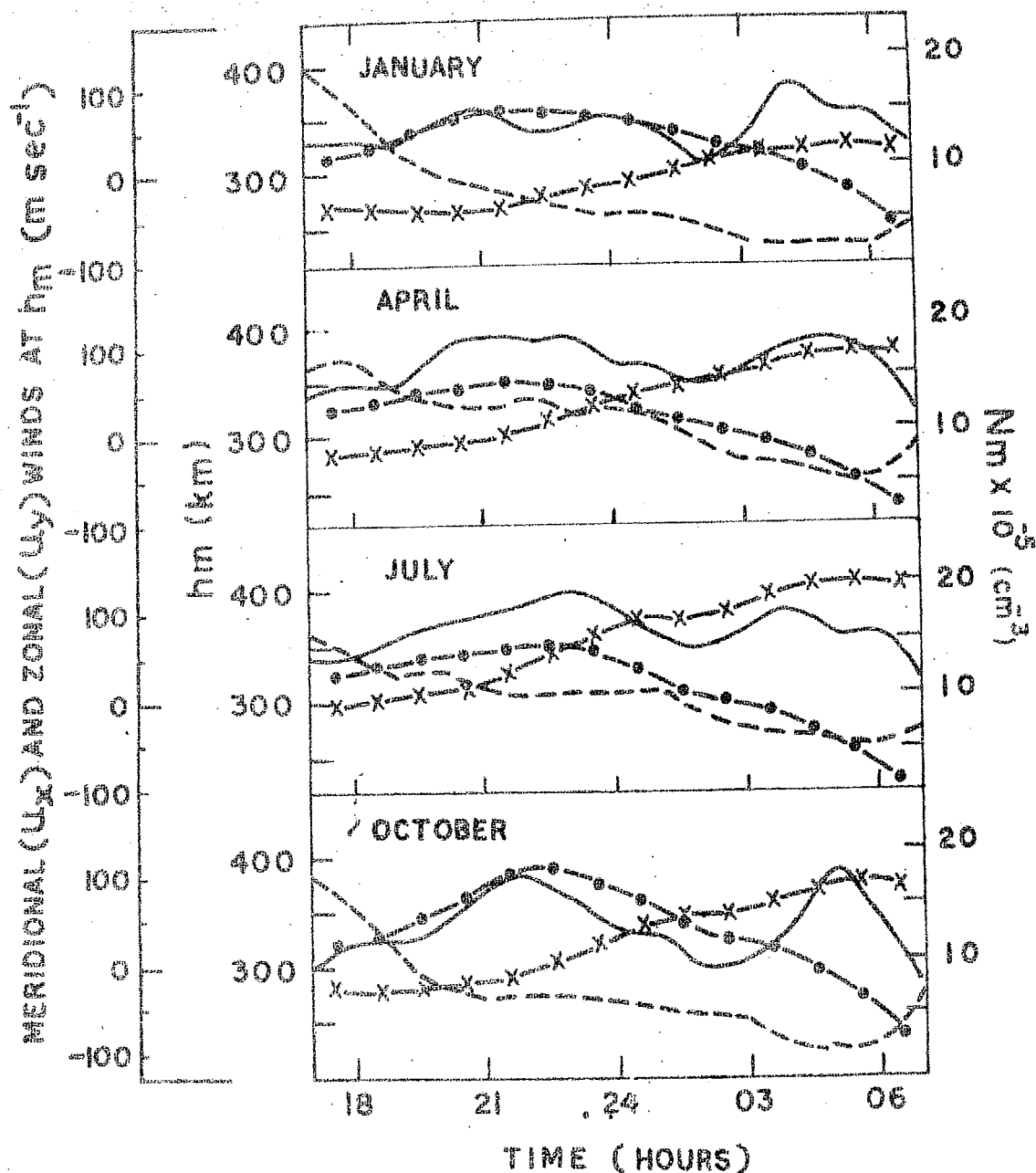
#### 4.9 EXPLANATION OF OBSERVED $h_m$ AND $N_m$ IN TERMS OF NEUTRAL WINDS AND PROTONOSPHERIC FLUX

The total drift velocity ( $v_z$ ), diffusion velocity ( $v_D$ ), protonospheric flux, neutral winds ( $u_x, u_y$ ) and drifts due to electric fields ( $v_E$ ) have been derived from the  $N(z, t)$  profiles for night-time hours, as discussed in the earlier sections. It remains to be seen how the neutral winds and flux (which includes diffusion and electric field drifts) would help to preserve the ionisation.

The times of reversal of the north-south wind are different for the four months, as will be seen from FIG 4.6, where results from 1800 hr to 0600 hr (night-time conditions) are shown. The layer preserving capacity of the meridional wind is prominently shown for July, and to a lesser extent for April and October. During these periods the tendency for the equatorward flow, which amounts to raising the layer to higher heights, is seen before 2100 hr. For January, the meridional flow reverses to equatorward flow only at later times (after about 0100 hr), and the winds too are very weak.

The time of reversal to equatorward direction depends on the atmospheric model chosen, and there are, indeed, discrepancies between the models derived from satellite drag and models based on incoherent scatter observations. As has been obtained by previous calculations, the present results also

## PUERTO RICO 1960



—  $h_m$ , ---  $N_m$ , x—x  $U_x$ , •—•  $U_y$

FIG 4.6 : Night-time meridional and zonal neutral wind velocities at  $h_m$ .

show that shifting the day-time temperature maximum by a few hours, shifts the phase of meridional winds and the reversal times by about an equal amount.

Table 4.2 summarises the mean day-time (from 0630 hr to 1730 hr) and mean night-time (2030 hr to 0530 hr)  $N_m$  and  $h_m$  values, the day-to-night increase in  $h_m$ , the day-to-night ratio of the average  $N_m$  and the reversal times of the meridional component. The maximum value of the southward component of wind velocity observed during the night, and the average flux for all the four months are also tabulated.

In all cases it is observed that the layer had started rising much before the neutral wind had turned equatorward. Appreciable increase of  $h_m$  at night from its day-time value is discernible, only, for the months of April, July, and October, which is in agreement with the comparatively earlier reversal times in the direction of  $u_x$ . However, the behaviour of  $h_m$  during the month of July, out of the above three months, is worth special notice: whereas the meridional neutral wind had turned equatorward as early as 1830 hr, the rise of  $h_m$  was only 28 km, while in April and October, the winds turned equatorward about 3 hour later and still  $h_m$  had risen by as much as 40 km. It is worth noting, all the same that the day-to-night  $N_m$  ratio is lowest for July, despite the lowest flux obtained, from which it would appear that the ionisation had duly been maintained by neutral winds.

Table 4.2

## PUERTO RICO 1960

Month	Mean Day-Time (0630 hr - 1730 hr)		Mean Night-Time (2030 hr - 0530 hr)		$\Delta h_m$	$N_m$	$N_m$	$u_{xm}$	Reversal time of $u_x$	Flux
	$h_m$	$N_m$	$h_m$	$N_m$						
JANUARY	333	1600	346	503	13	3.2	30	0100	-0.7	
APRIL	335	1700	376	942	41	1.8	100	2100	-0.4	
JULY	345	1230	373	852	28	1.5	110	1830	-0.2	
OCTOBER	305	1700	344	481	39	3.5	90	2130	-0.36	

Units :  $h_m$  - km;  $N_m$  - electrons  $\text{cm}^{-3} \times 10^{-3}$ ; Flux - particles  $\text{cm}^{-2} \text{sec}^{-1} \times 10^{-9}$

Symbols :  $\Delta h_m = (\text{mean night-time } h_m) - (\text{mean day-time } h_m)$

$r_{N_m} = \frac{\text{mean day-time } N_m}{\text{mean night-time } N_m}$

$u_{xm}$  = maximum positive  $u_x$  during night time.

Again, in April, and October, the reversal times are almost the same, with not much of a difference in the wind magnitude. The total rise of the layer is almost equal, being about 40 km. The calculated flux values are also similar. But the night-time layer in October is as much as 32 km lower than the April value. Consequently the day-to-night  $N_m$  ratio in October is also as high as about 3.5, as compared to 1.8 in April.

Also, during January, the rise of  $h_m$  has been the lowest, being only 13 km, the corresponding night-time  $N_m$  has also been lower, as much as 3.2 times its day-time value. Naturally, the calculated fluxes have been the largest for this month.

It will, thus, be seen that for a proper understanding of the maintenance of F-region night-time ionisation, it is important to consider all the four parameters as given below:

- i) the maximum electron density,  $N_m$
- ii) the peak of ionisation,  $h_m$
- iii) the day-to-night increase in  $h_m$ ,
- and iv) the ratio of day-to-night  $N_m$ .

#### 4.10 EFFECTS OF DIFFERENT PARAMETERS IN NIGHT TIME F-REGION

The results, obtained by solving the continuity equation and equations of motion, pertaining to night-time equinox conditions, are presented in FIGs 4.7 and 4.8. The effect of neutral winds, electric fields and fluxes can be seen from

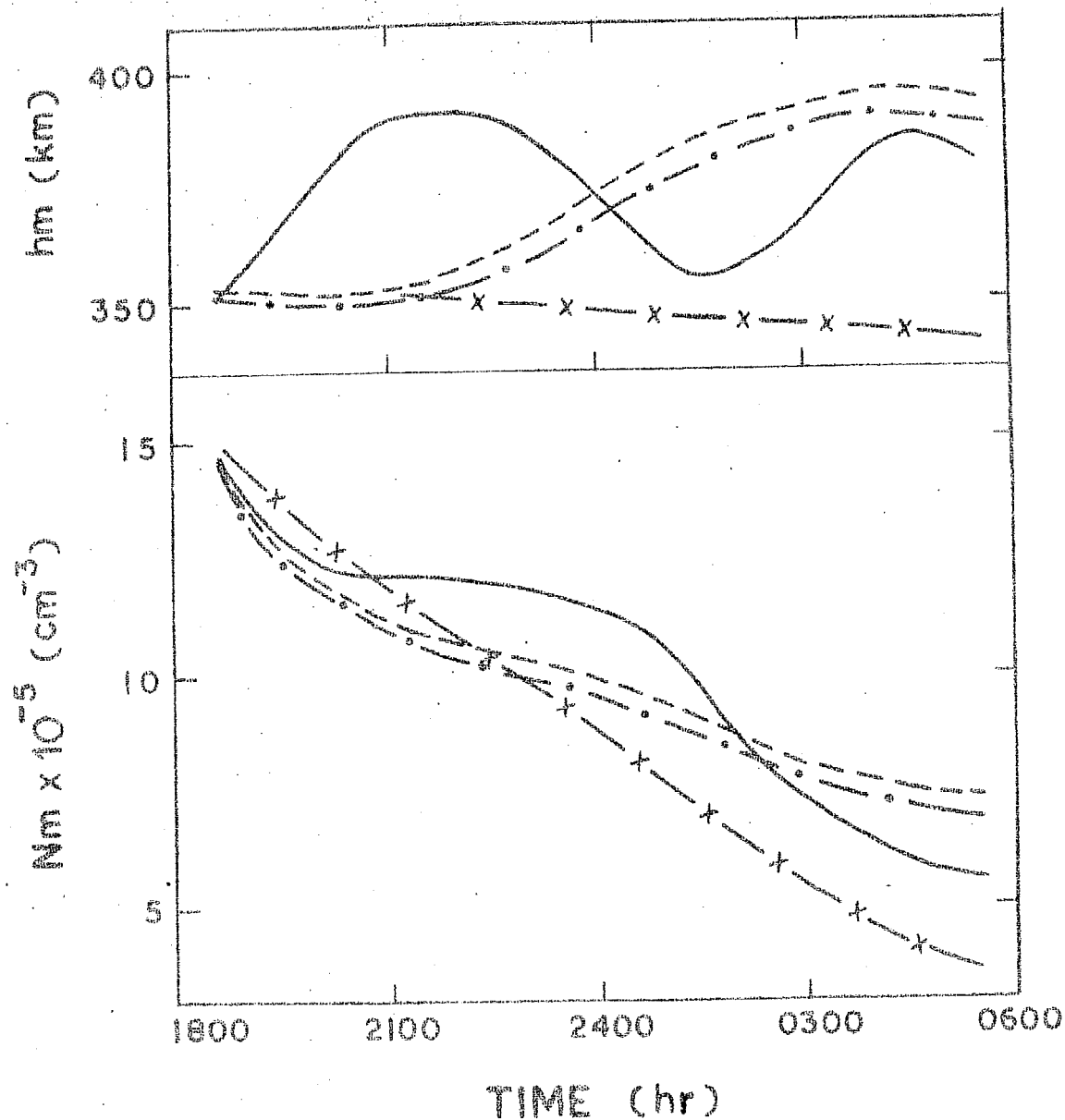
these figures, where night-time variation of  $h_m$  and  $N_m$  are plotted. The observed  $h_m$  and  $N_m$  behaviours are also shown for comparison.

It can be seen from FIG 4.7 that in the absence of winds and electric field, the  $h_m$  slowly descends, with the result that the  $N_m$  decreases continuously throughout the night. The effect of neutral wind, as can be seen, is to increase the layer height. But, as the meridional wind turns equatorward only around 2200 hr, sufficient decay has already occurred. Only after this time does the fast decay get halted. The layer continues to rise after this time. The effect of introduction of vertical electric field drift (assumed to be sinusoidally varying, with an amplitude of  $20 \text{ m sec}^{-1}$ , with maximum positive and negative values at 1200 hr and 2400 hr respectively, and zero drifts at 0600 hr and 1800 hr), however, makes little difference in the behaviour of  $h_m$  or  $N_m$ , except for the fact that  $h_m$  is reduced by a few km with a consequent small reduction in  $N_m$ . The observed behaviour of  $h_m$  is, however, not in consonance with that calculated. The observed behaviour is such that the layer rises immediately after 1830 hr, and falls gradually after about 2230 hr. It further rises after 0200 hr. These features are not reflected by including any parameter in the calculations.

The effect of variation of flux is presented in FIG 4.8. The larger flux keeps the layer height lower than that for



# PUERTO RICO : APRIL 1960



----- OBSERVED , x-----x NO WINDS OR ELECTRIC FIELD  
 ----- ONLY WINDS , ----- WINDS AND ELECTRIC FIELD

FIG 4.7 : Effect of neptural winds and electric fields on night-time F-region.

PUERTO RICO : APRIL 1960

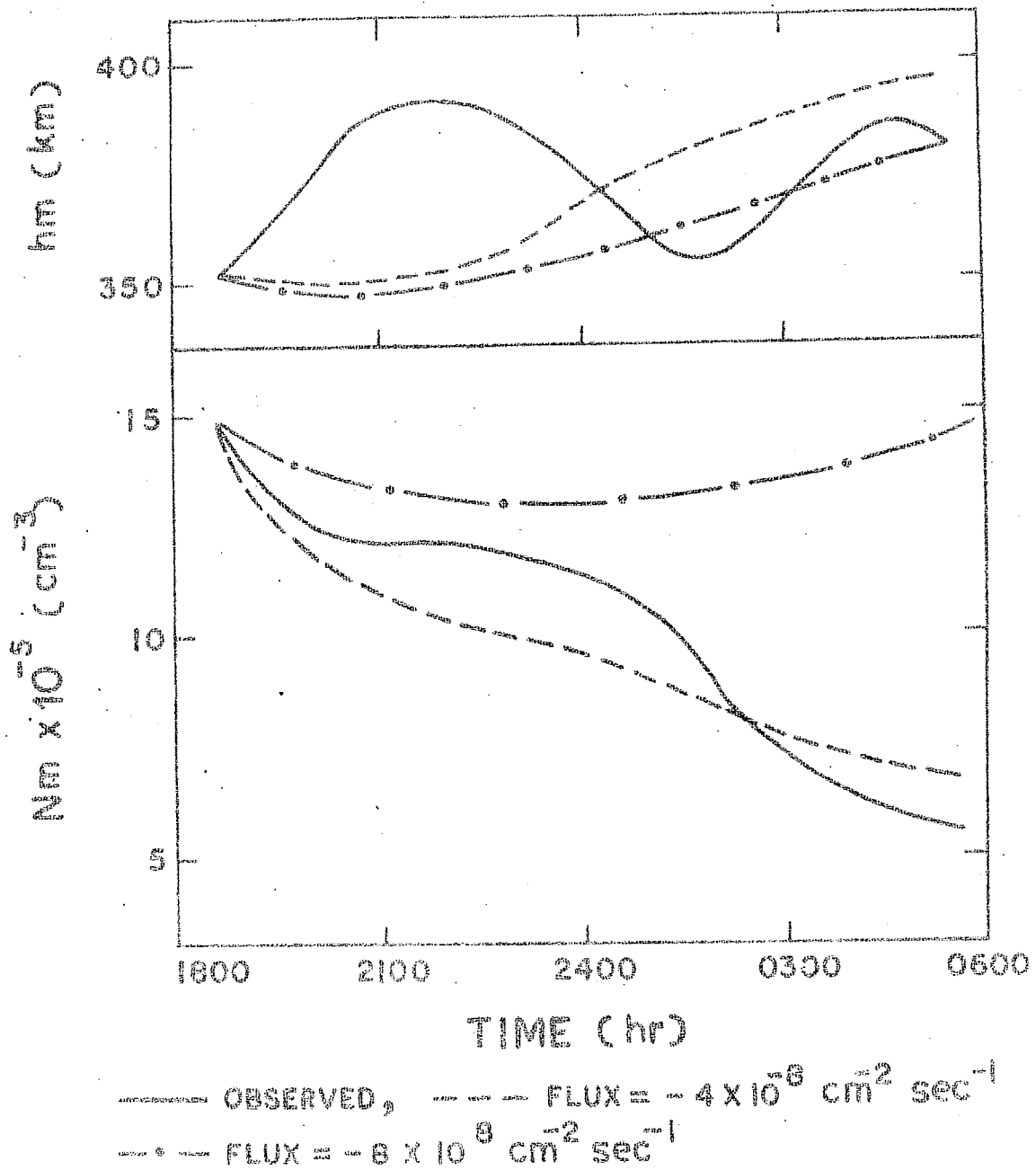


FIG 4.8 : Effect of plasma flux on night-time F-region.

smaller flux and after about 2200 hr, when the layer starts rising, due to equatorward winds, the  $N_m$  value also starts showing a rise. In the absence of winds a flux of the order of  $10^9$  electrons  $\text{cm}^{-2} \text{sec}^{-1}$  is needed to maintain  $N_m$  of about  $5 \times 10^5 \text{ cm}^{-3}$  at a height of 350 km.

Variation of loss coefficients by 20% demands a change in flux of around 30% to obtain almost the same results. The effect of variation of ion-drag is, to vary the magnitude of neutral wind velocities (as shown in Section 4.9) with a consequent change in the layer height and in  $N_m$ . Doubling the drag, reduces  $N_m$  by about 20% after about 0200 hr, when almost a steady value of  $N_m$  is reached.

It is, thus, seen that although the neutral wind may be able to explain some of the gross features, it has not been possible for any of the three mechanisms presented here (viz. neutral wind, electric field and protonospheric flux) to explain the observed behaviour of  $h_m$ , which shows two humps during the night. The declination being only  $8^\circ$  for Puerto Rico, the effect of east-west winds is also not likely to be significant for producing these features. The observed  $h_m$  behaviour suggests that the phase of reversal of meridional wind equatorward occurs about 3 to 4 hours earlier than the calculated time. This would be a violation of both Jacchia and incoherent scatter models. However, even this will not be able to explain the observed dip in  $h_m$  around 0130 hr.

These aspects, therefore, need further investigations. So is the case in regard to the seasonal variations in the behaviour of  $h_m$  and  $N_m$ , as pointed out in Section 4.9. These investigations are now being taken up.

## CHAPTER V

### SUMMARY AND CONCLUSIONS

THE thesis describes the experimental and theoretical investigations, carried out by the author at the Physical Research Laboratory, Ahmedabad, for understanding the structure and the dynamics of the Upper Atmosphere. The experimental observations were made by releasing chemical vapours with the help of rockets from the Thumba Equatorial Rocket Launchings Station (TERLS), near the magnetic equator. This launching station is only  $8^{\circ}$  north of the geographic equator.

By releasing the chemical vapours, neutral upper atmospheric winds were measured in the altitude region of 90 to 125 km at night-time, and upto about 200 km altitude at twilight hours. The night-time wind results from Thumba are presented for the first time. Atmospheric temperatures were also determined from the diffusion measurements of the vapour clouds in the height region of 130 to 200 km. These temperature results are also the first results of equatorial upper atmospheric temperatures above 100 km in the Indian Zone.

A systematic study of the neutral upper atmospheric wind measurements, carried out over the past several years, at different locations over the globe, has been conducted. An average general atmospheric circulation pattern for the prevailing winds, emerging out of this study, in the height region of 100 to 200 km, is presented. Seasonal and diurnal effects are also derived.

There are no proven experimental techniques for the direct measurement of atmospheric winds above about 250 km during twilight and above about 150 km at night-time. Vapour clouds diffuse away very rapidly at these great heights. The satellite drag measurements give only average zonal winds over a long period and the incoherent scatter measurements are useful only for the study of meridional motions. The author has, therefore, conducted a theoretical study and derived neutral winds at F-region heights from the known electron density profiles and model atmospheric parameters. Electron density profiles from the mid-latitude station Puerto Rico, for the year 1960, have been used for this study. The theoretical study has also revealed the effects of individual parameters, such as the neutral winds, electric fields and protonospheric influx of ionisation, on the F-region of the ionosphere; and has contributed to a furtherance of the present day knowledge about the maintenance of the night-time F-region ionisation.

The limitations of the experimental and theoretical methods employed, the errors involved in the measurements and the calculations, and the limitations imposed by the assumptions made, are also critically examined and discussed.

## 5.1 IMPORTANT CONCLUSIONS

The following are the important findings and conclusions drawn from the above mentioned studies :-

5.1.1 Results of Night Time Wind Measurements over Thumba

- i) The wind profiles over Thumba, observed during night-time in the 100-110 km region, do not show large wind shears, unlike in the case of profiles observed during twilight over Thumba (BHAVSAR AND RAMANUJA RAO, 1968) and over other latitudes, in the same height region.
- ii) The meridional winds, above an altitude of 115 km, are towards the equator (southward) around 2200 hr local time, but are in the opposite direction around 0200 hr local time.
- iii) Earlier observations of zonal winds in the height region of 115 to 140 km had shown winds during twilight to be regularly eastward in the height region of 115 to 140 km. The winds during night-time are now found to be westward around 2200 hr local time and eastward around 0200 hr local time.
- iv) The rotation of the wind vector with height, for night-time winds, does not show any regular pattern. This result is in agreement with the earlier findings for twilight hours over Thumba (BHAVSAR AND RAMANUJA RAO, 1968).

- v) There is a good agreement between the results of average E-region drifts, as measured by the spaced receiver technique at Thumba, and the night-time neutral motions in this region, in the east-west direction.
- vi) Evidences of turbulence features, both during the up- and down-leg releases of vapour clouds, have been observed.

#### 5.1.2 Results of Twilight Winds Determined from the Motions of Ba-Sr Neutral Clouds over Thumba

Ba-Sr clouds were only point releases at discrete heights, about 20 to 30 km apart in the vertical direction, and hence complete vertical wind profiles were not obtained as in the case of sodium or TMA trails. Accordingly, the wind shears as well as other vertical structures in the wind profiles could not be studied. These experiments were conducted at the end of March, which is the beginning of the summer in the Northern hemisphere, while all the earlier twilight wind measurements at Thumba had been made in the winter months of November - January.

- i) Earlier twilight results of meridional winds had shown that during the northern hemisphere winter, the winds over Thumba, in the 150 to 190 km altitude region, had a northward meridional component, continuously increasing



with height (BHAVSAR AND RAMANUJA RAO, 1968).

The present results suggest that the meridional flow is opposite in direction in summer to what was observed in winter.

ii) The zonal winds, observed by tracking the neutral strontium clouds at twilight, show predominantly westward winds with a maximum around 150 km and decreasing upwards thereafter and ultimately reversing direction to eastward, above 200 km. The results obtained for the summer months are in general agreement with those that had been obtained earlier (BHAVSAR AND RAMANUJA RAO, 1968) for the winter months, and therefore suggest that no seasonal effects prevail in the zonal component above 150 km in the neutral winds.

iii) The reversals of the zonal winds to the eastward direction at heights above 200 km seems to confirm the super-rotation hypothesis advanced by KING-HELE on the basis of satellite drag observations.

iv) During the Ba-Sr releases, the ion clouds were also tracked for electric field measurements. The results show that the ion clouds are affected by ambient neutral gas motions fully

upto about 160 km altitude and only along the field lines beyond this height.

### 5.1.3 General Circulation in the Upper Atmosphere

The prevailing flow of neutral air mass in the height range of 100 to 200 km has been derived from the results of about 200 vapour release experiments conducted from various locations over the globe over past several years. This general flow, however, is liable to have a bias towards conditions prevailing during evening twilight, since out of the total vapour releases, about 50% pertain to evening twilight, about 35% to night-time and only about 15% to the morning hours. The diurnal and seasonal changes in the average winds, above 150 km, have also been studied from the limited data available. The following conclusions have been arrived at :

- i) For latitudes below  $30^\circ$ , in the equatorial zone, the wind speed remains almost constant with altitude, whereas at higher latitudes, beyond  $30^\circ$ , an increasing wind speed with altitude is discerned.
- ii) The zonal prevailing circulation is easterly in the 140 to 180 km region for all the latitudes. For low latitudes, winds in the 120 to 140 km region are westerly.
- iii) The meridional flow shows strong seasonal trend above 150 km altitude. There is a

nett flow from the summer to winter hemisphere, which is more markedly evident from the evening twilight observations.

- iv) The super-rotation hypothesis, that the atmosphere above 180 km has a nett eastward velocity, finds support, particularly from mid-latitude evening observations. The absence of such a behaviour for high latitudes corroborates the model calculations done by ILL ET AL. (1973). However, the rather low nett eastward flow, observed at low latitudes by vapour release methods, does not support these model calculations.
- v) The morning winds above 180 km are mostly north-easterly, and this is in accordance with the model calculations.
- vi) Though the mean eastward flow, above 180 km, is in consonance with the models, the zonal motion in the 140 to 180 km altitude region, is westward. This calls for a re-thinking on interpolation of temperatures in the lower thermosphere.
- vii) The flow from the summer to the winter hemisphere also gives credence to the argument that neutral winds are the causative mechanisms for the observed asymmetry in the equatorial anomaly.

#### 5.1.4 Atmospheric Structure from the Study of Growth Rate of Artificial Vapour Releases

This study has been presented in Chapter III. A new procedure for correcting for sky background in the measurement of diffusion coefficient of vapour clouds has been developed and used. A new method for calculating atmospheric temperatures from the observed diffusion profile has also been presented in the study. This method of temperature determination, though indirect, will be of great value, when diffusion profiles are measured simultaneously with temperatures at a few altitudes. The effect of finite exposure and the mass motion of the cloud, on diffusion measurements has been studied. The results show that this effect is much smaller than what has been reported earlier. Other salient features of this study have been that the temperature profile derived from diffusion profiles below 150 km, shows negative gradients, not compatible with the present-day model atmosphere. Various possibilities for this anomalous behaviour have been investigated. Wave propagation and departures from barometric law of the atmospheric constituents seem to be the important causes, besides the possibility of additional diffusion at lower levels.

#### 5.1.5 Winds at F-region Heights and Interaction of Neutral and Ionised Atmospheres

In Chapter IV, from the observed electron density profiles at Puerto Rico and using model atmosphere parameters,

neutral atmospheric motions at F-region heights have been calculated. The protonospheric flux of plasma has also been estimated from the observed night-time electron-density profiles. The following conclusions emerge from these calculations :-

- i) The atmosphere at F-region heights has a nett eastward velocity of about  $35-40 \text{ m sec}^{-1}$ . This is in better agreement with the values quoted by KING-HELE (1972) from satellite drag analysis than the results of other workers.
- ii) The electron density maximum value ( $N_m$ ) and height of this maximum ( $h_m$ ) can be qualitatively explained on the basis of the meridional winds calculated from the model. Seasonal variations of the changeover of wind direction from poleward to equatorward are fairly well related to the decay and maintenance of ionisation.
- iii) Seasonal changes in the calculated values are in agreement with the observed average rises of night-time  $h_m$  over its day-time average value, and the ratios of the average day-time  $N_m$  to night-time  $N_m$  values.
- iv) Average protonospheric flux, of the order of  $4 \text{ to } 8 \times 10^8 \text{ particles cm}^{-2} \text{ sec}^{-1}$  throughout

the night for the different periods, has been estimated from the observed  $N(z,t)$  profiles, over Puerto Rico. These estimates are in good agreement with observational results.

#### 5.1.6 Effect of Various Atmospheric Parameters on Night-time Ionisation

The electron continuity equation and equations of motion for the neutral air and ions have all been simultaneously solved for equinox night-time conditions and the following conclusions have been arrived at :

- i) The effect of electric field drifts is insignificant on the night-time F-region parameters.
- ii) The neutral atmospheric winds at F-region heights and a flux of the order of  $4 \times 10^8$  electrons  $\text{cm}^{-2} \text{sec}^{-1}$  from above are able to explain broadly the observed  $N_m$  behaviour. The immediate rise of  $h_m$  after 1900 hr, as observed, is not evident from the calculations.
- iii) In the absence of neutral winds, a flux of about  $10^9$  electrons  $\text{cm}^{-2} \text{sec}^{-1}$  is required from above to maintain the observed average  $N_m$  during the night.

The dip in  $h_m$  observed at mid-night and the differences between the calculated and observed times of  $h_m$  increases,

are some other aspects which are yet to be investigated fully.

## 5.2 GENERAL CONCLUSIONS AND AREAS FOR FUTURE WORK

From what has been presented in Chapters II and III, it will be evident that the 100 to 150 km altitude region of the atmosphere needs further careful examination and exhaustive study. The temperature and other atmospheric parameters, as a function of altitude and latitude, as well as the various components of motion, need a better understanding. Paired observations, of the evening-morning twilight hours with some 4 or 5 night-time rocket launchings in between, would throw more light on the above aspects. Vapour cloud experiments above the 200 km altitude region are also necessary to study the super-rotation hypothesis more fully for a proper theoretical understanding.

The day-time wind measurement technique should be perfected and fully exploited in unravelling the diurnal and other behaviours of the neutral atmospheric dynamics. The development of techniques for measuring night-time winds above 150 km is also essential, as the present technique of TMA chemi-luminescent trail is limited to altitudes below 150 km. Simultaneous neutral and ion cloud movements have to be studied in more detail to understand the interaction between the two. Turbulence features will have to be studied

in more detail from the simultaneous up- and down-leg of the same vapour trail for a better understanding of the conditions which initiate turbulence.

Numerical methods have also to be improved for incorporating the non-linear term in the equations of motion for the neutral species. Dynamical model atmospheres have to be used for studying the motions and interactions.

Finally, although the F-region behaviour seems fairly well understood, there are, yet, conflicting opinions about the role of corpuscular radiation. Rocket experiments, at low latitudes for measuring the low energy electron fluxes, in conjunction with airglow observations of  $N_2^+$  bands, are necessary for this purpose.



## APPENDIX - I

### SOURCES OF WIND DATA FROM VAPOUR RELEASES

Wind data, for the analysis of Global Circulation presented in Chapter II, have mostly been taken from the sources referred to in the Thesis; a full list of the various references is given at the end. Some wind data have been taken from the following additional sources as well:

1. Space Research Volumes 1 to 12.
2. Bedinger J.F. and Constantinides E. (1968):  
GCA-TR-68-11-N.
3. Bedinger J.F. and Constantinides E. (1969):  
GCA-TR-69-3-N.
4. Justus C.G. and Edwards H.D. (1965):  
Georgia Tech. Proj. A-434, A-626, A-652,  
A-722, B-204, B-205.
5. Montgomery J.B., Justus C.G. and Edwards H.D. (1968):  
AFCRL-68-0503.
6. Smith L.B. (1971): Sardinia Laboratories Report  
(Revised) SC-RR-71, 0008.

# APPENDIX - II

## Mean Winds Above 150 km and Winds at the Highest Altitude of Observation Above 180 km

<u>Design-</u> <u>nation</u>	<u>Launch</u> <u>date</u>	<u>Season</u> <u>and</u> <u>Time</u>	<u>Mean Wind</u> <u>above 150 km</u> <u>(Vel/Dir)</u>	<u>Wind at the highest</u> <u>altitude</u>	
				<u>Altitude</u>	<u>Vel/Dir</u>
a) <u>LOW LATITUDE (&lt;30°)</u>					
1. <u>THUMBA (8° N, 77° E)</u>					
a1	21-11-63	W, E	185/350	180	260/345
a2	8- 1- 64	W, E	45/300	190	75/40
a3	12-1- 64	W, M	35/275		
a4	6-11-64	W, M	45/330		
a5	9-11-64	W, E	70/310		
a6	10-11-64	W, M	35/340		
a7	28- 3-68	S, E	35/235	205	35/170
a9	30- 3-68	S, E	10/200	204	14/140
a8	31- 3-68	S, M	25/300		
a34	31- 3-68	S, E	95/210		
2. <u>HAWAII (22° N, 16°W)</u>					
a10	11-10-62	W, E	75/340		
a11	21-10-62	W, E	35/300		
a12	29-10-62	W, E	35/290		
a13	25- 5-63	S, E	125/190		
a14	6- 2-64	W, E	40/160		
a15	23- 1-64	W, E	15/15		
a16	2- 1-64	W, E	72/310		
a17	16- 6-65	S, E	220/245		
a18	17- 6-65	S, E	70/210		
a19	17- 6-65	S, E	80/240		
a20	21- 6-65	S, E	120/150		
a21	21- 6-65	S, E	100/150		

: A-3 :

a22	23-6-65	S, E	85/190
a23	23-6-65	S, E	90/160
a24	8-6-66	S, E	90/280
a25	11-6-66	S, E	150/250
a26	31-5-67	S, E	110/270
a27	31-5-67	S, E	45/300
a28	1-6-67	S, E	125/130
a29	2-6-67	S, E	50/250

TONOPAH

a30	21-4-66	S, E	150/260
a31	15-12-66	W, E	85/85

3. SONMIANI (26° N, 67° E)

a32	1-12-64	W, M	30/270	205	40/240
-----	---------	------	--------	-----	--------

4. REGGAN (27° N, 0°)

a33	21- 5-63	S, M	90/170
-----	----------	------	--------

b) MID-LATITUDE (30°-35°)

1. EGLIN (30° N, 87° W)

b1	17- 5-63	S, E	100/200		
b2	18- 5-63	S, M	40/160		
b9	1-10-63	W, M	50/225		
b3	18-11-65	W, M	40/80		
b4	23- 6-66	S, M	140/250		
b5	16- 1-67	W, M	70/300		
b6	16- 1-67	W, E	25/180		
b7	12- 4-67	S, E	70/190		
b8	27- 4-67	S, E	50/130	230	55/130

2. HAMMAGUIR (31° N, 3° W)

b10	12- 3-59	W, M	65/100		
b13	2- 3-60	W, E	55/170	180	50/155
b11	5- 3-60	W, M	150/10		
b14	13- 6-60	S, E	75/180		

b12	16- 6-60	S, E	140/175		
b15	1-12-62	W, M	90/150		
b16	21- 5-63	S, E	65/150		

3. WOOMERA (31° S, 137° E)

b25	6- 3-61	W, E	130/300	180	130/300
b17	28-11-61	S, E	100/350	200	110/350
b18	5- 3-62	W, E	70/360		
b19	15-10-63	S, E	50/75	185	53/90
b20	16-10-63	S, M	70/270	190	73/280
b21	31- 5-68	W, M	100/170	240	115/170
b22	31- 5-68	W, E	75/110	240	105/85
b23	16-10-69	S, M	25/270	250	20/345
b24	17-10-69	S, E	90/50	240	100/50

4. CHAMICAL (32° S, 66° W)

b26	27-11-62	S, E	80/350		
b27	30-11-62	S, W	85/320		

5. NEW MEXICO (33° N, 107° W)

b28	26-11-57	W, M	40/220	200	40/240
-----	----------	------	--------	-----	--------

c) HIGH-LATITUDE (> 35°)1. WALLOPS ISLAND (38° N, 76° W)

c14	17- 8-59	S, M	170/230	225	110/225
c1	20- 4-61	S, E	125/195		
c15	21- 4-61	S, M	60/220		
c16	17- 9-61	S, M	100/300		
c17	17- 4-62	S, M	90/270	190	110/270
c18	30-11-62	W, M	100/160		
c2	21- 2-63	W, E	40/60		
c3	23- 5-63	S, E	70/210	200	60/260
c4	24- 5-63	S, E	100/190		
c19	16- 1-64	W, M	220/230	190	230/240
c5	14- 7-64	S, E	60/150	180	80/240
c20	15- 7-64	S, M	130/210	190	120/230
c21	8-10-64	W, M	120/270		
c6	10-11-64	W, E	60/90	185	70/70

c7	11-11-64	W, E	60/60	195	70/20
c22	23- 6-65	S, M	80/220		
c12	17- 1-66	W, E	70/60		
c26	18- 1-66	W, M	40/200	180	50/270
c13	16- 7-66	S, E	150/200		
c24	22- 2-68	W, M	90/120		
c25	22- 2-68	W, M	40/180		
c8	13- 2-69	W, E	100/90	250	100/90
c9	13- 2-69	W, E	80/90		
c23	14-2- 69	W, M	25/270		
c10	13-12-69	W, E	60/40		
c11	13-12-69	W, E	100/90	200	90/60

2. SARDINIA (40° N, 10° E)

c28	19- 4-61	S, E	130/180	185	145/170
c29	20- 4-61	S, M	135/220	190	135/230
c30	7- 9-61	S, E	100/145	200	100/140
c31	20- 5-63	S, E	80/180	195	80/180
c32	21- 5-63	S, M	80/210		
c33	21- 5-63	S, E	85/180	190	90/180

3. ILE DU LEVANT (43° N, 6° E)

c27	21- 5-63	S, M	65/210		
-----	----------	------	--------	--	--

4. FT. CHURCHILL (58° N, 94° W)

c34	21- 5-63	S, E	210/260		
c35	22- 5-63	S, M	220/230		
c37	22- 5-63	S, E	90/210		
c36	27- 5-63	S, E	60/330		
c38	15- 9-66	S, E	210/280		

Note : i) Direction of wind vector from north through east.

ii) S - Summer, W - Winter

M - Morning twilight, E - Evening twilight.

## REFERENCES

- ABUR ROBB M. F. K. & WINDLE D. W. (1969): PLANET. SPACE SCI. 17,97.  
ACKERMAN M. AND VAN HEMELREJCK E. (1971): J. GEOPHYS. RES. 76,3162.  
AINSWORTH J. E., FOX D. F. AND LAGOW H. E. (1961): J. GEOPHYS. RES. 66,3191.  
ALBRITTON D. L., YOUNG L. C., EDWARDS H. D. AND BROWN J. L. (1962): PHOTOGRAMMETRIC ENGG. 28,608.  
ALCAYDE D., BAUER P., JACK C. AND FALIN J. C. (1972): J. GEOPHYS. RES. 77,2368.  
ALLAN C. W. (1965): SPACE SCI. REV. 4,91.  
ALLAN R. R. (1972): PRESENTED AT THE 15TH COSPAR MEETING, MADRID, SPAIN.  
AMAYENC P. & REDDY C. A. (1972): PLANET. SPACE SCI. 20,1269.  
AMAYENC P. & VASSEUR G. (1972): J. ATMOS. TERR. PHYS. 34,351.  
AMAYENC P., FONTANARI J. AND ALCAYDE D. (1973): J. ATMOS. TERR. PHYS. 35,1499.  
ANDERSON A. D. AND SHARP G. W. (1971): EOS, TRANS. AGU. 52,293.  
AREFYEVA A. V., KORPUSOG V. N., LYSENKO I. A., ORLYANSKIY A. D., RYABCHIKOV A. N. AND SHUVARIKOV N. F. (1966): GEOMAG. & AERO. 6,537.  
AUTHIER B. (1964): ANN. GEOPHYS. 20,353.  
BABER H. T., CRUMBLY K. H. & ADAMSON D. (1971): NASA SP-264.  
BAILEY G. J., MOFFETT R. J. & RISHBETH H. (1969): J. ATMOS. TERR. PHYS. 31,253.  
BAILEY G. J. & MOFFETT R. J. (1972): PLANET. SPACE SCI. 20,1085.  
BALSIGER H., EBERHARDT P., GEISS J. AND KOPP E. (1971): REV. SCI. INSTR. 42,475.  
BALSLEY B. B. (1973): J. ATMOS. TERR. PHYS. 35,1035.  
BAMGBOYE D. K. AND LYON A. J. (1968): NATURE. 220,152.  
BANKS P. M. (1967): J. GEOPHYS. RES. 72,3365.  
BANKS P. M. & HOLZER T. E. (1969): J. GEOPHYS. RES. 74,6317.  
BARLIER F., FALIN J. L., ILL M. AND JACK C. (1972): PRESENTED AT THE 15TH COSPAR MEETING, MADRID, SPAIN.  
BATES D. R. (1950): J. GEOPHYS. RES. 55,347.  
BATES D. R. (1955): PROC. PHYS. SOC. A68,344.  
BATTEN E. S. (1961): J. METEOR. 18,283.  
BAUER P., WALDTEUFEL P. AND ALCAYDE D. (1970): J. GEOPHYS. RES. 75,4825.  
BEDINGER J. F. (1966): GCA TECH REP. 66-7-N.  
BEDINGER J. F. (1970 A): REV. SCI. INS. 41,1234.  
BEDINGER J. F. (1970 B): J. GEOPHYS. RES. 75,683.  
BEDINGER J. F. (1971): PRESENTED AT THE 14TH COSPAR MEETING, SEATTLE, WASHINGTON.  
BEDINGER J. F. (1973): J. ATMOS. TERR. PHYS. 35,377.  
BEDINGER J. F. & CONSTANTINIDES E. (1968): GCA TECH. REP. NO. T. R. 68-11-N.  
BEDINGER J. F., KNAFLICH H., MANRING E. AND LAYZER D. (1968): PLANET. SPACE SCI. 16,159.  
BERNARD R. AND SPIZZICHINO A. (1971): J. ATMOS. TERR. PHYS. 33,1345.  
BEST G. T. (1970): J. ATMOS. SCI. 27,979.  
BHAVSAR P. D. AND RAMANUJA RAO K. (1965): SPACE RES. 5,986.  
BHAVSAR P. D. AND RAMANUJA RAO K. (1968): SPACE RES. 8,655.  
BHAVSAR P. D., NARAYANAN M. S. AND RAMANUJA RAO K. (1969): SPACE RES. 9,374.

## REFERENCES

- ABUR ROBB M. F. K. & WINDLE D. W. (1969): PLANET. SPACE SCI. 17,97.  
ACKERMAN M. AND VAN HEEMELREJCK E. (1971): J. GEOPHYS. RES. 76,3162.  
AINSWORTH J. E., FOX D. F. AND LAGOW H. E. (1961): J. GEOPHYS. RES. 66,3191.  
ALBRITTON D. L., YOUNG L. C., EDWARDS H. D. AND BROWN J. L. (1962): PHOTOGRAMMETRIC ENGG. 28,608.  
ALCAYDE D., BAUER P., JACK C. AND FALIN J. C. (1972): J. GEOPHYS. RES. 77,2368.  
ALLAN C. W. (1965): SPACE SCI. REV. 4,91.  
ALLAN R. R. (1972): PRESENTED AT THE 15TH COSPAR MEETING, MADRID, SPAIN.  
AMAYENC P. & REDDY C. A. (1972): PLANET. SPACE SCI. 20,1269.  
AMAYENC P. & VASSEUR G. (1972): J. ATMOS. TERR. PHYS. 34,351.  
AMAYENC P., FONTANARI J. AND ALCAYDE D. (1973): J. ATMOS. TERR. PHYS. 35,1499.  
ANDERSON A. D. AND SHARP G. W. (1971): EOS, TRANS. AGU. 52,293.  
AREFYEVA A. V., KORPUSOG V. N., LYSENKO I. A., ORLYANSKIY A. D., RYABCHIKOV A. N. AND SHUVARIKOV N. F. (1966): GEOMAG. & AERO. 6,537.  
AUTHIER B. (1964): ANN. GEOPHYS. 20,353.  
BABER H. T., CRUMBLY K. H. & ADAMSON D. (1971): NASA SP-264.  
BAILEY G. J., MOFFETT R. J. & RISHBETH H. (1969): J. ATMOS. TERR. PHYS. 31,253.  
BAILEY G. J. & MOFFETT R. J. (1972): PLANET. SPACE SCI. 20,1085.  
BALSIGER H., EBERHARDT P., GEISS J. AND KOPP E. (1971): REV. SCI. INSTR. 42,475.  
BALSLEY B. B. (1973): J. ATMOS. TERR. PHYS. 35,1035.  
BAMBOYE D. K. AND LYON A. J. (1968): NATURE. 220,152.  
BANKS P. M. (1967): J. GEOPHYS. RES. 72,3365.  
BANKS P. M. & HOLZER T. E. (1969): J. GEOPHYS. RES. 74,6317.  
BARLIER F., FALIN J. L., ILL M. AND JACK C. (1972): PRESENTED AT THE 15TH COSPAR MEETING, MADRID, SPAIN.  
BATES D. R. (1950): J. GEOPHYS. RES. 55,347.  
BATES D. R. (1955): PROC. PHYS. SOC. A68,344.  
BATTEN E. S. (1961): J. METEOR. 18,283.  
BAUER P., WALDTEUFEL P. AND ALCAYDE D. (1970): J. GEOPHYS. RES. 75,4825.  
BEDINGER J. F. (1966): GCA TECH REP. 66-7-N.  
BEDINGER J. F. (1970 A): REV. SCI. INS. 41,1234.  
BEDINGER J. F. (1970 B): J. GEOPHYS. RES. 75,683.  
BEDINGER J. F. (1971): PRESENTED AT THE 14TH COSPAR MEETING, SEATTLE, WASHINGTON.  
BEDINGER J. F. (1973): J. ATMOS. TERR. PHYS. 35,377.  
BEDINGER J. F. & CONSTANTINIDES E. (1968): GCA TECH. REP. NO. T. R. 68-11-N.  
BEDINGER J. F., KNAFLICH H., MANRING E. AND LAYZER D. (1968): PLANET. SPACE SCI. 16,159.  
BERNARD R. AND SPIZZICHINO A. (1971): J. ATMOS. TERR. PHYS. 33,1345.  
BEST G. T. (1970): J. ATMOS. SCI. 27,979.  
BHAVSAR P. D. AND RAMANUJA RAO K. (1965): SPACE RES. 5,986.  
BHAVSAR P. D. AND RAMANUJA RAO K. (1968): SPACE RES. 8,655.  
BHAVSAR P. D., NARAYANAN M. S. AND RAMANUJA RAO K. (1969): SPACE RES. 9,374.

- BIRD R. B., STEWARD W. E. AND LIGHTFOOT E. N. (1960): 'TRANSPORT PHENOMENA', WILEY, N.YORK.
- BITTERBERG W., BRUTCHAUSEN K. OFFERMANN D. AND VON ZAHN U. (1970): J. GEOPHYS. RES. 75,4825.
- BLAMONT J. E. (1963): PLANET. SPACE SCI. 10,896.
- BLAMONT J. E. & DE JAGER C. (1961): ANN. GEOPHYS. 17,134.
- BLAMONT J. E., LORY M.L., SCHNEIDER J. P. AND COURTES G. (1962): SPACE RES. 2,974.
- BLAMONT J. E. & BARAT J. (1967): IN 'AURORA & AIRGLOW', ED. MCCORMAC B.M., P. 159, REINHOLD, N. YORK.
- BLAMONT J. E. AND LUTON J. M. (1972): J. GEOPHYS. RES. 77,3534.
- BLUM P. W. & HARRIS I. (1973): PLANET. SPACE SCI. 21,377.
- BLUMEN W. AND HENDL R.G. (1969): J. ATMOS. SCI. 26,210.
- BOWEN P. J., NORMAN K., WILLMORE A. P., BAGUETTE J. M., MURTY F. AND STOREY L. R. O. (1964): PLANET. SPACE SCI. 12,1173.
- BRAMLEY E. N. & PEART M. (1964): J. GEOPHYS. RES. 69,4609.
- BRAMLEY E. N. & PEART M. (1965): J. ATMOS. TERR. PHYS. 27,1201.
- BRAMLEY E. N. & YOUNG M. (1968): J. ATMOS. TERR. PHYS. 30,99.
- BRIERLY D. M. (1970): PLANET. SPACE SCI. 18,309.
- BRIGGS B. H. (1972): GEOPHYSISKE PUBLIKASJONER 39,121.
- BROGLIO L. (1965): SPACE RES. 5,1124.
- BROGLIO L. (1972): PRESENTED AT THE 15TH COSPAR MEETING, MADRID, SPAIN.
- BRUCE R. W. (1971): PRESENTED AT THE 14TH COSPAR MEETING, SEATTLE, WASHINGTON.
- CARLSON H. C. (1966): J. GEOPHYS. RES. 71,195.
- CARRU H., PETIT M. AND WALDTEUFEL P. (1967): PLANET. SPACE SCI. 15,944.
- CARTER V.L., CHING B.K. AND ELLIOT D.D. (1969): J. GEOPHYS. RES. 74,5083.
- CHALLINOR R. A. (1969): PLANET. SPACE SCI. 17,1097.
- CHAMPION K. S. W. (1967): SPACE RES. 7,1101.
- CHAMPION K. S. W. (1969): SPACE RES. 9,459.
- CHAMPION K. S. W. (1970): SPACE RES. 10,347.
- CHAMPION K. S. W. (1971): PRESENTED AT THE 14TH COSPAR MEETING, SEATTLE, WASHINGTON.
- CHAMPION K. S. W., MARCOS F.A. AND MCISAAC J. P. (1970 A): SPACE RES 10,450.
- CHAMPION K. S. W., MARCOS F. A. AND SCHWEINFURTH R. A. (1970 B): SPACE RES. 10,459.
- CHAMPION K. S. W. & SCHWEINFURTH R. A. (1971): PRESENTED AT THE 14TH COSPAR MEETING, SEATTLE, WASHINGTON.
- CHAMPION K. S. W. AND MARCOS F. A. (1972): PRESENTED AT THE 15TH COSPAR MEETING, MADRID, SPAIN.
- CHAMPION K. S. W., MARCOS F. A. AND SCHWEINFURTH R.A. (1972): PRESENTED AT THE 15TH COSPAR MEETING, MADRID, SPAIN.
- CHANDRA S. & STUBBE P. (1970): PLANET. SPACE SCI. 15,949.
- CHANDRA S. & STUBBE P. (1972): J. ATMOS. TERR. PHYS. 34,1627.
- CHANDRA S. AND SINHA A. K. (1973): PLANET. SPACE SCI. 21,593.
- CHAPMAN S. AND COWLING T. G. (1960): 'THE MATHEMATICAL THEORY OF NON-UNIFORM GASES', 2ND EDN., CAMBRIDGE UNIVERSITY PRESS, CAMBRIDGE.
- CHARNEY J. G. & DRAZIN P. G. (1961): J. GEOPHYS. RES. 66,83.
- CHIMONAS G. (1970): J. GEOPHYS. RES. 75,875.
- CHIMONAS G. & HINES C. O. (1970): J. GEOPHYS. RES. 75,875.



- CHUNG-MING-HUANG (1966): J. ATMOS. TERR. PHYS. 28,1151.  
CIRA (1965): COSPAR INTERNATIONAL REFERENCE ATMOSPHERE, NORTH HOLLAND, AMSTERDAM.  
COGGER L.L., NELSON G.J., BIONDI M.A., HAKE R.D. AND SIPLER D.P. (1970): J. GEOPHYS. RES. 75,4887.  
COLE K. D. (1962 A): NATURE 194,75.  
COLE K. D. (1962 B): AUST. J. PHYS. 15,223.  
COLE K. D. (1965): ANN. GEOPHYS. 21,156.  
COLE K. D. (1971): PLANET. SPACE SCI. 19,1010.  
COLEGROVE F.D., HANSON W. B. AND JOHNSON F.S. (1965): J. GEOPHYS. RES. 74,931.  
COLLIS R. T. H. (1969): ADV. GEOPHYS. 13,113.  
CONTE S.D. (1965): 'ELEMENTARY NUMERICAL ANALYSIS', MCGRAW HILL, N.YORK.  
COOK G. E. (1969 A): ANN. GEOPHYS. 25,451.  
COOK G. E. (1969 B): NATURE 222,969.  
CORMAN A. AND GUARINO N. J. (1965): GCA TECH. REP. NO. 65-2N.  
COTE O. (1965): GCA TECH. REP. NO. 65-5-N.  
COTE O. (1967): SPACE RES. 7,270.  
CRAIG R. A. (1965): 'THE UPPER ATMOSPHERE METEOROLOGY AND PHYSICS', INTERNATIONAL GEOPHYSICAL SERIES. VOL. 8, ACADEMIC PRESS, N.YORK.  
CRANK J. (1956): 'THE MATHEMATICS OF DIFFUSION', OXFORD UNIVERSITY PRESS, LONDON.  
CRPL (1960,1961): NATIONAL BUREAU OF STANDARDS, CENTRAL RADIO PROPAGATION LABORATORY PART A, IONOSPHERIC DATA, BOULDER, COLORADO.  
DALGARNO A. AND SMITH F. J. (1962): PLANET. SPACE SCI. 9,1.  
DANILOV A. D. (1962): ARTIFICIAL EARTH SATELLITE 8,233.  
DAVIS M. J. (1973): J. ATMOS. TERR. PHYS. 35,929.  
DESAI J. N. & NARAYANAN M. S. (1969): J. ATMOS. TERR. PHYS. 32,1235.  
DESHPANDE M.R. (1972): ANN. GEOPHYS. 28,809.  
DESHPANDE M. R. AND RASTOGI R.G. (1963): J. ATMOS. TERR. PHYS. 30,319.  
DESSLER A. J. (1958): J. GEOPHYS. RES. 63,507.  
DETWILER C. R, GARRET D. L., PURCELL J. D. AND TOUSEY R. (1961): ANN. GEOPHYS. 17,263.  
DEVRIES L. L. (1971): PRESENTED AT THE 14TH COSPAR MEETING, SEATTLE, WASHINGTON.  
DICKINSON R. E. (1968): J. ATMOS. SCI. 25,984.  
DICKINSON R. E. AND GEISLER J. E. (1968): MON. WEATH. REV. 96,606.  
DOUGHERTY J. P. (1961): J. ATMOS. TERR. PHYS. 20,167.  
DUBIN M. (1964): 'A GUIDE TO ROCKET LUMINOUS VAPOUR EXPERIMENTS', PUBLISHED BY COSPAR FOR THE IQSY.  
DUNCAN R. A. (1960): J. ATOMS.TERR. PHYS. 18,89.  
DUNGEY J. W. (1956): J. ATMOS. TERR. PHYS. 8,39.  
ECCLES D., KING J.W. AND KOHL H. (1971): J. ATMOS. TERR. PHYS. 33,1371.  
EDWARDS H. D. (1963): ED. 'STUDY OF PHOTO-CHEMISTRY, PHYSICAL STATE AND MOTION OF THE UPPER ATMOSPHERE', GEORGIA TECH. PROG. A-434.  
EDWARDS H.D., BEDINGER J. F., MANRING E. R. AND COPPER C. D. (1956): IN 'AIRGLOW & AURORA', ED. ARMSTRONG E. B. & DALGRAND A., P.122, PERGAMON PRESS, LONDON.  
EDWARDS H.D., COOKSEY M.M., JUSTUS C.G., FULLER R.N., ALBRITTON D.L. AND ROSENBERG N.W. (1963): J. GEOPHYS. RES. 68,3021.  
ELFORD W. G. (1959): PLANET. SPACE SCI. 1,94.

- EVANS J. V. (1965): J. GEOPHYS. RES. 70,4331.  
 EVANS J. V. (1969): PROC. IEEE. 57,496.  
 EVANS J. V. (1971): RADIO SCI. 6,843.  
 EVANS J. V. (1972): J. ATMOS. TERR. PHYS. 34,175.  
 EVANS J. V. (1973): PLANET. SPACE SCI. 21,763.  
 EVANS J. V. & TAYLOR G. N. (1961): PROC. ROY. SOC. A263,189.  
 EVANS J. V. & HOLT J. (1971): RADIO SCI 6,855.
- FARLEY D. T., MCCLURE J. P., STERLING D. L. AND GREEN J. L. (1967):  
 J. ATMOS. TERR. PHYS. 72,5837.
- FATKULIN M. N. (1973): J. ATMOS. TERR. PHYS. 35,453.  
 FATKULIN M. N. AND MURADOV A. (1971): GEOMAG. AND AERO. 11,61.  
 FEDDER J. A. AND BANKS P. M. (1972): J. GEOPHYS. RES. 77,2328.  
 FEDELE D. (1968): IN 'WINDS & TURBULENCE IN STRATOSPHERE, MESOSPHERE AND  
 IONOSPHERE', ED. K. RAWER, P.34, NORTH HOLLAND, AMSTERDAM.  
 FEDELE D. AND ZANCLA A. (1968): IN 'WINDS & TURBULENCE IN STRATOSPHERE,  
 MESOSPHERE AND IONOSPHERE', ED. K. RAWER, P.1, NORTH HOLLAND,  
 AMSTERDAM.
- FEES W. A. (1971): PRESENTED AT THE 14TH COSPAR MEETING, SEATTLE,  
 WASHINGTON.
- FEIBELMAN W. A., HAKE R. D., SIPLER D. P. AND BIONDI M. A. (1972):  
 J. GEOPHYS. RES. 77,1869.
- FOGLE B. AND HAURWITZ B. (1966): SPACE SCI. REV. 6,279.  
 FOPPL H., HAERENDEL G., LOIDL J., LUST R., MELZNER F., MAYER B., NEUSS H.  
 AND REIGER E. (1965): PLANET. SPACE SCI. 13,95.  
 FOPPL H., HAERENDEL G., HASER L., LOIDL J., LUTJENS P., LUST R., MELZNER F.,  
 MAYER B., NEUSS H. AND REIGER E. (1967): PLANET. SPACE SCI. 15,357.
- GEISLER J. E. (1967 A): J. ATMOS. TERR. PHYS. 29,1469.  
 GEISLER J. E. (1967 B): J. GEOPHYS. RES. 72,81.  
 GEISLER J. E. & BOWHILL S. A. (1965): AERONOMY REPORT NO. 5, UNIVERSITY  
 OF ILLINOIS, ILLINOIS.
- GILBERT J. C. AND REES D. (1971): PLANET. SPACE SCI. 19,669.  
 GIRAUD A., SCIALOM G. AND POKHUNKOV A. A. (1972): J. GEOPHYS. RES.  
 77,1251.
- GOLDBERG R. A. (1969): PROC. IEEE. 57,1119  
 GOLOMB D., HARANG O. AND DELGRECO F. P. (1967): J. GEOPHYS. RES. 72,2365.  
 GOLOMB D., DELGRECO F. P., HARANG O., JOHNSON R. H. AND MACLEOD M. A.  
 (1968): SPACE RES. 8,705.  
 GOLOMB D., GOOD R. E., KITROSSER D. F. AND JOHNSON R. H. (1969):  
 PRESENTED AT THE ANNUAL GENERAL MEETING OF AGU, WASHINGTON.
- GOOD R. E. AND GOLOMB D. (1972): PRESENTED AT THE 15TH COSPAR MEETING,  
 MADRID, SPAIN.
- GORDON W. E. (1958): PROC IRE 46, 1824.  
 GREENHOW J. S. (1959): J. ATMOS. TERR. PHYS. 16,384.  
 GREENHOW J. S. & NEUFELD E. L. (1960): PROC. PHYS. SOC. 75,228.  
 GREENHOW J. S. & NEUFELD E. L. (1961): QUART. J. ROY. MET. SOC. 87,472.  
 GROVES G. V. (1959): J. ATMOS. TERR. PHYS. 16,344.  
 GROVES G. V. (1963 A): PROC OF THE FIRST INT. SYM. ON ROCKET AND  
 SAT. MET., NORTH HOLLAND, AMSTERDAM.  
 GROVES G. V. (1963 B): J. GEOPHYS. RES. 68,3033.  
 GROVES G. V. (1971): AFCL REPORT NO. 71-0410.  
 GROVES G. V. & OWEN G. (1960): THE PHOTOGRAMMETRIC RECORD, VOL. III, NO. 16.  
 GULATTEE (1956): 'GRAVITY DATA IN INDIA', TECH. PAPER NO. 10,  
 SURVEY OF INDIA.

- HAKE R.D.JR., ARNOLD D.F., JACKSON D.W., EVANS W.E., FICKLIN B.P. AND LONG R.A. (1972): J. GEOPHYS. RES. 77,6839.
- HALL J.F. (1972): J.ATMOS. TERR. PHYS. 34,1337.
- HANSON W.B. & ORTENBURGER I.B. (1961): J. GEOPHYS. RES. 66,1425.
- HANSON W.B. & PATTERSON T.N.L. (1964): PLANET. SPACE SCI. 12,979.
- HANSON W.B. & MOFFETT R.J. (1966): J. GEOPHYS. RES. 71,5559.
- HARANG O. (1964): PLANET. SPACE SCI. 12,567.
- HARANG O. (1969): IN 'ATMOSPHERIC EMISSIONS', ED. MCCORMAC B.M. AND OMHOLD A., P. 489, VAN NOSTRAND, REINHOLD, N. YORK.
- HARANG O. AND STOFFREGEN W. (1969): PLANET. SPACE SCI. 17,261.
- HARRIS I. AND PRIESTER W. (1962 A): J. ATMOS SCI 19,286.
- HARRIS I. AND PRIESTER W. (1962 B): J. GEOPHYS. RES. 67,4585.
- HASER L. (1967): IN 'AURORA AND AIRGLOW', ED. MCCORMAC B.M., P.391, REINHOLD, LONDON.
- HAURWITZ B. (1961): PLANET. SPACE SCI. 5,92.
- HAURWITZ B. (1964): W. M. O. TECH. NOTE NO. 58.
- HAYS P.B., NAGY A.F. AND ROBLE R.G. (1969): J. GEOPHYS. RES. 74,4162.
- HAYS P.B., NAGY A.F. AND ROBLE R.G. (1970): J. GEOPHYS. RES. 75,4881.
- HAYS P.B. & ROBLE R.G. (1971): J. GEOPHYS. RES. 76,5316.
- HAYS P.B. & ROBLE R.G. (1973): PLANET. SPACE SCI. 21,339.
- HAYS P. B., JONES R. A. AND REES M.H. (1973): PLANET. SPACE SCI. 21,559.
- HEDIN A.E. AND MAYR H.G. (1972): PRESENTED AT THE 15TH COSPAR MEETING, MADRID, SPAIN.
- HERMAN J.R. & CHANDRA S. (1969): PLANET. SPACE SCI. 17,815.
- HICKS J.E. & JUSTUS C.G. (1970): J. GEOPHYS. RES. 75,5565.
- HILLIARD R. L. AND SHEPHERD G. G. (1966 A): PLANET. SPACE SCI.. 14,383.
- HILLIARD R.L. AND SHEPHERD G.G. (1966 B): J. OPT. SOC. AM. 56,362.
- HINES C.O. (1960): CAN. J. PHYS. 38,1441.
- HINES C.O. (1963): QUART. J. ROY MET SOC. 83,417.
- HINES C.O. (1964 A): J. GEOPHYS. RES. 69,2847.
- HINES C.O. (1964 B): J. GEOPHYS. RES. 69,1018.
- HINES C.O. (1965): J. GEOPHYS. RES. 70,177.
- HINES C.O. (1966): J. GEOPHYS. RES. 71,1453.
- HINES C.O. & RAGHAVA RAO. R (1968): J. ATMOS. TERR. PHYS. 30,979.
- HINTEREGGER H.E. (1962): J. ATMOS. SCI. 19,3519
- HINTEREGGER H.E. (1965): SPACE SCI. REV. 4,461.
- HINTEREGGER H.E. AND HALL J.E. (1969): SPACE RES. 9,519.
- HIRSCHFELDER J.O., CURTISS C.F. AND BIRD R.B. (1954): 'MOLECULAR THEORY OF GASES AND LIQUIDS', WILEY, N.YORK.
- HODGES R. J. JR. (1967): J. GEOPHYS. RES. 72,3455.
- HOOKE W. H. (1969): J. GEOPHYS. RES. 74,1870.
- HOROWITZ J. AND BANKS P.M. (1973): PLANET. SPACE SCI. 21,1975.
- HUNTEN D. M, RAWSON E.G. AND WALKER J.K. (1963) CAN. J. PHYS. 41,258.
- ILL M., CLAIREMIDI J. AND FALIN J.L. (1973): PRESENTED AT THE 16TH COSPAR MEETING, KONSTANZ, W. GERMANY.
- IVANOVA I.N., KOKIN G.A. AND CHIZHOV A.F. (1969): SPACE RES. 9,514.
- IVANOV-KHOLODNY G.S. (1965): SPACE RESEARCH. 5,19.
- JACCHIA L.G. (1963): REV MOD PHYS. 35,973.
- JACCHIA L.G. (1965): SMITHSON. CONTRIB. ASTOPHYS. 8,215.
- JACCHIA L.G. (1970 A): J. GEOPHYS. RES. 75,4347.
- JACCHIA L.G. (1970 B): S A O SPECIAL REPORT 313.
- JACCHIA L.G. (1971): S A O SPECIAL REPORT 332.

- JACCHIA L.G., SLOWEY J. AND VERNIANI F. (1967): J. GEOPHYS. RES. 72,1423.  
 JACCHIA L.G. AND SLOWEY J. (1968): PLANET. SPACE SCI. 16,509.  
 JARRETT A.H., MCGRATTEN G. & REES J.A. (1963): PLANET. SPACE SCI. 11,1309.  
 JARRETT A.H. AND HOEY M. (1965): PROC ROY SOC. A299,510.  
 JOHNSON E.R. & LLOYD K.H. (1963): AUST. J. PHYS. 16,490.  
 JOHNSON F.S. (1964): IN 'ELECTRON DENSITY DISTRIBUTION IN IONOSPHERE & EXOSPHERE', ED. THRANE E., P. 81, NORTH HOLLAND, AMSTERDAM.  
 JOHNSON F.S. & WILKINS E. M. (1965): J. GEOPHYS. RES. 70,1281.  
 JOHNSON F.S. & GOTTLEIB B. (1973): PLANET. SPACE SCI. 21,1001.  
 JOHNSON M.H. & HULBURT E.O. (1950): PHYS. REV. 79,802.  
 JUSTUS C.G. (1970): J. GEOPHYS. RES. 75,2171.  
 JUSTUS C.G., EDWARDS H.D. AND FULLER R.N. (1963): GEORGIA TECH. PROG. REP. NO. A-434, P.52.
- KANTOR A.J. & COLE A.E. (1964): J. GEOPHYS. RES. 69,5131.  
 KARANDIKAR R.V. (1968): PLANET. SPACE SCI. 16,539.  
 KASTLER A. AND BRICARD J. (1944): ANN. GEOPHYS 1,53.  
 KATO S. (1956): J. GEOMAG. GEOELEC. 8,24.  
 KATO S. (1957): J. GEOMAG. GEOELEC. 9,107.  
 KATO S. (1966 A): J. GEOPHYS. RES. 71,3201.  
 KATO S. (1966 B): J. GEOPHYS. RES. 71,3211.  
 KEATING G.M. (1969): SPACE RES. 9,534.  
 KEATING G. M. (1971): EOS, TRANS AGU. 52,498.  
 KEATING G.M. & PRIOR E.J. (1968): SPACE RES. 8,982.  
 KENNEL C. F. AND REES M.H. (1972): J. GEOPHYS. RES. 77,2294.  
 KENT G.S. (1970): REV. GEOPHYS. SPACE PHYS 8,229.  
 KENT G.S. & WRIGHT R.W.H. (1968): J. ATMOS. TERR. PHYS. 30,657.  
 KENT G.S., KEENLISIDE W., STANFORD M.C.W. & WRIGHT R.W.H. (1972): J. ATMOS. TERR. PHYS. 34,373.  
 KING G.A.M. (1964): J. ATMOS. SCI. 21,231.  
 KING J.W. & KOHL H. (1965): NATURE 206,699.  
 KING J.W., KOHL H. AND PRAT R. (1967): J. ATMOS. TERR. PHYS. 29,1529.  
 KING-HELE D.G. (1964): PLANET. SPACE SCI. 12,835.  
 KING-HELE D.G. (1966): ANN. GEOPHYS. 22,40.  
 KING-HELE D.G. (1972): SPACE RES. 12,847.  
 KING-HELE D.G. & ALLAN R.R. (1966): SPACE SCI. REV. 6,248.  
 KING-HELE D.G. & SCOTT D.W. (1967): PLANET. SPACE SCI. 15,1913.  
 KING-HELE D.G. AND WALKER D.M.C. (1969): PLANET. SPACE SCI. 17,2027.  
 KING-HELE D. G. AND WALKER D. M. C. (1970): PRESENTED AT THE 13TH COSPAR MEETING, LENINGRAD.  
 KNUDSEN W.C. (1968): J. GEOPHYS. RES. 73,841.  
 KNUDSEN W.C. (1969): J. GEOPHYS. RES. 74,4191.  
 KOCHANSKY A. (1963): J. GEOPHYS. RES. 68,213.  
 KOCHANSKY A. (1964): J. GEOPHYS. RES. 69,3651.  
 KOCHANSKY A. (1965): W.M.O. TECH. NOTE NO.70, ED. MURGATROYD R.J, P.140.  
 KOCHANSKY A. (1966): MONTH. WEA. REV. 94,199.  
 KOHL H. (1971): PRESENTED AT THE 14TH COSPAR MEETING, SEATTLE, WASHINGTON.  
 KOHL H. & KING J.W. (1967): J. ATMOS. TERR. PHYS. 29,1045.  
 KOHL H., KING J.W. & ECCLES D. (1968): J. ATMOS. TERR. PHYS. 30,1733.  
 KOHL H., KING J.W. AND ECCLES D. (1969): J. ATMOS. TERR. PHYS. 31,1011.  
 KRASSOVSKY V.I. (1972): PLANET. SPACE SCI. 20,1363.  
 KRASSOVSKY V.I., TRUTTSE YU.L. AND SHEFOV N.N. (1965): SPACE RES. 5,43.  
 KRISHNA MURTHY B.V. & SENGUPTA K. (1972): J. ATMOS. TERR. PHYS. 34,1155.

- LAYZER D. & BEDINGER J.F. (1969): PLANET. SPACE SCI. 17,1891.
- LEOVY C. (1969): ADV. GEOPHYS. 13,191.
- LILLER W. & WHIPPLE F.L. (1954): IN 'ROCKET EXPLORATION OF THE UPPER ATMOSPHERE', ED. BOYD R.L.F. & SEATON M.J., P. 112, PERGAMON PRESS, LONDON.
- LINDZEN R.S. (1966 A): MONTH. WEA. REV. 94,295.
- LINDZEN R. S. (1966 B): J. GEOPHYS. RES. 71,865.
- LINDZEN R.S. (1967 A): QUART. J. ROY. MET. SOC. 93,18.
- LINDZEN R.S. (1967 B): J. GEOPHYS. RES. 72,1591.
- LINDZEN R.S. (1969): J. ATMOS. TERR. PHYS. 31,449.
- LINDZEN R.S. & BLAKE D. (1970): J. GEOPHYS. RES. 75,6868.
- LLOYD K.H. (1965): AUST. J. PHYS. 18,349.
- LLOYD K.H. AND SHEPPARD L.M. (1966): AUST. J. PHYS. 19,323.
- LLOYD K.H., LOW C.H., MCAVANEY B.J., REES D. AND ROPER R.G. (1972): PLANET. SPACE SCI. 20,761.
- LLOYD K.H., LOW C.H. AND VINCENT R.A. (1973): PLANET. SPACE SCI. 21,653.
- LORY M.L. (1965): ANN. GEOPHYS. 21,303.
- LYON A.J. (1963): J. GEOPHYS. RES. 68,2531.
- LYON A.J. & THOMAS L. (1963): J. ATMOS. TERR. PHYS. 25,373.
- MACLEOD M.A. (1969): SPACE RES. 9,363.
- MAEDA H. (1955): J. GEOMAG. GEOELE. 7,121.
- MAEDA H. (1957): J. GEOMAG. GEOELE. 9,86.
- MAEDA K. (1965): J. ATMOS. TERR. PHYS. 27,259.
- MAEDA K. & KATO S. (1966): SPACE SCI. REV. 5,57.
- MAHAJAN K.K. (1969): J. ATMOS. TERR. PHYS. 31,93.
- MAHAJAN K. K. (1971): J. GEOPHYS. RES. 76,4621.
- MANRING E. AND LEVY R.J. (1961): GCA TECH. REP. NO. 61-4-N.
- MANRING E., BEDINGER J.F. AND KNAFLICH H. (1961): SPACE RES. 2,1107.
- MARTYN D.F. (1947): PROC. ROY. SOC. LONDON. A189,241.
- MARTYN D.F. (1953): PHIL. TRANS. ROY. SOC. LONDON. A246,306.
- MARTYN D. F. (1955): 'PHYSICS OF THE IONOSPHERE', P.254, PHYSICAL SOCIETY, LONDON.
- MATSUSHITA S. AND CHAMBELL W. H. (1967): ED. 'PHYSICS OF THE GEOMAGNETIC PHENOMENA', INTERNATIONAL GEOPHYSICAL SERIES, VOL. 11, ACADEMIC PRESS, N.YORK.
- MATSUSHITA S. & SMITH E.K. (1972): ED. RADIO SCI. 8,345.
- MAYR H.G. AND MAHAJAN K.K. (1971): J. GEOPHYS. RES. 76,1017.
- MAYR H.G. AND VOLLAND H. (1971): ANN. GEOPHYS. 27,513.
- MAYR H.G. & VOLLAND H. (1972): J. GEOPHYS. RES. 77,2359.
- MAYR H.G. & VOLLAND H. (1973): J. ATMOS. TERR. PHYS. 35,669.
- MCCLURE J.P. (1969): J. GEOPHYS. RES. 74,279.
- MERSON R.H., KING-HELE D.G. AND PLIMMER R.N.A. (1959): NATURE 183,239.
- MILLMAN P.M. (1959): J. GEOPHYS. RES. 64,2122.
- MISRA R.K. AND RASTOGI R. G. (1971): J. INST. TELECOM. ENGRS. 17,406.
- MITRA S.N. (1949): PROC. IEEE. 96,441.
- MITRA A.P., RAO B.C.N. AND MAHAJAN K.K. (1964): J. ATMOS. TERR. PHYS. 26,525.
- MITRA A.P., RAO B.C.N. AND MAHAJAN K.K. (1967): J. ATMOS. TERR. PHYS. 29,43.
- MOE K. (1967): PLANET. SPACE SCI. 15,1821.
- MOE K. (1973): J. GEOPHYS. RES. 78,1633.
- MOFFETT R.J. (1969): PLANET. SPACE SCI. 17,1850.

- MOFFETT R.J. AND HANSON W.B. (1965): NATURE 206,705.  
MULLER H.G. (1968): J. ATMOS. TERR. PHYS. 30,701.  
MURGATROYD R.J. (1957): QUART. J. ROY. MET. SOC. 83,417.  
MURGATROYD R.J. (1965): PROC. ROY. SOC. A288,575.  
MURGATROYD R.J. & GOODY R.M. (1958): QUART. J. ROY. MET. SOC. 84,225.  
MURPHY C.H. (1969): J. GEOPHYS. RES. 74,339.  
MURPHY C.H., BULL G.V. AND EDWARDS H.D. (1966): J. GEOPHYS. RES. 71,4535.  
MURPHY C.H. & BULL G.V. (1967): J. GEOPHYS. RES. 72,4831.  
MURPHY C.H. & BULL G.V. (1968): J. GEOPHYS. RES. 73,3005.
- NAGY A.F. & BANKS P.M. (1970): J. GEOPHYS. RES. 75,6260.  
NAGY A.F. WINNINGHAM J.D. AND BANKS P.M. (1973): J. ATMOS.  
TERR. PHYS. 35,2289.  
NARCISI R.S. (1971): IN 'PHYSICS OF THE UPPER ATMOSPHERE', ED. VERNIANI,  
P.12, EDITRICE COMPOSITORI, BOLOGNA.  
NATIONAL PHYSICAL LABORATORY (1960): 'MODERN COMPUTING METHODS', HER  
MAJESTY'S STATIONERY OFFICE, LONDON.  
NEWTON G.P. (1969): J. GEOPHYS. RES. 74,6409.  
NEWTON G.P. (1970): J. GEOPHYS. RES. 75,5510.  
NEWTON G. P., HOROWITZ R. AND PRIESTER W. (1965): PLANET. SPACE SCI.  
13,599.  
NEWTON G.P., PELZ D.T. AND KASPRZAK W.T. (1972): PRESENTED AT THE 15TH  
COSPAR MEETING, MADRID, SPAIN.  
NEWTON G.P. & PELZ D.T. (1973): J. GEOPHYS. RES. 78,725.  
NICOLET M. (1961): PLANET. SPACE SCI. 5,1.  
NIER A.O. (1971): PRESENTED AT THE 14TH COSPAR MEETING, SEATTLE, WASHINGTON.  
NIER A.O., HOFFMANN J.H., JOHNSON C.Y. AND HOLMES J.C. (1964):  
J. GEOPHYS. RES. 69,979.  
NISBET J.S. (1967): J. ATMOS. SCI. 24,586.  
NISBET J.S. & QUINN T.P. (1963): J. GEOPHYS. RES. 68,1031.  
NOEL T.M. (1966): J. GEOPHYS. RES. 71,5749.  
NORTON'S STAR ATLAS (1969): 'NORTON'S STAR ATLAS AND TELESCOPIC  
HANDBOOK', GALL AND INGLIS, LONDON.
- OFFERMANN D. AND VON ZAHN U. (1971): PRESENTED AT THE 14TH COSPAR  
MEETING, SEATTLE, WASHINGTON.  
O'NEIL R.R. (1972): PRESENTED AT THE 15TH COSPAR MEETING, MADRID, SPAIN.  
OSIPOV N. K. AND PIVOVAROVA N. B. (1971 A): GEOMAG. AERO. 11,233.  
OSIPOV N. K. AND PIVOVAROVA N. B. (1971 B): GEOMAG. AERO. 11,527.  
OSIPOV N. K. AND PIVOVAROVA N. B. (1971 C): GEOMAG. AERO. 11,715.
- PAETZOLD H.K. & ZSCHORNER H. (1961): SPACE RES. 1,24.  
PARK C.G. (1970): J. GEOPHYS. RES. 75,4249.  
PARK C.G. (1971): J. GEOPHYS. RES. 76,4560.  
PHILBRICK C.R., NARCISI R.S., BAKER D.W., TRZCINSKI E. AND GARDNER M.E.  
(1972 A): PRESENTED AT THE 15TH COSPAR MEETING, MADRID, SPAIN.  
PHILBRICK C.R., NARCISI R.S., GOOD R.E., HOFFMAN H.S. & KENESHEA T.J.  
(1972 B): PRESENTED AT THE 15TH COSPAR MEETING, MADRID, SPAIN.  
PHILBRICK C.R., GOLOMB D., ZIMMERMANN S.P., KENESHEA T.J. MACLEOD M.A.,  
GOOD R.E., DANDEKAR B.S. AND REINISCH B.W. (1973): PRESENTED AT THE  
16TH COSPAR MEETING, KONSTANZ, W. GERMANY.  
POKHUNKOV A.A. (1963): PLANET. SPACE SCI. 11,297.  
POKHUNKOV A.A. (1966): ANN. GEOPHYS. 22,92.

POLOSKOV S.M., TOULINOV G.F., BLAMONT J.E., LORY M.L., AND MAILLARD M.  
(1970): SPACE RES. 10,5199.

PRAG A. B. (1971): PRESENTED AT THE 14TH COSPAR MEETING. SEATTLE,  
WASHINGTON.

PRIESTER W., ROEMER M. AND VOLLAND H. (1967): SPACE SCI. REV. 6,707.  
PROCUNIER R.W. (1967): J. ATMOS. TERR. PHYS. 29,581.

QUESADA A.F. & MACLEOD M.A. (1972): PRESENTED AT THE 15TH  
COSPAR MEETING, MADRID, SPAIN.

RAGSDALE G.C. & WASKO P. E. (1963): NASA TECH. NOTE NO. D-1573.

RAMANUJA RAO K. (1966): PH.D. THESIS, GUJARAT UNIVERSITY, AHMEDABAD.

RASTOGI R G. (1959): J. GEOPHYS. RES. 64,727.

RASTOGI R. G., CHANDRA H. AND MISRA R. K. (1972): SPACE RES. 12,983.

RATCLIFF J. A. (1956): J. ATMOS. TERR. PHYS. 8,260.

REDDY C.A. AND DEVASIA C. V. (1973): PLANET. SPACE SCI. 21,811.

✓ REES D. (1967): PH. D. THESIS, UNIVERSITY OF LONDON, LONDON.

REES D. (1968): SPACE RES. 8,909.

REES D. (1969): J. BRIT. INTERPLANET. SOC. 22,275

REES D. (1971 A): PLANET. SPACE SCI. 19,233.

REES D. (1971 B): J BRIT. INTERPLANET. SOC. 24,643.

REES D. (1972): PHIL. TRANS. ROY. SOC. A271,563.

REES D., ROPER R.G., LLOYD K. H. AND LOW C.H. (1969): PRESENTED  
AT THE 12 TH COSPAR MEETING, PRAGUE.

REES D., ROPER R.G., LLOYD K.H. & LOW C.H. (1972 A): PHIL. TRANS. ROY.  
SOC., LONDON. A271,631.

REES D., NEAL M.P., LOW C.H., HIND A.D., BURROWS K. & FITCHEW R.S.  
(1972 B): NATURE 240,32.

REES D., HAERENDEL G., FELGATE D.G., LLOYD K.H. AND LOW C. H. (1973 A):  
PLANET. SPACE SCI. 21,1237.

REES D., KITROSSER D. F. AND GOLOMB D. (1973 B): PRESENTED AT THE 16TH  
COSPAR MEETING, KONSTANZ, W. GERMANY.

REES M. H. (1963): PLANET. SPACE SCI. 11,1209.

REES M. H. (1968): RADIO SCI. 3,645.

REVAH I. (1969): ANN. GEOPHYS. 25,1.

REVAH I. & SPIZZICHINO A. (1964): ANN. GEOPHYS. 20,248.

RISHBETH H. (1963): PROC. PHYS. SOC. 81,65.

RISHBETH H. (1964): J. ATMOS. TERR. PHYS. 26,657.

RISHBETH H. (1966): J. ATMOS. TERR. PHYS. 28,911.

RISHBETH H. (1967 A): PROC. IEEE 55,16.

RISHBETH H. (1967 B): J. ATMOS. TERR. PHYS. 29,225.

RISHBETH H. (1968 A): REV. GEOPHYS. 6,33.

RISHBETH H. (1968 B): J. ATMOS. TERR. PHYS. 30,63.

RISHBETH H. (1969): ANN. GEOPHYS. 25,495.

RISHBETH H. (1972 A): REV. GEOPHYS. SPACE PHYS. 10,711.

RISHBETH H. (1972 B): J. ATMOS. TERR. PHYS. 34,1.

RISHBETH H. & SETTY C. S. G. K. (1961): J. ATMOS. TERR. PHYS. 20,263.

RISHBETH H. & GARRIOT O. K. (1969): 'INTRODUCTION TO IONOSPHERIC  
PHYSICS', ACADEMIC PRESS, LONDON.

RISHBETH H., MOFFETT R.J. AND BAILEY G. J. (1969): J. ATMOS.  
TERR. PHYS. 31,1035.

- ROACH F.E., TANDGERG-HANSSSEN E. AND MEGILL L.R. (1958): J. ATMOS. TERR. PHYS. 13,122.
- ROBLE R.G., HAYS P.B. AND NAGY A.F. (1968): PLANET. SPACE SCI. 16,1109.
- ROBLE R.G., HAYS P.B. AND NAGY A.F. (1970): PLANET. SPACE SCI. 18,431.
- ROBLE R. G. AND NORTON R. B. (1972): J. GEOPHYS. RES. 77,3524.
- ROEMER M. (1971): IN 'PHYSICS OF THE UPPER ATMOSPHERE', ED. VERNIANI, P. 229, EDITRICE COMPOSITORI, BOLOGNA.
- ROSENBERG N. W. (1966): SCIENCE 152,1017.
- ROSENBERG N. W. (1968 A): SPACE RES. 8,673.
- ROSENBERG N. W. (1968 B): J. ATMOS. TERR. PHYS. 30,907.
- ROSENBERG N.W. (1968 C): J. GEOPHYS. RES. 73,4965.
- ROSENBERG N. W., GOLOMB D. AND ALLEN E.F. (1963 A): J. GEOPHYS. RES. 68,3329.
- ROSENBERG N. W., GOLOMB D. AND ALLEN E.F. (1963 B): J. GEOPHYS. RES. 68,5895.
- ROSENBERG N. W. & EDWARDS H. D. (1964): J. GEOPHYS. RES. 69,2819.
- ROSENBERG N. W., EDWARDS H. D. AND WRIGHT J.W. (1964): SPACE RES. 4,171.
- ROSENBERG N. W. & JUSTUS C. G. (1966): RAD. SCI. 1,149.
- RUSTER R. (1971): J. ATMOS. TERR. PHYS. 33,137.
- RUSTER R. & DUDENEY J. R. (1972): J. ATMOS. TERR. PHYS. 34,1075.
- RUSTER R. AND KING J. W. (1973): J. ATMOS. TERR. PHYS. 35,1317.
- SASTRY T. S. G., SAMPATH S. & HIRAO K. (1973): PRESENTED AT THE 16TH COSPAR MEETING, KONSTANZ, W. GERMANY.
- SATYA PRAKASH, SUBBARAYA B. H. AND GUPTA S P. (1968): J. ATMOS. TERR. PHYS. 30,1193.
- SAVENKO I. A., SHAVRIN P. I. AND PISARENTO N.K. (1963): PLANET. SPACE SCI. 11,431.
- SCIALOM G. (1971): IN 'PHYSICS OF THE UPPER ATMOSPHERE', ED. VERNIANI, P. 367, EDITRICE COMPOSITORI, BOLOGNA.
- SCHAEFER E. J. (1963): J. GEOPHYS. RES. 68,1175.
- SCHAEFER E. J. (1969): J. GEOPHYS. RES. 74,3488.
- SECHRIST C. F AND GELLER M. A. (1972): ED. COSPAR SYMPOSIUM ON D & E REGION CHEMISTRY, AERONOMY REPORT NO. 48, UNIVERSITY OF ILLINOIS, ILLINOIS.
- SHAFI AHMAD M. (1966): PRESENTED AT THE 9TH COSPAR MEETING, LONDON.
- SHAFI AHMAD M. (1967): PRESENTED AT THE 10TH COSPAR MEETING, TOKYO.
- SHEFOV N. N. (1971): PLANET. SPACE SCI. 19,129.
- SHEPHERD G.G. (1969): IN 'ATMOSPHERIC EMISSIONS', ED. MCCORMAC B.M. AND OMHOLD A., P. 411, VAN NOSTRAND, REINHOLD, N.YORK.
- SHIMAZAKI T. (1959): J. RADIO RES. LAB. TOKYO 6,107
- SHIMAZAKI T. (1965): J. ATMOS. TERR. PHYS. 27,593.
- SHIMAZAKI T. (1966): J. GEOPHYS. RES. 71,3177
- SHIRKE J.S., DESAI J.N. AND POKHUNKOV A.A. (1969): PROCEEDINGS OF THE 3RD INT. SYMP. ON EQUATORIAL AERONOMY, AHMEDABAD.
- SMITH E. K. AND MATSUSHITA S. (1962): 'IONOSPHERIC SPORADIC E', MACMILLAN, N.YORK.
- SMITH E. K. & MATSUSHITA S. (1966): ED. RAD. SCI. 1,129.
- SMITH F. J. (1963): PLANET. SPACE SCI. 11,1311.
- SMITH L. B. (1968): J. GEOPHYS. RES. 73,4959.
- SMITH L. B. (1972): J. GEOPHYS. RES. 77,2927.
- SMITH L. G. (1966): PLANET. SPACE SCI. 12,1173.



- SPENCER N. W., NEWTON G. P., CARIGNAN C. R. AND TAEUSCH D. B. (1970):  
SPACE RES. 10,389.
- SPENCER N. W. AND CARIGNAN C. R. (1972): PRESENTED AT 15TH COSPAR  
MEETING MADRID, SPAIN.
- SPIZZICHINO A. (1969 A): ANN. GEOPHYS. 25,693.
- SPIZZICHINO A. (1969 B): ANN. GEOPHYS. 25,755.
- SPIZZICHINO A. (1969 C): ANN. GEOPHYS. 25,773.
- SPIZZICHINO A. (1970 A): ANN. GEOPHYS. 26,9.
- SPIZZICHINO A. (1970 B): ANN. GEOPHYS. 26,25.
- SPIZZICHINO A., DELCOURT J., GIRAUD A., AND REVAH I. (1965): PROC. IEEE  
53,1084.
- STENING R. J. (1970): PLANET. SPACE SCI. 18,423.
- STUBBE P. (1968 A): J. ATOMS. TERR. PHYS. 30,243.
- STUBBE P. (1968 B): J. ATMOS. TERR. PHYS. 30,1965.
- STUBBE P. (1970): J. ATMOS. TERR. PHYS. 32,865.
- STUBBE P. (1972): PLANET. SPACE SCI. 20,209.
- STUBBE P. & CHANDRA S. (1970): J. ATMOS. TERR. PHYS. 32,1909.
- STROBEL D. F. & MCELROY M. B. (1970): PLANET. SPACE SCI. 18,1181.
- SUBBARAYA B. H., SATYA PRAKASH S. AND PAREEK P. N. (1972): J. ATMOS.  
TERR. PHYS. 34,1141.
- SWARTZ W. E., ROHRBAUGH J. L. AND NISBET J. S. (1972): J. ATMOS. TERR.  
PHYS. 34,1817.
- SWARTZ E. W. AND NISBET J. S. (1971): J. GEOPHYS. RES. 76,185.
- SWIDER W. (1971): EOS, TRANS. AGU. 52,505.
- TAEUSCH D. R. AND CARIGNAN G. R. (1972): J. GEOPHYS. RES. 77,4870.
- TAUBENHEIM J. (1971): J. ATMOS. TERR. PHYS. 33,1481.
- THOMAS L. (1966): J. GEOPHYS. RES. 71,1357.
- THOMAS L. (1968): J. ATMOS. TERR. PHYS. 30,1631.
- THOME G. (1968): J. GEOPHYS. RES. 73,6319.
- TITHERIDGE J. E. (1968): J. ATMOS. TERR. PHYS. 30,1857.
- TOHMATSU T. & NAGATA T. (1963): PLANET. SPACE SCI. 10,103.
- TORR D. G. & TORR M. R. (1970): J. ATMOS. TERR. PHYS. 32,15.
- USSA SUPPLEMENT (1966): UNITED STATES STANDARD ATMOSPHERE SUPPLEMENTS,  
U. S. GOVERNMENT PRINTING PRESS, WASHINGTON.
- VASSEUR G. (1969): J. ATMOS. TERR. PHYS. 31,397.
- VASSEUR G. & WALDTEUFEL P. (1969): J. ATMOS. TERR. PHYS. 31,885.
- VESTINE E. H. (1960): IN 'PHYSICS OF THE UPPER ATMOSPHERE', ED. J. A.  
RATCLIFFE, ACADEMIC PRESS, N. YORK.
- VINCENT R. A. (1972): J. ATMOS. TERR. PHYS. 34,1881.
- VOLLAND H. (1969): PLANET. SPACE SCI. 17,1581.
- VOLLAND H. (1970): J. GEOPHYS. RES. 75,5618.
- VOLLAND H. & MAYR H. G. (1972 A): J. ATMOS. TERR. PHYS. 34,1745.
- VOLLAND H. & MAYR H. G. (1972 B): J. ATMOS. TERR. PHYS. 34,1769.
- VOLLAND H. & MAYR H. G. (1972 C): J. ATMOS. TERR. PHYS. 34,1797.
- VON ZAHN U. (1967) J. GEOPHYS. RES. 72,5933.
- VON ZAHN U. (1970): J. GEOPHYS. RES. 75,5517.
- WALDTEUFEL P. (1970): PH. D. THESIS, UNIVERSITY OF PARIS, PAIRS.
- WALDTEUFEL P. (1971): J. GEOPHYS. RES. 76,6990.

- WALDTEUFEL P. AND MCCLURE J. P. (1969): ANN. GEOPHYS. 25,785.  
WALDTEUFEL P., BAUAR P. AND MCCLURE J. P. (1971): PRESENTED AT THE 14TH COSPAR/URSI MEETING, SEATTLE, WASHINGTON.  
WALDTEUFEL P. AND COGGER L. L. (1971): J. GEOPHYS. RES. 76,5322.  
WALDTEUFEL P. AND MCCLURE J. P. (1971): J. GEOPHYS. RES. 76,3106.  
WEBB W. L. (1968): SPACE RES. 8,1.  
WHITEHEAD J. D. (1961): J. ATMOS. TERR. PHYS. 20,49.  
WHITEHEAD J. D. (1967): SPACE RES. 7,89.  
WHITEHEAD J. D. (1970): REV. GEOPHYS. & SPACE PHYS. 8,65.  
WHITEHEAD J. D. (1972): PLANET. SPACE SCI. 20 ,1348.  
WILLMORE A. P. (1964): PROC. ROY. SOC. A281,140.  
WILLMORE A.P.(1970): SPACE SCI. REV. 11,607.  
WILT G. (1962): TELLUS 14,1.  
WOODRUM A. & JUSTUS C. G. (1968 A): J. GEOPHYS. RES. 73,467.  
WOODRUM A. & JUSTUS C. G. (1968 B): J. GEOPHYS. RES. 73,7535.  
WOODRUM A., JUSTUS C.G. AND ROPER R.G.(1969):J. GEOPHYS. RES. 74,4099.  
WOODMAN R. (1970): J. GEOPHYS. RES. 75,6249.  
WRIGHT J. W. (1968): J. ATMOS. TERR. PHYS. 30,919.  
WRIGHT J.W., MURPHY C.H. AND BULL G.V.(1967):J. GEOPHYS. RES. 72,1443.  
YONEZAVA T. (1965): J. RAD. RES. LABS. TOKYO. 12,65.  
YONEZAVA T. (1966): SPACE SCI REV. 5,3.  
ZIMMERMANN S. P. (1964): J. GEOPHYS. RES. 69,784.  
ZIMMERMANN S.P. & CHAMPION K.S.W.(1963):J. GEOPHYS. RES. 68,3049.  
ZIMMERMANN S.P. & MARKOS F.A.(1966):PRESENTED AT THE ICMVA SYMPOSIUM ON INTERACTION BETWEEN UPPER AND LOWER LAYERS OF THE ATMOSPHERE,VIENNA.  
ZIMMERMANN S. P & ROSENBERG N.W. (1971): PRESENTED AT THE 14TH COSPAR MEETING, SEATTLE, WASHINGTON.  
ZWICK H. H. AND SHEPHERD G. G. (1973): PLANET. SPACE SCI. 21,605.